

AD _____
(Leave blank)

Award Number:
W81XWH-07-1-0445

TITLE:
**Institute for Advanced Pharmaceutical Sciences: Molecular Targets
and Drug Screens to Combat Bioterrorism**

PRINCIPAL INVESTIGATOR:
Jerry L. Bauman, Ph.D.

CONTRACTING ORGANIZATION:
**University of Illinois
Chicago, Illinois 60612**

REPORT DATE:
December 2008

TYPE OF REPORT:
Final

PREPARED FOR: U.S. Army Medical Research and Materiel Command
Fort Detrick, Maryland 21702-5012

DISTRIBUTION STATEMENT: (Check one)

- ☒ Approved for public release; distribution unlimited
- ☐ Distribution limited to U.S. Government agencies only;
report contains proprietary information

The views, opinions and/or findings contained in this report are those of the author(s) and should not be construed as an official Department of the Army position, policy or decision unless so designated by other documentation.

| REPORT DOCUMENTATION PAGE | | | Form Approved OMB No. 0704-0188 | |
|--|------------------|-------------------------|--|--|
| Public reporting burden for this collection of information is estimated to average 1 hour per response, including the time for reviewing instructions, searching existing data sources, gathering and maintaining the data needed, and completing and reviewing this collection of information. Send comments regarding this burden estimate or any other aspect of this collection of information, including suggestions for reducing this burden to Department of Defense, Washington Headquarters Services, Directorate for Information Operations and Reports (0704-0188), 1215 Jefferson Davis Highway, Suite 1204, Arlington, VA 22202-4302. Respondents should be aware that notwithstanding any other provision of law, no person shall be subject to any penalty for failing to comply with a collection of information if it does not display a currently valid OMB control number. PLEASE DO NOT RETURN YOUR FORM TO THE ABOVE ADDRESS. | | | | |
| 1. REPORT DATE (DD-MM-YYYY) 30-12-2008 | | 2. REPORT TYPE Final | | 3. DATES COVERED (From - To) 1 JUL 2007 - 30 NOV 2008 |
| 4. TITLE AND SUBTITLE Institute for Advanced Pharmaceutical Sciences: Molecular Targets and Drug Screens to Combat Bioterrorism | | | 5a. CONTRACT NUMBER W81XWH-07-1-0445 | |
| | | | 5b. GRANT NUMBER | |
| | | | 5c. PROGRAM ELEMENT NUMBER | |
| 6. AUTHOR(S) Jerry L. Bauman | | | 5d. PROJECT NUMBER | |
| | | | 5e. TASK NUMBER | |
| | | | 5f. WORK UNIT NUMBER | |
| 7. PERFORMING ORGANIZATION NAME(S) AND ADDRESS(ES) University of Illinois Chicago, Illinois 60612-7205 | | | 8. PERFORMING ORGANIZATION REPORT NUMBER | |
| 9. SPONSORING / MONITORING AGENCY NAME(S) AND ADDRESS(ES) U.S. Army Medical Research and Materiel Command Fort Detrick, MD 21702 | | | 10. SPONSOR/MONITOR'S ACRONYM(S) | |
| | | | 11. SPONSOR/MONITOR'S REPORT NUMBER(S) | |
| 12. DISTRIBUTION / AVAILABILITY STATEMENT Approved for public release; distribution unlimited | | | | |
| 13. SUPPLEMENTARY NOTES | | | | |
| 14. ABSTRACT Anthrax continues to be a major threat to our national security and economy. We used multiple approaches for the development of novel therapeutics.(1)We engineered three isogenic mutant <i>E.coli</i> strains to be used for HTS screening for selective and specific inhibitors of anthrax protein synthesis.(2)We developed 2 assays for quantitation of peptide self-assembly and showed that ACDs inhibit specific aggregation pathways.(3)We demonstrated that inhibitors of FabI exhibit broad spectrum of activity against a variety of pathogens, and started to develop additional enzymatic targets in the fatty acid biosynthetic pathway.(4) We developed synthetic schemes for series of Antibiotic A-33853 derivatives and improved the potency of the original A-33853 two-fold against <i>B. anthracis</i> , and demonstrated that these derivatives are effective against wide spectrum of pathogens, including <i>L. donovani</i> .(5)We have developed automated MIC assay that can be used to screen up to 100K compounds/day against bacteria, and identified three structural classes as potential lead scaffolds for future medicinal chemistry improvement. | | | | |
| 15. SUBJECT TERMS Anthrax therapeutics, protein synthesis inhibitors, blockade of anthrax infiltration, FabI inhibitors as therapeutics, HTS and natural products-based discovery for anthrax therapeutics | | | | |
| 16. SECURITY CLASSIFICATION OF: | | | 17. LIMITATION OF ABSTRACT UU | 18. NUMBER OF PAGES 153 |
| a. REPORT U | b. ABSTRACT U | c. THIS PAGE | | |
| | | | 19a. NAME OF RESPONSIBLE PERSON USAMRMC | |
| | | | 19b. TELEPHONE NUMBER (include area code) | |

Table of Contents

| | <u>Page</u> |
|-----------------------------------|-------------|
| Introduction..... | 4 |
| Body..... | 5 |
| Project 1 report..... | 5 |
| Project 2 report..... | 9 |
| Project 3 report..... | 16 |
| Project 4 report..... | 19 |
| HTS core report..... | 22 |
| Key Research Accomplishments..... | 24 |
| Reportable Outcomes..... | 26 |
| Conclusion..... | 27 |
| References..... | 28 |
| Appendices..... | 29 |

Institute for Advanced Pharmaceutical Sciences: Molecular Targets and Drug Screens to Combat Bioterrorism

Introduction

Anthrax, the only biological agent used in US terrorist attacks in recent history, continues to be a major threat to our national security and economy and the potential for its use remains high. In addition, the potential for developing drug-resistant forms of anthrax is also high since it has been demonstrated that drug resistance forms, i.e. against Cipro, are easy to produce with common laboratory supplies and equipment. The program described herein consisted of multiple projects encompassing themes of developing novel sites in bacterial ribosomes for new antibiotic action (Project 1), development of amino cyclodextrins to block pore assembly by the anthrax pathogen (and others) in host tissues (Project 2), rational development of new inhibitors of a key enzyme in fatty acid biosynthesis, FabI, in many gram-positive and gram-negative bacteria (Project 3), and development and screening of natural products for their therapeutic potential against anthrax and other infectious agents (Project 4).

As we have previously notified your agency, the laboratories participating in this contract were affected by fire in the College of Pharmacy (COP), and flooding in Molecular Biology Research Building (MBRB), both events happening on the weekend of January 19, 2008. The fire originated on the 4th floor South of COP building and as a result the spaces on the 4th floor (Dr. Thatcher's laboratory) and 5th floor (Dr. Kozikowski's laboratory and mass specs) suffered significant smoke and soot damage, while the 3rd floor South (Dr. Gemeinhart's and Dr. Onyuksel's labs) suffered water damage, both to the space and to the equipment. Reagents in some refrigerators and freezers were also damaged due to temperature extremes, power outages, and failure of these appliances. The building itself was closed for the first 2 weeks post-fire, and after that access was limited to people in the parts of the building that were not affected, and to recovery workers. Full access to the space was restored on March 17, 2008. After that, great effort was spent on equipment inspections, repair, and replacement, and inventorying reagents that were affected post-fire; accordingly, most personnel in each of the labs described above were not able to resume research activities until May. Breakdown in the heating system and ensuing flood in MBRB affected work in the labs of Dr. Johnson, Dr. Mesecar, and to the lesser extent Dr. Mankin. Researchers located in MBRB were able to resume their work to nearly 100% of pre-flood level by February 15, 2008. We requested and were granted a six month no cost extension to complete this work.

Despite the disaster-caused delay, we have successfully completed Projects 1 and 4, and although we had some fire-related setbacks in Projects 2 and 3, we made substantive progress with these. Detailed Final reports for each project and for the HTS core follow; each report is structured into required sections. For even more detail, we appended scientific portions of the quarterly reports for each project (organized by project), and publications resulting from this research so far.

Project 1. Protein synthesis inhibitors acting upon new sites in bacterial ribosomes

A. Mankin

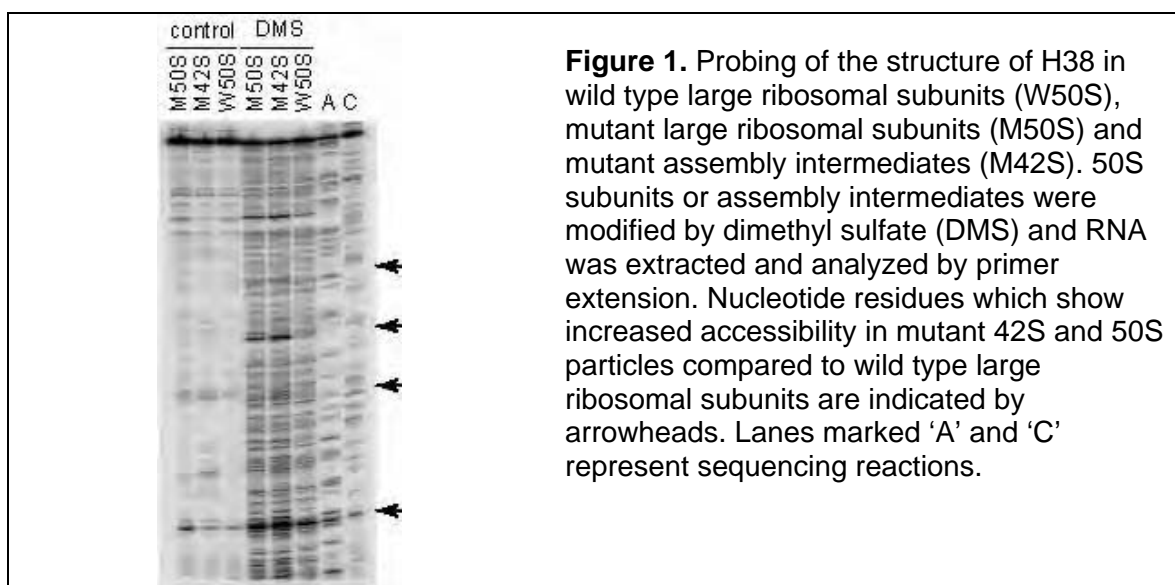
Introduction

The ribosome represents an evolutionary and clinically validated antibiotic target [1]. Many clinically useful antibiotics inhibit bacterial growth by interfering with protein synthesis in the target cells. However, the number of sites targeted by known antibiotics in the ribosome is limited, and natural resistance mechanisms operating upon these sites have curbed the usefulness of the known antibiotics. Therefore, the aim of this project was to characterize and validate a putative new site of antibiotic action in the ribosome of pathogenic bacteria, including *B. anthracis*, and develop approaches for identification of protein synthesis inhibitors acting upon this site.

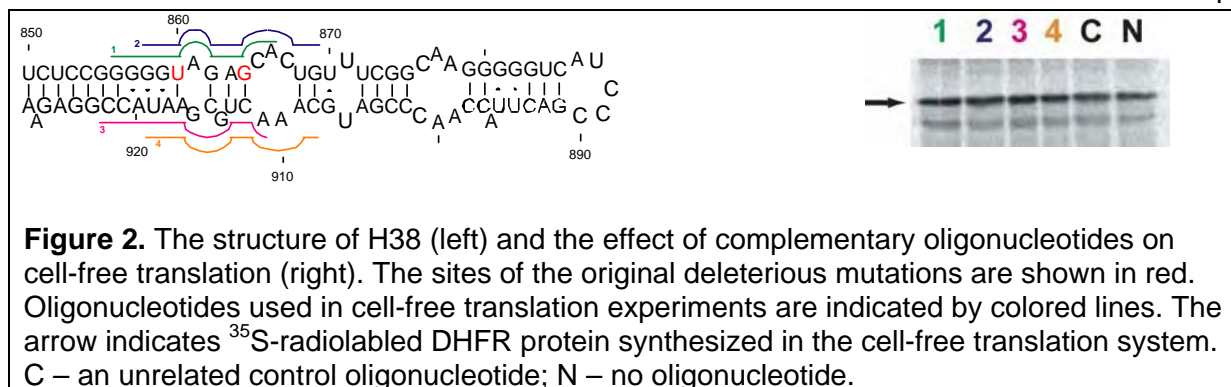
Body

In the course of this work we have investigated helix 38 in rRNA of the large ribosomal subunit as a new antibiotic target, characterized mutants with nucleotide alterations in this site, tested inhibitory action of several oligonucleotides targeted against the corresponding rRNA region and finally, devised a novel strategy suitable for high-throughput screening of chemical and natural libraries.

Two mutations in helix 38 (H38) of bacterial 23S rRNA were found initially to be highly deleterious [2]. Sucrose gradient analysis revealed that the presence of any of these mutations affect both assembly of the large ribosomal subunit as well as the structure of the mature subunits. RNA chemical probing demonstrated that the structure of mutant H38 in the assembly intermediates as well as in the fully assembled 50S subunits is less compact than in wild type ribosomes (Figure 1), thereby establishing a link between the lethal effect of the mutations and the ribosomal structure.

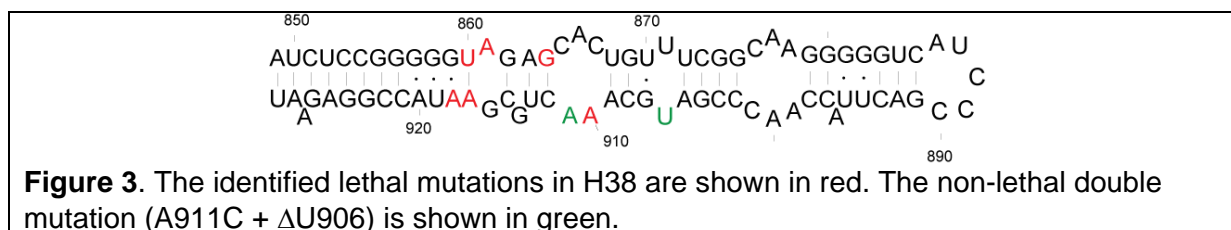


In order to test whether the structure of H38 (and thus the function of the ribosome) could be distorted by complementary oligonucleotides, a cell-free translation system was employed. Several oligonucleotides targeting the structurally- and functionally critical element of H38 were synthesized (Figure 2) and their effect on translation was analyzed.



None of the tested oligonucleotides produced a discernable effect on cell-free translation of a reporter protein (DHFR), suggesting that this oligonucleotide-based approach does not hold much promise for developing therapeutic agents targeted against this ribosomal site.

This result prompted us to further investigate H38 in order to better delineate its functionally-critical elements. A series of mutations were introduced at the nucleotide positions of H38 conserved in bacteria and the effects of these mutations on cell viability (and thus protein synthesis) were analyzed. In these studies we found that mutations A861C, A910C, A917C and A918C, together with the previously identified U860C and G864A, have dominant lethal phenotypes, indicating the importance of the corresponding residues for the function of the ribosome (Figure 3). In contrast, the mutations at positions U906 and A911 had little effect on cell viability. Two additional mutations (A78C and A99C) engineered in 5S rRNA in a segment which comes into direct contact with H38 had little effect on translation.

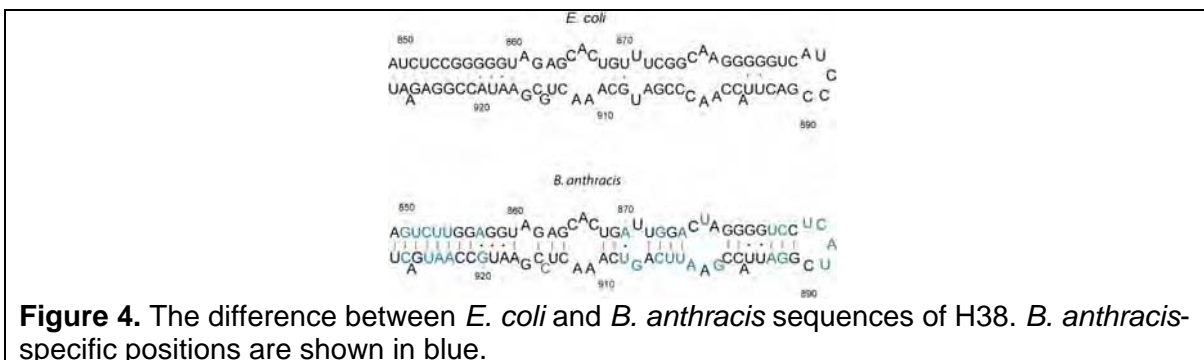


As a result of these studies, we now realize that the best region of H38 to be targeted by putative new antibiotics is a structure in the vicinity of the base pair U860-A917.

Our subsequent experimental effort was focused on designing a strategy that could lead to identification of selective antibiotic compounds acting upon the identified ribosomal site in pathogenic bacteria. Upon consultation with experts in the pharmaceutical industry and based on the results of our colleagues, we decided to avoid the common high-throughput screening approach which is based on identification of *in vitro* inhibitors of target enzymes. Years of futile attempts to develop drugs by this method serve as a strong deterrent from walking down this path. Instead, we came up with a novel approach which can result in identification of lead compounds that not only reach their target in the living bacterial cell, but also show sufficient selectivity against the bacterial ribosome.

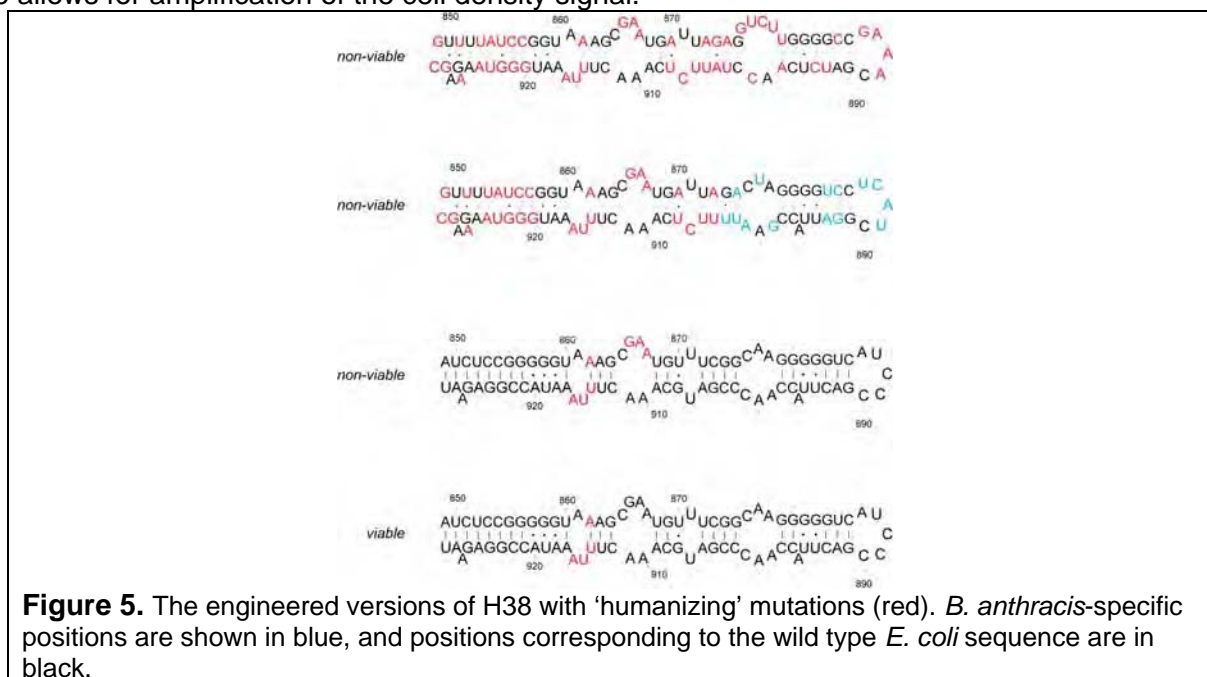
In the context of this novel approach, we engineer the *B. anthracis* and human sequences of H38 in the context of the *E. coli* ribosome. We then developed a protocol which would allow screening a library of chemical compounds for selective inhibitors of the engineered *E. coli* cells presenting the desired antibiotic target. In the initial experiments, we tested whether *E. coli* cells carrying the *B. anthracis* version of H38 are viable. Thirty out of 80 positions constituting H38 are different between *E. coli* and *B. anthracis* (Figure 4). Nevertheless, introducing all 30 nucleotide alterations in 23S rRNA of the *E. coli* ribosome had almost no effect on the viability of cells expressing exclusively mutant ribosomes. This result confirmed the idea that it is

possible to engineer elements of the pathogenic ribosome in the ribosome of a non-pathogenic laboratory strain to use the resulting mutant in library screening.



The next step was to alter the *E. coli* H38 so that it resembles the corresponding site in the human ribosome. The availability of *E. coli* with the 'humanized' ribosome would allow for direct screening of chemical or natural compound libraries for selective inhibitors acting upon the desired ribosomal site. This task turned out to be rather difficult. Introducing the 46 mutations in the *E. coli* H38 that converted its sequence into that found in human cytoplasmic ribosomes produced non-viable cells (Figure 5). Therefore, we had to progressively reduce the number of the mutated positions. In this effort, we tried to retain the 'humanizing' mutations in the vicinity of the functionally-critical site (the base pair U860-A917) identified in our previous studies.

As a result of this effort, we found that the ribosome with human-like mutations at positions 862, 914, 915 and 916 can support bacterial growth (Figure 5). These studies culminated in preparation of three isogenic *E. coli* strains: 1) wild type, 2) the strain with the *B. anthracis* version of the entire H38 and 3) the strain with the human-like structure of the functionally-critical site of H38. Protein synthesis in all these strains relies exclusively on the activity of plasmid-encoded engineered ribosomes. These strains can be used in high-throughput screens for specific and selective inhibitors of ribosome function which bind to the engineered site in H38 in the living cell. Though we did not have a chance to test the strains in a high-throughput screen (HTS), we have optimized the HTS protocol to adapt it for analysis of growth of the engineered *E. coli* strains. After several attempts, we settled on using the Alomar blue dye to monitor cell growth in 384-well microtiter plates. The dye is metabolized by living cells resulting in the development of an intensive blue color; the use of this dye allows for amplification of the cell density signal.



Previously, the dye was used exclusively with Gram-positive bacteria and we needed to optimize the assay for Gram-negative *E. coli*. We found that prolonged (90 min) incubation with the dye at 37° compensates for the low permeability of the Gram-negative membrane and provides sufficient signal to be used in the high throughput assay. The assay was tested with several protein synthesis inhibitors and was shown to be robust. In conclusion, in the course of work on this project, we have dissected the structure of H38 in the bacterial ribosome and identified a potential antibiotic target site in it. We have engineered tester strains with alterations in H38 that can be used in a high-throughput format and optimized the protocol for HTS of chemical or natural compound libraries for specific and selective inhibitors of protein synthesis.

Key Research Accomplishments

- Identified the nucleotide alterations in helix 38 of 23S rRNA resulting in the distortion of the helix structure which correlates with defects in protein synthesis.
- Delineated the segment of helix 38 which is critical for ribosome activity.
- Engineered a viable *E. coli* cells relying on the function of ribosomes which carry the *B. anthracis* version of helix 38.
- Engineered a viable *E. coli* strain which relies on the function of ribosomes which helix 38 with humanized functional segments.
- Optimized a high-throughput protocol for screening libraries of chemical and natural compounds for selective and specific inhibitors of protein synthesis.

Reportable outcomes

Three isogenic mutant *E. coli* strains have been developed which can be used for screening libraries of chemical and natural compounds for selective and specific inhibitors of protein synthesis. In the near future, a manuscript describing the results of the study will be prepared for publication.

Conclusions

The two main results of the study are identification a functionally-important segment of helix 38 in 23S ribosomal RNA as a potential antibiotic target and designing a novel approach that can be used for identifying selective and specific protein synthesis inhibitors using whole-cell high-throughput screening. The drawback is that the actual screening was not carried out because the appropriate compound libraries were not made available to us. The important future direction is preparing additional sets of *E. coli* strains with other engineered 'pathogenic' and 'humanized' sites in rRNA. Such strains can be used in screens for new protein synthesis inhibitors.

References

1. Poehlsgaard, J. and Douthwaite, S., *The bacterial ribosome as a target for antibiotics*. Nat Rev Microbiol, 2005. **3**(11): p. 870-81.
2. Yassin, A. and Mankin, A.S., *Potential new antibiotic sites in the ribosome revealed by deleterious mutations in RNA of the large ribosomal subunit*. J Biol Chem, 2007.

Project 2. Multiple target molecular counter-measures to biowarfare pathogens; blockade of infiltration and boosting of host defenses.

G. Thatcher

Introduction

The hypothesis of this research is that appropriately substituted aminocyclodextrins (ACDs) represent polyvalent ligands that can be synthesized to inhibit selectively the assembly of polypeptides that are cytotoxic and cause death to humans. The anthrax associated polypeptide protective antigen (PA) forms an organized aggregate that permits access of lethal factor (LF) and edema factor (EF) into the host human cell leading to cell death. It is argued that assembly of multiple PA polypeptides and insertion into the cell membrane results in formation of an ion channel. The hypothesis of this research is that appropriately substituted aminocyclodextrins (ACDs) represent polyvalent ligands that can be synthesized to inhibit selectively the assembly of PA, blocking intracellular delivery of LF and EF. We have previously demonstrated that ACDs are able to inhibit assembly of β -amyloid peptide into aggregates. These aggregates are soluble oligomers, sometimes coined amyloid derived diffusible ligands (ADDLs). It is currently agreed that these soluble oligomers are the neurotoxic form of amyloid that is causal in Alzheimer's disease, which is a human disease of the brain leading to death. The detailed mechanism of neurotoxicity of these oligomers is not fully elucidated, several proposals involve interaction with a membrane receptor, and one posits formation of an ion channel in the neuronal cell membrane leading to influx of calcium and cell death [1-3]. Regardless, it has been clearly demonstrated that $A\beta_{1-42}$ forms cyclic oligomers *in simile* with PA. A number of laboratories including our own, have demonstrated that substituted CDs can show specific recognition of substrates [4-12]. In order to pursue these studies, we developed, published, and patented novel and highly efficient synthetic techniques [13-15]. Based upon the hypothesis that proteoglycans have neurite growth promoting and inhibitory activity associated with the anionic glycosaminoglycan sulfate (GAGS) side chains[16], we synthesized amino-cyclodextrins (ACDs) in which the primary face was persubstituted with an amine and the secondary face was unmodified, methylated or acylated. ACDs were shown to selectively recognize different GAGs and in primary cell culture to inhibit and/or provide a substrate for neurite growth[10], showing a surprising degree of selectivity, explored further in studies using small anionic guest molecules, such as nucleotides and aryl phosphates [17, 18]. These studies demonstrated that ACDs differ significantly from other CD derivatives. We reported that ACDs inhibited self-assembly of a potentially neurotoxic form of β -amyloid protein ($A\beta$) implicated in Alzheimer's disease using an $A\beta$ specific immunoassay [19-22]. ACDs inhibit self-assembly of $A\beta$ into neurotoxic ADDLs with nanomolar potency through a combination of electrostatic and hydrophobic recognition [21]. ACDs can be viewed to present a topology of binding sites akin to an antibody-like binding pocket but without the inherent problems in antibody therapeutics [23, 24].

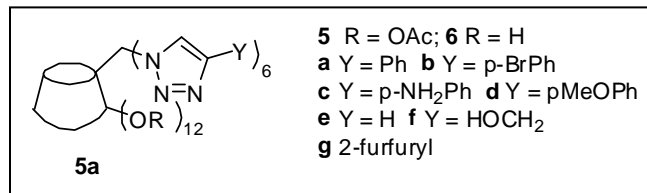
Body

Aim 1. Synthesis. Synthesis of a small library of 18 ACDs derived from α , β , and/or γ CD that contain pendant groups at the primary face to provide electrostatic or hydrophobic recognition or a combination of both. Synthesis of a combinatorial library of >2000 ACDs based upon either an α , β , or γ CD scaffold that utilizes different amine pendant groups in various combinations.

Three synthetic routes were studied for preparation of CD derivatives: (1) condensation of per-NH₂-ACD with the appropriate aldehydes followed by reduction to the desired ACD; (2) the standard route to derivatized CDs employing reaction of a thiol with per-Br-CD and subsequent functionalization, leading eventually to derivatives which contain amine pendant groups, but which are derivatized CDs, rather than ACD derivatives; (3) a new application of the Cu-catalyzed coupling of azides to alkynes (coined "click chemistry") whereby per-N₃-CD is reacted with the appropriate alkyne to yield a CD with a corona of amine pendant groups and an annulus of triazole groups. Since these may have different properties than CDs, we term these qCD derivatives. We have further explored routes (1) and (2) and confirmed that only in very few cases do reactions go to completion. Although the click chemistry proved more general than the first two synthetic methods attempted, drawbacks to this method were seen, in particular, long reaction times and very different rates of reaction with different alkynes. The importance of a quantitative synthetic methodology is that chromatography on derivatized CDs is complex and unsuitable for scale-up. The drawback with varied alkyne reactivity is the problem in preparing combinatorial libraries using different alkynes that react at very different rates.

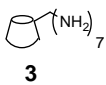
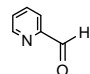
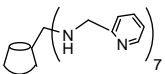
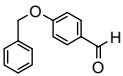
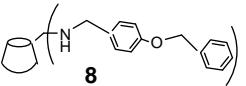
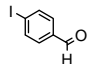
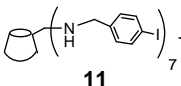
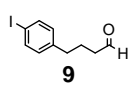
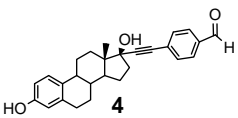
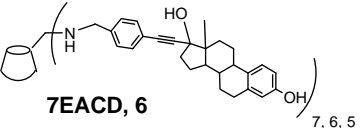
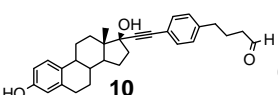
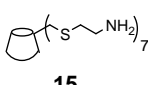
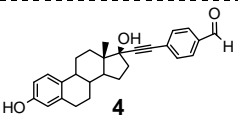
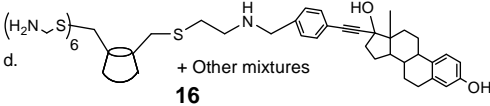
Click chemistry was optimized for library synthesis. The new method enjoys great advantage: (1) shortened reaction time (2 min in microwave oven versus 2 to 10 days previously); (2) the reaction can be easily monitored by TLC to ensure complete conversion; (3) removal of the new catalyst system CuI-P(OEt)₃ is more convenient than CuI alone, therefore improving the isolated yield.

A small qCD library of 14 compounds was prepared:



The postdoctoral researcher who developed the microwave procedure was incapable of optimizing the procedure for library preparation. However, the graduate student, Hye-yeong Kim, by focusing on preparation of homogeneous ACD and qCD derivatives, was able to produce a number of important compounds, achieving a comparison of the different synthetic methods (Tables 1-3); and generating interesting new compounds in sufficient yield for biological study.

Table I. Per-6-amino- β -CD derivatives and aldehydes condensation reactions.

| entry | CD | ligand | reaction condition | product |
|----------------|--|---|--------------------|--|
| 1 ^a |  3 | 8 eq.  | r.t, 5 h |  7 |
| 2 ^b | | 8 eq.  | r.t, 7 d |  8 |
| 3 ^c | | 8 eq.  | 60-70 °C, 18 h |  11 + Other mixtures |
| 4 ^c | | 8 eq.  9 | 60-70 °C, 18 h | S.M recovered |
| 5 ^d | | 10-70 eq.  4 | 60-70 °C, 10 d. |  7EACD, 6 |
| 6 ^d | | 10 eq.  10 | 60-70 °C, 10 d. | S.M recovered |
| 7 ^d |  15 | 21 eq.  4 | 60-70 °C, 10 d. |  16 + Other mixtures |

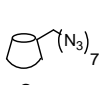
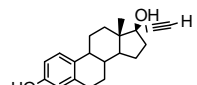
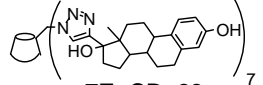
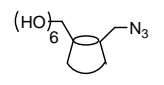
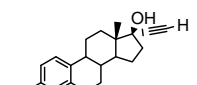
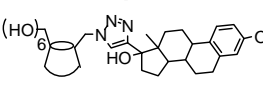
a. 1. r.t, 5 h, 2.

NaBH₄, MeOH, 2 h; **b.** 1. DMF, r.t, 7 d, 2. NaBH₄, MeOH, 2 h; **c.** 1. DMF, 60-70 °C, 18 h, 2. NaBH₄, MeOH, 2 h; **d.** 1. DMF, 60-70 °C, 10 d, 2. NaBH₄, MeOH, 2 h.

Rationale for synthetic targets. As stated above, it has been proposed that CD derivatives inhibit the actions of Anthrax lethal factor by blocking self-assembly of PA in the host cell membrane. The current clinical use of simple CDs has been as drug carriers solubilizing and increasing membrane permeability of these drugs, however CDs are in general assumed to be poorly membrane permeable. The question of membrane permeability of derivatized CDs of MW>1500 has not been unambiguously determined. Therefore, experiments were conducted with qCD and ACD derivatives to answer the question of membrane permeability, since this is an important question for future use. One approach to this question would be the use of an

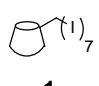
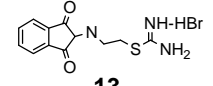
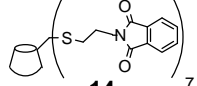
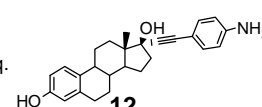
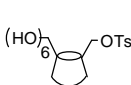
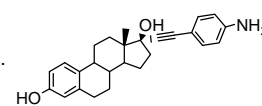
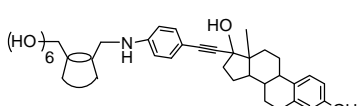
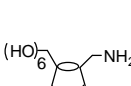
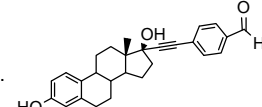
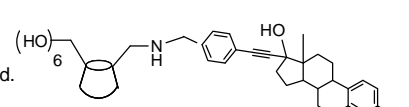
ACD/qCD derivatized with a fluorophore combined with use of confocal fluorescence microscopy. An alternate novel approach was taken: classical estrogenic action is widely believed to operate through ligand binding to the estrogen receptor (ER) in the cytoplasm, causing conformational change, dimerization, and translocation to the nucleus, leading to gene transcription and protein expression. The ER, when combined with a gene reporter construct, represents a high sensitivity reporter with nanomolar affinity for estrogens. It was therefore hypothesized that if qACD and ACD derivatives were synthesized containing an estrogen pendant group that cell and nuclear membrane permeability would be revealed. Two cellular assays were already established in our labs to measure estrogen-dependent gene transcription (ERE-luciferase in MCF-7 breast cancer cells and alkaline phosphatase in human endometrial cancer Ishikawa cells). Ethynylestradiol was used as the pendant estrogen ligand, yielding ACD (e.g. EE β ACD) and qCD derivatives (e.g. E β qCD) (Tables 1-3).

Table II. 'Click chemistry' with hepta- and mono-azido- β -CD **2** and **18** with EE₂.

| entry | CD | ligand | reaction condition | product |
|-----------------|--|---|--------------------|--|
| 14 ⁱ |  2 | 7 eq.  | r.t, 1 d |  7EqCD, 23 |
| 15 ⁱ |  18 | 1 eq.  | r.t, 1 d |  1EqCD, 24 |

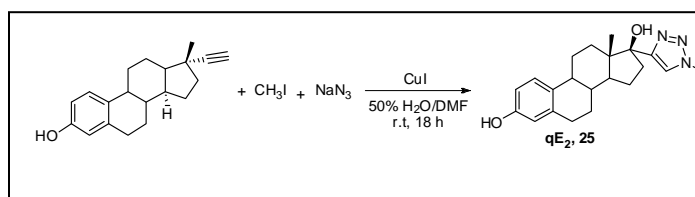
i. CuI, DIEA, DMF/MeOH, r.t, 1 d.

Table III. Substitution reactions and mono-modifications.

| entry | CD | ligand | reaction condition | product |
|-----------------|--|--|--------------------|--|
| 8 ^e |  1 | 15 eq.  13 | r.t, 2 d |  14 |
| 9 ^f | | 10-70 eq.  12 | 60-70 °C, 10 d | S.M recovered |
| 10 ^f |  17 | 21 eq.  12 | 60-70 °C, 7 d |  21 |
| 11 ^g |  19 | 1-3 eq.  4 | 60-70 °C, 3 d. |  1EACD, 20 |

e. DMF, Cs₂CO₃, r. t, 2 d; **f.** DMF, 60-70 °C, 10 d.; **g.** 1. DMF, 60-70 °C, 3 d, 2. NaBH₄, MeOH, 2 h.

Synthesis of triazole-modified control compound, qE₂ **25**.

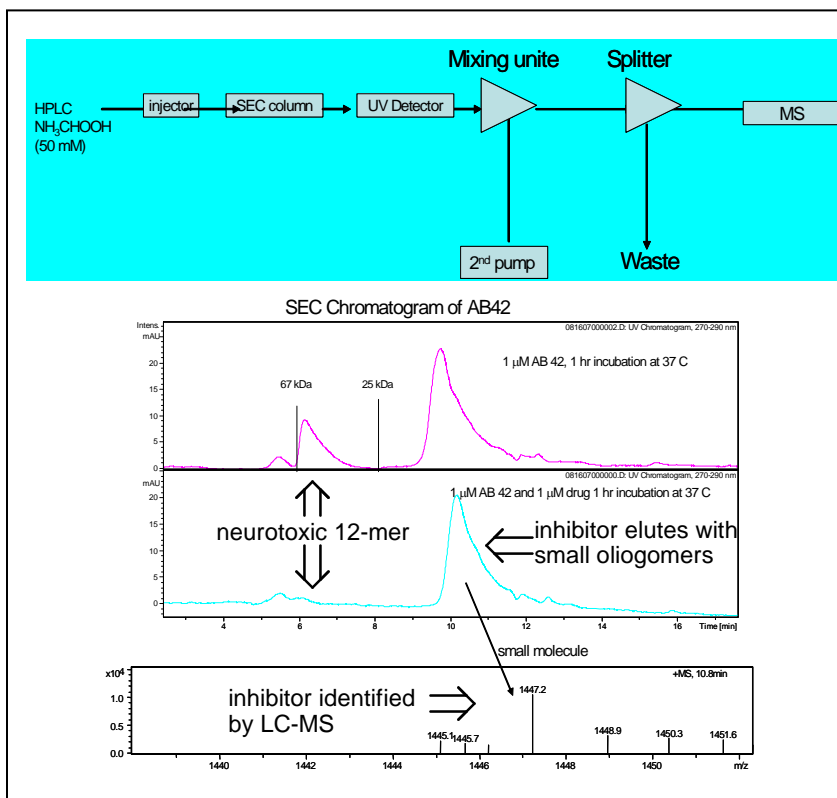


Aim 2. Assay of binding of ACDs to peptides and proteins using electrospray mass spectrometry to indicate the most potent ACD capable of inhibition of peptide self-assembly and to derive a structure-activity relationship for ACDs. In the original proposal, recombinant PA was to be provided from Dr. Andy Mesecar, a co-investigator on this grant, however, Dr Mesecar's lab had ceased to express and purify this protein; the commercial costs of these proteins was beyond the proposed budget. We adjusted our approach to optimize methods for assembly of alternative peptides before any study of PA. As described above, the original rationale for use of ACDs in Anthrax treatment was based upon the simile between PA and other peptides that self-assemble into cytotoxic oligomeric structures; and the ability of ACDs to inhibit such self-assembly: specifically, this includes neurotoxic amyloid peptide associated with Alzheimer's disease. This work in this aim was completed with the assistance of Dr Praneeth Edirisinghe who was not funded by this grant.

Inhibition of Self-Assembly - Methodology 1. An LC-MS method was developed to study the inhibition of self-assembly of β -amyloid peptide ($A\beta_{1-42}$) by ACD. This approach confirmed that the ACD under testing completely inhibited $A\beta_{1-42}$ self-assembly to the neurotoxic 12-mer form, but did not inhibit assembly of other oligomers. The methodology is not specific to $A\beta$, but should be general for screening of inhibitors of peptide self-assembly.

The details of the methodology (shown in the schematic to the right) are as follows: (1) inhibitor and peptide are incubated with stirring allowing self-assembly; (2) molecular weight cut-off filters are used to remove uncomplexed inhibitor; prior to (3) elution through a size exclusion chromatography (SEC) column, separating and detecting oligomeric forms by UV-detection; followed by (4) post-column disaggregation of oligomers; and finally (5) electrospray injection into mass spec and detection of small molecule inhibitors as a function of time. This SEC-LS-MS methodology is shown for the ACD inhibitor (MW = 14472); the neurotoxic 12-mer has MW 56kDa and is not observed in the presence of ACD.

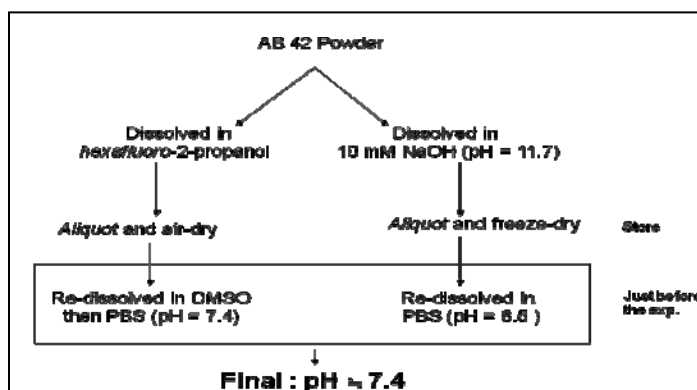
Further work on Methodology 1 yielded an unwanted observation: that the solid phase of the SEC column was not inert towards $A\beta$, i.e. the peptide aggregates were binding to the solid phase and presumably aggregation was perturbed by the column. This is not anticipated to be such a problem for other peptides, with less rapid self-assembly and less avid hydrophobic domains.



Inhibition of Self-Assembly - Methodology 2.

The difficulty encountered in Methodology 1 resulted from the rapid peptide self-aggregation of $A\beta_{1-42}$ and interference of the chromatography column during the aggregation process which continues during elution down the column. The solution to this problem was to incorporate a method for "quenching" aggregation to give a relatively stable mixture of $A\beta_{1-42}$ oligomers.

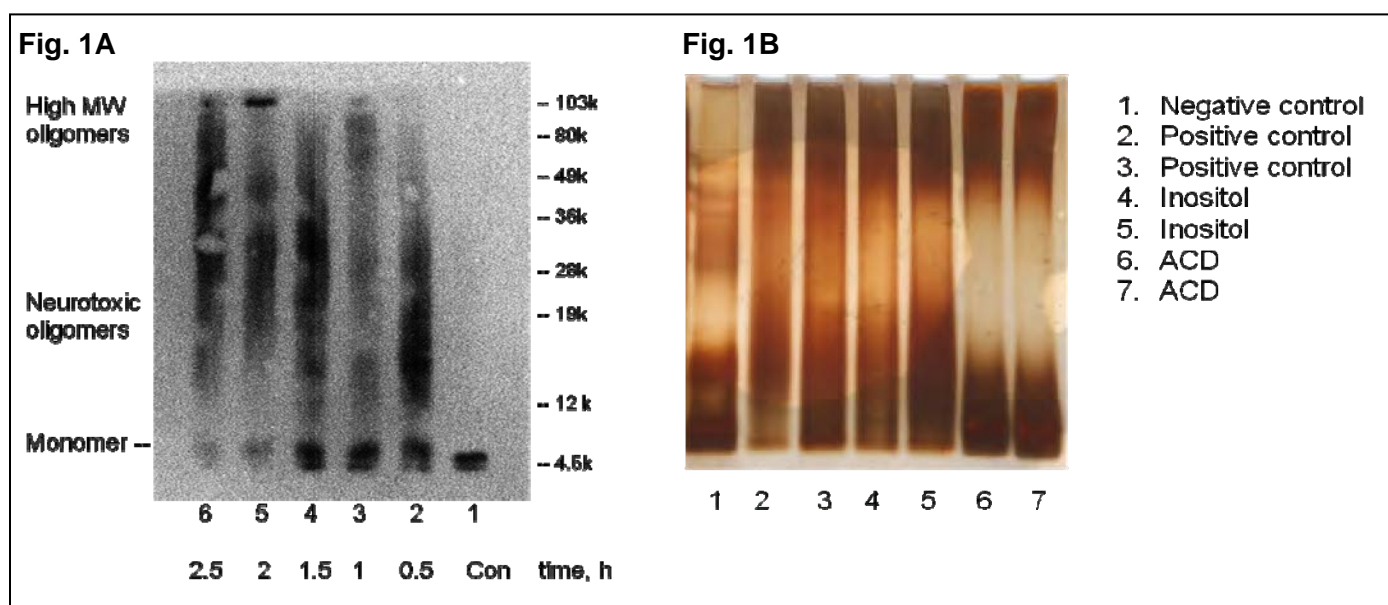
1. Preparation of $A\beta$ oligomers (see schematic).
2. Trapping of $A\beta$ oligomers by rapid photo-cross-linking using a ruthenium photocatalyst.



Free radical peptide cross-linking was achieved by photoactivation of ammonium persulfate (10 mM) in the presence of a Ru(II) salt (1 mM) generating oxygen radicals. An apparatus was constructed to focus the light source on the A β sample, optimizing: focal length; exposure time (10 s); and sample path length. Sample preparation following cross-linking required considerable optimization to remove ruthenium from the peptide sample

3. Analysis of cross-linked A β oligomers using 1D electrophoresis. The photo-cross-linked peptide mixtures were run on a 10% NuPAGE gel with MES as the running buffer. The gel was visualized by silver staining. Control experiments were run as a function of A β incubation time, showing a time-dependent loss of monomer and formation of oligomers. Notable was the very rapid formation of oligomers with 9,000 < MW < 30,000, followed by formation of higher molecular weight oligomers at later time points (Fig. 1A).

4. Assay of inhibition of A β oligomerization by ACD using gel electrophoresis. A simple ACD, modified with aminomethylfuran, previously demonstrated to inhibit ADDL formation was tested by co-incubating with A β for 48 h. A second agent was tested in parallel, *scyllo*-inositol, a natural product in Phase 2 clinical trials for Alzheimer's that reportedly inhibits A β aggregation and inhibits formation of A β fibrils and plaques in amyloid transgenic mice. The results were remarkable, in that ACD treatment inhibited formation of the smaller soluble oligomers that are thought to be the amyloid neurotoxic agents in humans (Fig. 1B).

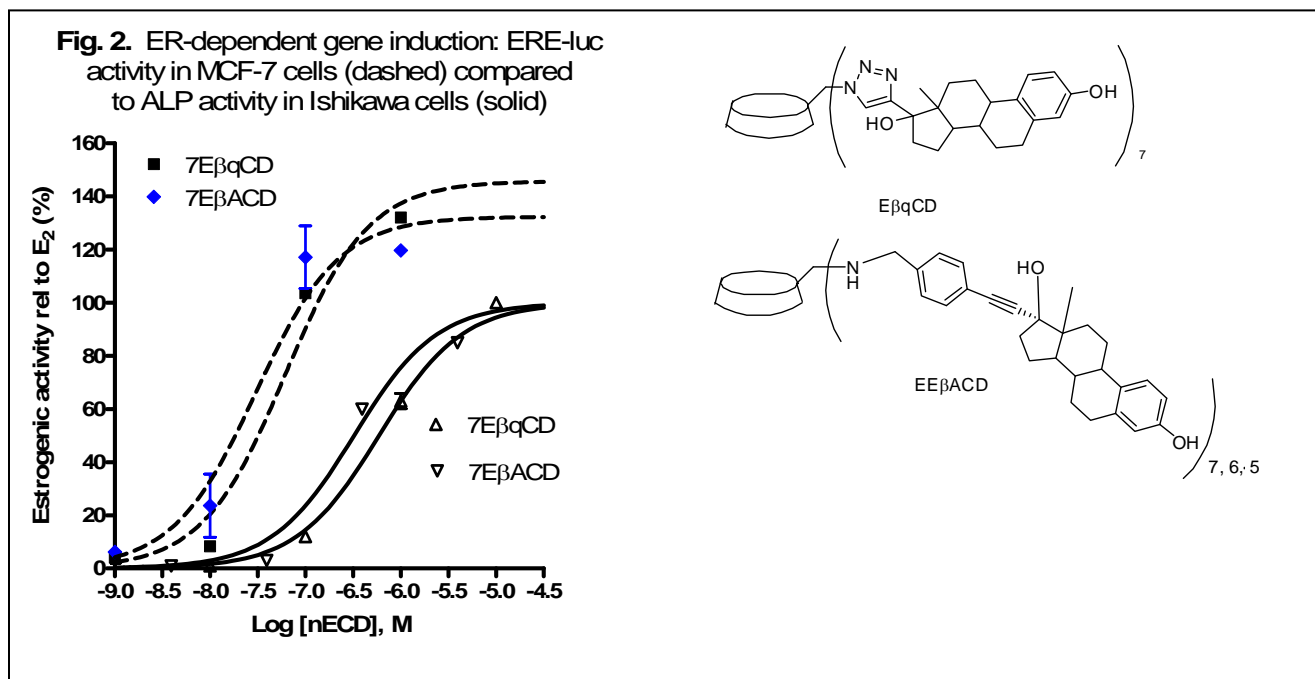


5. Mass spectrometric examination of inhibition of oligomerization by ACD. MALDI-TOF was used to identify cross-linked oligomers; at the end of the funding period this aspect was not optimized.

Aim 3. Assay of ACD activity in cell culture. It has been proposed that CD derivatives inhibit the actions of Anthrax lethal factor by blocking self-assembly of PA in the host cell membrane. The major clinical use of simple CDs has been as drug carriers solubilizing and increasing membrane permeability of these drugs. The question of membrane permeability of derivatized CDs of MW>1500 has not been unambiguously determined. Therefore, in the absence of LT to pursue aim 3, experiments were conducted with a pair of qCD and ACD derivatives to answer the question of membrane permeability. Experimental hypothesis: the intracellular estrogen receptor (ER) is a high sensitivity reporter with nanomolar affinity for estrogens; estrogen derivatized qCD and ACD will induce estrogen-dependent gene transcription (ERE-luciferase or Alkaline phosphatase expression) if they permeate the cell into the cytosol. An ethynylestradiol derivative of ACD (EE β ACD) and an estradiol derivative of qCD were synthesized (E β qCD).

Both the qCD and ACD estrogen conjugates were observed to be estrogenic in both ER positive endometrial and breast cancer cell lines (Fig. 2). This would seem to confirm the postulate that activity at a nuclear receptor confirms membrane permeability not only through the plasma membrane, but also through the nuclear membrane. However, there remains a question as to whether an impurity from the synthesis, such as ethynylestradiol (EE₂) itself, might be the cause of the observed estrogenic activity. The potency of EE₂ at the

ER is 10^{-11} M making it almost impossible to rule out analytically the level of contamination that would result in observed potency of 10^{-8} – 10^{-6} M.



Key research accomplishments

- Comparative analysis of synthetic methods for synthesis of ACD derivatives leading to a new methodology for synthesis of the related qCD derivatives.
- Synthesis of novel estrogen conjugates of ACD and qCD demonstrating nanomolar to micromolar estrogenic activity. These compounds represent useful tools for study of estrogenic activity in cell culture and provide evidence that high molecular weight estrogen conjugates have membrane permeability.
- Development of two new assays for quantitation of peptide self-assembly and demonstration of the ability of ACDs to inhibit specific aggregation pathways leading to formation of neurotoxic soluble oligomers.

Reportable outcomes

Hye-Yeong Kim, Gregory R. J. Thatcher, et al. Poster: Synthesis of Estradiol-Cyclodextrin Conjugates toward Studying Extranuclear Estrogen Signaling Pathway. Division of Medicinal Chemistry. The American Chemical Society 235th National Meeting & Exposition, New Orleans, LA, April 2008.

References

1. Arispe, N., Diaz, J.C. and Simakova, O., *Abeta ion channels. Prospects for treating Alzheimer's disease with Abeta channel blockers*. Biochim Biophys Acta, 2007. **1768**(8): p. 1952-65.
2. Simakova, O. and Arispe, N.J., *Early and late cytotoxic effects of external application of the Alzheimer's Abeta result from the initial formation and function of Abeta ion channels*. Biochemistry, 2006. **45**(18): p. 5907-15.
3. Arispe, N., *Architecture of the Alzheimer's A beta P ion channel pore*. J Membr Biol, 2004. **197**(1): p. 33-48.
4. Palmer, D.R.J., Buncel, E. and Thatcher, G.R.J., *Re-evaluation of cyclodextrin as a model of chymotrypsin: acceleration and inhibition of tertiary anilide hydrolysis*. J. Org. Chem., 1994. **59**(18): p. 5286-91.

5. Tabushi, I., *Cyclodextrin catalysis as a model for enzyme action*. Acc. Chem. Res., 1982. **15**: p. 66-72.
6. Breslow, R., *Biomimetic chemistry and artificial enzymes: catalysis by design*. Acc. Chem. Res., 1995. **28**: p. 146-153.
7. Murakami, Y., Kikuchi, J.-i., Hisaeda, Y. and Hayashida, O., *Artificial Enzymes*. Chemical Reviews (Washington, D. C.), 1996. **96**(2): p. 721-58.
8. Thatcher, G.R.J., *PI-specific phospholipase C: inhibition and enzyme model studies*. Book of Abstracts, 214th ACS National Meeting, Las Vegas, NV, September 7-11, 1997: p. CARB-058.
9. Breslow, R. and Dong, S.D., *Biomimetic Reactions Catalyzed by Cyclodextrins and Their Derivatives*. Chem Rev, 1998. **98**(5): p. 1997-2012.
10. Borrajo, A.M.P., Gorin, B.I., Dostaler, S.M., Riopelle, R.J. and Thatcher, G.R.J., *Derivatized cyclodextrins as peptidomimetics: influence on neurite growth*. Bioorg Med Chem Lett, 1997. **7**: p. 1185-1190.
11. Karginov, V.A., Nestorovich, E.M., Schmidtman, F., Robinson, T.M., Yohannes, A., Fahmi, N.E., Bezrukov, S.M. and Hecht, S.M., *Inhibition of S. aureus alpha-hemolysin and B. anthracis lethal toxin by beta-cyclodextrin derivatives*. Bioorg Med Chem, 2007. **15**(16): p. 5424-31.
12. Karginov, V.A., Nestorovich, E.M., Yohannes, A., Robinson, T.M., Fahmi, N.E., Schmidtman, F., Hecht, S.M. and Bezrukov, S.M., *Search for cyclodextrin-based inhibitors of anthrax toxins: synthesis, structural features, and relative activities*. Antimicrob Agents Chemother, 2006. **50**(11): p. 3740-53.
13. Gorin, B.D., Riopelle, R.J. and Thatcher, G.R.J., *Efficient perfacial derivatization of cyclodextrins at the primary face*. Tetrahedron Lett, 1996: p. 4647-4650.
14. Dow, K.E., Gorine, B.I., Riopelle, R.J. and Thatcher, G., *Cyclodextrin derivatives, preparation thereof, and use as nerve process growth modulators*. 1997, (Queen's University at Kingston, Can.). Application: WO WO. p. 36 pp.
15. Vizitiu, D., Walkinshaw, C.S. and Thatcher, G.R.J., *Synthesis of mono-facially functionalized cyclodextrins bearing amino pendent groups*. J. Org. Chem., 1997. **62**(25): p. 8760-8766.
16. Palmer, D.R.J., Buncel, E. and Thatcher, G.R.J., *Re-Evaluation of Cyclodextrin as a Model of Chymotrypsin: Acceleration and Inhibition of Tertiary Anilide Hydrolysis*. Journal of Organic Chemistry, 1994. **59**(18): p. 5286-91.
17. Vizitiu, D. and Thatcher, G.R.J., *Binding of phosphates to aminocyclodextrin biomimetics*. Journal of Organic Chemistry, 1999. **64**(17): p. 6235-6238.
18. Thatcher, G.R.J. and Borrajo, A.M.P., *Molecular recognition of nucleotides and other biologically relevant anions by amino-cyclodextrins*. Abstracts of Papers, 222nd ACS National Meeting, Chicago, IL, United States, August 26-30, 2001, 2001: p. ORGN-631.
19. Wang, Z., Fernandez, P.A., Chang, L., Klein, W.L., Venton, D.L. and Thatcher, G.R.J., *Design and synthesis of functionalized cyclodextrins as inhibitors of amyloid-b-peptide derived toxins*. Abstracts of Papers, 229th ACS National Meeting, San Diego, CA, United States, March 13-17, 2005, 2005: p. MEDI-195.
20. Venton, D.L., Klein, W.L., Thatcher, G.R.J., Chang, L., Liu, R., Wang, Z. and Holterman, M., *Preparation of per-6-amino-substituted-deoxy-cyclodextrins to treat Alzheimer's diseases*. 2005, (The Board of Trustees of the University of Illinois, USA; Northwestern University). Application: WO WO. p. 54 pp.
21. Wang, Z., Chang, L., Klein, W.L., Thatcher, G.R.J. and Venton, D.L., *Per-6-substituted-per-6-deoxy beta-cyclodextrins inhibit the formation of beta-amyloid peptide derived soluble oligomers*. J Med Chem, 2004. **47**(13): p. 3329-33.
22. Chang, L., Bakhos, L., Wang, Z., Venton, D.L. and Klein, W.L., *Femtomole immunodetection of synthetic and endogenous amyloid-beta oligomers and its application to Alzheimer's disease drug candidate screening*. J Mol Neurosci, 2003. **20**(3): p. 305-13.
23. Park, H.S., Lin, Q. and Hamilton, A.D., *Modulation of protein-protein interactions by synthetic receptors: design of molecules that disrupt serine protease-proteinaceous inhibitor interaction*. Proc Natl Acad Sci U S A, 2002. **99**(8): p. 5105-9.
24. Mourez, M., Kane, R.S., Mogridge, J., Metallo, S., Deschatelets, P., Sellman, B.R., Whitesides, G.M. and Collier, R.J., *Designing a polyvalent inhibitor of anthrax toxin*. Nat Biotechnol, 2001. **19**(10): p. 958-61.

Project 3. Rational discovery of new FabI inhibitors as biodefense antibacterial therapeutics

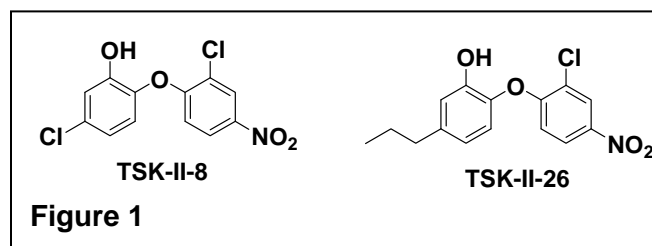
M. Johnson

Introduction

The goal of this research was to develop new inhibitors of the fatty acid biosynthetic pathway as potential antibiotic agents against the Class A bacterial agents, with particular emphasis on the enoyl reductase, FabI. This goal was approached through computational design of inhibitors to increase potency, chemical synthesis of proposed inhibitors, and biological testing to evaluate efficacy.

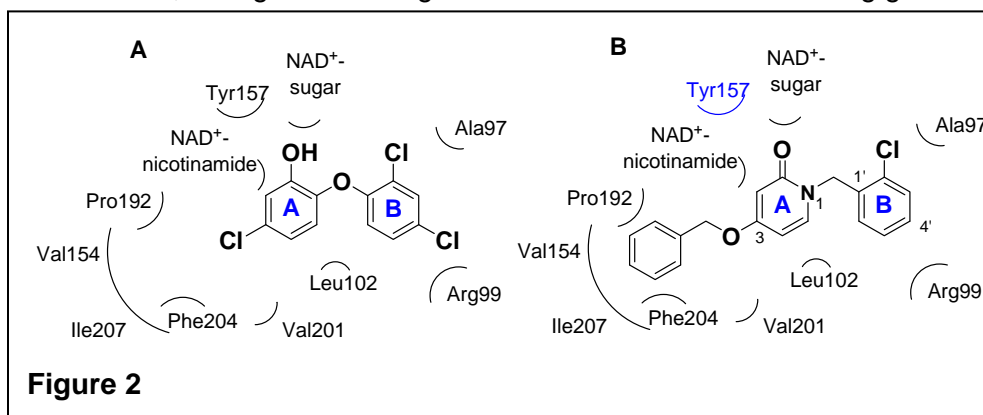
Body

At the time of project initiation, we had two aryl ether FabI inhibitors, shown schematically below in Figure 1, that exhibited significant activity against a variety of pathogenic bacteria. We pursued an extensive series of synthetic modifications to improve activity. The synthetic work, biological testing and antibacterial activities against the Sterne strain of *B. anthracis* and a variety of other pathogens has been described fully in a publication that is appended to this report, and is thus not described further here [Tipparaju, S. K.; Mulhearn, D. C.; Klein, G. M.; Chen, Y.; Tapadar, S.; Bishop, M. H.; Yang, S.; Chen, J.; Ghassemi, M.; Santarsiero, B. D.; Cook, J. L.; Johlfs, M.; Mesecar, A. D.; Johnson, M. E.; Kozikowski, A. P. "Design and Synthesis of Aryl Ether Inhibitors of the Bacillus Anthracis Enoyl-ACP Reductase." *ChemMedChem*. 2008, **3**, 1250-1268.] Although *in vitro* antibacterial activity was excellent, the hydroxyl group of these inhibitors was subject to *in vivo* metabolic processing, thus an alternative series of inhibitors was developed.



Substitution of phenolic group of the aryl ether inhibitors by a 2-pyridone provides a structure that computer modeling predicts should maintain the key interactions with the enzyme, as shown in the Figure 2 below. This figure results from docking triclosan and one of the synthesized pyridones to BaFabI. We observed that the 2-pyridones dock to BaENR in the same binding pocket as that of triclosan, and maintain similar H-bonding interactions with the residues in the active site; the figure to the right shows the similarities in binding geometry.

We thus pursued an extensive series of synthetic modifications to improve activity. The synthetic work, biochemical testing and antibacterial activities against a non-pathogenic (Δ ANR) strain of *B. anthracis* and a variety of other pathogens has been described fully in a publication that is appended to this report, and is thus not described further here [Tipparaju, S. K.;



Joyasawal, S.; Forrester, S.; Mulhearn, D. C.; Pegan, S.; Johnson, M. E.; Mesecar, A. D.; Kozikowski, A. P. "Design and Synthesis of 2-Pyridones As Novel Inhibitors of the Bacillus Anthracis Enoyl-ACP Reductase." *Bioorg. Med. Chem. Lett.* 2008, **18**, 3565-3569.] Although enzymatic activity was good for this series, the antibacterial was limited, perhaps due to limited bacterial permeability.

With the depletion of funds for further synthetic work, we focused our efforts on theoretical evaluation of alternative molecular scaffolds that might provide promising foundations for future work and on development of additional enzymatic targets within the fatty acid biosynthetic pathway for which inhibition might act synergistically with FabI inhibitors. Three new base structures, imidazoles, pyrazoles, and pyrrolidine carboxamides, and an alternate pyridone, shown in the Figure 3, were investigated utilizing computational modeling methods, docking the small compounds against BaFabI with GOLD. All three of the new scaffolds

have been reported to be good inhibitors against the enoyl acyl carrier protein reductases from other organisms, such as *S. pneumoniae*, *S. aureus*, *E. coli*, *P. falciparum*, or *M.*

tuberculosis, organisms for which triclosan has also been effective. Computational modeling suggests that all four of these scaffolds can potentially bind to the FabI catalytic site with reasonable affinity, and that they provide a good foundation for future developmental work.

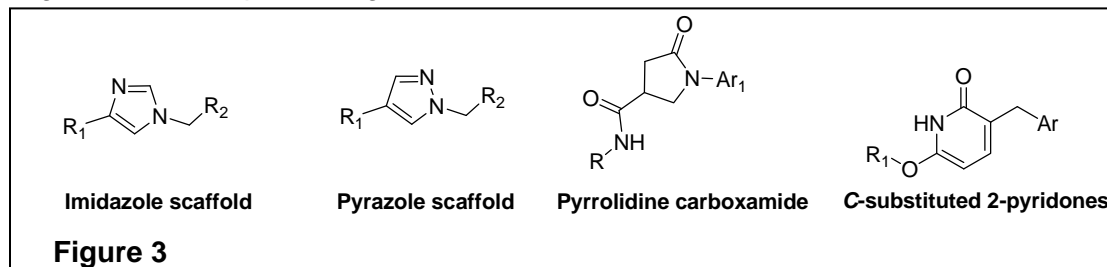


Figure 3

To further expand the potential library of leads for development, we have also computationally docked the “lead-like” subset of the ZINC dataset (with molecular weights < 350 and < 3 H-bond donors or acceptors) against FabI. Initial results from Surflex-Dock calculations provide approximately 100,000 compounds that will be further narrowed by clustering and additional computational strategies. This further refinement should generate ~1-10,000 compounds for experimental evaluation.

We have also pursued development of additional targets in the biosynthetic pathway whose inhibition may be synergistic with that of FabI. We have cloned, expressed, and are in the process of developing assays for FabF, FabH, FabG and FabD from *B. anthracis*. We have also completed computational screening of the “lead-like” subset of the ZINC dataset against FabF, FabG and FabH, and plan to screen it against FabD.

Key Research Accomplishments

- Extensive series of aryl ether FabI inhibitors with a wide range of antibacterial activities against gram positive bacteria, including *B. anthracis*.
- Extensive series of N-substituted 2-pyridones with better metabolic stability, and with at least one showing significant activity against *B. anthracis*.
- Computational development of four new molecular scaffolds as alternative foundations for future lead development against FabI.
- Computational screening of approximately 800,000 “lead-like” and “fragment” molecular structures against FabI for additional potential leads to be experimentally tested.
- Experimental development of four additional enzymatic targets, including FabF, FabH, FabG and FabD, within the fatty acid biosynthetic pathway that may provide opportunities for synergistic inhibition complementary to inhibition of FabI.

Reportable Outcomes

The principal reportable outcomes of this research are the two scientific papers detailed below, and provided in the Appendix. Additionally, the research has developed results from computational screening and additional target development that can be the foundation for additional research to develop better antibiotics against the Category A agents.

- (1) Tipparaju, S. K.; Mulhearn, D. C.; Klein, G. M.; Chen, Y.; Tapadar, S.; Bishop, M. H.; Yang, S.; Chen, J.; Ghassemi, M.; Santarsiero, B. D.; Cook, J. L.; Johlfs, M.; Mesecar, A. D.; Johnson, M. E.; Kozikowski, A. P. Design and Synthesis of Aryl Ether Inhibitors of the Bacillus Anthracis Enoyl-ACP Reductase. *ChemMedChem*. **2008**, 3, 1250-1268.
- (2) Tipparaju, S. K.; Joyasawal, S.; Forrester, S.; Mulhearn, D. C.; Pegan, S.; Johnson, M. E.; Mesecar, A. D.; Kozikowski, A. P. Design and Synthesis of 2-Pyridones As Novel Inhibitors of the Bacillus Anthracis Enoyl-ACP Reductase. *Bioorg. Med. Chem. Lett.* **2008**, 18, 3565-3569.

Conclusion

Although the initial leads proved not to be metabolically stable, they demonstrated that inhibitors of FabI can be developed that exhibit broad spectrum activity against a variety of gram positive pathogens, particularly including both *B. anthracis* and methicillin-resistant *S. aureus*, an increasingly serious problem. The further computational analysis of potential alternate scaffolds and leads provides a foundation for continued development.

Antibiotic resistance arises partly since most antibiotics target a single enzyme active site or receptor site where one mutation can compromise antibiotic activity. Recent studies suggest that polypharmacology, or drugs acting on multiple biological targets within a metabolic pathway, may be more therapeutically effective than those targeting a single enzymatic target (1). We have accordingly developed four additional enzymatic targets within the fatty acid biosynthetic pathway that will provide a foundation for development of antibiotics with enhanced efficacy.

References

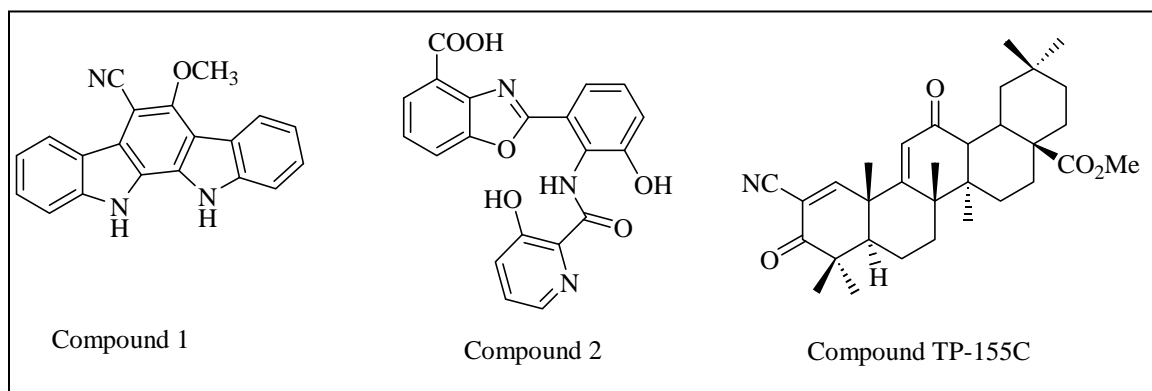
1. Hopkins AL: Network pharmacology. *Nature biotechnology* 2007; 25:1110-1111

Project 4. Natural products-based discovery of therapeutics for biodefense

A. Mesecar

Introduction

Anthrax, the only biological agent used in US terrorist attacks in recent history, continues to be a major threat to our national security and economy and the potential for its use remains high. For decades, natural products and natural product derived compounds have been the principle therapeutics used by man. Today, over 40% of drugs marketed worldwide are still natural product derived. Since natural products still hold significant promise as both therapeutics and lead compounds, we are pioneering an integrative, natural products based discovery program that incorporates traditional plant & terrestrial microorganism based natural product discovery, with modern, marine microorganism based natural product drug discovery which holds great promise for antibiotics development. We discovered two new natural product compounds, and one natural product derived compound (shown below), that have antibiotic activity towards *Bacillus anthracis* better than or equivalent to that of Ciprofloxacin (Cipro). These compounds were found to be non-toxic to normal, cultured human cells. Therefore, this project was conducted to improve the potency of two of these compounds.



Body

During the first quarter, we successfully completed the total synthesis of **Antibiotic A-33853**. In addition, we synthesized 6, first-generation analogs of A-33853 and have evaluated their antibiotic activities against the *Bacillus anthracis* ΔANR strain (see Figure 1). Antibiotic A-33853 was the most potent inhibitor against *Bacillus anthracis* in cell culture with a minimum inhibitor concentration (MIC) of approximately 6 μM. We tested all of the A-33853 compounds for their ability to inhibit the enzyme enoylreductase (ENR) from *B. anthracis*. However, none of the compounds inhibited the enzyme suggesting that this enzyme is not the target for these compounds. We also evaluated a series of natural Ambiquine and Hapalindole compounds isolated from a cyanobacteria strain for inhibitory activity towards *B. anthracis* (see Figure 2). We found that Ambiquine A has an MIC value of 1 to 3 μM placing it in the potency range of A-33853.

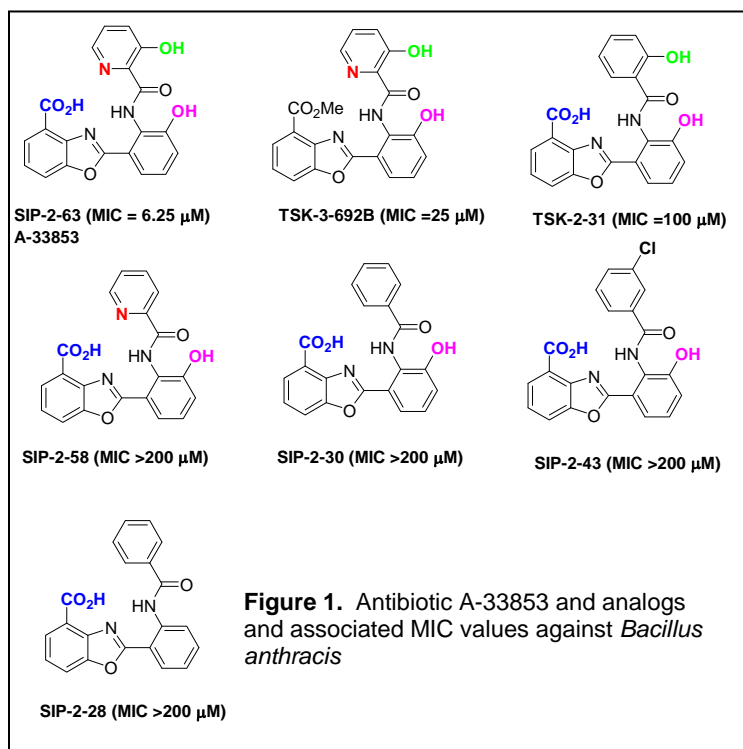
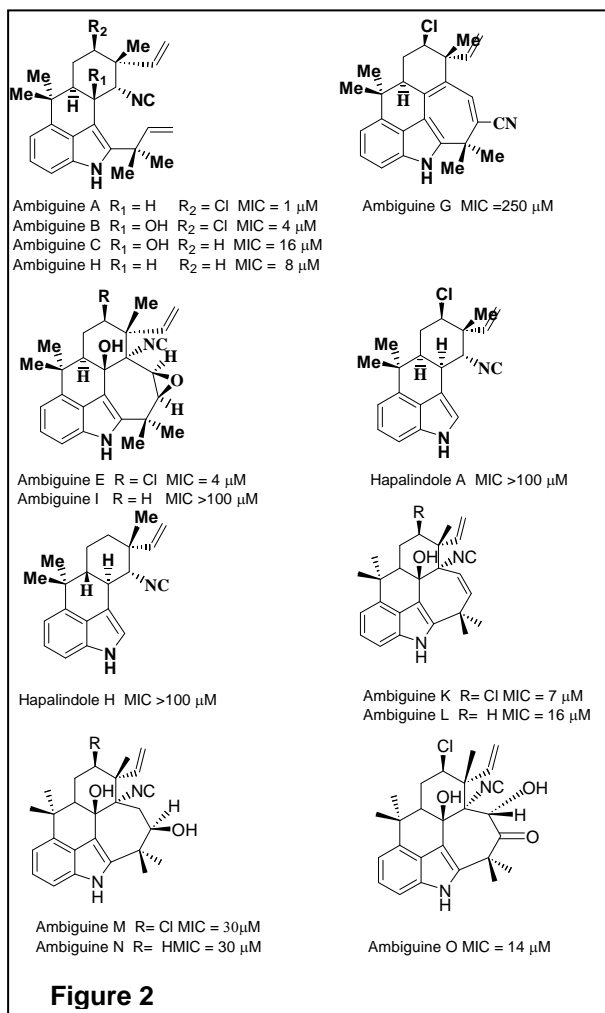


Figure 1. Antibiotic A-33853 and analogs and associated MIC values against *Bacillus anthracis*



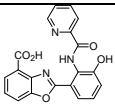
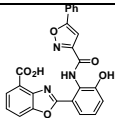
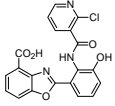
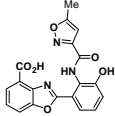
During the second quarter, we successfully completed the synthesis of a series of 2nd and 3rd generation derivatives of **Antibiotic A-33853** and have tested them against the *Bacillus anthracis* ΔANR strain. We also achieved the synthesis of one compound (compound **9** in Table 1) that has an MIC value of 12.5 μM which is near that of A-33853.

During the third quarter, we successfully completed the synthesis of additional analogs of Antibiotic A-33853 and tested them against the *Bacillus anthracis* ΔANR strain. In addition, we have tested A-33853 against a series of other pathogens to test for its spectrum of activity. Significantly, we have been able to improve upon the potency of the original lead, A-33853, against *B. anthracis*. Compound SIP-3-4 (MIC 3.125 μM) is 2-fold more potent. In addition, we have found that A-33853 potently inhibits another of other pathogens including various *Staphylococcus*, *Salmonella*, *Pasteurella*, *Mycoplasma* and *Aeromonas* strains.

During the fourth quarter, we have successfully completed the synthesis of a series of additional analogs of Antibiotic A-33853 and the staurosporine-like lead natural product (compound **1** above) and tested them against the *Bacillus anthracis* ΔANR strain. Significantly, we were able to improve upon the inhibitory potency of the original lead of the series against *B. anthracis*. Compound GSP3-32 has an MIC value of 1.56 μM .

TABLE 1

| Compounds | Structure of acids | MIC (μM) | Compounds | Structure of acids | MIC (μM) |
|-----------|--------------------|-----------------|-----------|--------------------|-----------------|
| 1 | A-33853 | 6.25 | 7 | | >200 |
| 2 | | 25 | 8 | | 50 |
| 3 | | 25 | 9 | | 12.5 |
| 4 | | 200 | 10 | | 50 |

| | | | | | |
|---|---|------|----|---|------|
| 5 |  | 200 | 11 |  | >200 |
| 6 |  | >200 | 12 |  | 50 |

Key research accomplishments

- First successful completion of the total synthesis of Antibiotic A-33853 (Compound 2 above).
- Synthetic schemes developed for a series of Antibiotic A-33853 derivatives
- Improvement of potency of original Antibiotic A-33853 (MIC = 6.25 μ M) two-fold against *Bacillus anthracis* (MIC = 3.125 μ M)
- Demonstrated that Antibiotic A-33853 and its derivatives are effective against a wide spectrum of pathogens including *Leishmania donovani* where a potency of 0.08 μ M was achieved

Reportable outcomes

- Two publications have so far resulted from this work. They are listed below.
 - Proposal applications are in the process of being drafted and submitted to continue this work.
 - Compounds have been designed and synthesized which should serve as additional lead templates and scaffolds for the continued development of other antibiotics against *Bacillus anthracis* and other bacteria as well as anti-infectives against other pathogens such as *Leishmania donovani*.
1. Suresh K. Tipparaju, Sipak Joyasawal, Marco Pieroni, Marcel Kaiser, Reto Brun, and Alan P. Kozikowski (2008) In Pursuit of Natural Product Leads: Synthesis and Biological Evaluation of 2-[3-hydroxy-2-[(3-hydroxypyridine-2-carbonyl)amino]phenyl]benzoxazole-4-carboxylic acid (A-33853) and Its Analogues: Discovery of *N*-(2-Benzoxazol-2-ylphenyl)benzamides as Novel Antileishmanial Chemotypes. *J. Med. Chem.*, 51 (23), 7344-7347.
 2. Scott D. Pegan, Kamolchanok Rukseeree, Scott G. Franzblau and Andrew D. Mesecar (2009), Structural Basis for Catalysis of a Tetrameric Class IIa Fructose 1,6-Bisphosphate Aldolase from *Mycobacterium tuberculosis*.

Conclusion

A series of lead compounds were identified and synthesized with significant potency against *Bacillus anthracis* and other pathogens. Continued lead development is necessary to improve potency and pharmacological properties necessary to enter the compounds into clinical trials. Since it traditionally takes 10 to 12 years on average to bring a drug to market, the one year of funding provided will not sufficient to fully develop any of the compounds.

High Throughput Screening (HTS) Core

A. Mesecar

Introduction

Anthrax, the only biological agent used in US terrorist attacks in recent history, continues to be a major threat to our national security and economy and the potential for its use remains high. In addition, the potential for developing drug-resistant forms of anthrax is also high since it has been demonstrated that drug resistance forms, i.e. against Cipro, are easy to produce with common laboratory supplies and equipment. The overall goals of this project were to develop an assay capable of screening tens-of-thousands of compounds against whole cell anthrax to identify new drug leads and to identify new candidate drug targets that are inhibited by these compounds.

Body

During the first quarter, the HTS Core developed an HTS assay capable of detecting natural products that inhibit or eliminate growth of *B. anthracis*. The adaptation of the Alamar Blue dye, a popular colorimetric assay used for the determination of MIC values of compounds against bacteria and other pathogens, to our HTS platform was accomplished. This assay has been shown to be successful for a wide range of mammalian, fungal, and bacteria cell assays. We were able to successfully adapt and miniaturize this assay for use in HTS of *B. anthracis*.

During the second quarter, we adapted and automated the Alamar Blue for *B. anthracis* (ABBA) assay on our Tecan robotics platform. We first screened over 2,500 natural product extracts and compounds. The assay was so successful that we were also able to screen over 50,080 compounds from commercial library sources.

During the 3rd Quarter, a structure-activity-analysis was completed on the HTS data acquired during the second quarter. A series of different structural templates were identified that served as our leads for follow-up activity analysis to confirm the hits. Follow-up included performing MICs on three distinct structural templates which identified one compound with an MIC value of 12.5 μ M. We also performed an extensive literature search and found a patent that states that one of our templates, a β -carboline, is an inhibitor of the enzyme Phosphopantetheine adenyltransferase (PPAT) from *E.coli*. To follow-up on this possibility, we successfully cloned and expressed PPAT from *Bacillus anthracis*, *Mycobacterium tuberculosis*, and *E.coli* so that we could test for inhibition of these enzymes by our identified lead compounds.

During the Fourth Quarter, the HTS core tested the hypothesis that β -carbolines inhibit the enzyme PPAT from *B. anthracis*, *M. tuberculosis* and *E.coli*. Most significantly, we found that the β -carbolines do not act as inhibitors of PPAT, at least in our current in vitro enzyme assays suggesting that they have a different molecular target in bacteria or that our enzymatic assay, which utilizes the reverse reaction, is not capable of sensing inhibition. We also crystallized and determined the X-ray structure of the essential enzyme fructose-1,6 biphosphate from *T. tuberculosis* which may serve as a drug target in both *M. tuberculosis* and *B. anthracis*. A manuscript on the structure of this enzyme has been accepted for publication (see Reference 2 below).

Key research accomplishments

- Development of an automated MIC assay that can be used to screen tens to one hundred thousand compounds against bacteria in a single day depending on the liquid handling robotics.
- Screened over 50,000 compounds against *B. anthracis* and identified 3 structural classes as potential lead scaffolds for further medicinal chemistry improvement.
- Cloned, expressed and purified phosphopantetheine adenyltransferase (PPAT) from three different bacteria including *B. anthracis*, *M. Tuberculosis* and *E.coli*. Determined that these enzymes are not inhibited by the β -carboline compounds identified in HTS when the enzymes are assayed in the reverse direction.

Reportable outcomes

- A protocol for an HTS assay that is capable of screening over 100,000 compounds per day against anthrax has been developed and should be universal for any lab wishing to screen for inhibitors against this bioweapon.
 - Two publications have so far resulted from this work. They are listed below and appended. Other publications are being drafted.
 - Proposal applications are in the process of being drafted and submitted to continue this work.
 - Compounds have been identified that should serve as additional lead templates and scaffolds for the continued development of other antibiotics against *Bacillus anthracis* and other bacteria.
 - Expression vectors have been created for the enzyme phosphopantetheine adenylyltransferase (PPAT) from three different bacteria including *B. anthracis*, *M. Tuberculosis* and *E.coli*. These vectors will be available to the public upon request for any research efforts aimed at identifying lead drug candidates against these potential enzyme targets.
1. Suresh K. Tipparaju, Sipak Joyasawal, Marco Pieroni, Marcel Kaiser, Reto Brun, and Alan P. Kozikowski (2008) In Pursuit of Natural Product Leads: Synthesis and Biological Evaluation of 2-[3-hydroxy-2-[(3-hydroxypyridine-2-carbonyl)amino]phenyl]benzoxazole-4-carboxylic acid (A-33853) and Its Analogues: Discovery of *N*-(2-Benzoxazol-2-ylphenyl)benzamides as Novel Antileishmanial Chemotypes. *J. Med. Chem.*, 51 (23), 7344-7347.
 2. Scott D. Pegan, Kamolchanok Rukseree, Scott G. Franzblau and Andrew D. Mesecar (2009), Structural Basis for Catalysis of a Tetrameric Class IIa Fructose 1,6-Bisphosphate Aldolase from *Mycobacterium tuberculosis*.

Conclusion

An HTS assay against *Bacillus anthracis* and other bacteria was developed that will be of universal use to the scientific community. We utilized this assay and screened over 50K compounds against *B. anthracis* and identified potential drug leads. There are no open reports of such large-scale screening efforts against whole cell anthracis. This work and results should therefore be of general interest and significance to the public.

Key Research Accomplishments

Project 1:

- Identification of the nucleotide alterations in helix 38 of 23S rRNA resulting in the distortion of the helix structure which correlates with defects in protein synthesis.
- Delineation of the segment of helix 38 which is critical for ribosome activity.
- Engineering of a viable *E. coli* cells relying on the function of ribosomes which carry the *B. anthracis* version of helix 38.
- Engineering of a viable *E. coli* strain which relies on the function of ribosomes which helix 38 with humanized functional segments.
- Optimization of a high-throughput protocol for screening libraries of chemical and natural compounds for selective and specific inhibitors of protein synthesis.

Project 2:

- Comparative analysis of synthetic methods for synthesis of ACD derivatives leading to a new methodology for synthesis of the related qCD derivatives.
- Synthesis of novel estrogen conjugates of ACD and qCD demonstrating nanomolar to micromolar estrogenic activity. These compounds represent useful tools for study of estrogenic activity in cell culture and provide evidence that high molecular weight estrogen conjugates have membrane permeability.
- Development of two new assays for quantitation of peptide self-assembly and demonstration of the ability of ACDs to inhibit specific aggregation pathways leading to formation of neurotoxic soluble oligomers.

Project 3:

- Extensive series of aryl ether FabI inhibitors with a wide range of antibacterial activities against gram positive bacteria, including *B. anthracis*.
- Extensive series of N-substituted 2-pyridones with better metabolic stability, and with at least one showing significant activity against *B. anthracis*.
- Computational development of four new molecular scaffolds as alternative foundations for future lead development against FabI.
- Computational screening of approximately 800,000 "lead-like" and "fragment" molecular structures against FabI for additional potential leads to be experimentally tested.
- Experimental development of four additional enzymatic targets, including FabF, FabH, FabG and FabD, within the fatty acid biosynthetic pathway that may provide opportunities for synergistic inhibition complementary to inhibition of FabI.

Project 4:

- First successful completion of the total synthesis of Antibiotic A-33853.
- Synthetic schemes developed for a series of Antibiotic A-33853 derivatives.
- Improvement of potency of original Antibiotic A-33853 (MIC = 6.25 μ M) two-fold against *Bacillus anthracis* (MIC = 3.125 μ M).
- Demonstration of the fact that Antibiotic A-33853 and its derivatives are effective against a wide spectrum of pathogens including *Leishmania donovani* where a potency of 0.08 μ M was achieved.

HTS Core:

- Development of an automated MIC assay that can be used to screen tens to one hundred thousand compounds against bacteria in a single day depending on the liquid handling robotics.
- Screening of over 50,000 compounds against *B. anthracis* and identification of 3 structural classes as potential lead scaffolds for further medicinal chemistry improvement.

- Cloning, expression and purification of phosphopantetheine adenylyltransferase (PPAT) from three different bacteria including *B. anthracis*, *M. Tuberculosis* and *E.coli*. Determined that these enzymes are not inhibited by the β -carboline compounds identified in HTS when the enzymes are assayed in the reverse direction.

Reportable Outcomes

- The principal reportable outcomes of this research are the six scientific papers and one abstract detailed below, and provided in the Appendix.
 1. Tipparaju, S.K., Mulhearn, D.C., Klein, G.M., Chen, Y., Tapadar, S., Bishop, M.H., Yang, S., Chen, J., Ghassemi, M., Santarsiero, B.D., Cook, J.L., Johlfs, M., Mesecar, A.D., Johnson, M.E. and Kozikowski, A.P., *Design and synthesis of aryl ether inhibitors of the Bacillus anthracis enoyl-ACP reductase*. ChemMedChem, 2008. 3(8): p. 1250-68.
 2. Tipparaju, S.K., Joyasawal, S., Forrester, S., Mulhearn, D.C., Pegan, S., Johnson, M.E., Mesecar, A.D. and Kozikowski, A.P., *Design and synthesis of 2-pyridones as novel inhibitors of the Bacillus anthracis enoyl-ACP reductase*. Bioorg Med Chem Lett, 2008. 18(12): p. 3565-9.
 3. Tipparaju, S.K., Joyasawal, S., Pieroni, M., Kaiser, M., Brun, R. and Kozikowski, A.P., *In Pursuit of Natural Product Leads: Synthesis and Biological Evaluation of 2-[3-hydroxy-2-[(3-hydroxypyridine-2-carbonyl)amino]phenyl]benzoxazole-4-carboxylic acid (A-33853) and Its Analogues: Discovery of N-(2-Benzoxazol-2-ylphenyl)benzamides as Novel Antileishmanial Chemotypes*. J Med Chem, 2008.
 4. Pegan, S.D., Rukseere, K., Franzblau, S.G. and Mesecar, A.D., *Structural Basis for Catalysis of a Tetrameric Class IIa Fructose 1,6-Bisphosphate Aldolase from Mycobacterium tuberculosis*. J Mol Biol, 2009.
 5. Onyuksel, H., Mohanty, P.S. and Rubinstein, I., *VIP-grafted sterically stabilized phospholipid nanomicellar 17-allylamino-17-demethoxy geldanamycin: A novel targeted nanomedicine for breast cancer*. Int J Pharm, 2009. 365(1-2): p. 157-61.
 6. Cesur, H., Rubinstein, I., Pai, A. and Onyuksel, H., *Self-associated indisulam in phospholipid-based nanomicelles: a potential nanomedicine for cancer*. Nanomedicine, 2008.

Abstract: Hye-Yeong Kim, Gregory R. J. Thatcher, et al. Poster: Synthesis of Estradiol-Cyclodextrin Conjugates toward Studying Extranuclear Estrogen Signaling Pathway. Division of Medicinal Chemistry. The American Chemical Society 235th National Meeting & Exposition, New Orleans, LA, April 2008.

- Three isogenic mutant *E. coli* strains have been developed which can be used for screening libraries of chemical and natural compounds for selective and specific inhibitors of protein synthesis.
- Compounds have been designed and synthesized which should serve as additional lead templates and scaffolds for the continued development of other antibiotics against *Bacillus anthracis* and other bacteria as well as anti-infectives against other pathogens such as *Leishmania donovani*.
- A protocol for an HTS assay that is capable of screening over 100,000 compounds per day against anthrax has been developed and should be universal for any lab wishing to screen for inhibitors against this bioweapon.
- Compounds have been identified that should serve as additional lead templates and scaffolds for the continued development of other antibiotics against *Bacillus anthracis* and other bacteria.
- Expression vectors have been created for the enzyme phosphopantetheine adenylyltransferase (PPAT) from three different bacteria including *B. anthracis*, *M. Tuberculosis* and *E.coli*. These vectors will be available to the public upon request for any research efforts aimed at identifying lead drug candidates against these potential enzyme targets.
- Proposal applications are in the process of being drafted and submitted to continue this work.
- Additional manuscripts are in preparation for publication.

Conclusion

The IAPS project enabled us to integrate our cutting-edge research activities focused on infectious agents used in bioterrorism; and to accelerate the drug discovery process through the application of novel experimental methodologies. We developed two promising novel screens for compounds targeting anthrax and potentially other infectious agents, and identified potential lead compounds as well as additional drug targets.

The first screen is based on identification of a functionally-important segment of helix 38 in 23S ribosomal RNA as a potential antibiotic target and designing a novel approach that can be used for identifying selective and specific protein synthesis inhibitors using whole-cell high-throughput screening. The important future direction is preparing additional sets of *E. coli* strains with other engineered 'pathogenic' and 'humanized' sites in rRNA. Such strains can be used in screens for new protein synthesis inhibitors. The actual screening was not carried out because the appropriate compound libraries were not available during this project, which can be remedied with additional funding.

Second, an HTS assay against *Bacillus anthracis* and other bacteria was developed that will be of universal use to the scientific community. We utilized this assay and screened over 50K compounds against *B. anthracis* and identified potential drug leads. There are no open reports of such large-scale screening efforts against whole cell anthracis. This work and results should therefore be of general interest and significance to the public.

A series of lead compounds were identified and synthesized with significant potency against *Bacillus anthracis* and other pathogens. Continued lead development is necessary to improve potency and pharmacological properties necessary to enter the compounds into clinical trials. Since it traditionally takes 10 to 12 years on average to bring a drug to market, the one year of funding provided was not sufficient to fully develop any of the compounds.

Although the initial leads proved not to be metabolically stable, they demonstrated that inhibitors of FabI can be developed that exhibit broad spectrum activity against a variety of gram positive pathogens, particularly including both *B. anthracis* and methicillin-resistant *S. aureus*, an increasingly serious problem. The further computational analysis of potential alternate scaffolds and leads provides a foundation for continued development.

Antibiotic resistance arises partly since most antibiotics target a single enzyme active site or receptor site where one mutation can compromise antibiotic activity. Recent studies suggest that polypharmacology, or drugs acting on multiple biological targets within a metabolic pathway, may be more therapeutically effective than those targeting a single enzymatic target. We have accordingly developed four additional enzymatic targets within the fatty acid biosynthetic pathway that will provide a foundation for development of antibiotics with enhanced efficacy.

References

Relevant references can be found at the end of each individual project report.

Institute for Advanced Pharmaceutical Sciences: Molecular Targets and Drug Screens to Combat Bioterrorism

Jerry L. Bauman

Appendices to the final report

6 publications and 1 abstract are attached as PDF files.

For further reference, the scientific parts of the individual quarterly progress reports are also attached, organized by project.

Project personnel

Design and Synthesis of Aryl Ether Inhibitors of the *Bacillus Anthracis* Enoyl-ACP Reductase

Suresh K. Tipparaju,^[b] Debbie C. Mulhearn,^[a] Gary M. Klein,^[a, b] Yufeng Chen,^[b] Subhasish Tapadar,^[b] Molly H. Bishop,^[a] Shuo Yang,^[a] Juan Chen,^[c] Mahmood Ghassemi,^[c] Bernard D. Santarsiero,^[a] James L. Cook,^[c] Mary Johlfs,^[a] Andrew D. Mesecar,^{*,[a, b]} Michael E. Johnson,^{*,[a]} and Alan P. Kozikowski^{*,[b]}

The problem of increasing bacterial resistance to the current generation of antibiotics is well documented. Known resistant pathogens such as methicillin-resistant *Staphylococcus aureus* are becoming more prevalent, while the potential exists for developing drug-resistant pathogens for use as bioweapons, such as *Bacillus anthracis*. The biphenyl ether antibacterial agent, triclosan, exhibits broad-spectrum activity by targeting the fatty acid biosynthetic pathway through inhibition of enoyl-acyl carrier protein reductase (ENR) and provides a potential scaffold for the development of new, broad-spectrum antibiotics. We used a structure-based approach to develop novel aryl ether analogues of triclosan that target ENR, the product of the *fabI* gene, from *B. anthracis*

(BaENR). Structure-based design methods were used for the expansion of the compound series including X-ray crystal structure determination, molecular docking, and QSAR methods. Structural modifications were made to both phenyl rings of the 2-phenoxy-phenyl core. A number of compounds exhibited improved potency against BaENR and increased efficacy against both the Sterne strain of *B. anthracis* and the methicillin-resistant strain of *S. aureus*. X-ray crystal structures of BaENR in complex with triclosan and two other compounds help explain the improved efficacy of the new compounds and suggest future rounds of optimization that might be used to improve their potency.

Introduction

The increasing prevalence of antibiotic-resistant bacteria is well documented. The 2004 monograph by the Infectious Diseases Society of America noted that the incidence of methicillin-resistant *S. aureus* (MRSA) in particular, has increased quite rapidly over the last two decades.^[1] Recent summaries have documented that *Staphylococci* are among the most common causes of nosocomial infections, and that resistance to β -lactams and glycopeptides is complicating treatment of those infections.^[2] Particularly alarming is a recent JAMA article and accompanying editorial, which noted that deaths from invasive MRSA in 2005 were comparable to, or exceeded those from HIV/AIDS.^[3,4] This rapid increase in bacterial resistance to current antibiotics is a strong motivation for the development of new antibacterials with alternate modes of action.

Drug resistance in pathogens that might be used as bioweapons is also of concern. Natural isolates of *B. anthracis* have been reported to show resistance to some antibiotics such as penicillin G, amoxicillin, erythromycin, cefuroxime, sulfamethoxazole, trimethoprim, cefotaxime-sodium, aztreonam, deflazidime^[5–8] and ofloxacin,^[9] as well as tetracycline and penicillin.^[10] Furthermore, two reports described the potential to develop resistant *B. anthracis* strains through standard microbial selection procedures.^[11,12] While previous acts of bioterrorism used a *B. anthracis* strain that was susceptible to conventional antibiotics, future incidents may involve more virulent *B. anthracis* strains resistant to conventional antibiotics. Because anthrax has been rated first or second for potential bioterrorism impact, comparable to smallpox,^[13,14] and may be readily

adapted to biowarfare applications,^[14] there is an incentive for the development of antibiotics with novel modes of action that could be used to combat drug-resistant bacteria.^[15]

Validated targets for antibiotic development are the fatty acid biosynthesis pathways essential for bacterial growth.^[16,17] Fatty acids are synthesized by mammals (FAS I) and bacteria (FAS II) by substantially different biosynthetic mechanisms, enabling bacteria-specific drug targeting. FAS I involves a single multifunctional enzyme-acyl carrier protein (ACP) complex,

[a] Dr. D. C. Mulhearn,⁺ G. M. Klein, M. H. Bishop, S. Yang, Dr. B. D. Santarsiero, Dr. M. Johlfs, Dr. A. D. Mesecar, Prof. Dr. M. E. Johnson
Center for Pharmaceutical Biotechnology, University of Illinois at Chicago
900 S. Ashland Ave., Chicago, IL 60607-7173 (USA)
Fax: (+1) 312-413-9303
E-mail: mesecar@uic.edu
mjohanson@uic.edu

[b] Dr. S. K. Tipparaju,⁺ G. M. Klein, Dr. Y. Chen, Dr. S. Tapadar, Dr. A. D. Mesecar, Prof. Dr. A. P. Kozikowski
Drug Discovery Program
Department of Medicinal Chemistry and Pharmacognosy
University of Illinois at Chicago
833 S. Wood St., Chicago, IL 60612 (USA)
Fax: (+1) 312-413-0577
E-mail: kozikowa@uic.edu

[c] Dr. J. Chen, Dr. M. Ghassemi, Dr. J. L. Cook
Department of Medicine, University of Illinois at Chicago
808 S. Wood St., Chicago IL 60612 (USA)

[*] These authors contributed equally to this work.

Supporting information for this article is available on the WWW under <http://dx.doi.org/10.1002/cmdc.200800047>.

whereas FAS II incorporates several small monofunctional enzymes that operate in conjunction with ACP-associated substrates.^[18] Recent studies have revealed that the genes responsible for FAS II are essential in *Bacillus subtilis*, a close relative of *B. anthracis*.^[19]

Enoyl-ACP reductase (ENR), the product of the *fabI* gene in *B. anthracis* (*BaENR*), is a key NADH-dependent enzyme in FAS II that catalyzes the final and rate-determining step of chain elongation.^[20] Research has shown that enoyl-ACP reductase is efficiently inhibited in some pathogens by antibacterial agents including isoniazid,^[21] diazaboranes,^[22–24] triclosan,^[25–28] and several other small-molecule inhibitors.^[29–35] API-1252, a recently developed *FabI* inhibitor, shows excellent in vitro activity against clinical isolates of *Staphylococcus epidermidis* and *S. aureus*.^[36a] Another novel *FabI* inhibitor, CG400462, was recently reported to show efficacy against *S. aureus* infected mice.^[36b] These studies clearly indicate that inhibition of enoyl-ACP reductase is a viable approach to develop new antibacterials with novel modes of action.

Triclosan, a 2-phenoxyphenol, is a well-known, broad-spectrum antibacterial that is used in a number of consumer products, such as toothpastes, soaps and plastics. It has been shown to inhibit the growth of *Escherichia coli*,^[26,37] *Pseudomonas aeruginosa*,^[38] and *S. aureus*.^[32] Originally, triclosan was thought to be a nonspecific antibacterial acting against bacterial cell membranes, however, the mode of action was later shown to be inhibition of bacterial fatty acid synthesis at the enoyl-acyl carrier protein reductase step.^[39,40] Triclosan inhibits ENR, the gene product of *fabI*, *fabL*, and *inhA* in a number of microorganisms, leading to several attempts to develop new triclosan-derived antibacterials.^[26,41–45] Further investigation into the broad-spectrum activity of triclosan derivatives has been deterred by the variability in effectiveness against different species; the IC₅₀ values range from 70 and 73 nM respectively in *S. aureus*^[32] and *Plasmodium falciparum* (*PfENR*)^[42] to only 7.25 μM in *E. coli*.^[26,37] Due to this large range in activity, it would be valuable to explore the inhibitory action of additional triclosan-like aryl ether analogues against individual organisms to maximize the specificity. Initially focusing on *B. anthracis*, we determined the IC₅₀ value of triclosan against *BaENR* to be 0.6 μM with a minimum inhibitory concentration (MIC) of 3.1 $\mu\text{g mL}^{-1}$.^[46] Herein we describe our approaches to improve its efficacy through structural modifications to the 2-phenoxyphenol core using a structure-based design approach that relies on the crystal structure of *BaENR* with triclosan bound in the active site.^[46] Additional *BaENR* crystal structures involving newly designed diphenyl ethers are also presented and discussed. We found that at least two compounds exhibit improved activity against both the ΔANR , and Sterne strain of *B. anthracis*, as well as MRSA.¹

Results and Discussion

Synthesis of the inhibitors

The 2-phenoxyphenol core was prepared from the corresponding methoxy derivatives, synthesized from commercially available materials by nucleophilic aromatic substitution reaction (Method A) or Cu-catalyzed coupling reaction (Methods B and C)^[47] followed by demethylation (Method D) (Scheme 1).

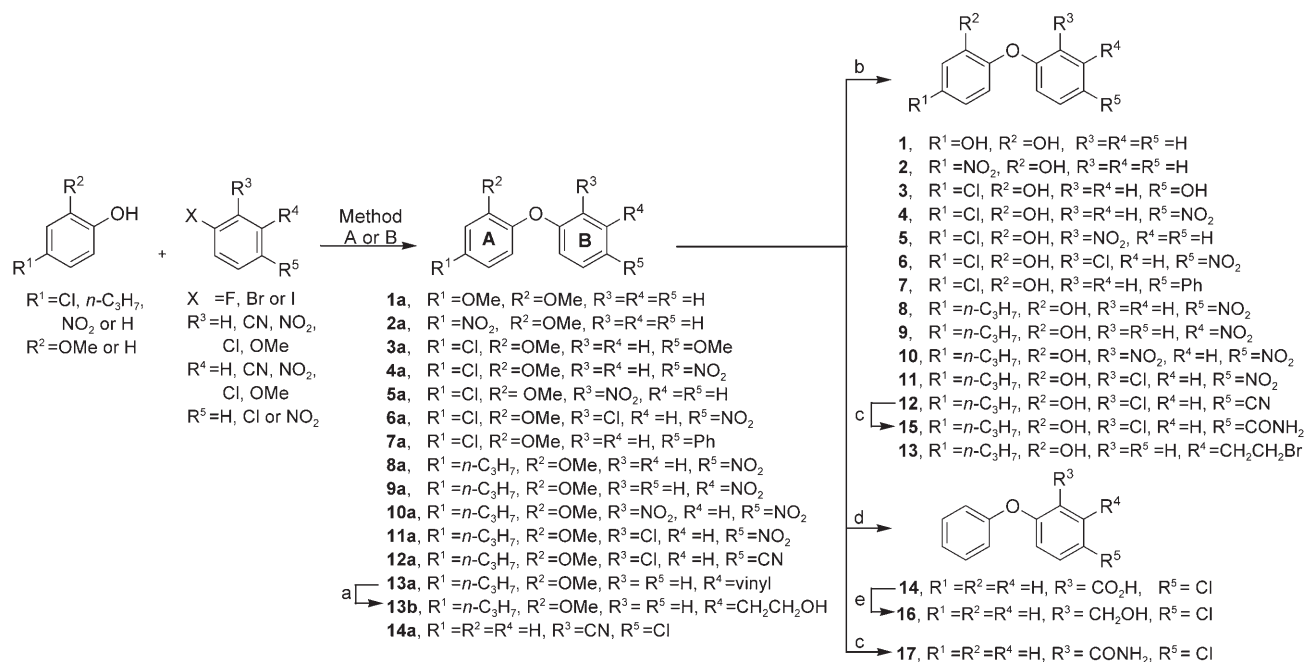
Method A involves the reaction of an appropriate phenol with a fluoro-aromatic compound in the presence of K₂CO₃ and was used to prepare a variety of 2-phenoxyphenol derivatives bearing an electron-withdrawing group on ring B, namely NO₂, or CN groups (**4–6**, **8–12**, and **14**). Compound **14** was synthesized by base-catalyzed hydrolysis of the benzonitrile **14a** in EtOH at reflux.^[48] Subsequent reduction of the carboxylic acid using NaBH₄ in the presence of BF₃·Et₂O gave benzylic alcohol **16**.^[49] Attempts to demethylate **13b** using excess BBr₃ resulted in the formation of brominated analogue **13** as a major product. Carboxamides **15** and **17** were prepared from the corresponding benzonitriles by base-catalyzed hydrolysis in the presence of hydrogen peroxide.^[48] Anilines **20** and **21** were synthesized by catalytic hydrogenation followed by demethylation of nitro intermediates **4a** and **8a**, respectively. The aniline intermediates **19a** and **20a** were acetylated and subsequently demethylated to give acetamides **19** and **18**. Similarly, tosylation followed by demethylation under standard conditions gave sulfonamide **22** from aniline **20a** (Scheme 2).

Method B involves the Cu-catalyzed coupling reaction of an appropriate phenol with a variety of aromatic halides under thermal conditions. This method is versatile, and was used to synthesize electron-rich diphenyl ethers **1**, **3**, and **7** (Scheme 1). Heteroaromatic B ring analogues (**23–25**) were prepared similarly (Scheme 3).

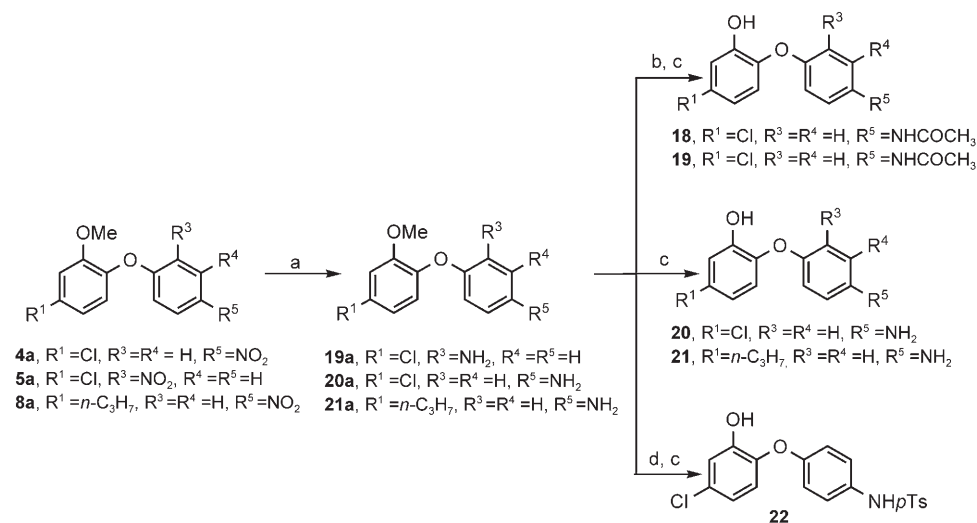
Method C is a mild copper-promoted C–O coupling reaction between arylboronic acids and phenols that was employed to synthesize a variety of aryl ethers (Schemes 4–7). This coupling reaction complements nucleophilic aromatic substitutions (Method A) and Ullman-type couplings (Method B) described above for the synthesis of aryl ethers. Although this reaction worked well with *meta*- and *para*-substituted phenylboronic acids, coupling of 2-methoxyphenols with *ortho*-substituted phenylboronic acids, as well as with heteroaromatic boronic acids failed, presumably due to unfavorable steric interactions.

In Scheme 4, coupling of phenylboronic acid with commercially available 4-allyl-2-methoxyphenol and 4-hydroxy-3-methoxybenzaldehyde gave diphenyl ether intermediates **27a** and **28a**, respectively, in high yields. Allyl and aldehyde functional groups were tolerated under these mild reaction conditions. The allyl group of **27a** was further functionalized to the 1,2-diol **26** via dihydroxylation and demethylation, or the *n*-propyl-substituted diphenyl ether **27** via catalytic hydrogenation and demethylation. Similarly, the aldehyde **28a** was either reduced to an alcohol and demethylated (to give **28**), or transformed into a series of alkyl amines by reductive amination to give compounds **29–31** after demethylation.

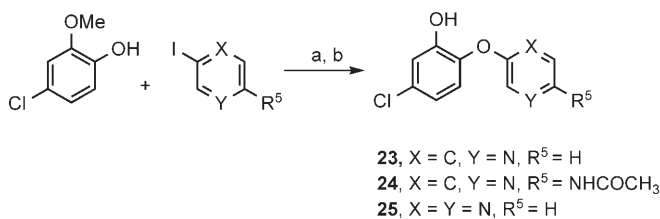
¹ The ΔANR strain, containing neither *pXO1* (toxin) nor *pXO2* (capsule) plasmids, was used for enzymatic assays. The Sterne strain, containing only the *pXO1* (toxin) plasmid, was used in antibacterial testing.



Scheme 1. Synthesis of compounds 1–17: When X = F and R³ = R⁴ = H, NO₂, CN, Cl, Method A: K₂CO₃, DMSO, 100 °C, 8–12 h. When X = Br or I and R³ = R⁴ = H, OMe, Ph, Method B: K₂CO₃, DMF, (CuOTf)₂·PhH, 140 °C, 16–20 h. a) BH₃·THF, 3 M NaOH, H₂O₂, RT, 4–6 h; b) Excess BBr₃, CH₂Cl₂, –78 °C to RT, 2–6 h; c) 35% H₂O₂, 3 M NaOH, EtOH, 30 °C, 18 h; d) 14 a, 25% NaOH, EtOH, reflux, 20 h; e) NaBH₄, BF₃·Et₂O, THF, RT to reflux, 1 h.



Scheme 2. Synthesis of compounds 18–22: a) Pd/C, H₂, EtOH, RT, 2–6 h; b) Ac₂O, DMAP, Et₃N, CH₂Cl₂, RT, 3–6 h; c) Excess BBr₃, CH₂Cl₂, –78 °C to RT, 2–6 h; d) 4-toluenesulfonyl chloride, Et₃N, CH₂Cl₂, 0 °C to RT, 3 h.

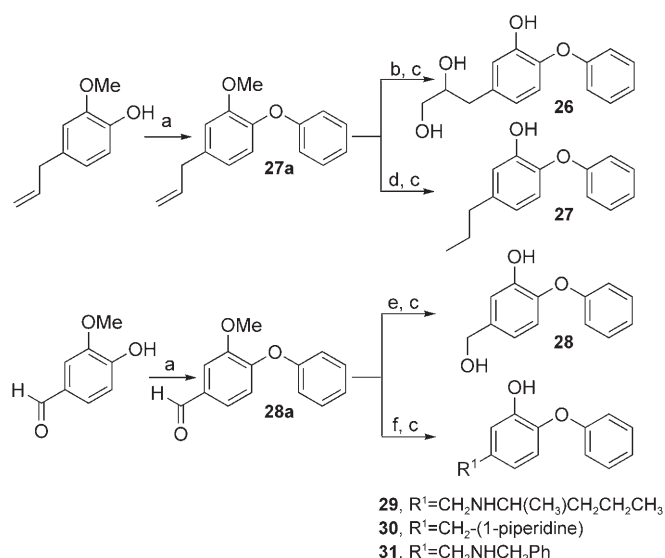


Scheme 3. Synthesis of compounds 23–25: a) Method B: K₂CO₃, DMF, (CuOTf)₂·PhH, 140 °C, 14–18 h; b) Excess BBr₃, CH₂Cl₂, –78 °C to RT, 2–6 h.

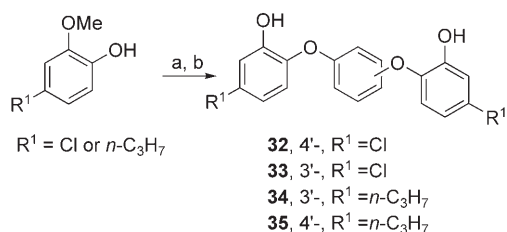
Scheme 5 illustrates the coupling of 2-methoxy-4-chlorophenol or 2-methoxy-4-propylphenol with commercially available *meta*- and *para*-substituted phenyldiboronic acids to give the triphenyl ethers 32–35 in two steps. While the coupling of *meta*-substituted phenyldiboronic acid and phenols resulted in high yields, *para*-substituted phenyldiboronic acid did not react well (less than 10% yield).

Schemes 6 and 7 illustrate the synthetic routes to *meta*- and *para*-substituted ring B diphenyl ether analogues from commercially available arylboronic acids bearing both electron-donating and electron-withdrawing functional groups. These functional groups were further elaborated

to obtain diverse substitutions on ring B. Benzoic acid 39 was obtained by hydrolysis of the corresponding methyl benzoate 37 while compound 42 was obtained by the reduction of the ketone 40 using NaBH₄. Oxidation of the methylthioether group in 41 a afforded the methyl sulfoxide 43 and methyl sulfone 44, respectively, after demethylation. Coupling 4-allyl-2-methoxyphenol with the corresponding arylboronic acids gave allylic intermediates 45 a and 46 a; reduction of the allylic side



Scheme 4. Synthesis of compounds **26–31**: a) Phenylboronic acid, Cu(OAc)₂, Et₃N, CH₂Cl₂, air, RT, 16 h; b) OsO₄, NMO, THF, RT, overnight; c) BBr₃, CH₂Cl₂, –78 °C, 2 h; d) H₂, Pd/C, EtOAc, RT, 2 h; e) NaBH₄, MeOH, 0 °C, 1 h; f) amine, NaBH(OAc)₃, AcOH, CH₂Cl₂, RT, overnight.



Scheme 5. Synthesis of compounds **32–35**: a) Cu(OAc)₂, *meta*- or *para*-phenyldiboronic acid, Et₃N, CH₂Cl₂, air, RT, 16 h; b) BBr₃, CH₂Cl₂, –78 °C, 2 h.

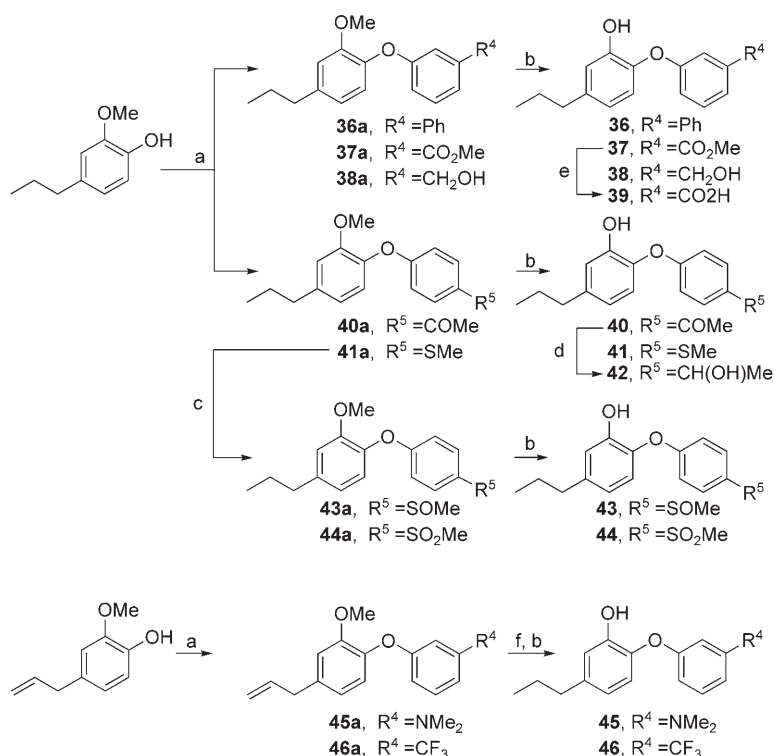
chain via catalytic hydrogenation, and subsequent demethylation gave compounds **45** and **46**.

In Scheme 7, 2-methoxy-4-propylphenol was coupled with 3-formylphenylboronic acid to give the aldehyde **47a**; subsequent demethylation gave compound **47**. The *meta*-aldehyde group in **47** underwent a Wittig reaction, and two-carbon elongated side chain analogues **48–51** were obtained by following similar hydrogenation and hydrolysis protocols.

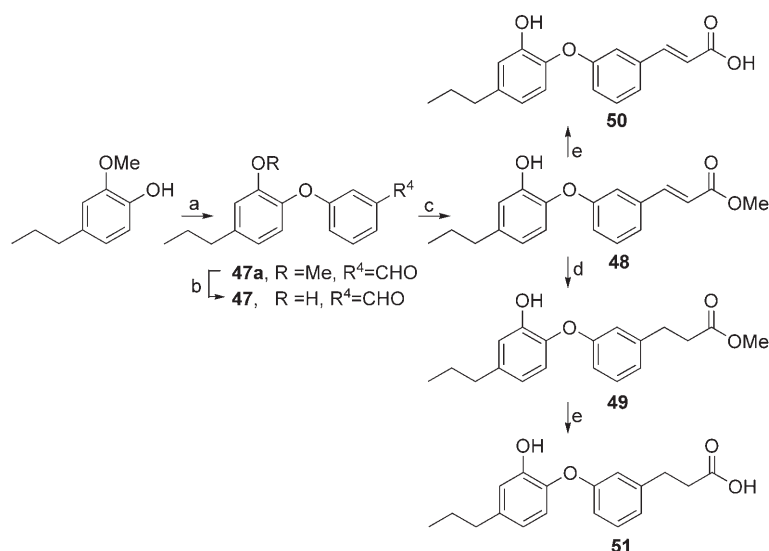
Evaluation of the active site

Initial assay results indicate that triclosan is an effective inhibitor of *Ba*ENR, and has good antibacterial activity against *B. anthracis* (Table 1). We conducted structure-activity relationship studies on a number of aryl ether derivatives to improve the potency of this lead compound, with the goal of optimizing the activity against *Ba*ENR. The first structural modifications were directed at ring A of triclosan. As expected, the hydrogen bonding interaction of the phenolic hy-

droxy group on ring A is critical for *Ba*ENR inhibitory activity. Conversion of the phenol group to an ether resulted in complete loss of activity (compounds **52** and **53**), while substitution by an amino functionality (compound **54**), carboxylic acid (compound **14**), or a carboxamide (compound **17**) resulted in no inhibition at 1 μM. Replacing the phenol with benzylic alcohol (compound **16**) gave no improvement in activity. We recently reported the X-ray structure of triclosan bound to *Ba*ENR,^[46] which helps explain this lack of activity. The binding geometry of triclosan, shown in Figure 1a, is similar to that seen with analogous proteins from other organisms. The phenolic "ring A" of triclosan π stacks with the nicotinamide ring of NAD⁺ while the hydroxy group is involved in hydrogen bonds with the phenol side chain of Tyr 157 and the 2'-hydroxy group of nicotinamide ribose. Removal of these hydrogen bonds by substitution at the 2-position would have a substantial impact on the binding energy of these compounds, confirmed by the experimental results (Table 1). The diphenyl ether linkage is also within hydrogen bonding distance to the 2'-hydroxy group of nicotinamide ribose, thereby adding increased binding energy between *Ba*ENR and the NAD⁺-triclosan complex. Based on these findings, our design efforts focused on 2-phenoxyphenol as the key scaffold, and on optimizing the substitution of rings A and B to maximize the van der Waals, electrostatic, and hydrogen bonding interactions in the active site. The design of compounds in this investigation was also based on comparison of calculated molecular properties (ClogP, ALOGpS and TPSA) with those of triclosan.^[50]



Scheme 6. Synthesis of compounds **36–46**: a) Cu(OAc)₂, substituted phenylboronic acids, Et₃N, CH₂Cl₂, air, RT, 16 h; b) BBr₃, CH₂Cl₂, –78 °C to RT, 2 h; c) *m*-CPBA, CH₂Cl₂, 0 °C, 10 min; d) NaBH₄, MeOH, 0 °C, 1 h; e) LiOH·H₂O, MeOH, H₂O, RT, 2 h; f) H₂, Pd/C, EtOAc, RT, 2 h.



Scheme 7. Synthesis of compounds 47–51: a) $\text{Cu}(\text{OAc})_2$, 3-formylphenylboronic acid, Et_3N , CH_2Cl_2 , air, RT, 16 h; b) BBr_3 , CH_2Cl_2 , -78°C to RT, 2 h; c) $\text{Ph}_3\text{P}=\text{CHCO}_2\text{Me}$, THF, reflux, overnight; d) H_2 , Pd/C, EtOAc, RT, 2 h; e) $\text{LiOH}\cdot\text{H}_2\text{O}$, MeOH, H_2O , RT, 2 h.

Connolly surface maps with various properties were generated for the active site of *Ba*ENR; Figure 2a maps the charge distribution to the surface, Figure 2b maps the lipophilicity, and Figure 2c maps the hydrogen bonding opportunities found on the active site surface. Full evaluation and consideration of these active site surface maps contribute significantly to the structure-based design approach. For this system, the shape of the active site indicates that the R^1 position on ring A and the R^4 and/or R^5 positions on ring B are suitable sites for introduc-

ing bulky substituents. The ring A pocket appears to be neutral in charge (Figure 2a), lacking in hydrogen bonding opportunities (Figure 2c), and highly hydrophobic (Figure 2b); for these reasons, we designed inhibitors with increased lipophilic R^1 substituents on ring A to maximize the hydrophobic interactions in this pocket, and minimize steric constraints.

Substitutions on ring A

Compound 55, bereft of substituents on ring B, was previously shown to be a potent inhibitor of *E. coli* ENR.^[37] Compound 55, used as a reference in this study, shows similar activity to that of triclosan against *Ba*ENR, although its MIC value against ΔANR *B. anthracis* is an order of magnitude lower (Table 1). Replacement of the R^1 chloro substituent with polar, hydrophilic functionalities, such as OH (compound 1) and NO_2 (compound 2), decreased the inhibitory activity against *Ba*ENR. Although compound 2 has fair antibacterial activity ($\text{MIC}=5.8\text{ }\mu\text{g mL}^{-1}$), its poor enzyme inhibitory activity suggests a different mechanism of action. Poor solubility of these diphenyl ether derivatives made the introduction of hydrophilic groups at the R^1 position necessary (in 26, 28, and 29–31), which resulted in decreased inhibitory activity (Table 1). This is in agreement with the surface-map property analysis of the active site from the *Ba*ENR–triclosan X-ray structure (Figure 2a–c). The surface maps show a hydrophobic pocket, approximately 6 Å in diameter, near the R^1 position of ring A. Moreover, Figure 2c shows there are no opportunities for additional hydrogen bonds to

Table 1. *Ba*ENR inhibition and antibacterial activity for modifications of ring A.

| Compound | R^1 | | IC_{50} [μM] or % inhibition at 1 μM | $\text{MIC}^{[b]}$ [$\mu\text{g mL}^{-1}$] |
|-----------|--|------------------------|---|--|
| Triclosan | | | 0.6 ± 0.0 | 3.1 |
| 52 | Cl | | 0.5% | NT |
| 53 | Cl | OMe | 0% | NT |
| 54 | Cl | NH_2 | 4.4% | NT |
| 14 | Cl | CO_2H | 0% | NT |
| 16 | Cl | CH_2OH | 1.8% | NT |
| 17 | Cl | CONH_2 | 0% | NT |
| 55 | Cl | OH | 0.5 ± 0.1 | 32 |
| 1 | OH | OH | 6.3 ± 0.4 | 64 |
| 2 | NO_2 | OH | > 50 | 5.8 |
| 26 | $\text{CH}_2\text{CH}(\text{OH})\text{CH}_2\text{OH}$ | OH | 9.8% | > 104 |
| 28 | CH_2OH | OH | 5.0% | 43 |
| 29 | $\text{CH}_2\text{NHCH}(\text{CH}_3)\text{CH}_2\text{CH}_2\text{CH}_3$ | OH | 0% | > 109 |
| 30 | CH_2 -(1-piperidine) | OH | 0% | > 113 |
| 31 | $\text{CH}_2\text{NHCH}_2\text{Ph}$ | OH | 7.9% | > 122 |
| 27 | <i>n</i> -propyl | OH | > 0.8 ^[a] | 22.8 |

[a] Saturation with inhibitor was not obtained over the concentration range tested. The percent inhibition of *Ba*ENR showed a linear response to increasing inhibitor concentrations. [b] MIC values are against ΔANR *B. anthracis*. NT = Not tested.

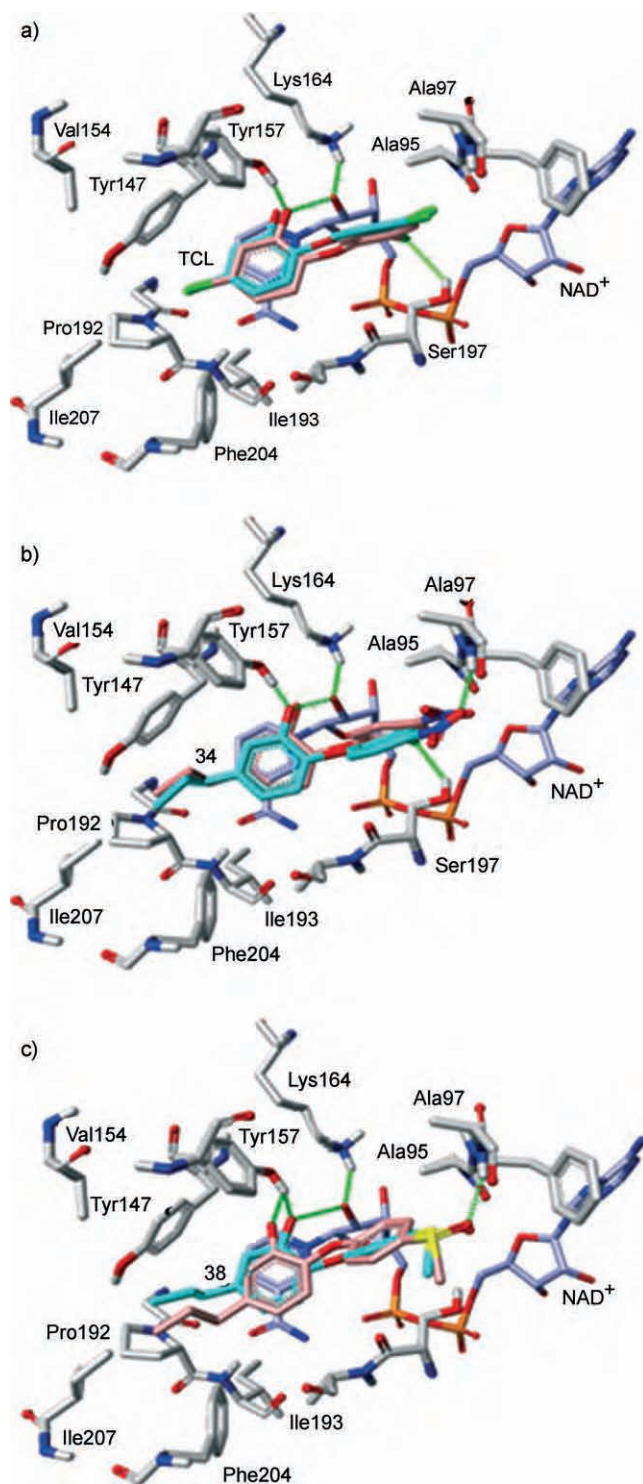


Figure 1. Comparison of ligand-bound crystal structures of *Ba*ENR and the predicted GOLD docking conformation: side chains (gray), NAD⁺ (blue-gray, behind the ligand); a) The triclosan crystal structure (coral) and GOLD docking conformation for triclosan (cyan); b) Compound 11 crystal structure (coral) and GOLD conformation (cyan); c) Compound 43 crystal structure (coral) and the GOLD conformation (cyan). Hydrogen bonding (green) is shown between the ligands and Tyr 157, as well as between the 2'-hydroxy of NAD⁺ with the 2-hydroxy and the ether linkage of the ligands. Also shown is a hydrogen bond between 2'-chloro of triclosan and Ser 197.

occur within the ring A pocket, further explaining the experimental results.

From the crystal structure shown in Figure 1, it is clear that hydrophobic residues dominate the region surrounding ring A. Sullivan et al. recently reported potent inhibition of ENR (InhA) from *Mycobacterium tuberculosis* by triclosan analogues bearing long aliphatic chains at the R¹ position.^[43,51] Because the ring A pocket in *Ba*ENR is much smaller than in InhA, numerous aliphatic chain lengths (2–8 carbons) were evaluated by GOLD docking prior to synthesis to optimize the chain length. We are confident that GOLD docking can accurately predict the binding conformation of these diphenyl ether analogues; an overlay of the predicted GOLD docking conformation and the crystal structure of triclosan show that they are in very good agreement (RMSD = 0.32 Å) (Figure 1a). The best result from the docking studies (conformation and scoring), where R¹ is *n*-propyl (compound 27), was synthesized and tested. The IC₅₀ value of 27 was higher than 55, presumably because it could not saturate the *Ba*ENR active site under the experimental concentrations. Sparing solubility made accurate determination of IC₅₀ values difficult; however, the *n*-propyl derivative 27 had a MIC value similar to that of compound 55. We chose to expand two series of compounds: the first was based on a chloro group at R¹ of ring A (55), and the second was based on the *n*-propyl group at R¹ (in 27).

Substitutions on ring B

Preliminary structure–activity relationship (SAR) studies on ring B involved the modification of R³–R⁵, while R¹ (Cl) and R² (OH) of ring A remained unchanged. The goal was to increase the binding affinities of these compounds by increasing the hydrogen bonding interactions in the ring B pocket, specifically to the backbone of Ala95–Ala97; from analysis of the modeling results and crystal structure presented in Figures 1 and 2, these residues appear to be potential hydrogen bond donors/acceptors. Several functional groups capable of hydrogen bonding were introduced at the 4'-position of ring B (R⁵) (Table 2). Introduction of a hydroxy group did not improve the activity (compound 3). Substitution with an amino group (compound 20) led to improved antibacterial activity, but weaker inhibition of *Ba*ENR (IC₅₀ = 7 μM). Acetylation or sulfonylation of the amino group was not effective in improving the *Ba*ENR activity (compounds 18, 19, and 22).

Compound 6, where R³ = Cl, and R⁵ = NO₂, a known inhibitor of malarial ENR from *P. falciparum*,^[41] was the best inhibitor in this series (IC₅₀ = 290 nM and MIC = 3.1 μg mL⁻¹). The nitro group decreases the electron density of ring B, but perhaps more importantly, it adds two potential hydrogen bond acceptors. Compound 7, where R⁵ = Ph, is more active against the bacterium (MIC = 1.9 μg mL⁻¹) than triclosan, but not as effective against *Ba*ENR, indicating a nonspecific or alternative mode of action, or that the biphenyl ring improves bacterial membrane penetration. Similarly, the symmetrical triaryl ethers 32 and 33 were ineffective against *Ba*ENR, even though 33 showed improved antibacterial activity.

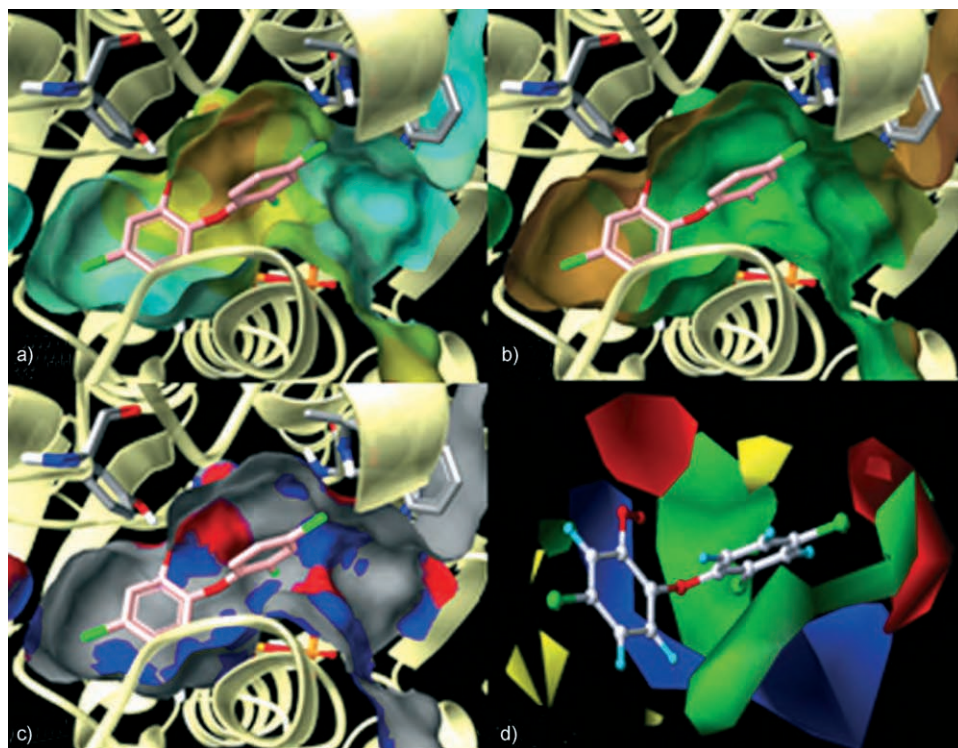


Figure 2. Surface maps of the *BaENR* active site: a) Electrostatic potential surface map showing regions of moderate positive charge (orange/yellow) and areas of neutral charge (cyan) on *BaENR*; b) Lipophilic map with a brown to green scale, where brown depicts the more hydrophobic areas; c) Hydrogen bonding map where the blue and red areas indicate places for either hydrogen bonding acceptors or donors, respectively; d) Steric and electrostatic fields from the CoMFA based on IC_{50} values. Steric fields are green and yellow, indicating regions of favorable and unfavorable steric expansion. Electrostatic fields are red and blue, indicating preferred regions of negative and positive charge. Surface maps were generated using the Benchware software and CoMFA fields were generated using Sybyl 7.2, (both softwares from Tripos, Inc., St. Louis, MO).

Considerable improvement in the IC_{50} values of compound **6** over **4** (0.3 μM versus 7.2% inhibition at 1 μM) suggests that a 2'-chloro group considerably increases binding affinity. From the crystal structure of triclosan bound to *BaENR* (Figure 1a), the hydroxy group of Ser 197 is 2.6 Å from the 2'-chloro group, which is sufficiently close for a favorable halogen–oxygen interaction,^[52] and also 2.7 Å from one of the oxygen atoms of the bridging phosphate group of NAD^+ . The improved activity of the 2'-chloro compounds may be due to this hydrogen bond network, rendering ring B in a “locked” orientation, favorably positioning R^5 substituents to form hydrogen bonds with the backbone of Ala97. Hydrogen bonding to Ser197 (OH) may also stabilize positioning of the substrate binding or “flipping” loop, which is flexible in a number of organisms.^[16, 17, 46]

To improve the solubility of these diphenyl ethers, we synthesized heteroaromatic ring B analogues of **55**, such as the pyridine and pyrazine (data shown in Supporting Information). These compounds failed to show promising activity; acetamidopyridine derivative **24** gave a moderate IC_{50} value (IC_{50} = 4.1 μM), but proved to be inactive against the bacterium ($MIC > 111.5 \mu\text{g mL}^{-1}$), and so no further such modifications were investigated.

Combining the SAR data of rings A and B, we synthesized compounds in which ring A was the more hydrophobic 2-hy-

droxy-4-*n*-propylphenyl moiety (**27**, Table 1), and ring B was modified to provide additional hydrogen bond donors/acceptors, both at the R^4 and the R^5 positions, allowing close interactions with the residues in the region of Ala97, and positioning the ring B substituents toward the entrance of the active site, closer to the protein surface.

The *n*-propyl series of compounds showed an overall improvement in both the IC_{50} and MIC values over those listed in Tables 1 and 2 (Table 3). Introduction of small, hydrophilic hydrogen bond acceptor groups, which have the ability to withdraw electron density from ring B, increases activity. The best results were obtained when ring B contained a nitro or a cyano substituent (**8–12**, Table 3). As discussed above, the presence of a 2'-chloro group contributed to the binding affinity of these inhibitors (**8** versus **11**). Compounds with either an amide (in **15**), or methyl ketone (in **40**) group also had inhibitory activities similar to triclosan. The compounds with an electron-rich

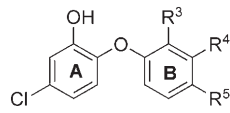
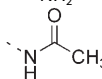
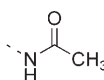
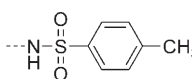
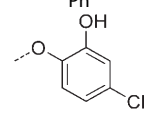
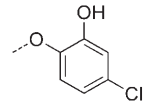
amino group at the R^5 position were found to be weak inhibitors of *BaENR* (e.g. **8** versus **21**), consistent with the results of compound **55** versus **20** (Table 2).

The correlation of inhibitory activities with the electron-donating or -withdrawing ability of R^5 substituents, such as NH_2 (compound **21**) and NO_2 (compound **8**), does not hold for the sulfur-containing derivatives. Improved IC_{50} values were seen with the more electron-donating methylthioether group (**41**, IC_{50} = 0.6 μM), while compounds bearing relatively stronger electron-withdrawing groups were only moderately active (methylsulfoxide **43**, IC_{50} = 3.6 μM , or methylsulfone **44**, IC_{50} = 2.2 μM). An electrostatic effect and a steric contribution and/or orientation of the hydrogen bond acceptor in the active site contribute to the inhibitory activity of these compounds. The different geometry of a sulfone compared with a nitro group means that the oxygen atoms are positioned differently, leading to distinct hydrogen bonding capabilities. It is notable here that methyl ketone **40**, which is a close structural analogue of methylsulfoxide **43**, exhibits improved inhibitory activity against *BaENR* and ΔANR *B. anthracis* (IC_{50} = 0.8 μM , MIC = 13.5 $\mu\text{g mL}^{-1}$).

To better understand the binding interactions of these inhibitors at the active site, we determined the X-ray crystal structures of inhibitors **11** and **43** bound to *BaENR* in the presence

Table 2. *Ba*ENR inhibition and antibacterial activity for modification of ring B.

Table 2. *In vitro* inhibition and antifungal activity for modification of ring 2.

| Compound | R ³ | R ⁴ | R ⁵ | IC ₅₀ [μM] or % inhibition at 1 μM | MIC ^[b] [μg mL ⁻¹] |
|-----------|---|--|---|---|---|
| | | |  | | |
| Triclosan | Cl | H | Cl | 0.6 ± 0.0 | 3.1 |
| 55 | H | H | H | 0.5 ± 0.1 | 32 |
| 3 | H | H | OH | 2.6% | > 64 |
| 20 | H | H | NH ₂ | 7.1 ± 1.2 | 12 |
| 18 | H | H |  | 1.6% | 111 |
| 19 |  | H | H | 0% | 111 |
| 22 | H | H |  | > 12 ^[a] | 4.9 |
| 4 | H | H | NO ₂ | 7.2% | 3.3 |
| 5 | NO ₂ | H | H | 7.7 ± 0.7 | 13.3 |
| 6 | Cl | H | NO ₂ | 0.3 ± 0.0 | < 0.1–3.1 |
| 7 | H | H | Ph | > 6.25 | 1.9 |
| 32 | H | H |  | 15.5% | > 145 |
| 33 | H |  | H | 9.9% | 2.3 |

[a] Saturation with inhibitor was not obtained over the concentration range tested. The percent inhibition of *Ba*ENR showed a linear response to increasing inhibitor concentrations. [b] MIC values are against Δ ANR *B. anthracis*.

of NAD⁺ (2.3 Å resolution, Figure 1b and c), and compared them to the structure of *Ba*ENR in complex with triclosan. As expected from modeling studies, the binding conformations of these inhibitors were nearly identical to that of triclosan. The most significant difference between the structures was the interaction between R⁵ and the protein. Improved activity of compound 11 can be attributed to the additional hydrogen bond between the 4'-nitro group and Ala97(NH) (~2.2 Å), accurately predicted by the GOLD docking results, as well as the proposed orientation of the 2'-chloro group within hydrogen bonding distance to the side chain of Ser197. Figure 1b is an overlay of the X-ray crystal structure of compound 11 and its GOLD docking conformation in the active site of *Ba*ENR (RMSD=0.45 Å). Figure 1c is an overlay of the X-ray crystal structure of compound 43 and its GOLD docking conformation in the active site of *Ba*ENR (RMSD=0.69 Å). Again, there is very good agreement between the two, as well as the correct prediction of the hydrogen bond between the sulfoxide and Ala97(NH) (~1.8 Å).

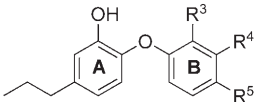
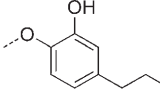
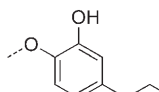
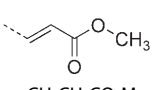
Ring B modifications at the *meta* position (R⁴) involved the addition of heteroatoms close to the aromatic ring, including compounds 45 (NMe₂), 46 (CF₃), and 38 (CH₂OH). Only compound 46 showed improved activities against *Ba*ENR and the bacterium. Compounds 36 and 34, where R⁴=Ph, were more active toward the bacterium than triclosan itself (MIC=1.9 and

1.2 μ g mL⁻¹ respectively), but exhibited weaker activities against *Ba*ENR. It is well documented that the ENR from various organisms has a very flexible substrate binding loop,^[46,53] the bulky phenyl substituent may induce a shift in this loop, opening up the active site, and leading to a decrease in the binding affinity of the compound for *Ba*ENR.

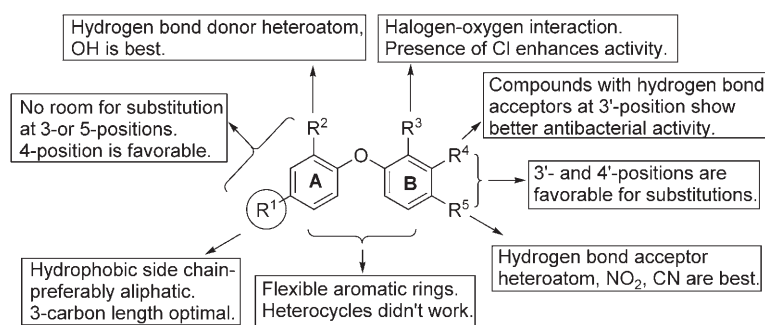
Compounds 37–39 and 48–51 are closely related R⁴ ester and acid analogues. As previously noted, modeling and structural analysis suggests that hydrogen bonds may be formed between ring B substituents and the residues surrounding Ala97 in the active site of *Ba*ENR. Hydrogen bonding is optimal when the acceptor/donor R⁴ group is 1–2 atoms away from ring B, as seen in compounds 37–39, while longer chain substituents result in weaker inhibition (48–51). Although this modification proved disappointing, these results indicate that esters are better than acids at inhibiting *Ba*ENR (37 versus 39, 49 versus 51).

While some of the 3'-substituted analogues show IC₅₀ values near 1 μ M, the majority had little activity against *Ba*ENR (less than 20% inhibition at 1 μ M). This is in contrast to the 4'-substituted analogues, which generally had IC₅₀ values \leq 3.6 μ M. MIC values suggest that 3'-substituted compounds have greater antibacterial activity than analogous 4'-derivatives (34 versus 35, Table 3). Figure 3 summarizes the SAR of the di-

Table 3. *Ba*ENR inhibition and antibacterial activity for modification of ring B, where ring A is a 2-hydroxy-4-propylphenyl group.

| Compound | R ³ | R ⁴ | R ⁵ | IC ₅₀ [μM] or % inhibition at 1 μM | MIC ^[c] [μg mL ⁻¹] |
|---|-----------------|---|--|---|---|
|  | | | | | |
| Triclosan | | | | 0.6 ± 0.0 | 3.1 |
| 27 | H | H | H | > 0.8 ^[a] | 22.8 |
| 8 | H | H | NO ₂ | 1.1 ± 0.1 | 3.4 |
| 9 | H | NO ₂ | H | > 0.8 ^[a] | 1.7 |
| 10 | NO ₂ | H | NO ₂ | 3.6 ± 0.8 | 4 |
| 11 | Cl | H | NO ₂ | 0.5 ± 0.0 | 1.9–3.1 |
| 12 | Cl | H | CN | > 0.8 ^[a] | 1.8 |
| 15 | Cl | H | C(=O)NH ₂ | 1.1 ± 0.1 | 30.6 |
| 40 | H | H | C(=O)Me | 0.8 ± 0.1 | 13.5 |
| 43 | H | H | S(=O)Me | 3.6 ± 0.3 | 116 |
| 44 | H | H | SO ₂ Me | 2.2 ± 0.3 | 61.3 |
| 42 | H | H | CH(OH)Me | 17.1 % | 54.5 |
| 21 | H | H | NH ₂ | 8.8 ± 1.0 | > 97 |
| 41 | H | H | SMe | 0.6 ± 0.0 | 13.5 |
| 45 | H | N(Me) ₂ | H | 12.6 % | 13.6 |
| 46 | H | CF ₃ | H | 1.24 | 7.4 |
| 37 | H | CO ₂ Me | H | 2.0 ± 0.3 | 3.6 |
| 39 | H | CO ₂ H | H | 9.2 % | 6.8 |
| 38 | H | CH ₂ OH | H | 20.3 ± 1.3 | 12.9 |
| 36 | H | Ph | H | 0.5 ± 0.1 ^[b] | 1.9 |
| 34 | H |  | H | 20.6 % | 1.2 |
| 35 | H | H |  | 10.0 % | > 151 |
| 48 | H |  | H | > 6.25 | 2 |
| 49 | H | CH ₂ CH ₂ CO ₂ Me | H | 7.5 ± 1.9 | 7.9 |
| 50 | H | CH=CHCO ₂ H | H | 17.9 % | 14.9 |
| 51 | H | CH ₂ CH ₂ CO ₂ H | H | 17.6 % | 60.1 |
| 13 | H | CH ₂ CH ₂ Br | H | 6.0 ± 1.5 | 1.7 |

[a] Saturation with inhibitor was not obtained over the concentration range tested. The percent inhibition of *Ba*ENR showed a linear response to increasing inhibitor concentrations. [b] 100% inhibition was not observed. The response of the enzyme to inhibitor showed maximum saturation at ~50% inhibition. [c] MIC values are against ΔANR *B. anthracis*.

**Figure 3.** Summary of the SAR of diaryl ether inhibitors of *Ba*ENR.

phenyl ethers studied, showing the key pharmacophore functionalities required for effective *Ba*ENR inhibition.

Considering the enzyme assay alone, the *n*-propyl R¹ series of compounds show better inhibitory activity against *Ba*ENR

than the chloro series shown in Table 2. More importantly, this series has resulted in nine compounds (**8**, **9**, **11**, **12**, **15**, **27**, **36**, **40**, and **41**) that are equipotent or near-equipotent with triclosan. Of these, **15**, **40**, and **41** have the potential for further structural modification and expansion. Compounds where R³=Cl have also shown increased activity against *Ba*ENR. Interestingly, we observed a similar improvement in the binding affinity of 2-pyridone derivatives with *Ba*ENR in a recent study;^[54] hence, introduction of a chloro group to **40** and **41** is predicted to improve their inhibitory activities. Additionally, carboxamide **15**, methyl ketone **40**, and thioether **41** possess R⁵ functionalities that are amenable to further derivatization and therefore useful in the design of the next generation of compounds.

CoMFA maps and future design implications

GOLD accurately predicted the binding conformations of simple substitutions; however, it is unable to account for the flexibility in the *Ba*ENR substrate binding loop. A ligand-based approach, 3D-QSAR, or comparative molecular field analysis (CoMFA), is needed for further drug design. We performed a CoMFA on the results obtained against *Ba*ENR, presented in Tables 1–3 and the Supporting Information. The CoMFA model has $q^2=0.831$, and $r^2=0.929$. Figure 2d shows the steric and electrostatic fields generated from the CoMFA. The R² hydroxy group and R⁵ substituent protrude favorably into negatively charged regions (red). The CoMFA map suggests that steric expansion of R⁴ and R⁵ would be beneficial, while ring A expansion should be limited, as shown by the yellow regions here. The large green region behind the molecule could potentially be misleading; from the crystal structure, we know this to be the NAD⁺ binding region. Modifications that occupy this region are not likely to be beneficial because triclosan and its analogues co-bind with NAD⁺ for optimal binding energy.^[37,46,55] The CoMFA model provides insight for the further structural expansion of these aryl ethers and will be used to predict the activities of the next generation of compounds.

Antibacterial testing of lead compounds

Table 4 shows the MIC and MBC values of **6** and **11** against several bacterial pathogens compared to ciprofloxacin. The broth microdilution method (National Committee for Clinical Laboratory Standards) was validated using a panel of ATCC strains of bacterial pathogens with known MIC values for ciprofloxacin, and then employed to determine the MIC and MBC values for **6** and **11**. The results show that **6** and **11** are equally active against Sterne and Δ ANR strains of *B. anthracis*. These compounds also have noticeable activity against both Gram(+) and Gram(–) bacteria, suggesting their potential expansion to a more broad-spectrum application. A notable exception is their lack of activity against *P. aeruginosa*, which was reported for triclosan also,^[56] and may be explained by bacterial efflux

pump activity.^[29] Both compounds exhibited impressive activity against MRSA (MIC = 0.3 $\mu\text{g mL}^{-1}$), and an MBC/MIC ratio of 1.6–1.9, compared with a ratio of ~20 for methicillin-sensitive *S. aureus* (MSSA); the comparable activities against MRSA and MSSA are consistent with previous reports.^[56] Should the 10-fold increase in antibacterial activity against MRSA over MSSA be reproducible in further tests against multiple strains of each, it might be interesting to pursue further mechanistic investigations.

Previous studies have indicated that the bactericidal activity of triclosan against *S. aureus* (both MRSA and MSSA) may be unrelated to specific enzyme inhibition but rather involve multiple bacterial targets.^[57] It is likely that compounds **6** and **11** target FabI in *S. aureus*, however, in the absence of an X-ray crystal structure of ENR from *S. aureus*, this increased activity must be explained by secondary structures. Sequence alignment of ENR from *S. aureus* and *B. anthracis* indicates 62% homology, with all residues in the substrate binding loop (residues 190–210), and all residues within 5 Å radius of the active site fully conserved between species with the exception of a single residue, where Met99 (*S. aureus* ENR) is substituted by Arg99 (*Ba*ENR). Arg99 is located near the surface of *Ba*ENR, with the arginine side chain partially covering the entrance to the active site. Substitution with methionine (*S. aureus* ENR) is likely to leave the active site more accessible for the ligands, and could partially explain the increased activity of the biaryl ethers against *S. aureus* compared with *B. anthracis*. Further investigation is needed to assess the strain specificity and ENR pathway dependence of these MBC/MIC results. Preliminary cytotoxicity evaluation of **6** and **11** showed an EC₅₀/MIC ratio of approximately 15–20 against HeLa cells (footnote, Table 4). Further testing is needed to validate these values and assess whether structural modifications are necessary to minimize toxicity.

Conclusions

A number of novel aryl ethers, including triphenyl ethers and heteroaromatic analogues, have been prepared and tested for

Table 4. MIC and MBC values of ENR inhibitors against *B. anthracis* and other bacterial pathogens.

| Bacteria | Cipro ^[a] MIC ^[b] | MIC | Compound 6 ^[e] MBC | MBC/MIC | MIC | Compound 11 ^[e] MBC | MBC/MIC |
|-----------------------------|--|---------------|---|---------|---------------|--|---------|
| Δ ANR ^[c] | 0.1 \pm 0.0 | 2.2 \pm 0.4 | 3.1 \pm 1.1 | 1.4 | 2.2 \pm 0.0 | 3.9 \pm 0.8 | 1.8 |
| Sterne ^[d] | 0.1 \pm 0.0 | 1.9 \pm 0.3 | 3.9 \pm 0.8 | 2.1 | 1.9 \pm 0.0 | 3.9 \pm 0.8 | 2.1 |
| <i>S. aureus</i> | 0.4 \pm 0.0 | 0.1 \pm 0.1 | 2.9 \pm 1.2 | 20.9 | 0.1 \pm 0.1 | 2.9 \pm 1.2 | 20.9 |
| MRSA | 0.5 \pm 0.2 | 0.3 \pm 0.3 | 0.4 \pm 0.1 | 1.6 | 0.3 \pm 0.3 | 0.5 \pm 0.2 | 1.9 |
| <i>E. fecalis</i> | 0.7 \pm 0.1 | 4.4 \pm 0.8 | 31.3 \pm 6.3 | 7.1 | 4.4 \pm 0.5 | 12.5 \pm 0.0 | 2.9 |
| VRE | 0.6 \pm 0.2 | 5.7 \pm 0.6 | 37.5 \pm 12.5 | 6.6 | 5.7 \pm 0.3 | 15.6 \pm 3.1 | 2.7 |
| <i>L. monocytogenes</i> | 0.9 \pm 0.3 | 2.8 \pm 0.3 | 14.1 \pm 3.9 | 5.0 | 2.8 \pm 0.9 | 14.1 \pm 3.9 | 5.0 |
| <i>P. aeruginosa</i> | 0.3 \pm 0.1 | > 25 | NT | | > 25 | NT | |
| <i>K. pneumoniae</i> | 0.5 \pm 0.1 | 1.8 \pm 0.4 | 12.5 | 7.1 | 1.8 \pm 0.9 | 8.3 \pm 2.1 | 4.7 |
| <i>E. coli</i> | 0.1 \pm 0.0 | 0.3 \pm 0.1 | 12.50 | 48.0 | 0.3 \pm 0.2 | 1.2 \pm 0.4 | 4.5 |

[a] Drug concentrations = $\mu\text{g mL}^{-1}$. Results = mean \pm SEM, $n=3$. [b] MIC = minimum inhibitory concentration; MBC = minimum bactericidal concentration; Bactericidal drug: MBC/MIC ≤ 4 . [c] Plasmid-negative strain of *B. anthracis*, lacking both pXO1 and pXO2 plasmids. [d] Sterne strain of *B. anthracis* that contains pXO1 (toxin production) but lacks pXO2 (capsule). [e] The EC₅₀ against the HeLa cell line is 29.3 $\mu\text{g mL}^{-1}$ for **6** and 41.4 $\mu\text{g mL}^{-1}$ for **11**. EC₅₀ against the MHS cell line is 9.9 $\mu\text{g mL}^{-1}$ for **6** and 22.6 $\mu\text{g mL}^{-1}$ for **11**.

inhibition of purified BaENR and cultured Δ ANR *B. anthracis*. These efforts have led to an improved understanding of the enzyme active site, and provided clear SAR data for these inhibitors. The X-ray crystal structures coupled with molecular modeling studies have demonstrated the importance of hydrophobic interactions of substituents located at the R¹ position with the enzyme active site, and underscore the H-bonding contribution of the *ortho* (R³) and *para* (R⁵) substituents on ring B with Ser197 (OH) and Ala97. In particular, the importance of the *ortho*-chloro group on ring B for optimized activity warrants further investigation. These results highlight the biological activity's sensitivity towards changes in electron distribution in either ring of the 2-phenoxyphenol. For example, although replacement of a chloro for a *n*-propyl group at R¹ improved activity, simultaneous and complementary substitution is needed on ring B. Structure-based design efforts are ongoing with a focus on R⁵ modifications and linking groups such as thioethers, amides, and esters, as well as nitro group modification.

Several compounds have been synthesized that exhibit structural diversity and improved antibacterial activity over triclosan, and offer an opportunity to identify new inhibitory pathways and drug candidates. Encouraging inhibitory activities of these compounds against a number of pathogens suggests potential for broad-spectrum applications. The intriguing activity shown by compounds **6** and **11** against MRSA provides potential leads against a serious and increasingly common pathogen. To advance these compounds further, pharmacokinetic and drug metabolism studies are planned.

Experimental Section

¹H NMR and ¹³C NMR spectra were recorded on a Bruker DPX-400, and an AVANCE-400 spectrometer with TMS as an internal standard. HRMS data were performed using a Q-TOF-2TM (Micromass). Preparative TLC was performed with 1000 μ m silica gel GF plates (Analtech). Column chromatography was performed using 40–60 mesh silica gel (Merck). HPLC was carried out on an ACE AQ columns (100 \times 4.6 and 250 \times 10 mm), with detection at 254 nm on a Shimadzu SPD-10 A VP detector; flow rate = 2.0–3.5 mL min⁻¹; from 10% CH₃CN in water to 100% CH₃CN with 0.05% TFA. Compound **54** was commercially available from Sigma-Aldrich. Compounds **53**, **55**,^[37] and **28**^[26,37] were synthesized according to published methods.

Synthesis of inhibitors

General Methods: **Method A:** A solution of aryl halide (1 mmol), phenol (1 mmol), and K₂CO₃ (2–4 mmol) in DMSO (1.5 mL) were heated to 100 °C under nitrogen until completion (8–12 h). The reaction was cooled to RT, diluted with EtOAc, and washed with aq NaOH (5%). The aqueous layer was further extracted with EtOAc, and the combined organic layers washed with brine. The organic layer was dried (Na₂SO₄), filtered and concentrated in vacuo to give the crude product, which was purified by chromatography. **Method B:** KOtBu (1.1 mmol) was added to a solution of phenol (1 mmol) in DMF (1.75 mL) in one portion, and the reaction heated at 45 °C under mild vacuum (2 h). The reaction was cooled to RT, and treated with aryl halide (1 mmol) and (CuOTf)₂-PhH

(0.05 mmol), then heated to reflux (16–20 h). The reaction was cooled to RT, diluted with EtOAc, and filtered over Celite. The filtrate was washed with aq NaOH (5%), extracted with EtOAc, and the combined organic layers washed with brine. The organic phase was dried (Na₂SO₄), filtered and concentrated in vacuo to give the crude product, which was purified by chromatography. **Method C:** A suspension of arylboronic acid (1–2 mmol), phenol (1 mmol), Cu(OAc)₂ (2–5 mmol), Et₃N (5–10 mmol) and powdered molecular sieves (5 Å) in CH₂Cl₂ (10 mL) was stirred open to the air until completion (3–16 h). The reaction mixture was diluted with EtOAc, filtered over Celite, and the filtrate was washed with aq NaOH (5%). The aqueous layer was extracted with EtOAc, and the combined organic layers were washed with brine. The organic phase was dried (Na₂SO₄), filtered and concentrated in vacuo to give the crude product, which was purified by chromatography. **Method D:** A solution of BBr₃ (2–8 mmol, 1.0 M in CH₂Cl₂) was added to a solution of diphenyl ether (1 mmol) in anhyd CH₂Cl₂ (4 mL) under nitrogen at –78 °C and stirred (1 h) before warming to RT and stirring until completion (3–8 h). The reaction was cooled to –78 °C and quenched with MeOH. The reaction was concentrated in vacuo then redissolved in EtOAc, washed with 10% aq NaHCO₃, water and brine; the aqueous layer was extracted with EtOAc (\times 2). The combined organic layers were then dried (Na₂SO₄), filtered, concentrated in vacuo and purified by chromatography.

4-Phenoxybenzene-1,3-diol (1): Method B was used to prepare the intermediate **1a** from 2,4-dimethoxyphenol (1.00 g, 6.5 mmol), KOtBu (0.87 g, 7.8 mmol), (CuOTf)₂-PhH (0.17 g, 0.3 mmol) and iodobenzene (1.59 g, 7.8 mmol) in 50% yield, and method D was used to convert it to the title compound. Purification by flash chromatography (10% EtOAc/hexanes) gave **1** as a viscous brown oil (80%). ¹H NMR (400 MHz, CDCl₃): δ = 4.86 (s, 1H), 5.56 (s, 1H), 6.36 (dd, *J* = 9.0, 3.0 Hz, 1H), 6.58 (d, *J* = 2.8 Hz, 1H), 6.83 (d, *J* = 8.7 Hz, 1H), 7.08 (d, *J* = 7.6 Hz, 2H), 7.09 (t, *J* = 7.4 Hz, 1H), 7.33 ppm (t, *J* = 7.4 Hz, 2H); ¹³C NMR (100 MHz, CDCl₃): δ = 103.4, 107.3, 116.4, 120.6, 122.7, 129.5, 136.3, 148.0, 152.5, 157.3 ppm; HRMS (ESI+): *m/z* calcd for C₁₂H₁₀O₃ ([M+H]⁺): 201.0557, found: 201.0556.

5-Nitro-2-phenoxyphenol (2): Method A was used to prepare the intermediate **2a** from phenol (0.66 g, 7.0 mmol), 1-fluoro-2-methoxy-4-nitrobenzene (1.12 g, 7.0 mmol) and K₂CO₃ (1.80 g, 12.8 mmol) in 48% yield, and method D was used to convert it to the title compound. Purification by flash chromatography (15% EtOAc/hexanes) gave **2** as a greenish yellow oil (75%). ¹H NMR (400 MHz, CDCl₃): δ = 6.53 (br s, 1H), 7.08–7.14 (m, 3H), 7.26 (t, *J* = 7.6 Hz, 1H), 7.43 (t, *J* = 7.6 Hz, 2H), 7.70 (d, *J* = 2.8 Hz, 1H), 7.97 ppm (dd, *J* = 4.0, *J* = 2.0 Hz, 1H); ¹³C NMR (100 MHz, CDCl₃): δ = 112.5, 115.3, 118.8, 120.1, 124.9, 130.0, 140.7, 143.9, 154.5, 152.4 ppm; HRMS (ESI–): *m/z* calcd for C₁₂H₉NO₄ ([M–H][–]): 230.0459, found: 230.0458.

5-Chloro-2-(4-hydroxyphenoxy)phenol (3): Method B was used to prepare the intermediate **3a** from 4-chloro-2-methoxyphenol (1.00 g, 6.3 mmol), KOtBu (0.85 g, 7.6 mmol), (CuOTf)₂-PhH (0.17 g, 0.3 mmol) and 4-iodoanisole (1.80 g, 7.6 mmol) in 49% yield, and method D was used to convert it to the title compound. Purification by flash chromatography (10% EtOAc/hexanes) gave **3** as a colorless oil (82%). ¹H NMR (400 MHz, CDCl₃): δ = 4.68 (s, 1H), 5.72 (s, 1H), 6.70 (d, *J* = 8.8 Hz, 1H), 6.79 (dd, *J* = 8.0, *J* = 2.0 Hz, 1H), 6.84 (dd, *J* = 7.0, *J* = 2.0 Hz, 2H), 6.94 (dd, *J* = 7.0, *J* = 2.0 Hz, 2H), 7.04 ppm (d, *J* = 2.4 Hz, 1H); ¹³C NMR (100 MHz, CDCl₃): δ = 115.8, 116.1, 117.4, 119.8, 119.9, 128.2, 143.3, 147.1, 149.1, 151.7 ppm; HRMS (ESI–): *m/z* calcd for C₁₂H₉ClO₃ ([M–H][–]): 235.0168, found: 235.0166.

5-Chloro-2-(4-nitrophenoxy)phenol (4): Method A was used to prepare the intermediate **4a** in 96% yield, as described in the synthesis of **20**, and method D was used to convert it to the title compound. Purification by flash chromatography (3% MeOH/CHCl₃) gave the **4** as a brown solid (70%). ¹H NMR (400 MHz, CDCl₃): δ = 5.42 (s, 1H), 6.95 (s, 2H), 7.14–7.02 (m, 3H), 8.26 ppm (d, *J* = 9.2 Hz, 2H); ¹³C NMR (100 MHz, CDCl₃): δ = 116.5, 117.3, 120.9, 121.1, 125.7, 131.2, 139.7, 142.9, 147.9, 161.7 ppm; HRMS (ESI[−]): *m/z* calcd for C₁₂H₈ClNO₄ ([*M*−H][−]): 264.0069, found: 264.0069.

5-Chloro-2-(2-nitrophenoxy)phenol (5): Method A was used to prepare the intermediate **5a** in 96% yield, as described in the synthesis of **19**, and method D was used to convert it to the title compound. Purification by flash chromatography (1% MeOH/CHCl₃) gave **5** as an off-white solid (76%). ¹H NMR (400 MHz, CDCl₃): δ = 6.89 (dd, *J* = 4.0, *J* = 2.0 Hz, 1H), 6.98 (d, *J* = 4.0 Hz, 1H), 7.12–7.08 (m, 2H), 7.28–7.23 (m, 1H), 7.57–7.53 (m, 1H), 7.94 ppm (dd, *J* = 4.0, *J* = 1.0 Hz, 1H); ¹³C NMR (100 MHz, CDCl₃): δ = 117.8, 118.9, 120.6, 121.3, 123.9, 125.9, 131.5, 134.6, 140.9, 148.7, 150.0 ppm; HRMS (ESI[−]): *m/z* calcd for C₁₂H₈ClNO₄ ([*M*−H][−]): 264.0069, found: 264.0068.

5-Chloro-2-(2-chloro-4-nitrophenoxy)phenol (6): Method A was used to prepare the intermediate **6a** from 4-chloro-2-methoxyphenol (1.00 g, 6.3 mmol), 2-chloro-1-fluoro-4-nitrobenzene (1.10 g, 6.3 mmol) and K₂CO₃ (1.80 g, 12.6 mmol) in 91% yield, and method D was used to convert it to the title compound. Purification by flash chromatography (3% MeOH/CHCl₃) gave **6** as a light yellow solid (79%). ¹H NMR (400 MHz, CDCl₃): δ = 5.73 (s, 1H), 6.97–6.91 (m, 3H), 7.14 (d, *J* = 1.2 Hz, 1H), 8.11 (dd, *J* = 4.0, *J* = 1.0 Hz, 1H), 8.41 ppm (d, *J* = 2.0 Hz, 1H); ¹³C NMR (400 MHz, CDCl₃): δ = 116.1, 117.5, 120.8, 121.0, 123.4, 124.2, 126.3, 131.5, 139.7, 142.9, 147.7, 157.4 ppm; HRMS (ESI[−]): *m/z* calcd for C₁₂H₇Cl₂NO₄ ([*M*−H][−]): 297.9679, found: 297.9679.

2-(Biphenyl-4-yloxy)-5-chlorophenol (7): Method B was used to prepare the intermediate **7a** from 4-chloro-2-methoxyphenol (1.00 g, 6.3 mmol), KOtBu (0.78 g, 6.9 mmol), (CuOTf)₂-PhH (0.16 g, 0.3 mmol) and 4-bromobiphenyl (1.47 g, 6.3 mmol) in 69% yield, and method D was used to convert it to the title compound. Purification by flash chromatography (2% EtOAc/hexanes) gave **7** as a white solid (65%). ¹H NMR (400 MHz, CDCl₃): δ = 5.83 (br s, 1H), 6.90 (s, 2H), 7.12 (d, *J* = 8.8 Hz, 3H), 7.40 (t, *J* = 7.2 Hz, 1H), 7.49 (t, *J* = 7.2 Hz, 2H), 7.61 ppm (d, *J* = 8.0 Hz, 4H); ¹³C NMR (100 MHz, CDCl₃): δ = 116.3, 117.9, 119.1, 120.3, 126.6, 126.9, 128.3, 128.5, 129.39, 129.2, 136.8, 139.8, 142.9, 147.7, 155.5 ppm; HRMS (ESI⁺): *m/z* calcd for C₁₈H₁₃ClO₂ ([*M*+H]⁺): 297.0621, found: 297.0652.

2-(4-Nitrophenoxy)-5-propylphenol (8): Method A was used to prepare the intermediate **8a** from 2-methoxy-4-propylphenol (1.00 g, 6.3 mmol), 1-fluoro-4-nitrobenzene (0.89 g, 6.3 mmol) and K₂CO₃ (1.80 g, 12.6 mmol) in 93% yield, and method D was used to convert it to the title compound. Purification by flash chromatography (10% EtOAc/hexanes) gave **8** as a yellow solid (96%). ¹H NMR (400 MHz, CDCl₃): δ = 0.99 (t, *J* = 3.2 Hz, 3H), 1.65 (q, *J* = 3.6 Hz, 2H), 2.59 (t, *J* = 3.6 Hz, 2H), 6.77 (d, *J* = 8.0 Hz, 1H), 6.90–6.91 (m, 2H), 7.07 (d, *J* = 9.2 Hz, 2H), 8.21 ppm (d, *J* = 1.2 Hz, 2H); ¹³C NMR (100 MHz, CDCl₃): δ = 13.4, 23.9, 37.2, 116.1, 116.8, 120.3, 120.9, 125.6, 138.6, 141.5, 146.9, 162.5 ppm; HRMS (ESI[−]): *m/z* calcd for C₁₅H₁₅NO₄ ([*M*−H][−]): 272.0928, found: 272.0925.

2-(3-Nitrophenoxy)-5-propylphenol (9): Method A was used to prepare the intermediate **9a** from 2-methoxy-4-propylphenol (1.00 g, 6.3 mmol), 1-fluoro-3-nitrobenzene (0.89 g, 6.3 mmol) and K₂CO₃ (1.8 g, 12.6 mmol) in 65% yield, and method D was used to convert it to the title compound. Purification by flash chromatography (5% EtOAc/hexanes) gave **9** as a yellow solid (83%). ¹H NMR (400 MHz, CDCl₃): δ = 0.99 (t, *J* = 7.2 Hz, 3H), 1.67 (quin, *J* = 7.6 Hz, 2H), 2.59 (t, *J* = 7.6 Hz, 2H), 5.37 (s, 1H), 6.76 (dd, *J* = 4.0, *J* = 2.0 Hz, 1H), 6.89 (d, *J* = 8.0 Hz, 1H), 6.93 (d, *J* = 1.6 Hz, 1H), 7.36 (dd, *J* = 5.0, *J* = 2.0 Hz, 1H), 7.50 (t, *J* = 8.2 Hz, 1H), 7.83 (t, *J* = 2.0 Hz, 1H), 7.96 ppm (dd, *J* = 4.0, *J* = 1.0 Hz, 1H); ¹³C NMR (100 MHz, CDCl₃): δ = 13.4, 23.9, 37.1, 111.5, 116.7, 117.3, 119.6, 120.8, 122.7, 129.9, 139.2, 141.0, 146.9, 148.8, 157.9 ppm; HRMS (ESI[−]): *m/z* calcd for C₁₅H₁₅NO₄ ([*M*−H][−]): 272.0928, found: 272.0926.

2-(2,4-Dinitrophenoxy)-5-propylphenol (10): Method A was used to prepare the intermediate **10a** from 2-methoxy-4-propylphenol (0.50 g, 3.0 mmol), 1-fluoro-2,4-dinitrobenzene (0.56 g, 3.0 mmol) and K₂CO₃ (0.84 g, 6.0 mmol) in 93% yield, and method D was used to convert it to the title compound. Purification by flash chromatography (10% EtOAc/hexanes) gave **10** as a yellow solid (81%). ¹H NMR (400 MHz, CDCl₃): δ = 0.95 (t, *J* = 7.2 Hz, 3H), 1.65 (quin, *J* = 7.2 Hz, 2H), 2.59 (t, *J* = 7.2 Hz, 2H), 5.72 (s, 1H), 6.83 (d, *J* = 8.2 Hz, 1H), 7.02 (s, 1H), 7.06–7.04 (m, 1H), 7.18–7.13 (m, 1H), 8.36 (dd, *J* = 4.0, *J* = 3.0 Hz, 1H), 8.84 ppm (t, *J* = 2.8 Hz, 1H); ¹³C NMR (100 MHz, CDCl₃): δ = 13.3, 24.0, 36.9, 117.4, 117.5, 120.8, 121.2, 121.6, 127.6, 128.7, 136.2, 137.8, 141.2, 142.9, 144.8, 146.8, 155.4 ppm; HRMS (ESI[−]): *m/z* calcd for C₁₅H₁₄N₂O₆ ([*M*−H][−]): 317.0779, found: 317.0776.

2-(2-Chloro-4-nitrophenoxy)-5-propylphenol (11): Method A was used to prepare the intermediate **11a** from 2-methoxy-4-propylphenol (0.50 g, 3.0 mmol), 2-chloro-1-fluoro-4-nitrobenzene (0.53 g, 3.0 mmol) and K₂CO₃ (0.84 g, 6.1 mmol) in 93% yield, and method D was used to convert it to the title compound. Purification by flash chromatography (10% EtOAc/hexanes) gave **11** as a pale yellow solid (82%). ¹H NMR (400 MHz, CDCl₃): δ = 0.97 (t, *J* = 7.2 Hz, 3H), 1.66 (quin, *J* = 7.6 Hz, 2H), 2.57 (t, *J* = 7.6 Hz, 2H), 5.55 (s, 1H), 6.77 (dd, *J* = 4.0, *J* = 2.0 Hz, 1H), 6.91–6.89 (m, 3H), 8.02 (dd, *J* = 5.0, *J* = 2.0 Hz, 1H), 8.33 ppm (d, *J* = 2.0 Hz, 1H); ¹³C NMR (100 MHz, CDCl₃): δ = 13.4, 23.9, 37.1, 115.3, 117.1, 120.2, 121.1, 123.3, 123.5, 125.9, 138.5, 141.9, 142.1, 146.7, 158.3 ppm; HRMS (ESI[−]): *m/z* calcd for C₁₅H₁₄ClNO₄ ([*M*−H][−]): 306.0539, found: 306.0541.

3-Chloro-4-(2-hydroxy-4-propylphenoxy)benzonitrile (12): Method A was used to prepare the intermediate **12a** from 2-methoxy-4-propylphenol (1.00 g, 6.3 mmol), 3-chloro-4-fluorobenzonitrile (0.94 g, 6.0 mmol) and K₂CO₃ (1.7 g, 12.0 mmol) in 80% yield, and method D was used to convert it to the title compound. Purification by flash chromatography (10% EtOAc/hexanes) gave **12** as a white crystalline solid (79%). ¹H NMR (400 MHz, CDCl₃): δ = 7.76 (d, *J* = 2.0 Hz, 1H), 7.47 (dd, *J* = 4.0, *J* = 2.0 Hz, 1H), 6.93–6.87 (m, 3H), 6.78–6.75 (m, 1H), 5.42 (s, 1H), 2.58 (t, *J* = 7.6 Hz, 2H), 1.67 (quin, *J* = 7.6 Hz, 2H), 0.98 ppm (t, *J* = 7.2 Hz, 3H); ¹³C NMR (100 MHz, CDCl₃): δ = 13.4, 23.9, 37.1, 106.3, 116.4, 117.0, 120.1, 120.9, 124.1, 131.8, 133.8, 138.5, 141.7, 146.9, 156.9 ppm; HRMS (ESI[−]): *m/z* calcd for C₁₆H₁₄ClNO₂ ([*M*−H][−]): 286.0640, found: 286.0637.

2-[3-(2-Hydroxy-ethyl)phenoxy]-5-propylphenol (13): Method B was used to prepare the intermediate **13a** from 2-methoxy-4-propylphenol (1 g, 6.0 mmol) and 3-bromostyrene (1.32 g, 7.2 mmol) (62%). Compound **13a** was treated with BH₃·THF (1 M in anhyd THF, 0.5 equiv) and the reaction was stirred at RT (3 h). The reaction was cooled to 0 °C and treated dropwise with aq NaOH (7 mL, 3 M), then hydrogen peroxide (4 mL, 30%), and stirred at RT (12 h) before work-up. Purification using flash column chromatography (2% MeOH/CHCl₃) gave **13b** (68%), and method D was used to convert it to the title compound. Purification by flash chromatography (5% EtOAc/hexanes) gave **13** as a colorless oil (75%).

¹H NMR (400 MHz, CDCl₃): δ = 0.98 (t, J = 7.2 Hz, 3H), 1.67 (t, J = 7.6 Hz, 2H), 2.57 (t, J = 7.6 Hz, 2H), 3.16 (t, J = 7.6 Hz, 2H), 3.57 (t, J = 7.2 Hz, 2H), 5.47 (s, 1H), 6.69 (dd, J = 4.0 Hz, J = 2.0 Hz, 1H), 6.84 (d, J = 8.4 Hz, 1H), 6.93–6.89 (m, 3H), 6.97 (d, J = 7.2 Hz, 1H), 7.30 ppm (t, J = 7.2 Hz, 1H); ¹³C NMR (100 MHz, CDCl₃): δ = 13.9, 24.5, 32.6, 37.6, 39.1, 116.0, 116.3, 117.8, 119.1, 120.7, 123.6, 129.9, 140.0, 140.9, 141.0, 147.3, 157.5 ppm; HRMS (ESI[−]): m/z calcd for C₁₇H₁₉BrO₂ ([M −H][−]): 333.0496, found: 333.0492.

5-Chloro-2-phenoxybenzoic acid (14): Method A was used to prepare the intermediate **14a** from 5-chloro-2-fluorobenzonitrile (1.00 g, 6.4 mmol), phenol (0.66 g, 7.0 mmol) and K₂CO₃ (1.8 g, 12.8 mmol) (75%). A solution of **14a** (0.20 g, 0.9 mmol) in aq NaOH (0.4 mL, 25%) and EtOH (2 mL) was refluxed (20 h), then cooled to RT and acidified with dil HCl; the crude product was isolated by filtration. Purification by flash chromatography (6% MeOH/CHCl₃) gave **14** as a white solid (143 mg, 64%). ¹H NMR (400 MHz, CD₃OD): δ = 6.95 (m, 3H), 7.1 (t, J = 8.0 Hz, 1H), 7.33 (t, J = 8.0 Hz, 2H), 7.46 (dd, J = 9.0, J = 3.0 Hz, 1H), 7.84 ppm (d, J = 2.0 Hz, 1H); ¹³C NMR (100 MHz, CD₃OD): δ = 119.6, 123.1, 124.8, 129.6, 131.1, 132.4, 134.4, 156.5, 158.6 ppm; MS (ESI) m/z : 249 [M +H]⁺; HRMS (ESI⁺): m/z calcd for C₁₃H₉ClO₃ ([M +Na]⁺): 271.0133, found: 271.0129.

3-Chloro-4-(2-hydroxy-4-propylphenoxy)benzamide (15): A solution of **12** (0.38 g, 1.3 mmol), hydrogen peroxide (1 mL, 30%) and aq NaOH (0.18 mL, 3 M) in EtOH was stirred at 35 °C (20 h), then acidified with H₂SO₄ (1 N). The organic solvent was removed in vacuo and the resulting suspension diluted with EtOAc. The two phases were separated and the organic phase washed with water, then brine, dried (Na₂SO₄), filtered and concentrated in vacuo to give the crude product. Purification by flash chromatography (3% MeOH/CHCl₃) gave **15** as a white solid (65%). ¹H NMR (400 MHz, CD₃OD): δ = 0.91 (t, J = 7.6 Hz, 3H), 1.58 (quin, J = 7.6 Hz, 2H), 2.50 (t, J = 7.6 Hz, 2H), 6.62 (d, J = 8.0 Hz, 1H), 6.68 (dd, J = 4.0, J = 2.0 Hz, 1H), 6.82 (d, J = 2.0 Hz, 1H), 6.95 (d, J = 8.0 Hz, 1H), 7.39 (br s, 1H), 7.73 (dd, J = 4.0, J = 2.0 Hz, 1H), 7.97 (br s, 1H), 8.03 ppm (d, J = 2.0 Hz, 1H); ¹³C NMR (100 MHz, CDCl₃): δ = 115.5, 117.7, 120.2, 121.5, 122.3, 128.3, 129.1, 129.9, 139.7, 141.1, 149.1, 156.3, 166.6 ppm; HRMS (ESI[−]): m/z calcd for C₁₆H₁₆ClNO₃ ([M −H][−]): 304.0746, found: 304.0743.

5-Chloro-2-phenoxyphenylmethanol (16): A solution of BF₃·Et₂O (17 μ L, 0.13 mmol) in THF (2 mL) was added slowly to a solution of NaBH₄ (0.012 g, 0.31 mmol) and **14** (0.051 g, 0.21 mmol) in THF (1 mL) at RT under an inert atmosphere. The mixture was held at reflux (1 h) before it was cooled to 0 °C, and quenched with water and stirred (10 min). The organic solvent was removed in vacuo, and CH₂Cl₂ was added to the aqueous phase. After stirring (1 h), the organic layer was separated, washed with brine, dried (Na₂SO₄), filtered and concentrated in vacuo. Purification by flash chromatography (18% EtOAc/hexanes) gave **16** as a white solid (39 mg, 80%). ¹H NMR (400 MHz, CDCl₃): δ = 2.11 (br s, 1H), 4.72 (s, 2H), 6.79 (d, J = 9.0 Hz, 1H), 6.96 (d, J = 8.0 Hz, 2H), 7.12 (t, J = 8.0 Hz, 1H), 7.20 (dd, J = 8.0, J = 2.0 Hz, 1H), 7.34 (t, J = 8.0 Hz, 2H), 7.47 ppm (d, J = 3.0 Hz, 1H); ¹³C NMR (100 MHz, CDCl₃): δ = 60.7, 118.6, 119.9, 123.4, 129.0, 129.1, 130.2, 133.9, 153.3, 157.0 ppm; HRMS (ESI⁺): m/z calcd for C₁₃H₁₁ClO₂ ([M]⁺): 234.0448, found: 234.0458.

5-Chloro-2-phenoxybenzamide (17): A solution of **14a** (0.20 g, 0.9 mmol), hydrogen peroxide (0.37 mL, 35%) and aq NaOH (0.36 mL, 3 M) in EtOH (5 mL) was stirred at 30 °C (18 h), then acidified with H₂SO₄ (1 N); the crude product was isolated by filtration. Purification by flash chromatography (60% EtOAc/hexanes) gave

17 as a white solid (171 mg, 70%). ¹H NMR (400 MHz, CDCl₃): δ = 6.55 (br s, 1H), 6.76 (d, J = 8.0 Hz, 1H), 7.07 (d, J = 6.0 Hz, 2H), 7.26 (t, J = 8.0 Hz, 1H), 7.34 (dd, J = 9.0, J = 3.0 Hz, 1H), 7.42 (t, J = 8.0 Hz, 2H), 7.55 (br s, 1H), 8.24 ppm (d, J = 2.0 Hz, 1H). ¹³C NMR (100 MHz, CDCl₃): δ = 119.6, 120.0, 125.4, 129.2, 130.6, 132.4, 133.2, 154.9, 133.2, 165.0 ppm; MS (ESI⁺): m/z 248 [M +H]⁺; HRMS (ESI⁺): m/z calcd for C₁₃H₁₀ClNO₂ ([M +Na]⁺): 270.0293, found 270.0286.

N-[4-(4-Chloro-2-hydroxyphenoxy)phenyl]acetamide (18): The intermediate **20a** (0.14 g, 0.6 mmol), prepared as described in the synthesis of **20**, was treated with Ac₂O (0.07 g, 0.7 mmol), catalytic DMAP and Et₃N (0.07 g, 0.7 mmol) in CH₂Cl₂ (2 mL) at 0 °C (3 h), and method D was used to convert it to the title compound. Purification by flash chromatography (3% MeOH/CHCl₃) gave **18** as a white solid (92%). ¹H NMR (400 MHz, CD₃OD): δ = 2.11 (s, 3H), 7.00–6.78 (m, 5H), 7.52–7.45 ppm (m, 2H); ¹³C NMR (100 MHz, CD₃OD): δ = 21.9, 116.4, 116.9, 119.0, 120.6, 121.2, 121.3, 124.2, 128.6, 133.1, 142.6, 149.2, 153.6, 169.8 ppm; HRMS (ESI[−]): m/z calcd for C₁₄H₁₂ClNO₃ ([M −H][−]): 276.0433, found: 276.0432.

N-[2-(4-Chloro-2-hydroxyphenoxy)phenyl]acetamide (19): Method A was used to prepare the intermediate **5a** from 4-chloro-2-methoxyphenol (1.00 g, 6.3 mmol), 1-fluoro-2-nitrobenzene (0.89 g, 6.3 mmol) and K₂CO₃ (1.80 g, 12.6 mmol) in 96% yield. A mixture of **5a** (1.70 g, 6.1 mmol) and 10% Pd/C (0.30 mg) in EtOH (24 mL) was stirred at RT under H₂ (6 h). The reaction was filtered through Celite, the filter pad was washed with EtOH and the filtrate was concentrated in vacuo. Purification by flash chromatography (10% EtOAc/hexane) gave **19a** as a brown liquid (0.82 g, 92%). A solution of **19a** (0.12 g, 0.47 mmol) in CH₂Cl₂ (3 mL) was treated with Ac₂O (0.06 g, 0.56 mmol), catalytic DMAP (0.006 g) and Et₃N (0.06 g, 0.56 mmol) at 0 °C and stirred (3 h) to give **N**-[2-(4-chloro-2-methoxyphenoxy)-phenyl]acetamide (85%), and method D was used to convert it to the title compound. Purification by flash chromatography (3% MeOH/CHCl₃) gave **19** as a white solid (92%). ¹H NMR (400 MHz, CD₃OD): δ = 2.17 (s, 3H), 6.73 (dd, J = 4.0, J = 1 Hz, 1H), 6.84 (dd, J = 4.0, J = 2.0 Hz, 1H), 6.98–6.93 (m, 2H), 7.09–7.03 (m, 2H), 7.76 ppm (dd, J = 3.0, J = 1 Hz, 1H); ¹³C NMR (100 MHz, CD₃OD): δ = 21.7, 115.1, 116.7, 119.1, 121.7, 122.2, 123.8, 125.1, 127.1, 129.5, 141.5, 149.0, 149.3, 170.3 ppm; HRMS (ESI[−]): m/z calcd for C₁₄H₁₂ClNO₃ ([M −H][−]): 276.0433, found: 276.0429.

2-(4-Aminophenoxy)-5-chlorophenol (20): Method A was used to prepare intermediate **4a** from 4-chloro-2-methoxyphenol (1.00 g, 6.3 mmol), 1-fluoro-4-nitrobenzene (0.89 g, 6.3 mmol) and K₂CO₃ (1.8 g, 12.6 mmol) in 96% yield. A mixture of **4a** (1.00 g, 3.6 mmol) and 10% Pd/C (0.36 g) in EtOH (20 mL) was stirred at RT under H₂ (4 h). The reaction was filtered through Celite, the filter pad was washed with MeOH and the filtrate was concentrated in vacuo. Purification by flash chromatography (20% EtOAc/hexanes) gave **20a** as a brown liquid (0.82 g, 92%). Method D was used to convert **20a** to the title compound. Purification by flash chromatography (20% EtOAc/hexanes) gave **20** as brown solid (82%). ¹H NMR (400 MHz, (CD₃)₂SO): δ = 4.89 (br s, 2H), 6.54 (d, J = 8.8 Hz, 2H), 6.67 (d, J = 8.8 Hz, 2H), 6.74 (dd, J = 4.0, J = 2.0 Hz, 2H), 6.90 ppm (d, J = 2.4 Hz, 2H); ¹³C NMR (100 MHz, CD₃OD): δ = 115.3, 116.9, 119.3, 119.5, 119.7, 119.9, 126.8, 145.2, 145.5, 147.3, 149.5 ppm; HRMS (ESI⁺): m/z calcd for C₁₂H₁₀ClNO₂ ([M +H]⁺): 236.0473, found: 236.0471.

2-(4-Aminophenoxy)-5-propylphenol (21): Method A was used to prepare the intermediate **8a** from 2-methoxy-4-propylphenol (1.00 g, 6.3 mmol), 1-fluoro-4-nitrobenzene (0.89 g, 6.3 mmol) and K₂CO₃ (1.80 g, 12.6 mmol) in 93% yield. A mixture of **8a** (1.00 g,

3.6 mmol) and 10% Pd/C (0.36 g) in MeOH (20 mL) was stirred at RT under H₂ (4 h). The reaction mixture was filtered through Celite, the filter pad was washed with MeOH and the filtrate was concentrated in vacuo. Purification by flash chromatography (20% EtOAc/hexanes) gave **21a** as a brown liquid (0.82 g, 92%). Method D was used to convert **21a** to the title compound. Purification by flash chromatography (3% MeOH/CHCl₃) gave **21** as a grey solid (84%). ¹H NMR (400 MHz, CDCl₃): δ = 0.96 (t, *J* = 7.6 Hz, 3H), 1.65 (quin, *J* = 7.6 Hz, 2H), 2.53 (t, *J* = 7.6 Hz, 2H), 6.62 (d, *J* = 8.0 Hz, 1H), 6.71–6.67 (m, 3H), 6.89–6.87 ppm (m, 3H); ¹³C NMR (100 MHz, CDCl₃): δ = 13.4, 24.1, 37.1, 115.3, 115.9, 116.6, 119.4, 119.8, 138.1, 142.1, 142.5, 146.2, 148.6 ppm; HRMS (ESI[−]): *m/z* calcd for C₁₅H₁₇NO₂ ([*M*−H][−]): 242.1236, found: 242.1238.

4-(4-Chloro-2-hydroxyphenoxy)-1-(4-methylphenylsulphonamido) benzene (22): A solution of **20a** (0.16 g, 0.63 mmol) in anhyd CH₂Cl₂ (3 mL) was cooled to 0 °C and treated with Et₃N (0.2 mL, 1.25 mmol). The reaction was stirred (10 min) and then treated with TsCl (0.18 g, 0.94 mmol), and stirring was continued at RT (3 h). The reaction was quenched with HCl (10 mL, 1 M), diluted with EtOAc (100 mL), the organic layer was separated and the aqueous layer was extracted with EtOAc (×2). The combined organic layers were washed with water then brine, dried (Na₂SO₄), filtered and concentrated in vacuo, and method D was used to convert the crude intermediate to the title compound. Purification by flash chromatography (22% EtOAc/hexanes) gave **22** as a white solid (122 mg, 50%). ¹H NMR (300 MHz, CDCl₃): δ = 2.41 (s, 3H), 5.66 (s, 1H), 6.68 (s, 1H), 6.72 (d, *J* = 9.0 Hz, 1H), 6.81 (dd, *J* = 9.0, *J* = 2.0 Hz, 1H), 6.90 (m, 2H), 7.04 (m, 3H), 7.26 (d, *J* = 8.0 Hz, 2H), 7.64 ppm (d, *J* = 9.0 Hz, 2H); ¹³C NMR (75 MHz, CDCl₃): δ = 21.8, 116.9, 118.9, 119.6, 120.8, 124.7, 127.5, 129.9, 136.2, 142.3, 144.2, 154.5 ppm; MS (ESI[−]): *m/z* 412 [*M*+Na]⁺; HRMS (ESI[−]): *m/z* calcd for C₁₉H₁₅ClNO₄S ([*M*−H][−]): 388.0416, found 388.0415.

5-Chloro-2-(pyridin-3-yloxy)phenol (23): Method B was used to prepare the intermediate **23a** from 4-chloro-2-methoxyphenol (1 g, 6.3 mmol), KOtBu (0.85 g, 7.6 mmol), (CuOTf)₂·PhH (0.33 g, 0.63 mmol) and 3-iodopyridine (1.60 g, 7.6 mmol) in 48% yield, and method D was used to convert the crude intermediate to the title compound. Purification by flash chromatography (3% MeOH/CHCl₃) gave **23** as an off-white solid (52%). ¹H NMR (400 MHz, CD₃OD): δ = 4.83 (s, 1H), 5.56 (s, 1H), 6.36 (dd, *J* = 8.0, *J* = 2.0 Hz, 1H), 6.58 (d, *J* = 2.8 Hz, 1H), 6.88 (dd, *J* = 4.0, *J* = 2.0 Hz, 1H), 7.03–6.97 (m, 2H), 7.39–7.29 (m, 2H), 8.23 ppm (br s, 2H); ¹³C NMR (100 MHz, CD₃OD): δ = 116.7, 119.3, 122.2, 123.3, 124.1, 130.2, 137.8, 140.6, 141.9, 149.8 ppm; HRMS (ESI[−]): *m/z* calcd for C₁₁H₈ClNO₂ ([*M*−H][−]): 220.0171, found: 220.0170.

***N*-[5-(4-Chloro-2-hydroxyphenoxy)-pyridin-2-yl]acetamide (24):** Method B was used to prepare the intermediate **24a** from 4-chloro-2-methoxyphenol (1.00 g, 6.3 mmol), *N*-(5-iodo-pyridin-2-yl)acetamide (1.4 g, 5.3 mmol), KOtBu (0.78 g, 7.0 mmol) and (CuOTf)₂·PhH (0.49 g, 0.95 mmol) in 15% yield, and method D was used to convert it to the title compound. Purification by flash chromatography (8% MeOH/CHCl₃) gave **24** as a white solid (60%). ¹H NMR (400 MHz, CDCl₃): δ = 2.16 (s, 3H), 6.84 (dd, *J* = 4.0, *J* = 2.0 Hz, 1H), 6.93–6.98 (m, 2H), 7.31 (dd, *J* = 8.0, *J* = 3.0 Hz, 1H), 7.98 (d, *J* = 2.8 Hz, 1H), 8.02 ppm (d, *J* = 8.9 Hz, 1H); ¹³C NMR (100 MHz, CDCl₃): δ = 114.9, 117.0, 119.6, 119.9, 120.7, 121.6, 125.4, 125.9, 126.0, 129.9, 136.6, 136.7, 142.2, 146.6, 148.9, 149.8, 151.1, 170.3 ppm; HRMS (ESI[−]): *m/z* calcd for C₁₃H₁₁ClN₂O₃ ([*M*−H][−]): 277.0385, found: 277.0384.

5-Chloro-2-(pyrazin-2-yloxy)phenol (25): Method B was used to prepare the intermediate **25a** from 4-chloro-2-methoxyphenol

(1.00 g, 6.3 mmol), 2-iodopyrazine (1.10 g, 5.3 mmol), KOtBu (0.78 g, 7.0 mmol) and (CuOTf)₂·PhH (0.49 g, 0.95 mmol) in 67% yield, and method D was used to convert it to the title compound. Purification by flash chromatography (3% MeOH/CHCl₃) gave **25** as a white solid (73%). ¹H NMR (400 MHz, CD₃OD): δ = 6.88 (dd, *J* = 4.0, *J* = 3.0 Hz, 1H), 6.96 (d, *J* = 2.4 Hz, 1H), 7.09 (d, *J* = 8.8 Hz, 1H), 8.1 (dd, *J* = 2.0, *J* = 1.0 Hz, 1H), 8.25 (d, *J* = 2.8 Hz, 1H), 8.41 ppm (d, *J* = 1.6 Hz, 1H); ¹³C NMR (100 MHz, CD₃OD): δ = 116.4, 117.2, 118.9, 122.5, 123.3, 125.7, 130.5, 134.4, 137.4, 137.5, 140.6 ppm; HRMS (ESI[−]): *m/z* calcd for C₁₀H₇ClN₂O₂ ([*M*−H][−]): 221.0123, found: 221.0123.

3-(3-Hydroxy-4-phenoxyphenyl)propane-1,2-diol (26): A solution of **27a** (0.10 g, 0.41 mmol) in THF (20 mL) was treated with *N*-methyl-morpholine *N*-oxide (0.20 g, 1.66 mmol) and OsO₄ (0.24 mL, 0.038 mmol, 4 wt.% in H₂O) and stirred until completion (12 h). The reaction was poured into aq Na₂SO₃ (50 mL, 15%) and extracted with CH₂Cl₂. The organic phase was washed with brine, dried (MgSO₄), filtered and concentrated in vacuo. Conversion of the crude intermediate using method D gave **26** as a viscous colorless oil without the need for further purification (31 mg, 28%). ¹H NMR (400 MHz, CDCl₃): δ = 2.75 (t, *J* = 7.7 Hz, 2H), 3.58–3.54 (m, 1H), 3.75–3.72 (m, 1H), 3.97 (br s, 1H), 5.47 (s, 1H), 6.68 (dd, *J* = 8.0, *J* = 1.0 Hz, 1H), 6.82 (d, *J* = 8.1 Hz, 1H), 5.66 (s, 1H), 6.72 (dd, *J* = 8.0, *J* = 1.0 Hz, 1H), 6.85 (d, *J* = 8.2 Hz, 1H), 6.95 (s, 1H), 7.04 (d, *J* = 8.0 Hz, 2H), 7.14 (t, *J* = 7.3 Hz, 1H), 7.36 ppm (t, *J* = 7.8 Hz, 2H); ¹³C NMR (100 MHz, CDCl₃): δ = 39.2, 66.0, 72.8, 116.8, 117.8, 118.9, 121.3, 123.6, 129.8, 134.4, 142.1, 147.4 ppm; HRMS (ESI[−]): *m/z* calcd for C₁₅H₁₆O₄ ([*M*−H][−]): 259.0975, found: 259.0978.

2-Phenoxy-5-propylphenol (27): A suspension of **27a** (0.10 g, 0.41 mmol) and 10% Pd/C (0.02 g) in EtOAc (5 mL) was stirred under H₂ at RT (4 h). The reaction was filtered through Celite, the filter pad was washed with EtOAc, and the filtrate was concentrated in vacuo. Method D was used to convert the crude intermediate to the title compound. Purification by preparative TLC (30% EtOAc/hexanes) gave **27** as an off-white solid (54 mg, 71%). ¹H NMR (400 MHz, CDCl₃): δ = 0.97 (t, *J* = 7.3 Hz, 3H), 1.69–1.62 (m, 2H), 2.56 (t, *J* = 7.5 Hz, 2H), 5.49 (s, 1H), 6.68 (dd, *J* = 8.0, *J* = 1.0 Hz, 1H), 6.83 (d, *J* = 8.2 Hz, 1H), 6.90 (d, *J* = 1.6 Hz, 1H), 7.03 (d, *J* = 7.8 Hz, 2H), 7.12 (t, *J* = 7.3 Hz, 1H), 7.35 ppm (t, *J* = 7.7 Hz, 2H); ¹³C NMR (100 MHz, CDCl₃): δ = 13.7, 24.4, 37.5, 116.0, 117.5, 118.9, 120.5, 123.2, 129.7, 139.8, 141.0, 147.2, 157.1 ppm; MS (ESI[−]): *m/z* 227 [*M*−H][−]; HRMS (ESI⁺): *m/z* calcd for C₁₅H₁₆O₂ ([*M*+H]⁺): 229.1223, found 229.1224.

5-Hydroxymethyl-2-phenoxyphenol (28): Method D was used to prepare the title compound from **28a** (0.08 g, 0.34 mmol) and BBr₃ (1 M, 6.9 mL, 6.9 mmol). Purification by preparative TLC (40% EtOAc/hexanes) gave **28** as a colorless oil (64 mg, 85%). ¹H NMR (400 MHz, CDCl₃): δ = 4.48 (s, 2H), 5.66 (s, 1H), 6.82 (d, *J* = 7.3 Hz, 1H), 6.89 (dd, *J* = 8.0, *J* = 2.0 Hz, 1H), 7.06 (d, *J* = 8.3 Hz, 2H), 7.12 (d, *J* = 2.0 Hz, 1H), 7.17 (t, *J* = 7.3 Hz, 1H), 7.38 ppm (t, *J* = 7.8 Hz, 2H); ¹³C NMR (100 MHz, CDCl₃): δ = 33.2, 116.7, 118.2, 118.4, 121.3, 124.0, 129.9, 134.0, 143.9, 147.2, 156.1 ppm; MS (ESI⁺): *m/z* 239 [*M*+Na]⁺.

5-[(1-Methyl-butylamino)methyl]-2-phenoxyphenol (29): Method D was used to prepare the title compound from **29a** (0.10 g, 0.33 mmol) and BBr₃ (1 M, 6.6 mL, 6.6 mmol). Purification by preparative TLC (10% MeOH/CH₂Cl₂) gave **29** as a colorless oil (65 mg, 68%). ¹H NMR (400 MHz, CDCl₃): δ = 0.91 (t, *J* = 7.4 Hz, 3H), 1.09 (d, *J* = 11.0 Hz, 3H), 1.41–1.34 (m, 1H), 1.58–1.51 (m, 1H), 2.67–2.62 (m, 1H), 3.78–3.67 (m, 2H), 6.79–6.77 (m, 1H), 6.84 (d, *J* = 8.1 Hz, 1H), 6.99 (d, *J* = 7.9 Hz, 2H), 7.01 (d, *J* = 1.4 Hz, 1H), 7.10 (d, *J* = 7.3 Hz,

1 H), 7.33 ppm (t, $J=7.8$ Hz, 2H); ^{13}C NMR (100 MHz, CDCl_3): $\delta=10.2, 19.5, 29.6, 50.7, 53.9, 116.6, 117.5, 119.2, 120.1, 123.1, 129.7, 137.4, 142.3, 147.7, 157.1, 165.0$ ppm.

2-Phenoxy-5-piperidin-1-ylmethylphenol (30): Method D was used to prepare the title compound from **30a** (0.07 g, 0.23 mmol) and BBr_3 (4.7 mL, 1 M in CH_2Cl_2). Purification by preparative TLC (1:10 MeOH/ CH_2Cl_2) gave **30** as a grey solid (34 mg, 50%). ^1H NMR (400 MHz, CDCl_3): $\delta=1.47$ (br s, 2H), 1.70–1.60 (m, 4H), 2.47 (br s, 4H), 3.49 (s, 2H), 6.83 (s, 2H), 7.03 (d, $J=7.8$ Hz, 2H), 7.12 (t, $J=7.3$ Hz, 1H), 7.07 (s, 1H), 7.35 ppm (t, $J=8.0$ Hz, 2H); ^{13}C NMR (100 MHz, CDCl_3): $\delta=24.1, 25.5, 54.2, 63.0, 117.2, 117.8, 118.6, 121.4, 123.4, 129.8, 142.5, 147.3, 156.9$ ppm; HRMS (ESI+): m/z calcd for $\text{C}_{18}\text{H}_{21}\text{NO}_2$ ($[\text{M}+\text{H}]^+$): 284.1645, found 284.1652.

5-(Benzylaminomethyl)-2-phenoxyphenol (31): Method D was used to prepare the title compound from **31a** (0.08 g, 0.25 mmol) and BBr_3 (1 M, 5 mL, 5.0 mmol). Purification by preparative TLC (10% MeOH/ CH_2Cl_2) gave **31** as a white solid (42 mg, 54%). ^1H NMR (400 MHz, CDCl_3): $\delta=3.78$ (s, 2H), 3.86 (s, 2H), 6.84 (s, 2H), 7.00 (d, $J=8.0$ Hz, 2H), 7.14–7.10 (m, 2H), 7.42–7.28 ppm (m, 7H); ^{13}C NMR (100 MHz, CDCl_3): $\delta=51.5, 52.0, 116.6, 117.8, 119.0, 120.6, 123.4, 127.5, 128.5, 128.6, 128.7, 129.8, 134.4, 137.6, 142.9, 147.7, 156.8$ ppm. HRMS (ESI–): m/z calcd for $\text{C}_{20}\text{H}_{19}\text{NO}_2$ ($[\text{M}-\text{H}]^-$): 304.1343, found: 304.1352.

2-[4-(2-Hydroxy-4-chlorophenoxy)phenoxy]-5-chlorophenol (32): Method C was used to prepare intermediate **32a** from 2-methoxy-4-propylphenol (0.20 g, 1.2 mmol) and benzene-1, 4-diboronic acid (0.20 g, 1.2 mmol). Purified by preparative TLC (30% EtOAc/hexanes) gave **32a** (35 mg, 7%). Method D was used to prepare the title compound from **32a** (0.03 g, 0.076 mmol) and BBr_3 (1 M, 1.5 mL, 1.5 mmol). Purification by preparative TLC (40% EtOAc/hexanes) gave **32** as a grey solid (12 mg, 43%). ^1H NMR (400 MHz, $(\text{CD}_3)_2\text{SO}$): $\delta=6.86$ – 6.83 (m, 6H), 6.93 (d, $J=7.5$ Hz, 2H), 6.98 (d, $J=2.3$ Hz, 2H), 10.06 ppm (s, 2H); ^{13}C NMR (100 MHz, $(\text{CD}_3)_2\text{SO}$): $\delta=117.3, 118.3, 119.7, 122.6, 128.5, 143.1, 150.4, 152.9$ ppm. HRMS (ESI–): m/z calcd for $\text{C}_{18}\text{H}_{12}\text{Cl}_2\text{O}_4$ ($[\text{M}-\text{H}]^-$): 361.0040, found: 361.0047.

2-[3-(2-Hydroxy-4-chlorophenoxy)phenoxy]-5-chlorophenol (33): Method C was used to prepare intermediate **33a** from 2-methoxy-4-propylphenol (0.20 g, 1.20 mmol), and benzene-1, 3-diboronic acid (0.20 g, 1.20 mmol). Purification by preparative TLC (30% EtOAc/hexanes) gave **33a** (207 mg, 41%). Method D was used to prepare the title compound from **33a** (0.1 g, 0.25 mmol) and BBr_3 (1 M, 5.1 mL, 5.1 mmol). Purification by preparative TLC (40% EtOAc/hexanes) gave **33** as a white solid (65 mg, 70%). ^1H NMR (400 MHz, CDCl_3): $\delta=0.96$ (t, $J=7.3$ Hz, 3H), 1.69–1.62 (m, 2H), 2.55 (t, $J=7.4$ Hz, 4H), 5.68 (s, 2H), 6.76–6.71 (m, 3H), 6.86 (s, 4H), 7.08 (t, $J=1.2$ Hz, 2H), 7.30 ppm (t, $J=8.2$ Hz, 1H); ^{13}C NMR (100 MHz, CDCl_3): $\delta=107.2, 111.9, 112.2, 116.4, 116.5, 119.1, 119.7, 120.4, 129.7, 130.5, 141.1, 147.7, 157.6$ ppm. HRMS (ESI–): m/z calcd for $\text{C}_{18}\text{H}_{12}\text{Cl}_2\text{O}_4$ ($[\text{M}-\text{H}]^-$): 361.0040, found: 361.0051.

2-[3-(2-Hydroxy-4-propylphenoxy)phenoxy]-5-propylphenol (34): Method C was used to prepare intermediate **34a** from 2-methoxy-4-propylphenol (0.20 g, 1.2 mmol) and benzene-1,3-diboronic acid (0.20 g, 1.2 mmol). Purification by preparative TLC (30% EtOAc/hexanes) gave **34a** (27 mg, 5%). Method D was used to prepare the title compound from **34a** (0.10 g, 0.24 mmol) and BBr_3 (1 M, 4.9 mL, 4.9 mmol). Purification by preparative TLC (40% EtOAc/hexanes) gave **34** as a viscous oil (67 mg, 71%). ^1H NMR (400 MHz, CDCl_3): $\delta=0.97$ (t, $J=7.3$ Hz, 6H), 1.70–1.60 (m, 4H), 2.56 (t, $J=7.4$ Hz, 4H), 5.40 (s, 2H), 6.75–6.65 (m, 5H), 6.86 (s, 1H), 6.88 (t, $J=1.8$ Hz, 3H), 7.27–7.22 ppm (m, 1H); ^{13}C NMR (100 MHz, CDCl_3): $\delta=$

13.3, 24.0, 37.1, 106.4, 111.3, 115.9, 119.0, 120.3, 130.1, 139.9, 146.8, 158.2 ppm; HRMS (ESI–): m/z calcd for $\text{C}_{24}\text{H}_{26}\text{O}_4$ ($[\text{M}-\text{H}]^-$): 377.1758, found: 377.1763.

2-[4-(2-Hydroxy-4-propylphenoxy)phenoxy]-5-propylphenol (35): Method C was used to prepare intermediate **35a** from 2-methoxy-4-propylphenol (0.20 g, 1.2 mmol) and benzene-1,4-diboronic acid (0.20 g, 1.2 mmol). Purification by preparative TLC (30% EtOAc/hexanes) gave **35a** (27 mg, 5%). Method D was used to prepare the title compound from **35a** (0.02 g, 0.049 mmol) and BBr_3 (1 M, 0.98 mL, 0.98 mmol). Purification by preparative TLC (40% EtOAc/hexanes) gave **35** as a viscous oil (13 mg, 69%). ^1H NMR (400 MHz, CDCl_3): $\delta=0.96$ (t, $J=7.3$ Hz, 6H), 1.70–1.60 (m, 4H), 2.55 (t, $J=7.4$ Hz, 4H), 5.51 (s, 2H), 6.67 (dd, $J=8.0, J=2.0$ Hz, 2H), 6.79 (d, $J=8.2$ Hz, 2H), 6.89 (d, $J=1.8$ Hz, 2H), 7.00 ppm (s, 4H); ^{13}C NMR (100 MHz, CDCl_3): $\delta=13.3, 24.0, 37.1, 115.6, 117.8, 118.7, 120.1, 139.2, 141.1, 146.5, 152.3$ ppm; HRMS (ESI–): m/z calcd for $\text{C}_{24}\text{H}_{26}\text{O}_4$ ($[\text{M}-\text{H}]^-$): 377.1758, found: 377.1747.

2-(Biphenyl-3-yloxy)-5-propylphenol (36): Method C was used to prepare intermediate **36a** from 4-propyl-2-methoxyphenol (0.10 g, 0.6 mmol) and 3-biphenylboronic acid (0.36 g, 1.8 mmol) in 46% yield. Method D was used to prepare the title compound from **36a** (0.08 g, 0.25 mmol) and BBr_3 (1 M, 5.0 mL, 5.0 mmol). Purification by preparative TLC (40% EtOAc/hexanes) gave **36** as a white solid (34 mg, 44%). ^1H NMR (400 MHz, CDCl_3): $\delta=0.99$ (t, $J=7.3$ Hz, 3H), 1.75–1.65 (m, 2H), 2.58 (t, $J=7.4$ Hz, 2H), 5.56 (s, 1H), 6.71 (d, $J=8.2$ Hz, 1H), 6.90 (d, $J=8.2$ Hz, 1H), 6.93 (s, 1H), 7.01 (d, $J=6.7$ Hz, 1H), 7.42–7.35 (m, 3H), 7.46 (t, $J=7.3$ Hz, 2H), 7.59 ppm (d, $J=7.4$ Hz, 2H); ^{13}C NMR (100 MHz, CDCl_3): $\delta=13.4, 24.0, 37.1, 115.7, 115.9, 116.0, 118.6, 120.2, 121.7, 126.7, 127.2, 128.4, 129.7, 139.5, 139.9, 140.6, 142.8, 146.8, 157.2$ ppm; HRMS (ESI+): m/z calcd for $\text{C}_{29}\text{H}_{34}\text{N}_4\text{O}_5$ ($[\text{M}+\text{H}]^+$): 519.2602, found: 519.2595.

3-(2-Hydroxy-4-propylphenoxy)benzoic acid methyl ester (37): Method C was used to prepare intermediate **37a** from 4-propyl-2-methoxyphenol (0.10 g, 0.6 mmol) and 3-(ethoxycarbonyl) phenylboronic acid (0.32 g, 1.8 mmol) in 41% yield. Method D was used to prepare the title compound from **37a** (0.07 g, 0.23 mmol) and BBr_3 (1 M, 4.6 mL, 4.6 mmol). Purification by preparative TLC (50% EtOAc/hexanes) gave **37** as a white solid (44 mg, 65%). ^1H NMR (400 MHz, CDCl_3): $\delta=0.97$ (t, $J=7.3$ Hz, 3H), 1.69–1.62 (m, 2H), 2.57 (t, $J=7.5$ Hz, 2H), 3.91 (s, 3H), 5.56 (s, 1H), 6.72 (dd, $J=8.0, J=2.0$ Hz, 1H), 6.82 (d, $J=8.2$ Hz, 1H), 6.91 (d, $J=1.8$ Hz, 1H), 7.22–7.19 (m, 1H), 7.40 (t, $J=8.0$ Hz, 1H), 7.68–7.67 (m, 1H), 7.77 ppm (d, $J=7.7$ Hz, 1H); ^{13}C NMR (100 MHz, CDCl_3): $\delta=13.7, 24.4, 37.5, 52.2, 116.4, 118.4, 119.0, 120.7, 121.9, 124.3, 129.8, 131.9, 140.3, 140.6, 147.2, 157.3, 166.4$ ppm; HRMS (ESI–): m/z calcd for $\text{C}_{17}\text{H}_{18}\text{O}_4$ ($[\text{M}-\text{H}]^-$): 285.1132, found: 285.1139.

2-(3-Hydroxymethyl-phenoxy)-5-propylphenol (38): Method C was used to prepare intermediate **38a** from 4-propyl-2-methoxyphenol (0.10 g, 0.6 mmol) and 3-(hydroxymethyl) phenylboronic acid (0.27 g, 1.8 mmol) in 18% yield. Method D was used to prepare the title compound from **38a** (0.03 g, 0.11 mmol) and BBr_3 (1 M, 2.2 mL, 2.2 mmol). Purification by preparative TLC (60% EtOAc/hexanes) gave **38** as an oil (12 mg, 42%). ^1H NMR (300 MHz, CDCl_3): $\delta=0.98$ (t, $J=7.3$ Hz, 3H), 1.78–1.62 (m, 2H), 2.57 (t, $J=7.4$ Hz, 2H), 5.45 (s, 1H), 6.70 (dd, $J=8.0, J=2.0$ Hz, 1H), 6.84 (d, $J=8.2$ Hz, 1H), 6.91 (d, $J=1.8$ Hz, 1H), 6.94 (dd, $J=8.0, J=2.0$ Hz, 1H), 7.06 (d, $J=1.9$ Hz, 1H), 7.14 (d, $J=7.6$ Hz, 1H), 7.29 ppm (d, $J=8.8$ Hz, 1H); ^{13}C NMR (100 MHz, CDCl_3): $\delta=13.8, 24.4, 32.7, 37.5, 116.2, 117.3, 117.9, 119.1, 120.7, 123.8, 125.8, 130.1, 139.7, 140.2, 140.5, 147.2, 157.4$ ppm; MS (ESI–): m/z 257 $[\text{M}-\text{H}]^-$.

3-(2-Hydroxy-4-propylphenoxy)benzoic acid (39): A solution of **37** (0.02 g, 0.073 mmol) in MeOH/H₂O (10 mL, 1:1) was treated with LiOH·H₂O (0.03 g, 0.73 mmol) and stirred at RT (2 h). The reaction was acidified with saturated aq. KHSO₄ and extracted with EtOAc. The organic phase was washed with brine, dried (Na₂SO₄), filtered and concentrated in vacuo. Purification by preparative TLC (1:10 MeOH/CH₂Cl₂) gave **39** as a white solid (11 mg, 55%). ¹H NMR (300 MHz, CDCl₃): δ = 0.98 (t, *J* = 7.3 Hz, 3H), 1.70–1.60 (m, 2H), 2.57 (t, *J* = 7.5 Hz, 2H), 6.71 (dd, *J* = 8, *J* = 1 Hz, 1H), 6.84 (d, *J* = 8.2 Hz, 1H), 6.92 (d, *J* = 1.5 Hz, 1H), 7.27 (dd, *J* = 8, *J* = 2 Hz, 1H), 7.45 (t, *J* = 8.0 Hz, 1H), 7.74 (s, 1H), 7.86 ppm (d, *J* = 7.6 Hz, 1H); ¹³C NMR (100 MHz, CDCl₃): δ = 13.7, 24.4, 37.5, 116.4, 118.8, 119.1, 120.8, 122.8, 124.9, 129.9, 130.2, 131.0, 140.4, 147.2, 157.4, 171.2 ppm; HRMS (ESI[−]): *m/z* calcd for C₁₆H₁₆O₄ ([*M*−H][−]): 271.0975, found: 271.0982.

1-[4-(2-Hydroxy-4-propylphenoxy)phenyl]ethanone (40): Method C was used to prepare intermediate **40a** from 2-methoxy-4-propylphenol (0.10 g, 0.6 mmol) and 4-acetylphenylboronic acid (0.30 g, 1.8 mmol) in 39% yield. Method D was used to prepare the title compound from **40a** (0.06 g, 0.21 mmol) and BBr₃ (1 M, 4.2 mL, 4.2 mmol). Purification by preparative TLC (40% EtOAc/hexanes) gave **40** as a grey solid (42 mg, 73%). ¹H NMR (400 MHz, CDCl₃): δ = 0.98 (t, *J* = 7.2 Hz, 3H), 1.75–1.62 (m, 2H), 2.60–2.50 (m, 5H), 5.37 (s, 1H), 6.74 (d, *J* = 8.0 Hz, 1H), 6.90 (d, *J* = 8.5 Hz, 1H), 6.92 (s, 1H), 7.05 (d, *J* = 8.5 Hz, 2H), 7.96 ppm (d, *J* = 8.5 Hz, 2H); ¹³C NMR (100 MHz, CDCl₃): δ = 13.7, 24.4, 26.4, 37.5, 116.4, 116.6, 120.1, 120.9, 130.6, 132.2, 139.5, 141.1, 147.4, 161.5, 196.6 ppm; HRMS (ESI[−]): *m/z* calcd for C₁₇H₁₈O₃ ([*M*−H][−]): 269.1183, found: 269.1188.

2-(4-Methylsulfonylphenoxy)-5-propylphenol (41): Method D was used to prepare the title compound from **41a** (0.05 g, 0.17 mmol) and BBr₃ (1 M, 3.4 mL, 3.4 mmol). Purification by preparative TLC (40% EtOAc/hexanes) gave **41** as a grey solid (32 mg, 67%). ¹H NMR (400 MHz, CDCl₃): δ = 0.97 (t, *J* = 7.2 Hz, 3H), 1.72–1.62 (m, 2H), 2.49 (s, 3H), 2.56 (t, *J* = 6.4 Hz, 2H), 5.47 (s, 1H), 6.67 (d, *J* = 8.2 Hz, 1H), 6.80 (d, *J* = 8.2 Hz, 1H), 6.89 (s, 1H), 6.97 (d, *J* = 8.7 Hz, 2H), 7.29–7.27 ppm (m, 2H); ¹³C NMR (100 MHz, CDCl₃): δ = 13.7, 17.1, 24.4, 37.5, 116.1, 118.3, 118.6, 120.5, 125.8, 129.2, 132.3, 139.8, 141.1, 147.0, 155.2 ppm; HRMS (ESI[−]): *m/z* calcd for C₁₆H₁₈O₂S ([*M*−H][−]): 273.0954, found: 273.0958.

2-[4-(1-Hydroxyethyl)phenoxy]-5-propylphenol (42): NaBH₄ (0.008 g, 0.22 mmol) was added in a single portion to a solution of **40** (0.02 g, 0.073 mmol) in anhyd MeOH (5 mL) at 0 °C and the reaction was stirred for 1 h. After quenching with H₂O (2 mL), the reaction was diluted with EtOAc (15 mL). The organic phase was washed with brine, dried (NaSO₄), filtered and concentrated in vacuo. Purification by preparative TLC (50% EtOAc/hexanes) gave **42** as a clear oil (14 mg, 69%). ¹H NMR (300 MHz, CDCl₃): δ = 0.96 (t, *J* = 7.3 Hz, 3H), 1.70–1.55 (m, 2H), 2.56 (t, *J* = 7.4 Hz, 2H), 4.91 (q, *J* = 6.4 Hz, 1H), 5.50 (s, 1H), 6.67 (dd, *J* = 8, *J* = 2 Hz, 1H), 6.82 (d, *J* = 8.2 Hz, 1H), 6.89 (d, *J* = 1.7 Hz, 1H), 7.00 (d, *J* = 8.2 Hz, 2H), 7.35 ppm (d, *J* = 8.5 Hz, 2H); ¹³C NMR (100 MHz, CDCl₃): δ = 13.7, 24.4, 25.1, 37.5, 69.8, 116.1, 117.5, 118.9, 120.5, 126.9, 139.8, 140.7, 141.0, 147.1, 156.5 ppm; HRMS (ESI[−]): *m/z* calcd for C₁₇H₂₀O₃ ([*M*−H][−]): 271.1339, found: 271.1342.

2-(4-Methanesulfonylphenoxy)-5-propylphenol (43): Method C was used to prepare intermediate **41a** from 2-methoxy-4-propylphenol (0.20 g, 1.2 mmol) and 4-(methylsulfonyl) phenylboronic acid (0.61 g, 3.61 mmol) in 59% yield. A solution of **41a** (0.15 g, 0.52 mmol) in CH₂Cl₂ (20 mL) was cooled to 0 °C and treated with a solution of *m*-CPBA (80%, 0.17 g, 0.78 mmol) in CH₂Cl₂ (3 mL) to give a mixture of **43a** (35 mg, 22%) and **44a** (54 mg, 32%).

Method D was used to prepare the title compound from **43a** (0.03 g, 0.098 mmol) and BBr₃ (1 M, 1.9 mL, 1.9 mmol). Purification by preparative TLC (60% EtOAc/hexanes) gave **43** as a grey solid (19 mg, 66%). ¹H NMR (400 MHz, CDCl₃): δ = 0.97 (t, *J* = 7.1 Hz, 3H), 1.70–1.58 (m, 2H), 2.57 (t, *J* = 6.7 Hz, 2H), 2.73 (s, 3H), 5.86 (s, 1H), 6.72 (d, *J* = 8.0 Hz, 1H), 6.88 (d, *J* = 8.1 Hz, 1H), 6.92 (s, 1H), 7.12 (d, *J* = 6.9 Hz, 2H), 7.60 ppm (d, *J* = 6.9 Hz, 2H); ¹³C NMR (100 MHz, CDCl₃): δ = 13.7, 24.4, 37.5, 43.9, 116.8, 117.6, 120.1, 120.8, 125.5, 138.9, 139.8, 141.0, 147.5, 160.1 ppm; HRMS (ESI[−]): *m/z* calcd for C₁₆H₁₈O₃S ([*M*−H][−]): 289.0903, found: 289.0910.

2-(4-Methanesulfonylphenoxy)-5-propylphenol (44): Method D was used to prepare the title compound from **44a** (0.05 g, 0.15 mmol) and BBr₃ (1 M, 3.1 mL, 3.1 mmol). Purification by preparative TLC (60% EtOAc in hexane) gave **44** as a white solid (24 mg, 50%). ¹H NMR (400 MHz, CDCl₃): δ = 0.98 (t, *J* = 7.2 Hz, 3H), 1.75–1.65 (m, 2H), 2.59 (t, *J* = 6.6 Hz, 2H), 3.06 (s, 3H), 5.41 (s, 1H), 6.76 (d, *J* = 8 Hz, 1H), 6.91 (d, *J* = 8 Hz, 1H), 6.93 (s, 1H), 7.12 (d, *J* = 6.7 Hz, 2H), 7.89 ppm (d, *J* = 6.6 Hz, 2H); ¹³C NMR (100 MHz, CDCl₃): δ = 13.7, 24.3, 37.5, 44.7, 116.9, 117.0, 120.4, 121.1, 129.7, 134.4, 139.1, 141.6, 147.4, 162.0 ppm; HRMS (ESI[−]): *m/z* calcd for C₁₆H₁₈O₄S ([*M*−H][−]): 305.0853, found: 305.0858.

2-(3-Dimethylaminophenoxy)-5-propylphenol (45): Method D was used to prepare the title compound from **45b** (0.09 g, 0.31 mmol) and BBr₃ (1 M, 6.3 mL, 6.3 mmol). Purification by flash chromatography (40% EtOAc/hexanes) gave **45** as an off-white solid (70 mg, 81%). ¹H NMR (400 MHz, CDCl₃): δ = 0.97 (t, *J* = 7.3 Hz, 3H), 1.68–1.63 (m, 2H), 2.56 (t, *J* = 7.5 Hz, 2H), 2.95 (s, 6H), 5.52 (s, 1H), 6.32 (d, *J* = 7.6 Hz, 1H), 6.44 (s, 1H), 6.49 (d, *J* = 8.3 Hz, 1H), 6.66 (d, *J* = 7.1 Hz, 1H), 6.85 (d, *J* = 8.2 Hz, 1H), 6.86 (s, 1H), 7.18 ppm (t, *J* = 8.1 Hz, 2H); ¹³C NMR (100 MHz, CDCl₃): δ = 13.4, 24.0, 37.1, 40.0, 101.7, 104.8, 107.2, 115.4, 118.4, 120.2, 129.6, 139.0, 140.9, 146.7, 151.6, 157.7 ppm; HRMS (ESI[−]): *m/z* calcd for C₁₇H₂₁NO₂ ([*M*−H][−]): 270.1499, found: 270.1501.

5-Propyl-2-(3-trifluoromethylphenoxy)phenol (46): Method D was used to prepare the title compound from **46b** (0.08 g, 0.25 mmol) and BBr₃ (1 M, 5.1 mL, 5.1 mmol). Purification by preparative TLC (40% EtOAc/hexanes) gave **46** as a grey solid (45 mg, 58%). ¹H NMR (400 MHz, CDCl₃): δ = 0.98 (t, *J* = 7.3 Hz, 3H), 1.72–1.62 (m, 2H), 2.58 (t, *J* = 6.8 Hz, 2H), 5.40 (s, 1H), 6.72 (d, *J* = 8.1 Hz, 1H), 6.85 (d, *J* = 8.1 Hz, 1H), 6.92 (s, 1H), 7.17 (d, *J* = 8.1 Hz, 1H), 7.37 (d, *J* = 7.3 Hz, 1H), 7.45 ppm (t, *J* = 7.9 Hz, 1H); ¹³C NMR (100 MHz, CDCl₃): δ = 13.3, 24.0, 37.1, 113.9, 113.9, 116.1, 118.9, 119.4, 119.4, 119.9, 120.5, 121.8, 124.5, 130.0, 131.4, 131.7, 132.0, 139.7, 140.4, 146.8, 157.2 ppm; HRMS (ESI[−]): *m/z* calcd for C₁₆H₁₉F₃O₂ ([*M*−H][−]): 295.0951, found: 295.0973.

3-(2-Hydroxy-4-propylphenoxy)benzaldehyde (47): Method D was used to prepare the title compound from **47a** (0.25 g, 0.92 mmol) and BBr₃ (1 M, 18.4 mL, 18.4 mmol). Purification by flash chromatography (60% EtOAc/hexanes) gave **47** (187 mg, 78%). ¹H NMR (300 MHz, CDCl₃): δ = 0.98 (t, *J* = 7.2 Hz, 3H), 1.70–1.63 (m, 2H), 2.57 (t, *J* = 6.7 Hz, 2H), 6.71 (dd, *J* = 8, *J* = 2 Hz, 1H), 6.85 (d, *J* = 8.3 Hz, 1H), 6.97 (d, *J* = 1.7 Hz, 1H), 7.32–7.29 (m, 1H), 7.49 (s, 1H), 7.53 (d, *J* = 7.9 Hz, 1H), 7.63 (d, *J* = 7.3 Hz, 1H), 9.98 ppm (s, 1H).

3-[3-(2-Hydroxy-4-propylphenoxy)phenyl]acrylic acid methyl ester (48): A solution of **47** (0.18 g, 0.70 mmol) and methyl (triphenylphosphoranylidene) acetate (0.47 g, 1.40 mmol) in THF (20 mL) was heated at reflux overnight, cooled and concentrated in vacuo. Purification by flash chromatography (1:3 EtOAc/hexanes) gave **48** as a white solid (177 mg, 80%). ¹H NMR (400 MHz, CDCl₃): δ = 0.98 (t, *J* = 7.3 Hz, 3H), 1.72–1.60 (m, 2H), 2.57 (t, *J* = 7.0 Hz, 2H), 3.82 (s,

3H), 5.43 (s, 1H), 6.40 (d, $J=16.0$ Hz, 1H), 6.70 (d, $J=8.1$ Hz, 1H), 6.84 (d, $J=8.1$ Hz, 1H), 6.91 (s, 1H), 7.05 (d, $J=8.3$ Hz, 1H), 7.16 (s, 1H), 7.36 (t, $J=7.8$ Hz, 1H), 7.64 ppm (d, $J=16.0$ Hz, 1H); ^{13}C NMR (100 MHz, CDCl_3): $\delta=13.7, 24.4, 37.5, 51.7, 116.3, 116.4, 118.7, 119.2, 120.7, 123.0, 130.2, 136.2, 140.3, 140.4, 144.0, 147.2, 157.7, 167.1$ ppm; HRMS (ESI $^-$): m/z calcd for $\text{C}_{19}\text{H}_{20}\text{O}_4$ ($[\text{M}-\text{H}]^-$): 311.1288, found: 311.1299.

3-[3-(2-Hydroxy-4-propylphenoxy)phenyl]propionic acid methyl ester (49): A suspension of **48** (0.10 g, 0.32 mmol) and 10% Pd/C (0.02 g) in EtOAc (10 mL) was stirred under H_2 (2 h), filtered over Celite and concentrated in vacuo to give **49** as a colorless oil (88 mg, 87%) without the need for further purification. ^1H NMR (400 MHz, CDCl_3): $\delta=0.97$ (t, $J=7.3$ Hz, 3H), 1.69–1.62 (m, 2H), 1.64 (t, $J=7.8$ Hz, 1H), 2.56 (t, $J=7.4$ Hz, 2H), 2.63 (t, $J=7.9$ Hz, 2H), 2.94 (t, $J=7.6$ Hz, 2H), 5.47 (s, 1H), 3.68 (s, 3H), 6.68 (dd, $J=8, J=2$ Hz, 1H), 6.82 (d, $J=8.1$ Hz, 1H), 6.87–6.85 (m, 2H), 6.89 (d, $J=1.5$ Hz, 1H), 6.95 (d, $J=7.4$ Hz, 1H), 7.25 ppm (t, $J=7.8$ Hz, 1H); ^{13}C NMR (100 MHz, CDCl_3): $\delta=13.7, 24.4, 30.7, 35.4, 37.5, 51.6, 115.3, 116.0, 117.3, 118.9, 120.5, 123.1, 129.8, 139.8, 140.9, 142.6, 147.2, 157.3, 173.1$ ppm; HRMS (ESI $^-$): m/z calcd for $\text{C}_{19}\text{H}_{22}\text{O}_4$ ($[\text{M}-\text{H}]^-$): 313.1445, found: 313.1451.

3-[3-(2-Hydroxy-4-propylphenoxy)phenyl]propionic acid (50): A solution of **48** (0.05 g, 0.16 mmol) in MeOH (10 mL) was treated with $\text{LiOH}\cdot\text{H}_2\text{O}$ (0.07 g, 1.62 mmol) and stirred until completion (2 h) to give **50** as a white solid (29 mg, 60%) without the need for further purification. ^1H NMR (400 MHz, CDCl_3): $\delta=0.98$ (t, $J=7.3$ Hz, 6H), 1.70–1.60 (m, 4H), 2.58 (t, $J=7.4$ Hz, 4H), 6.41 (d, $J=16.0$ Hz, 1H), 6.71 (d, $J=8.0$ Hz, 1H), 6.85 (d, $J=8.0$ Hz, 1H), 6.92 (s, 1H), 7.07 (d, $J=8.0$ Hz, 1H), 7.18 (s, 1H), 7.29 (d, $J=8.0$ Hz, 1H), 7.38 (t, $J=7.6$ Hz, 1H), 7.62 ppm (d, $J=16.0$ Hz, 1H); ^{13}C NMR (100 MHz, CDCl_3): $\delta=13.8, 24.4, 37.5, 116.4, 116.6, 118.1, 119.2, 119.6, 120.8, 123.2, 130.3, 135.8, 140.3, 140.4, 146.2, 147.2, 157.8, 171.7$ ppm; HRMS (ESI $^-$): m/z calcd for $\text{C}_{18}\text{H}_{18}\text{O}_4$ ($[\text{M}-\text{H}]^-$): 297.1132, found: 297.1137.

3-[3-(2-Hydroxy-4-propylphenoxy)phenyl]propionic acid (51): A solution of **49** (0.05 g, 0.16 mmol) in MeOH (10 mL) was treated with $\text{LiOH}\cdot\text{H}_2\text{O}$ (0.07 g, 1.62 mmol) and stirred until completion (2 h) to give **50** as a white solid (37 mg, 75%) without the need for further purification. ^1H NMR (300 MHz, CDCl_3): $\delta=0.97$ (t, $J=7.3$ Hz, 3H), 1.72–1.60 (m, 2H), 2.56 (t, $J=7.4$ Hz, 2H), 2.68 (t, $J=7.8$ Hz, 2H), 2.95 (t, $J=7.5$ Hz, 2H), 6.67 (dd, $J=8, J=2$ Hz, 1H), 6.82 (d, $J=8.2$ Hz, 1H), 6.92–6.85 (m, 3H), 6.93 (d, $J=7.4$ Hz, 1H), 7.24 ppm (d, $J=7.8$ Hz, 1H); ^{13}C NMR (100 MHz, CDCl_3): $\delta=13.7, 24.4, 30.4, 35.1, 37.5, 115.4, 116.1, 117.4, 119.0, 120.5, 123.1, 129.8, 139.9, 140.8, 142.2, 147.2, 157.3, 177.7$ ppm; HRMS (ESI $^-$): m/z calcd for $\text{C}_{18}\text{H}_{20}\text{O}_4$ ($[\text{M}-\text{H}]^-$): 299.1288, found: 299.1298.

3-[5-Chloro-2-(2,4-dichlorophenoxy)phenoxy]pyridine (52): Method C was used to prepare the title compound from triclosan (0.10 g, 0.34 mmol), 3-pyridineboronic acid (0.13 g, 1.03 mmol), $\text{Cu}(\text{OAc})_2$ (0.31 g, 1.72 mmol), Et_3N (0.35 g, 3.45 mmol) and 5 Å molecular sieves (0.6 g) in CH_2Cl_2 (20 mL). Purification by preparative TLC (1:3 EtOAc/hexanes) gave **52** as a grey solid (45 mg, 35%). ^1H NMR (400 MHz, CDCl_3): $\delta=6.83$ (d, $J=8.7$ Hz, 1H), 6.94 (d, $J=8.6$ Hz, 1H), 7.20–7.13 (m, 3H), 7.27–7.26 (m, 2H), 7.42 (d, $J=2.4$ Hz, 1H), 8.33 (s, 1H), 8.39 ppm (d, $J=2.4$ Hz, 1H); ^{13}C NMR (100 MHz, CDCl_3): $\delta=119.5, 121.1, 122.0, 124.0, 124.4, 125.5, 125.6, 127.9, 129.3, 129.9, 130.5, 140.2, 144.7, 145.8, 146.5, 150.8, 153.2$ ppm; HRMS (ESI $^-$): m/z calcd for $\text{C}_{17}\text{H}_{11}\text{O}_2\text{NCl}_3$ ($[\text{M}-\text{H}]^-$): 365.9849, found: 365.9843.

X-ray crystallography

Details on the crystal structure of the triclosan-bound complex have been reported elsewhere.^[46] The atomic coordinates and structure factors have been deposited in the Protein Data Bank (<http://www.rcsb.org/pdb>) under the PDB code 2QIO. A summary of crystallographic data collection and refinement information for inhibitors **11** and **43** bound to BaENR is provided in the Supporting Information (unpublished results).

Computational methods

Compounds were modeled into our triclosan-BaENR crystal structure using the GOLD docking program.^[58] The triclosan crystal structure was used as a reference ligand, and default parameters were chosen. After testing different algorithms, ChemScore was selected from within Gold as the best scoring function. A CoMFA was performed using up to 10 docking conformations for each of our ligands. The best scoring conformation was initially selected, then alternative conformations were systematically replaced to determine whether a better alignment could be achieved over the initial one, by way of a cross-validated PLS analysis. After all the conformations were evaluated, the conformation associated with the highest q^2 was selected. Using a training set of 22 compounds, an acceptable model was developed, shown by the PLS results of $q^2=0.831$, $r^2=0.929$, and $\text{SEE}=0.36$. The steric and electrostatic fields were graphed, and used in the design of new compounds.

Purification of BaENR and activity assays

BaENR was expressed in, and purified from *E. coli* according to the procedures of Klein et al.^[46] The assay was conducted at 30 °C in a 96-well plate using purified BaENR (1 μM), NADH (175 μM), and crotonyl-CoA (200 μM) with 200 μL of buffer containing Tris-HCl (20 mM), NaCl (150 mM). Crotonyl-CoA was added last to initiate the reaction. BaENR activity, determined by the decrease in NADH absorbance at 340 nm ($\epsilon=6220 \text{ m}^{-1} \text{ cm}^{-1}$), was recorded using a Molecular Devices SpectraMax384 Plus plate reader. The path length of the well in the 96-well microtiter plate cell was determined by measuring the rate ($\Delta\text{AU}/\text{min}$) in a 1 mL reaction volume with a 1.00 cm cuvette, and then calculating the rate of reaction (NADH/min) using the Beer-Lambert equation ($\text{AU}=\epsilon\cdot l\cdot[\text{NADH}]$) where l =path length. The reaction was then aliquoted (200 μL) into 5 wells of the 96-well plate, and the reaction rates were measured ($\Delta\text{AU}/\text{min}$). Values for $\Delta\text{AU}/\text{min}$ ($[\text{NADH}]\text{min}^{-1}$), and ϵ ($6220 \text{ m}^{-1} \text{ cm}^{-1}$) allowed us to determine the path length for the reactions (0.45 cm).

Inhibition of BaENR by triclosan and other compounds

The maximum solubility of a compound was determined by adding a stock solution of the compound in DMSO to the reaction well (2 μL , 10 mM) with a final volume of 200 μL ; if precipitation was visible in the reaction well, sequential twofold dilutions of the stock solution in DMSO were carried out until precipitation in the reaction well was no longer visible. This protocol ensured a consistent 1% (v/v) of DMSO in the final solution. The percent inhibition (%) was tested at the maximum solubility concentration using the equation $\%I=((A_c-A_i)/A_c)100$, where A_c =activity of the control (uninhibited) and A_i =activity in the presence of an inhibitor. If $\%I\geq 50\%$, then the IC_{50} value was determined by fixing the non-varied substrates at subsaturating concentrations as described above, and then varying the inhibitor concentration. The reactions

were allowed to preincubate for 30 min before initiation with crotonyl-CoA. An equal concentration of DMSO was added to the control experiments to negate the effect of solvent on enzyme activity. Nonlinear regression and the Enzyme Kinetics Module 1.0 of the Sigma Plot (SYSTAT Inc) program were used to fit the data to the equation $%I = \%I_{\max}/(IC_{50}/[I] + 1)$.

Bacterial growth and MIC determination

The MIC values were determined against the Δ ANR (plasmid-cured Ames Strain) and Sterne strains of *B. anthracis*, and reference strains of the following bacteria: *S. aureus* (ATCC strain 29213), MRSA (ATCC strain 43300), *Enterococcus faecalis* (ATCC strain 29212), vancomycin-resistant *Enterococcus* (VRE) (ATCC strain 51299), *Listeria monocytogenes* (10403S),^[59] *P. aeruginosa* (ATCC strain 27853), *Klebsiella pneumoniae* (ATCC strain 700603) and *E. coli* (ATCC strain 25922). Luria–Bertani (LB) medium was added to each well in a row on a sterile, Falcon MICROTTEST 96-well U-bottom tissue culture plate; 96 μ L was added to each well of the first column, and 50 μ L was added to all subsequent wells. The compounds or control antibiotic to be tested were added to the first column for a final well volume of 100 μ L. The inhibitors were then serially diluted (twofold) across the columns of wells by pipetting and mixing 50 μ L of solution. Bacterial cultures were grown to mid-log phase ($OD_{600} = 0.4$ – 0.6), and diluted to $OD_{600} = 0.004$ using fresh LB medium. 50 μ L of the bacterial culture was added to each well of the plate and the plate was then incubated at 37 °C overnight (~14 h) without shaking. For each compound or antibiotic control, the first clear well with no visible signs of growth was reported as the MIC value. Medium from each clear well was then inoculated onto plates of LB agar medium that were incubated overnight. The first clear-medium dilution from which no bacterial colonies could be grown was reported as the MBC value.

Acknowledgements

This work was funded by a grant from NIH/NIAID (U19 AI056575), and a contract from DOD (W81XWH-07-1-0445). X-ray diffraction intensities were collected at Southeast Regional Collaborative Access Team (SER-CAT) 22-ID and 22-BM beamlines at the Advanced Photon Source, Argonne National Laboratory. Supporting institutions may be found at www.ser-cat.org/members.html. Use of the Advanced Photon Source was supported by the U. S. Department of Energy, Office of Science, Office of Basic Energy Sciences, under Contract No. W-31-109-Eng-38. *Listeria monocytogenes* (10403S) was provided by Nancy E. Freitag, University of Illinois at Chicago. Work in the Cook Laboratory was supported in part by the James A. and Marion C. Grant Fund.

Keywords: B. anthracis • enoyl reductase • inhibitors • structure–activity relationships • triclosan

- [1] Infectious Diseases Society of America, *Bad Bugs, No Drugs*, <http://www.idsociety.org/WorkArea/showcontent.aspx?id=5554> (Last accessed: June 18, 2008).
- [2] A. L. Casey, P. A. Lambert, T. S. Elliott, *Int. J. Antimicrob. Agents* **2007**, 29, S23–S32.
- [3] E. A. Bancroft, *JAMA J. Am. Med. Assoc.* **2007**, 298, 1803–1804.
- [4] R. M. Klevens, M. A. Morrison, J. Nadle, S. Petit, K. Gershman, S. Ray, L. H. Harrison, R. Lynfield, G. Dumyati, J. M. Townes, A. S. Craig, E. R. Zell, G. E.

- Fosheim, L. K. McDougal, R. B. Carey, S. K. Fridkin, *JAMA J. Am. Med. Assoc.* **2007**, 298, 1763–1771.
- [5] B. Weisblum, *Antimicrob. Agents Chemother.* **1995**, 39, 577–585.
- [6] J. G. Bartlett, T. V. Inglesby, Jr., L. Borio, *Clin. Infect. Dis.* **2002**, 35, 851–858.
- [7] J. D. Cavallo, F. Ramisse, M. Girardet, J. Vaissaire, M. Mock, E. Hernandez, *Antimicrob. Agents Chemother.* **2002**, 46, 2307–2309.
- [8] P. R. Coker, K. L. Smith, M. E. Hugh-Jones, *Antimicrob. Agents Chemother.* **2002**, 46, 3843–3845.
- [9] B. Vester, S. Douthwaite, *Antimicrob. Agents Chemother.* **2001**, 45, 1–12.
- [10] A. V. Stepanov, L. I. Marinin, A. P. Pomerantsev, N. A. Staritsin, *J. Biotechnol.* **1996**, 44, 155–160.
- [11] L. B. Price, A. Vogler, T. Pearson, J. D. Busch, J. M. Schupp, P. Keim, *Antimicrob. Agents Chemother.* **2003**, 47, 2362–2365.
- [12] A. Athamna, M. Athamna, N. bu-Rashed, B. Medlej, D. J. Bast, E. Rubinstein, *J. Antimicrob. Chemother.* **2004**, 54, 424–428.
- [13] C. R. MacIntyre, A. Seccull, J. M. Lane, A. Plant, *Mil. Med.* **2006**, 171, 589–594.
- [14] L. D. Rotz, A. S. Khan, S. R. Lillibridge, S. M. Ostroff, J. M. Hughes, *Emerging Infect. Dis.* **2002**, 8, 225–230.
- [15] J. C. Burnett, E. A. Henschel, A. L. Schmaljohn, S. Bavari, *Nat. Rev. Drug Discovery* **2005**, 4, 281–297.
- [16] S. W. White, J. Zheng, Y. M. Zhang, C. O. Rock, *Annu. Rev. Biochem.* **2005**, 74, 791–831.
- [17] Y. M. Zhang, Y. J. Lu, C. O. Rock, *Lipids* **2004**, 39, 1055–1060.
- [18] C. O. Rock, S. Jackowski, *Biochem. Biophys. Res. Commun.* **2002**, 292, 1155–1166.
- [19] K. Kobayashi, S. D. Ehrlich, A. Albertini, G. Amati, K. K. Andersen, M. Arnaud, K. Asai, S. Ashikaga, S. Aymerich, P. Bessieres, F. Boland, S. C. Brignell, S. Bron, K. Bunai, J. Chapuis, L. C. Christiansen, A. Danchin, M. Dæbarbouille, E. Dervyn, E. Deuerling, K. Devine, S. K. Devine, O. Dreesen, J. Errington, S. Fillinger, S. J. Foster, Y. Fujita, A. Galizzi, R. Gardan, C. Eschevins, T. Fukushima, K. Haga, C. R. Harwood, M. Hecker, D. Hosoya, M. F. Hullo, H. Kakeshita, D. Karamata, Y. Kasahara, F. Kawamura, K. Koga, P. Koski, R. Kuwana, D. Imamura, M. Ishimaru, S. Ishikawa, I. Ishio, D. Le Coq, A. Masson, C. Mauëel, R. Meima, R. P. Mellado, A. Moir, S. Moriya, E. Nagakawa, H. Nanamiya, S. Nakai, P. Nygaard, M. Ogura, T. Ohanan, M. O'Reilly, M. O'Rourke, Z. Pragai, H. M. Pooley, G. Rapoport, J. P. Rawlins, L. A. Rivas, C. Rivolta, A. Sadaie, Y. Sadaie, M. Sarvas, T. Sato, H. H. Saxild, E. Scanlan, W. Schumann, J. F. Seegers, J. Sekiguchi, A. Sekowska, S. J. Særor, M. Simon, P. Stragier, R. Studer, H. Takamatsu, T. Tanaka, M. Takeuchi, H. B. Thomaidis, V. Vagner, J. M. van Dijk, K. Watabe, A. Wipat, H. Yamamoto, M. Yamamoto, Y. Yamamoto, K. Yamane, K. Yata, K. Yoshida, H. Yoshikawa, U. Zuber, N. Ogasawara, *Proc. Natl. Acad. Sci. USA* **2003**, 100, 4678–4683.
- [20] R. J. Heath, C. O. Rock, *J. Biol. Chem.* **1995**, 270, 26 538–26 542.
- [21] D. A. Rozwarski, G. A. Grant, D. H. Barton, W. R. Jacobs, Jr., J. C. Sacchettini, *Science* **1998**, 279, 98–102.
- [22] C. Baldock, G. J. de Boer, J. B. Rafferty, A. R. Stuitje, D. W. Rice, *Biochem. Pharmacol.* **1998**, 55, 1541–1549.
- [23] C. Baldock, J. B. Rafferty, S. E. Sedelnikova, P. J. Baker, A. R. Stuitje, A. R. Slabas, T. R. Hawkes, D. W. Rice, *Science* **1996**, 274, 2107–2110.
- [24] C. W. Levy, C. Baldock, A. J. Wallace, S. Sedelnikova, R. C. Viner, J. M. Clough, A. R. Stuitje, A. R. Slabas, D. W. Rice, J. B. Rafferty, *J. Mol. Biol.* **2001**, 309, 171–180.
- [25] L. M. McMurry, P. F. McDermott, S. B. Levy, *Antimicrob. Agents Chemother.* **1999**, 43, 711–713.
- [26] R. J. Heath, Y. T. Yu, M. A. Shapiro, E. Olson, C. O. Rock, *J. Biol. Chem.* **1998**, 273, 30 316–30 320.
- [27] C. W. Levy, A. Roujeinikova, S. Sedelnikova, P. J. Baker, A. R. Stuitje, A. R. Slabas, D. W. Rice, J. B. Rafferty, *Nature* **1999**, 398, 383–384.
- [28] R. McLeod, S. P. Muench, J. B. Rafferty, D. E. Kyle, E. J. Mui, M. J. Kirisits, D. G. Mack, C. W. Roberts, B. U. Samuel, R. E. Lyons, M. Dorris, W. K. Milhous, D. W. Rice, *Int. J. Parasitol.* **2001**, 31, 109–113.
- [29] D. T. Moir, *Curr. Drug Targets Infect. Disord.* **2005**, 5, 297–305.
- [30] X. He, A. Alian, R. Stroud, P. R. Ortiz de Montellano, *J. Med. Chem.* **2006**, 49, 6308–6323.
- [31] S. Broussy, V. Bernardes-Gaënnison, A. Quémard, B. Meunier, J. Bernadoux, *J. Org. Chem.* **2005**, 70, 10 502–10 510.
- [32] W. H. Miller, M. A. Seefeld, K. A. Newlander, I. N. Uzinskis, W. J. Burgess, D. A. Heering, C. C. Yuan, M. S. Head, D. J. Payne, S. F. Rittenhouse, T. D.

- Moore, S. C. Pearson, V. Berry, W. E. DeWolf Jr., P. M. Keller, B. J. Polizzi, X. Qiu, C. A. Janson, W. F. Huffman, *J. Med. Chem.* **2002**, *45*, 3246–3256.
- [33] M. A. Seefeld, W. H. Miller, K. A. Newlander, W. J. Burgess, W. E. DeWolf Jr., P. A. Elkins, M. S. Head, D. R. Jakas, C. A. Janson, P. M. Keller, P. J. Manley, T. D. Moore, D. J. Payne, S. Pearson, B. J. Polizzi, X. Qiu, S. F. Rittenhouse, I. N. Uzinskas, N. G. Wallis, W. F. Huffman, *J. Med. Chem.* **2003**, *46*, 1627–1635.
- [34] I. I. Protasevich, C. G. Brouillette, M. E. Snow, S. Dunham, J. R. Rubin, R. Gogliotti, K. Siegel, *Biochemistry* **2004**, *43*, 13380–13389.
- [35] M. A. Seefeld, W. H. Miller, K. A. Newlander, W. J. Burgess, D. J. Payne, S. F. Rittenhouse, T. D. Moore, W. E. DeWolf, Jr., P. M. Keller, X. Qiu, C. A. Janson, K. Vaidya, A. P. Fosberry, M. G. Smyth, D. D. Jaworski, C. Slater-Radosti, W. F. Huffman, *Bioorg. Med. Chem. Lett.* **2001**, *11*, 2241–2244.
- [36] a) J. A. Karlowsky, N. M. Laing, T. Baudry, N. Kaplan, D. Vaughan, D. J. Hoban, G. G. Zhanel, *Antimicrob. Agents Chemother.* **2007**, *51*, 1580–1581; b) H. S. Park, Y. M. Yoon, S. J. Jung, I. N. R. Yun, C. M. Kim, J. M. Kim, J.-H. Kwak, *Int. J. Antimicrob. Agents* **2007**, *30*, 446–451.
- [37] S. Sivaraman, T. J. Sullivan, F. Johnson, P. Novichenok, G. Cui, C. Simmerling, P. J. Tonge, *J. Med. Chem.* **2004**, *47*, 509–518.
- [38] M. G. Escalada, J. L. Harwood, J. Y. Maillard, D. Ochs, *J. Antimicrob. Chemother.* **2005**, *55*, 879–882.
- [39] L. M. McMurtry, M. Oethinger, S. B. Levy, *Nature* **1998**, *394*, 531–532.
- [40] J. Regös, O. Zak, R. Solf, W. A. Vischer, E. G. Weirich, *Dermatologica* **1979**, *158*, 72–79.
- [41] a) J. S. Freundlich, J. W. Anderson, D. Sarantakis, H. M. Shieh, M. Yu, J. C. Valderramos, E. Lucumi, M. Kuo, W. R. Jacobs, Jr., D. A. Fidock, G. A. Schiehser, D. P. Jacobus, J. C. Sacchettini, *Bioorg. Med. Chem. Lett.* **2005**, *15*, 5247–5252; b) J. S. Freundlich, F. Wang, Han-Chun Tsai, M. Kuo, Hong-Ming Shieh, J. W. Anderson, L. J. Nkrumah, Juan-Carlos Valderramos, M. Yu, T. R. S. Kumar, S. G. Valderramos, W. R. Jacobs, Jr., G. A. Schiehser, D. P. Jacobus, P. David, D. A. Fidock, J. C. Sacchettini, *J. Biol. Chem.* **2007**, *282*, 25436–25444.
- [42] J. S. Freundlich, M. Yu, E. Lucumi, M. Kuo, H. C. Tsai, J. C. Valderramos, L. Karagoyozov, W. R. Jacobs, Jr., G. A. Schiehser, D. A. Fidock, D. P. Jacobus, J. C. Sacchettini, *Bioorg. Med. Chem. Lett.* **2006**, *16*, 2163–2169.
- [43] a) H. Lu, P. J. Tonge, *Acc. Chem. Res.* **2008**, *41*, 11–20; b) T. J. Sullivan, J. J. Truglio, M. E. Boyne, P. Novichenok, X. Zhang, C. F. Stratton, H. J. Li, T. Kaur, A. Amin, F. Johnson, R. A. Slayden, C. Kisker, P. J. Tonge, *ACS Chem. Biol.* **2006**, *1*, 43–53.
- [44] R. Perozzo, M. Kuo, A. S. Sidhu, J. T. Valiyaveetil, R. Bittman, W. R. Jacobs Jr., D. A. Fidock, J. C. Sacchettini, *J. Biol. Chem.* **2002**, *277*, 13106–13114.
- [45] M. Chhibber, G. Kumar, P. Parasuraman, T. N. Ramya, N. Surolia, A. Surolia, *Bioorg. Med. Chem.* **2006**, *14*, 8086–8098.
- [46] G. M. Klein, D. S. Bernard, S. K. Tipparaju, S. Pegan, M. H. Bishop, A. P. Kozikowski, A. D. Mesecar, *unpublished results*.
- [47] D. A. Evans, J. L. Katz, T. R. West, *Tetrahedron Lett.* **1998**, *39*, 2937–2940.
- [48] C. Papamicaël, G. Queguiner, J. Bourguignon, G. Dupas, *Tetrahedron* **2001**, *57*, 5385–5391.
- [49] C. Su-Dong, P. Yong-Dae, K. Jeum-Jong, J. R. Falck, Y.-J. Yoon, *Bull. Korean Chem. Soc.* **2004**, *25*, 407–409.
- [50] Molecular properties were calculated using a free web-based program: <http://146.107.217.178/lab/alogps/index.html> (Last accessed: June 18, 2008). A table showing comparison of values of synthesized compounds with those of triclosan is included in the Supporting Information.
- [51] M. E. Boyne, T. J. Sullivan, C. W. amEnde, H. Lu, V. Gruppo, D. Heaslip, A. G. Amin, D. Chatterjee, A. Lenaerts, P. J. Tonge, R. A. Slayden, *Antimicrob. Agents Chemother.* **2007**, *51*, 3562–3567.
- [52] P. Auffinger, F. A. Hays, E. Westhof, P. S. Ho, *Proc. Natl. Acad. Sci. USA* **2004**, *101*, 16789–16794.
- [53] L. S. Pidugu, M. Kapoor, N. Surolia, A. Surolia, K. Suguna, *J. Mol. Biol.* **2004**, *343*, 147–155.
- [54] S. K. Tipparaju, S. Joyasawal, S. Forrester, D. C. Mulhearn, S. Pegan, M. E. Johnson, A. D. Mesecar, A. P. Kozikowski, *Bioorg. Med. Chem. Lett.* **2008**, *18*, 3565–3569.
- [55] M. Kapoor, P. L. Mukhi, N. Surolia, K. Suguna, A. Surolia, *Biochem. J.* **2004**, *381*, 725–733.
- [56] R. J. Lambert, *J. Appl. Microbiol.* **2004**, *97*, 699–6711.
- [57] M. T. Suller, A. D. Russell, *J. Antimicrob. Chemother.* **2000**, *46*, 11–18.
- [58] M. L. Verdonk, J. C. Cole, M. J. Hartshorn, C. W. Murray, R. D. Taylor, *Proteins Struct. Funct. Genet.* **2003**, *52*, 609–623.
- [59] K. J. Mueller, N. E. Freitag, *Infect. Immun.* **2005**, *73*, 1917–1926.

Received: February 20, 2008

Revised: May 28, 2008

Published online on July 28, 2008



Contents lists available at ScienceDirect

Bioorganic & Medicinal Chemistry Letters

journal homepage: www.elsevier.com/locate/bmcl

Design and synthesis of 2-pyridones as novel inhibitors of the *Bacillus anthracis* enoyl-ACP reductase

Suresh K. Tipparaju^a, Sipak Joyasawal^a, Sara Forrester^b, Debbie C. Mulhearn^b, Scott Pegan^b, Michael E. Johnson^{b,*}, Andrew D. Mesecar^{a,b,*}, Alan P. Kozikowski^{a,*}

^a Drug Discovery Program, Department of Medicinal Chemistry and Pharmacognosy, University of Illinois at Chicago, 833 S. Wood Street, Chicago, IL 60612, USA

^b Center for Pharmaceutical Biotechnology, University of Illinois at Chicago, 900 S. Ashland Avenue, Chicago, IL 60607, USA

ARTICLE INFO

Article history:

Received 20 March 2008

Revised 28 April 2008

Accepted 1 May 2008

Available online 4 May 2008

Keyword:

Anthrax

ABSTRACT

Enoyl-ACP reductase (ENR), the product of the *FabI* gene, from *Bacillus anthracis* (*BaENR*) is responsible for catalyzing the final step of bacterial fatty acid biosynthesis. A number of novel 2-pyridone derivatives were synthesized and shown to be potent inhibitors of *BaENR*.

© 2008 Elsevier Ltd. All rights reserved.

Fatty acids are an essential source of energy for organisms from all taxa. Fatty acid synthesis in mammals is substantially different from that in bacteria. In mammals, the fatty acid synthesis involves a single multifunctional enzyme–acyl carrier protein (ACP) complex. In bacteria, the synthesis utilizes several small monofunctional enzymes that operate in conjunction with ACP-associated substrates.¹ Thus, it is possible to selectively target key enzymes in the bacterial fatty acid biosynthesis.²

The final and rate-determining step of chain elongation in the bacterial fatty acid biosynthesis is the reduction of enoyl-ACP to an acyl-ACP, which is catalyzed by the enzyme–enoyl-acyl carrier protein reductase. Considerable research over the past few years has shown that ENR is the target of a number of known antibacterial agents, including isoniazid,³ diazaboranes,⁴ and triclosan.⁵ Targeting ENR is an attractive approach for the development of novel antibacterials, which has been validated by the recent discovery of several other small molecule inhibitors,⁶ including those that exhibit potent in vitro activity against clinical isolates of methicillin-resistant *Staphylococcus epidermidis* and *Staphylococcus aureus*.⁷

As part of an on-going program to develop novel therapeutics for anthrax, we recently reported that the diphenyl ether–triclosan and a number of its aryl ether derivatives inhibit *BaENR*.⁸ Although triclosan is a potent inhibitor of *BaENR* (IC_{50} = 0.5 μ M, MIC = 3.1 μ g/mL),⁹ a major caveat in developing triclosan or its derivatives as drugs is the metabolic liability of the phenolic hydroxyl group.¹⁰

In addition, triclosan-like diphenyl ethers are fairly lipophilic molecules and pose serious solubility problems. In order to overcome these structural drawbacks, it is important to design compounds in which the phenolic group of ring A of triclosan is replaced by a more metabolically stable functionality. We report herein our efforts toward addressing these issues by developing novel scaffolds that replace the phenolic ring of triclosan with other heterocyclic rings that retain the essential structural features of triclosan required for interaction with ENR, such as π -stacking of the aromatic ring with NAD^+ , hydrogen bonding of the phenolic OH group with the ribose, as well as optimal flexibility of the two rings in order to allow complementary interactions with the active site.⁹

Our structure optimization studies were based on predicted binding interactions of 2-pyridones with the enzyme active site. Triclosan and synthesized pyridones were docked into the *BaENR* crystal structure⁹ using the GOLD-docking program.¹¹ It was observed that the 2-pyridones dock to *BaENR* in the same binding pocket as that of triclosan, and maintain similar H-bonding interactions with the residues in the active site. Figure 1 shows the similarities in the binding geometry of triclosan and a representative 2-pyridone, **2**. Figure 2 shows the crystal structure of triclosan bound to *BaENR* and the GOLD docking conformations of compounds **2** and **35** in the active site. The X-ray structure of triclosan bound to *BaENR* shows that the phenolic hydroxyl group on ring A is involved in two hydrogen bonds, one with Tyr157 (OH) and the other to the 2'-hydroxyl group of nicotinamide ribose (shown in Fig. 2A).⁹ These interactions appear to be preserved in the GOLD-docking conformation of the pyridones as well, and show that the oxygen on the carbonyl group of ring A is involved in a hydrogen bonding interaction with Tyr157 (OH) and the NAD^+ (shown in Fig. 2B and C). As seen in Figure 1, the ring A pocket of the

* Corresponding authors. Tel.: +1 312 996 9114; fax: +1 312 413 9303 (M.E.J.); tel.: +1 312 996 1877; fax: +1 312 413 9303 (A.D.M.); tel.: +1 312 996 7577; fax: +1 312 413 0577 (A.P.K.).

E-mail addresses: mjohnson@uic.edu (M.E. Johnson), mesecar@uic.edu (A.D. Mesecar), kozikowa@uic.edu (A.P. Kozikowski).

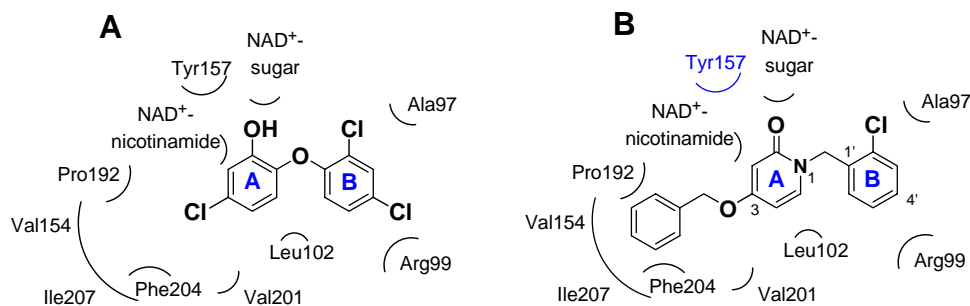


Figure 1. Schematic representation of residues in the binding pockets of rings A and B of (A) triclosan and (B) compound **2**.

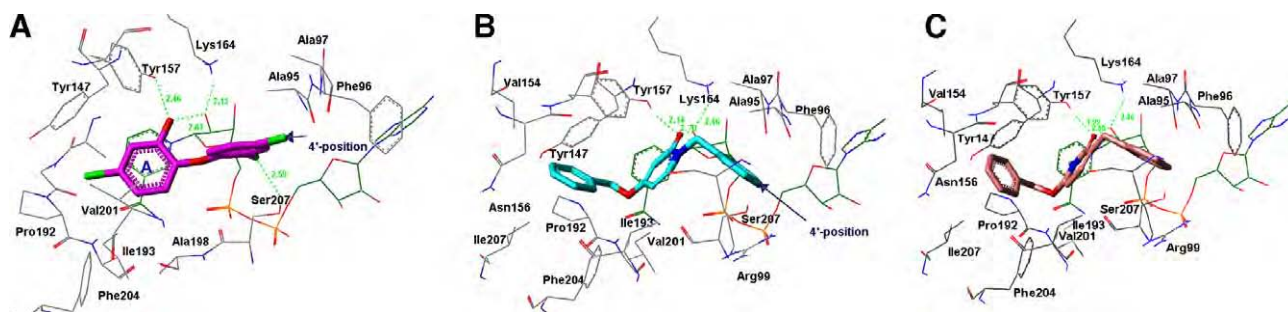
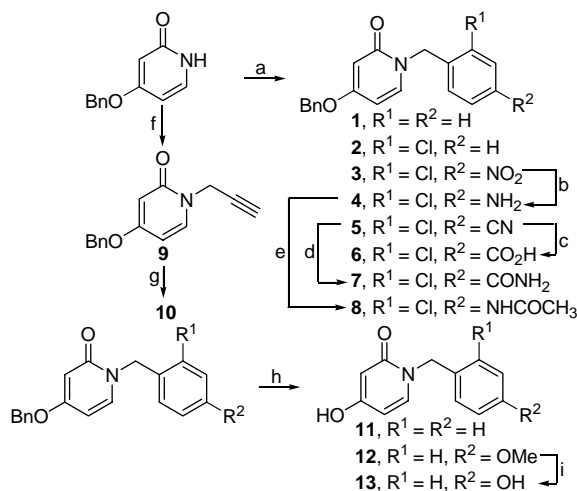


Figure 2. (A) Crystal structure of triclosan bound to BaENR. ENR atoms are colored by atom type, NAD⁺ is green, and triclosan is magenta. (B) GOLD-docking conformation of **2** against the crystal structure of BaENR. ENR atoms are colored by atom type, NAD⁺ is green, and **2** is cyan. Distances between atoms that are close enough to be within hydrogen bonding range are shown in green. (C) GOLD-docking conformation of **35** against the crystal structure of BaENR. ENR atoms are colored by atom type, NAD⁺ is green, and **35** is coral.

pyridones is surrounded by Val 154, Val 201, Ile 207, and Phe 204, and thus appears to be dominated by a high amount of hydrophobicity.

The synthesis of compounds **1–3**, **5**, and **9** involved selective N-alkylation of the commercially available 4-benzyloxy-2(1*H*)-pyridone with the corresponding benzyl halides according to the procedure described by Conreux et al. (Scheme 1).¹² Reduction of **3** gave the amino compound **4**, which was further converted to the acetamide **8**. While alkaline hydrolysis of the benzonitrile **5** re-



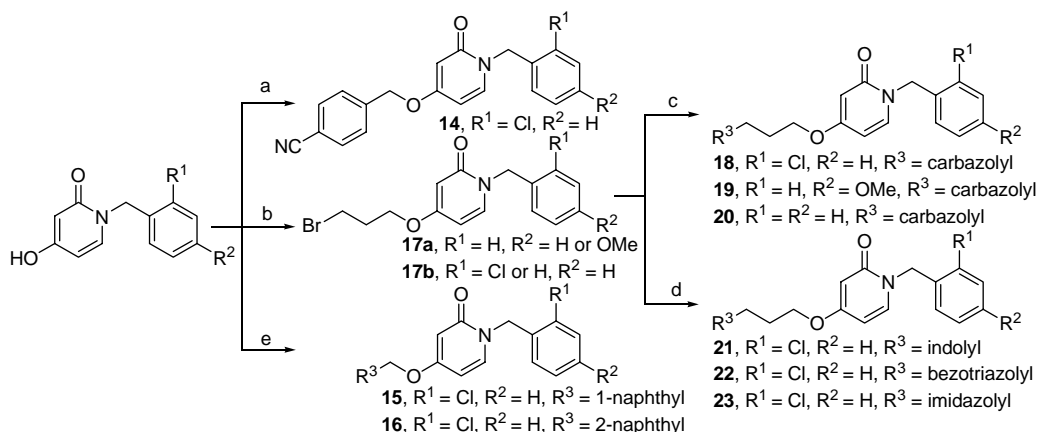
Scheme 1. Reagents and conditions: (a) KOtBu, TBAI, THF, ArCH₂X, 0–25 °C, 16 h; (b) NaBH₄, Cu(OAc)₂, THF, 0 °C, 40 min; (c) 25% NaOH, EtOH, reflux, 20 h; (d) 35% H₂O₂, 3 N NaOH, EtOH, 30 °C, 20 h; (e) Ac₂O, DMAP, Et₃N, CH₂Cl₂, 0–25 °C, 3 h; (f) KOtBu, TBAI, THF, propargyl bromide, 0–25 °C, 16 h; (g) ethyl chlorooxidoacetate, Et₃N, rt, 5 h; (h) Pd/C, H₂, MeOH, rt, 10–15 min; (i) BBr₃, CH₂Cl₂, –78 °C to rt, 12 h.

sulted in the carboxylic acid **6**, hydrolysis in the presence of hydrogen peroxide gave the carboxamide **7**. Isoxazole **10** was prepared by treating **9** with ethyl chlorooxidoacetate in the presence of a base.¹³ Rapid and selective O-debenzylation of 4-benzyloxy-2(1*H*)-pyridone derivatives occurred when treated with Pd/C under atmospheric pressure of hydrogen to give compounds **11** and **12**. Compound **13** was obtained by treatment of **12** with BBr₃.

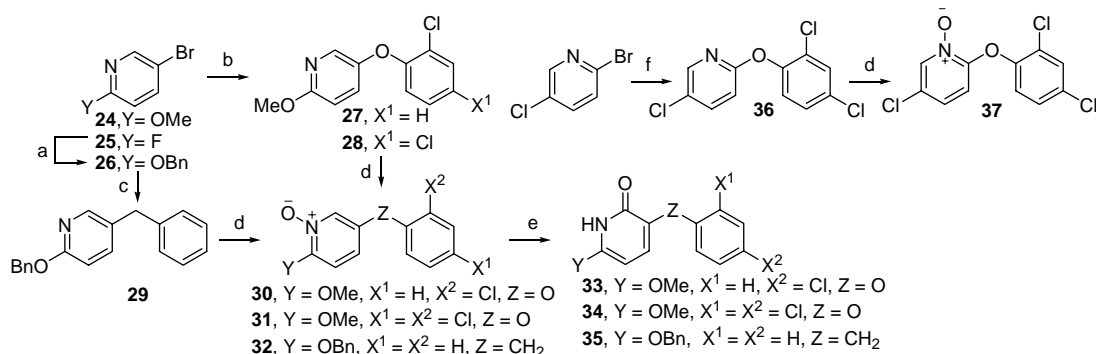
The above 4-hydroxy-pyridones were elaborated into a number of derivatives via a series of alkylation reactions (Scheme 2). Compound **14** was prepared by benzylation of 4-hydroxy-pyridone with 4-cyanobenzyl bromide. Naphthyl derivatives **15** and **16** were obtained by using a similar procedure. The common synthetic intermediates **17** were prepared by alkylating the 4-hydroxy-pyridones with 1,3-dibromopropane. Compounds **18–20** were prepared in turn by N-alkylation of carbazole with these intermediates. Compounds **21–23** were synthesized using a similar protocol.

The synthesis of the 3-substituted 2-pyridones and N-oxide derivatives is shown in Scheme 3. Pyridones **33–35** were synthesized by acetic anhydride mediated rearrangement of the corresponding N-oxides, followed by acidic hydrolysis.¹⁴ The N-oxides were synthesized from the corresponding pyridines by *m*-CPBA oxidation. While the ethers **27** and **28** were prepared by standard coupling reactions, intermediate **29** was obtained by treating 2-benzyloxy-5-bromopyridine with benzyltrimethyltin under Stille reaction conditions.

The compounds synthesized were evaluated for their BaENR inhibitory and antibacterial activities.¹⁵ Inhibitor **2** appears to be the best compound in this series and was considered as a lead. As expected from the interactions of hydrophobic residues located around the 3-position of the pyridone ring in the active site, replacing the benzyloxy group at this position with a more polar hydroxy group led to a substantial decrease in the ENR inhibitory activity (Table 1, compounds **11–13**). A four-fold improvement in the en-



Scheme 2. Reagents and conditions: (a) NaH, DMF/THF, 4-CN-PhCH₂Br, 0–25 °C, 12 h; (b) NaH, DMF, 1,3-dibromopropane, 0–25 °C, 6 h; (c) NaH, DMF, carbazole, 0–25 °C, 12 h; (d) For **21**: NaH, DMF, indole, rt, 16 h; for **22**: benzotriazole, DMF, K₂CO₃, rt, 12 h; for **23**: imidazole, KOH, THF, 85 °C, 16 h; (e) NaH, DMF/THF, 1- or 2-bromomethyl naphthalene, 0–25 °C, 12 h.



Scheme 3. Reagents and conditions: (a) benzyl alcohol, NaH, THF, rt, 12 h; (b) for **27**: KOH–CuCO₃, 2-chlorophenol, 180 °C, 15 h; for **28**: 2,4-dichlorophenol, KOtBu, DMF, rt, 3 h, then at 45 °C under vacuum, Cu(OTf)₂·PhCH₃, DMF, reflux, 16 h; (c) trimethylbenzylstannane, Pd(PPh₃)₄, DMF, 80 °C, 12 h; (d) *m*-chloroperbenzoic acid, CHCl₃, rt, 12 h; (e) Ac₂O, reflux, 5 h, 1 N HCl, 100 °C, 12 h; (f) KOH–CuCO₃, 2,4-dichlorophenol, 180 °C, 15 h.

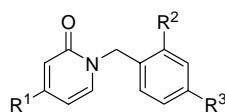
zyme inhibitory activity was observed when a chlorine atom is present at the 2'-position on the aromatic ring B (cf. **1** vs **2**). A similar improvement in the binding affinity of triclosan derivatives to the *Ba*ENR active site was recently observed by us.⁸ Attachment of an electron withdrawing cyano group to the aromatic ring of the benzyloxy moiety resulted in **14**, which showed an ENR inhibitory activity lower than the lead compound. Thus, we explored the activities of compounds with other hydrophobic substituents at the 3-position of the pyridone ring. Introduction of 1- and 2-naphthyl groups resulted in compounds **15** and **16** whose enzymatic activity was comparable to the lead compound. Introduction of a bulkier carbazole unit, tethered with a three-carbon chain on the other hand, decreased the *Ba*ENR inhibitory activity (Table 1, compounds **18–20**). Again, the importance of having a chlorine atom at the 2'-position on ring B to improve the inhibitory activity of these compounds is evident by comparing the activities of **18** and **20**. Replacing the carbazole unit with a smaller indole moiety resulted in twofold improvement in the ENR inhibitory activity (compound **21**), while a benzotriazolyl substitution resulted in the compound (**22**) with an ENR inhibitory activity comparable to that of the lead compound. Introduction of an imidazolyl unit did not improve the activity.

We explored the SAR of the 2-pyridones by functionalizing ring B. From the docking conformations of the lead compound into the *Ba*ENR X-ray crystal structure (Fig. 2B), we anticipated that hydrogen bond donors/acceptors at the 4'-position would be ideally positioned to interact with either Ala 97 or Arg 99. Hence, we synthesized

compounds **3–8** with various functional groups at the 4'-position of the ring B. Compound **4**, bearing an amino group at the 4'-position turned out to be the best compound with an IC₅₀ of 0.8 μM. Conversion of the amino functionality into an acetamide (compound **8**) reduced the *Ba*ENR inhibitory activity by half. Thus, it appears that the presence of an electron-donating group at the 4'-position is able to enhance the interaction of ligands with the enzyme active site. Attempts to replace the aromatic ring B of these 2-pyridones with an acetylene (compound **9**) or an isoxazole (compound **10**) were not successful in improving the activity (Table 2).

We briefly explored the activities of C-substituted 2-pyridones that are structurally similar to the N-substituted 2-pyridones discussed above (compounds **33–35**). These C-substituted pyridones are capable of existing in their enol form as hydroxypyridines, and thus closely mimic triclosan in structure. The activities of these compounds are shown in Table 2. It is gratifying to note that the novel C-substituted 2-pyridone, **35** showed a 10-fold improvement in ENR inhibitory activity over its N-substituted analog **1**. The GOLD-docking conformation of **35** in Figure 2C suggests a nearly identical orientation of the C-substituted 2-pyridones compared to the N-substituted pyridones. Although the origin of improved activity of compound **35** is not completely clear at this stage, the pyridone NH and the nicotinamide ring are about 3.6 Å apart and thus ligand binding stabilization from an N–H...π interaction cannot be ruled out.¹⁶ Moderate ENR inhibition was observed by the 3-phenoxy-2-pyridones **33** and **34**. Among the pyridine N-oxides, compound **37** exhibited modest ENR inhibition, while compound **30** was inactive.

Table 1
BaENR inhibitory activities of compounds



| Compound | R ¹ | R ² | R ³ | IC ₅₀ (μM) |
|----------------|--------------------------|----------------|-------------------|-----------------------|
| 11 | OH | H | H | >100 ^a |
| 12 | OH | H | OMe | >100 ^a |
| 13 | OH | H | OH | >100 ^a |
| 1 | BnO | H | H | 6.8 ± 0.8 |
| 2 ^b | BnO | Cl | H | 1.5 ± 0.1 |
| 14 | 4-CN-PhCH ₂ O | Cl | H | 2.7 ± 0.4 |
| 15 | | Cl | H | 1.5 ± 0.8 |
| 16 | | Cl | H | 1.1 ± 0.1 |
| 18 | | Cl | H | >6 ^c |
| 19 | | H | OMe | >3 ^d |
| 20 | | H | H | >100 ^a |
| 21 | | Cl | H | 0.8 ± 0.2 |
| 22 | | Cl | H | 1.6 ± 0.3 |
| 23 | | Cl | H | 28.0 ± 6.2 |
| 5 | BnO | Cl | CN | 7.0 ± 1.1 |
| 7 | BnO | Cl | CONH ₂ | 3.6 ± 0.3 |
| 6 ^b | BnO | Cl | COOH | 23.8 ± 2.5 |
| 3 | BnO | Cl | NO ₂ | 3.7 ± 1.1 |
| 4 | BnO | Cl | NH ₂ | 0.8 ± 0.1 |
| 8 | BnO | Cl | NHAc | 1.8 ± 0.5 |

^a BaENR inhibition was less than 30% at 100 μM.

^b MIC values against ΔANR *B. anthracis*¹⁵ for compound **2**: 16 μg/mL, for compound **6**: 74 μg/mL. MICs for all other compounds in the table are >80 μg/mL.

^c The inhibitor precipitated at concentrations >6 μM.

^d The inhibitor precipitated at concentrations >3 μM.

In conclusion, we have identified certain 2-pyridone derivatives as novel, small-molecule inhibitors of bacterial enoyl-ACP reductase (ENR) from *B. anthracis*. Compound **2** showed good ENR-inhibitory activity as well as reasonable antibacterial activity, thus providing a lead compound for further development. Compounds **4** and **21** show nearly a twofold improvement in ENR inhibitory activity over compound **2**. Compound **35**, a 'reversed' pyridone, is also an encouraging lead for the development of a new class of ENR inhibitors. Current efforts focus on further improvement of

Table 2
BaENR inhibitory activities of compounds

| Compound ^a | Structure | IC ₅₀ (μM) |
|-----------------------|-----------|-----------------------|
| 9 | | >100 ^b |
| 10 | | >100 ^b |
| 35 | | 0.7 ± 0.4 |
| 33 | | 18.8 ± 4.2 |
| 34 | | 23.7 ± 11.7 |
| 30 | | >100 ^b |
| 37 | | 21.4 ± 7.7 |

^a MIC values against ΔANR *B. anthracis* were >100 μg/mL.

^b BaENR inhibition was less than 30% at 100 μM.

BaENR inhibition and improving antibacterial activities of these compounds.

Acknowledgments

This work was funded by a grant from NIH/NIAID (U19 AI056575) and a contract from DOD (W81XWH-07-1-0445).

Supplementary data

Supplementary data associated with this article can be found, in the online version, at doi:10.1016/j.bmcl.2008.05.004.

References and notes

- (a) Rock, C. O.; Jackowski, S. *Biochem. Biophys. Res. Commun.* **2002**, 292, 1155; (b) Wakil, S. J. *Biochemistry* **1989**, 28, 4523.
- (a) Campbell, J. W.; Cronan, J. E., Jr. *Annu. Rev. Microbiol.* **2001**, 55, 305; (b) Heath, R. J.; White, S. W.; Rock, C. O. *Prog. Lipid Res.* **2001**, 40, 467.
- Rozwarski, D. A.; Grant, G. A.; Barton, D. H.; Jacobs, W. R., Jr.; Sacchettini, J. C. *Science (New York, NY)* **1998**, 279, 98.
- Levy, C. W.; Baldock, C.; Wallace, A. J.; Sedelnikova, S.; Viner, R. C.; Clough, J. M.; Stuitje, A. R.; Slabas, A. R.; Rice, D. W.; Rafferty, J. B. *J. Mol. Biol.* **2001**, 309, 171. and references cited therein.
- (a) McLeod, R.; Muench, S. P.; Rafferty, J. B.; Kyle, D. E.; Mui, E. J.; Kirisits, M. J.; Mack, D. G.; Roberts, C. W.; Samuel, B. U.; Lyons, R. E.; Dorris, M.; Milhous, W. K.; Rice, D. W. *Int. J. Parasitol.* **2001**, 31, 109; (b) Ref. 8 and references cited therein.
- (a) Kitagawa, H.; Kumura, K.; Takahata, S.; Iida, M.; Atsumi, K. *Bioorg. Med. Chem. Lett.* **2007**, 15, 1106; (b) Kitagawa, H.; Ozawa, T.; Takahata, S.; Iida, M.; Saito, J.; Yamada, M. *J. Med. Chem.* **2007**, 50, 4710. and references cited therein; (c) Moir, D. T. *Curr. Drug Targets Infect. Disord.* **2005**, 5, 297. and references cited therein.

7. Karlowsky, J. A.; Laing, N. M.; Baudry, T.; Kaplan, N.; Vaughan, D.; Hoban, D. J.; Zhanel, G. G. *Antimicrob. Agents Chemother.* **2007**, *51*, 1580.
8. Tipparaju, S. K.; Mulhearn, D. C.; Klien, G. M.; Chen, Y.; Tapadar, S.; Bishop, M. H.; Yang, S.; Chen, J.; Ghassemi, M.; Santarsiero, B. D.; Cook, J. L.; Johlfs, M.; Mesecar, A. D.; Johnson, M. E.; Kozikowski, A. P. *ChemMedChem*, in press.
9. Klein, G. M.; Bernard, D. S.; Tipparaju, S. K.; Pegan, S.; Bishop, M. H.; Kozikowski, A. P.; Mesecar, A. D. *Biochemistry* **2007**, accepted for publication.
10. Wang, L. Q.; Falany, C. N.; James, M. O. *Drug Metab. Dispos.* **2004**, *32*, 1162.
11. The synthesized pyridones were docked into the *B. anthracis* ENR active site from the crystal structure with PDB code 2QIT. GOLD docking was performed using the default parameters and the ChemScore scoring function. GOLD reference: Verdonk, M. L.; Cole, J. C.; Hartshorn, M. J.; Murray, C. W.; Taylor, R. D. *Proteins* **2003**, *52*, 609.
12. Conreux, D.; Bossharth, E.; Monteiro, N.; Desbordesb, P.; Balmea, G. V. *Tetrahedron Lett.* **2005**, *46*, 7917.
13. Kozikowski, A. P.; Adamczyk, M. J. *Org. Chem.* **1983**, *48*, 366.
14. Shone, R. L.; Coker, V. M.; Moormann, A. E. *J. Heterocycl. Chem.* **1975**, *12*, 389.
15. Detailed description of methods for biological assay is provided in [Supplementary information](#).
16. Meyer, E. A.; Castellano, R. K.; Diederich, F. *Angew. Chem., Int. Ed.* **2003**, *42*, 1210.

JMB

Available online at www.sciencedirect.com

ScienceDirect



Structural Basis for Catalysis of a Tetrameric Class IIa Fructose 1,6-Bisphosphate Aldolase from *Mycobacterium tuberculosis*

Scott D. Pegan^{1,2}, Kamolchanok Rukseree^{3,4}, Scott G. Franzblau³ and Andrew D. Mesecar^{1,2,3*}

¹Department of Medicinal Chemistry and Pharmacognosy, University of Illinois at Chicago, Chicago, IL 60607, USA

²Center for Pharmaceutical Biotechnology, University of Illinois at Chicago, Chicago, IL 60607, USA

³Institute for Tuberculosis Research, University of Illinois at Chicago, Chicago, IL 60612, USA

⁴National Center for Genetic Engineering and Biotechnology (BIOTEC), National Science and Technology Development Agency, Thailand Science Park, Pathumthani 12120, Thailand

Received 20 October 2008;
received in revised form
5 January 2009;
accepted 6 January 2009

Mycobacterium tuberculosis, the causative agent of tuberculosis (TB), currently infects one-third of the world's population in its latent form. The emergence of multidrug-resistant and extensive drug-resistant strains has highlighted the need for new pharmacological targets within *M. tuberculosis*. The class IIa fructose 1,6-bisphosphate aldolase (FBA) enzyme from *M. tuberculosis* (MtFBA) has been proposed as one such target since it is upregulated in latent TB. Since the structure of MtFBA has not been determined and since there is little information available on its reaction mechanism, we sought to determine the X-ray structure of MtFBA in complex with its substrates. By lowering the pH of the enzyme in the crystalline state, we were able to determine a series of high-resolution X-ray structures of MtFBA bound to dihydroxyacetone phosphate, glyceraldehyde 3-phosphate, and fructose 1,6-bisphosphate at 1.5, 2.1, and 1.3 Å, respectively. Through these structures, it was discovered that MtFBA belongs to a novel tetrameric class of type IIa FBAs. The molecular details at the interface of the tetramer revealed important information for better predictability of the quaternary structures among the FBAs based on their primary sequences. These X-ray structures also provide interesting and new details on the reaction mechanism of class II FBAs. Substrates and products were observed in geometries poised for catalysis; in addition, unexpectedly, the hydroxyl-enolate intermediate of dihydroxyacetone phosphate was also captured and resolved structurally. These concise new details offer a better understanding of the reaction mechanisms for FBAs in general and provide a structural basis for inhibitor design efforts aimed at this class of enzymes.

© 2009 Published by Elsevier Ltd.

Keywords: class II fructose 1,6-bisphosphate aldolase; *Mycobacterium tuberculosis*; dihydroxyacetone; glyceraldehyde 3-phosphate; aldol condensation

Edited by M. Guss

Introduction

Tuberculosis (TB) is one of the most prevalent infections in the world and a leader among the causes of mortality in developing countries. Infections by *Mycobacterium tuberculosis*, the causative agent of TB, have been estimated by the World Health Organization at 9.2 million new cases during 2006, with 1.7 million *M. tuberculosis*-related deaths. This is an increase over the 9.1 million new cases reported in 2005.¹ Additionally, one-third of the world's population is estimated to have latent *M. tuberculosis*.¹ Although the increase in new TB cases is attributed to population growth, new drug-resistant strains that

*Corresponding author. Center for Pharmaceutical Biotechnology, University of Illinois at Chicago, 900 South Ashland Avenue, M/C 870, Chicago, IL 60607, USA. E-mail address: mesecar@uic.edu.

Abbreviations used: TB, tuberculosis; FBA, fructose 1,6-bisphosphate aldolase; MtFBA, *M. tuberculosis* FBA; DHAP, dihydroxyacetone phosphate; FBP, fructose 1,6-bisphosphate; G3P, glyceraldehyde 3-phosphate; PGH, phosphoglycolohydroxamate; HEI, hydroxyl-enolate intermediate; TIM, triose-phosphate isomerase; PEG, polyethylene glycol.

threaten to increase this number and thwart efforts to eradicate this disease have also emerged. Incidences of multidrug-resistant TB and extensive drug-resistant TB are on the rise, requiring the development of new treatment regimens, drugs, and drug targets.²

One potential drug target for TB is class II fructose 1,6-bisphosphate aldolase (FBA) from *M. tuberculosis* (MtFBA; E.C. 4.1.2.13). MtFBA is one of two classes of FBAs located within *M. tuberculosis*. These FBAs are responsible for mediating the second reversible step of the glycolytic pathway, which supplies glyceraldehyde 3-phosphate (G3P) for downstream enzymes in the pathway and fructose 1,6-bisphosphate (FBP) for gluconeogenesis. Together, the substrates and products of the FBA reaction are crucial for the supply of these precursor molecules to other biochemical pathways essential for the survival of *M. tuberculosis*.

Class I and class II FBAs both catalyze the reversible adol condensation of dihydroxyacetone phosphate (DHAP) with G3P to form FBP,³ and both classes are hypothesized to have evolved independently from a common ancestor since they are both composed of (α/β)₈-barrel folds.⁴ However, the two classes differ in the mechanisms they utilize to catalyze the reaction, their prevalence among species, and their roles in autotrophic prokaryotes. For instance, although both aldolases form enolate anions from DHAP for their reaction with G3P, class I FBAs use the ϵ -amino group of a lysine to elicit a Schiff-base intermediate, whereas class II aldolases utilize a Zn(II) cation to stabilize the enolate intermediate. Class II FBAs are also activated by monovalent cations, such as Na(I).³

In addition to the differences in their reaction mechanisms, the two classes of FBAs also differ in their distribution among different species. Higher organisms possess only class I FBAs, whereas protozoa, bacteria, fungi, and blue-green algae primarily have class II FBAs, with a few possessing both.^{5–7} In those species in which both classes of FBAs are present, such as *Escherichia coli* and other autotrophic prokaryotes, only class II FBA genes appear to be essential.^{4,8,9} Single-gene knockout attempts of the *E. coli* *fbaA* gene (class II) have proven to be unsuccessful, whereas knockouts of the *fbaB* gene (class I) are viable.^{8,10} Significant expression levels of class I FBA in *E. coli* were only observed in the presence of gluconeogenic substrates, suggesting that class I FBAs are only conditionally present.¹¹ JM2087, an *E. coli* strain with 11 gene mutations, including the *fbaA*-1 gene, has been reported to be viable, but the precise reason for the viability and that for the nature of the mutation in the *fbaA*-1 gene are ambiguous.¹² Studies on the *E. coli* *fba* genes are consistent with studies on *M. tuberculosis* in which only the class I enzyme is observed during high aeration conditions, while under hypoxic conditions, the class II MtFBA is singularly expressed at high levels.^{13,14} Attempts to replace the wild-type *fba* (class II) gene in *M. tuberculosis* with a deleted allele (Δfba) by a two-step homologous recombination procedure have also proven to be unsuccessful.¹⁵

Since one of the difficulties in the successful treatment of *M. tuberculosis* infections is the bacterium's ability to adopt a latent phenotype that allows survival of the bacterium under hypoxic conditions, targeting enzymes that are essential for survival under these conditions is vital. The lack of a class II FBA in humans and its critical role in bacteria highlight MtFBA as a promising target for pharmaceutical development.¹⁶ Previous efforts to design inhibitors for class II FBAs have had limited success due to lack of robust selectivity for class II FBAs over class I FBAs.^{17,18} Efforts to further develop these and other new inhibitors through structure-based drug discovery efforts have been hindered by the lack of available MtFBA structures. Moreover, structures of any class II FBA in productive substrate-bound, intermediate-bound, and product-bound complexes are currently unavailable.

Class II FBAs can be further categorized into class IIa and class IIb families. Traditionally, class IIa and class IIb FBAs were categorized according to sequence homology and their oligomeric state. Class IIa FBAs were considered dimers, while class IIb FBAs could be dimers, tetramers, or octamers.^{5,6,19} Members belonging to each family are observed to exhibit 40% sequence similarity, with 25%–30% sequence similarity to all class II FBAs.²⁰ MtFBA has been traditionally classified as a class IIa FBA based on its significant sequence homology to other class IIa FBAs (*E. coli* and *Streptomyces galbus*; Fig. 1).^{20,21} However, in recent expression studies on MtFBA, the enzyme was observed to form a tetramer during analytical size-exclusion chromatography even though it is considered to be a member of class IIa FBAs.⁴

Structures have been determined for members of each family, and these structures have been assumed to be representative of each family in general. Structures of class IIa and class IIb FBAs in complex with the inhibitor phosphoglycolohydroxamate (PGH) have been determined.^{6,21} Although PGH and its analogs are potent inhibitors of FBAs due to their structural similarity to DHAP, this similarity also makes them potent inhibitors of the human class I FBAs, which makes them nonspecific and undesirable for drug development.¹⁷ Additionally, the available X-ray structures of PGH complexes only provide general insight into one reaction step in the class II FBA mechanism, thereby leaving all the other steps of reaction unexplored structurally. A more thorough understanding of the structural basis for the binding and catalysis of substrates and products by MtFBA would therefore significantly enhance our understanding of the overall catalytic mechanism of class II FBAs and provide a better rationale for the development and improvement of existing and new class II FBA inhibitors.

An in-depth X-ray structural characterization of MtFBA was conducted with its natural substrates and products to investigate the oligomeric nature of this unique member of the class IIa FBAs and to aid in future structure-based drug discovery efforts. X-ray structures of MtFBA in complex with DHAP, 202

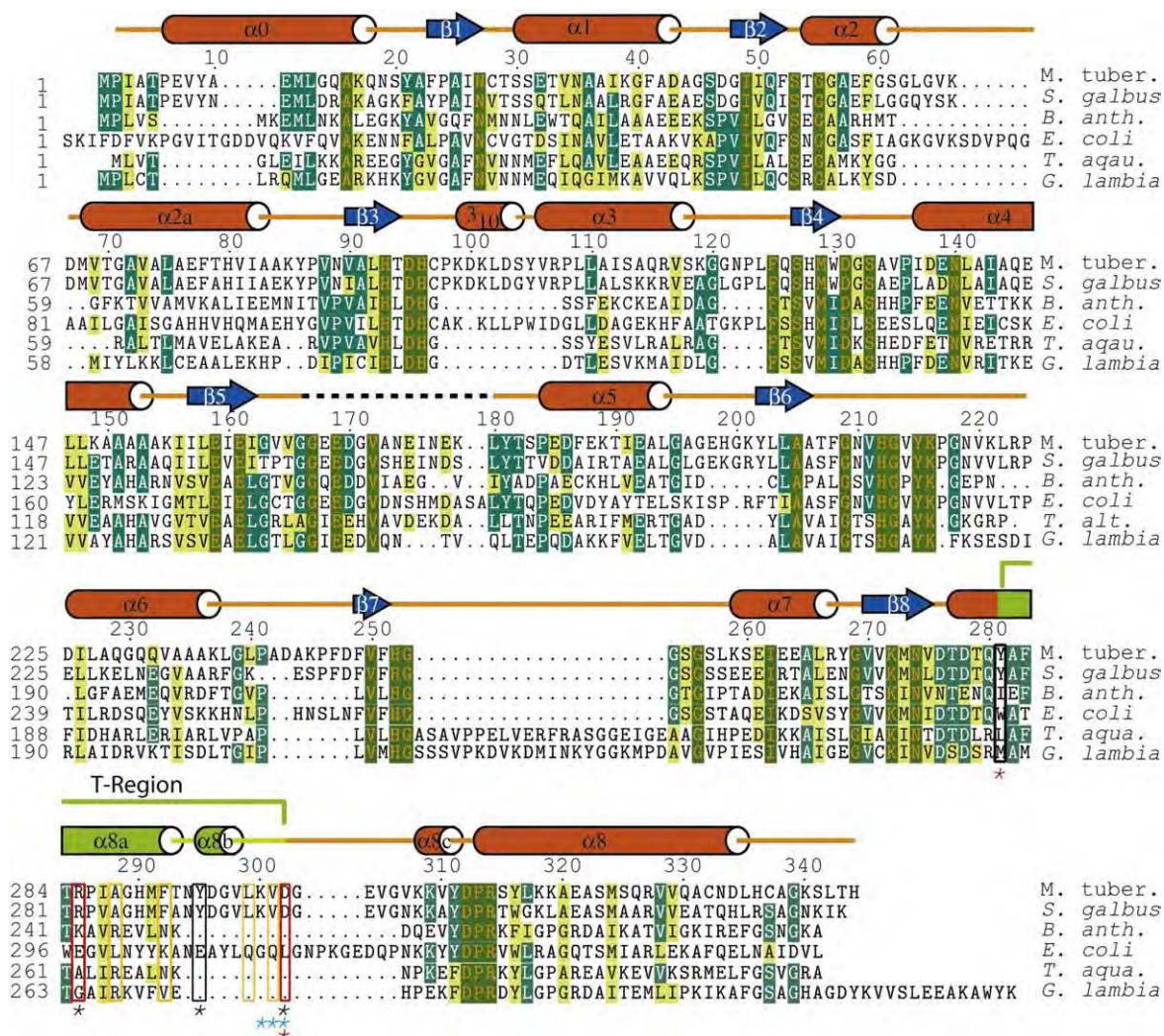


Fig. 1. Sequence alignment of various FBP aldolases. FBAs are from the H37RV strain of *M. tuberculosis* (protein accession code NP_334786), *S. galbus* (protein accession code CAA10483), *Bacillus anthracis* (protein accession code NP_847736), *E. coli* (PDB code 1B57_A), *T. aquaticus* (PDB code 1RV8_A), and *Giardia lamblia* (PDB code 2ISV_A). The alignment was generated using CLUSTALW, TEXSHADE, and BL2SEQ. Programs (<http://workbench.sdsc.edu/>) were used with the following parameters: matrix=BLOSUM62, gap opening penalty=11, gap extension penalty=1, and lambda ratio=0.85. Amino acids are color coded according to being nonconserved (white), similar (lime green), conserved (green), and completely conserved (dark green; orange lettering) across the six sequences. The secondary structure of MtFBA according to DSSP (Defined Secondary Structure of Proteins) is represented by orange cylinders (helical regions), blue arrows (β -sheet regions), yellow-orange shading (loops), green shading (T region), and dashed lines (missing residues). Residues in the T region are bracketed according to the type of tetrameric interactions they form. Residue side-chain properties are colored according to charge (red), hydrophobicity (yellow), or both (black). Red and black asterisks indicate interaction partners, while cyan asterisks indicate backbone H-bond interactions.

G3P, and FBP were determined to high resolution and revealed that MtFBA belongs to a novel tetrameric class of type IIa FBAs. The molecular details at the interface of the tetramer provide important information for better predictability of the oligomeric states among the FBAs based on their primary sequences. The structures also provide interesting and new details on the reaction mechanism of class II FBAs. The substrates and products were observed in geometries poised for catalysis; in addition, unexpectedly, the hydroxyl-enolate intermediate (HEI) of DHAP was also captured and resolved structurally.

Results

X-ray structural elucidation of MtFBA

A series of X-ray structures of MtFBA in complex with G3P, DHAP, and FBP were determined to resolutions between 1.3 and 2.1 Å (Table 1). The construct of MtFBA used for crystallization contained the full-length MtFBA enzyme with five additional histidine residues added to the C-terminal histidine, forming a hexahistidine affinity tag. MtFBA was co-crystallized with the substrate DHAP, and the

Table 1. Data collection and refinement

| | MtFBA-DHAP | MtFBA-DHAP-G3P | MtFBA-FBP |
|---|--------------------------|--------------------------|--------------------------|
| Data collection | | | |
| Space group | <i>I</i> 222 | <i>I</i> 222 | <i>I</i> 222 |
| Unit cell dimensions | | | |
| <i>a</i> , <i>b</i> , <i>c</i> (Å) | 61.3, 120.2, 164.8 | 61.2, 120.5, 164.3 | 60.6, 119.5, 164.0 |
| $\alpha = \beta = \gamma$ (°) | 90.0 | 90.0 | 90.0 |
| Resolution (Å) | 97.1–1.5 | 97.1–2.1 | 96.7–1.3 |
| No. of reflections observed | 421,305 | 105,670 | 688,310 |
| No. of unique reflections | 91,761 | 36,655 | 140,514 |
| R_{merge} (%) ^a | 5.4 (21.1) ^b | 5.0 (9.0) ^b | 5.8 (31.3) ^b |
| $I/\sigma I$ | 21.4 (4.6) ^b | 14.7 (10.6) ^b | 26.4 (4.1) ^b |
| Completeness (%) | 96.5 (89.6) ^b | 91.4 (78.5) ^b | 98.9 (94.8) ^b |
| Refinement | | | |
| Resolution range | 97.1–1.5 | 97.1–2.1 | 96.7–1.3 |
| No. of reflections in working set | 87,153 | 34,810 | 133,473 |
| No. of reflections in test set | 4602 | 1592 | 7033 |
| R_{work} (%) ^c | 16.7 | 15.8 | 15.8 |
| R_{free} (%) ^c | 17.8 | 18.1 | 17.0 |
| RMSD | | | |
| Bond lengths (Å) | 0.01 | 0.02 | 0.01 |
| Bond angles (°) | 0.73 | 1.74 | 1.20 |
| Protein/water atoms | 3274/533 | 2985/365 | 3257/533 |
| Average <i>B</i> -factors (Å ²) | 3274/533 | 2985/365 | 3257/533 |
| Total | 22.6 | 25.2 | 20.8 |
| Protein | 19.8 | 18.6 | 18.4 |
| Water | 34.6 | 34.6 | 41.0 |
| Ligands | 20.6 | 24.9 | 17.2 |
| Ions | 17.5 | 26.0 | 15.0 |

^a $R_{\text{merge}} = \sum_h \sum_i |I_i(h) - \langle I(h) \rangle| / \sum_h \sum_i I_i(h)$, where $I_i(h)$ is the *i*th measurement and $\langle I(h) \rangle$ is the weighted mean of all measurements of $I(h)$.

^b Data for the last resolution shell are shown in parentheses.

^c R_{work} and $R_{\text{free}} = h(|F(h)_o| - |F(h)_c|) / |F(h)_o|$ for reflections in the working and test sets, respectively.

complex crystallized as a monomer in the asymmetric unit (Fig. 2a and b). One sodium and two zinc cations were found bound to each monomer (Figs. 2 and 3). One of the two zinc cations (Zn1) is located within the active site, whereas the other zinc atom (Zn2) is located at a crystal contact between two symmetry-related MtFBA monomers formed through coordination to the hexahistidine tag (data not shown). Specifically, Zn2 coordinates with the δ -nitrogen of H344, the ϵ -nitrogen of H346, and the oxygen atom of water 105. The fourth and fifth coordination positions are occupied by the carboxyl group of E198 and ϵ -nitrogen of H199 of a symmetry-related MtFBA monomer.

The secondary structure of MtFBA resembles that of other bacterial class II aldolases^{5,22} (Fig. 2a and b). MtFBA has an eight-stranded β -sheet core in which each β -strand (β 1– β 8) is followed in general by an α -helix (α 1– α 8a), giving rise to an overall (β/α)₈-barrel fold. There are two deviations to the typical

(β/α)₈-barrel fold in MtFBA; one is the presence of a previously unobserved 3_{10} -helix between β -strand β 3 and α -helix α 3, and the other is an extra α -helix, α 2a, between α -helix α 2 and β -strand β 3 (Fig. 1). In addition to the (β/α)₈-barrel, four helices are also present within a monomer. One of these helices, α 0, blocks the entrance to the (β/α)₈-barrel on its N-terminal side (Fig. 2a). Two other helices, α 8b and α 8c, which are not observed in other FBA structures, form at the apex of an arm formed by α 8 and the fourth additional helix, α 8a (Fig. 2a). This arm and the (β/α)₈-barrel fold result in a monomer with dimensions of 78, 52, and 40 Å.

Quaternary structure and T region of MtFBA

The quaternary structure of MtFBA in solution is consistent with its being a tetramer based on our analytical size-exclusion chromatography experiments and those reported previously.⁴ Therefore,

Fig. 2. Overall monomer and tetramer structures of MtFBA illustrating the unique tetramerization interface of class IIa FBAs. (a) Cartoon representation of the MtFBP protomer bound with DHAP. Helical regions are rendered in orange; β -strands, in light blue; and loops, in yellow-orange. Zinc (gray) and sodium (purple) are illustrated as spheres. Missing residues 168–180 are represented by dashed lines. (b) Secondary structure matching alignment of MtFBA (orange) with chain A of FBA from *T. aquaticus* (PDB code 1RV8_A; blue). The T region of MtFBA is shown in green. (c) Tetramer of MtFBP with asymmetric unit protomer colored according to (a), with the T region highlighted in green. Symmetry-related protomers in pink, gray, and light blue with sodium (purple) and zinc (hot pink) are depicted as spheres. DHAP and HEI are shown in light cyan. Three axes are present (red, black, and magenta), illustrating crystallographic symmetry planes. Labels are in black for one protomer and in yellow for one of its symmetry-related protomers. (d) Close-up view of the T region rendered with residues represented as sticks and colored as in (c). Labels are in orange for protomer residues and outlined for symmetry-related residues.

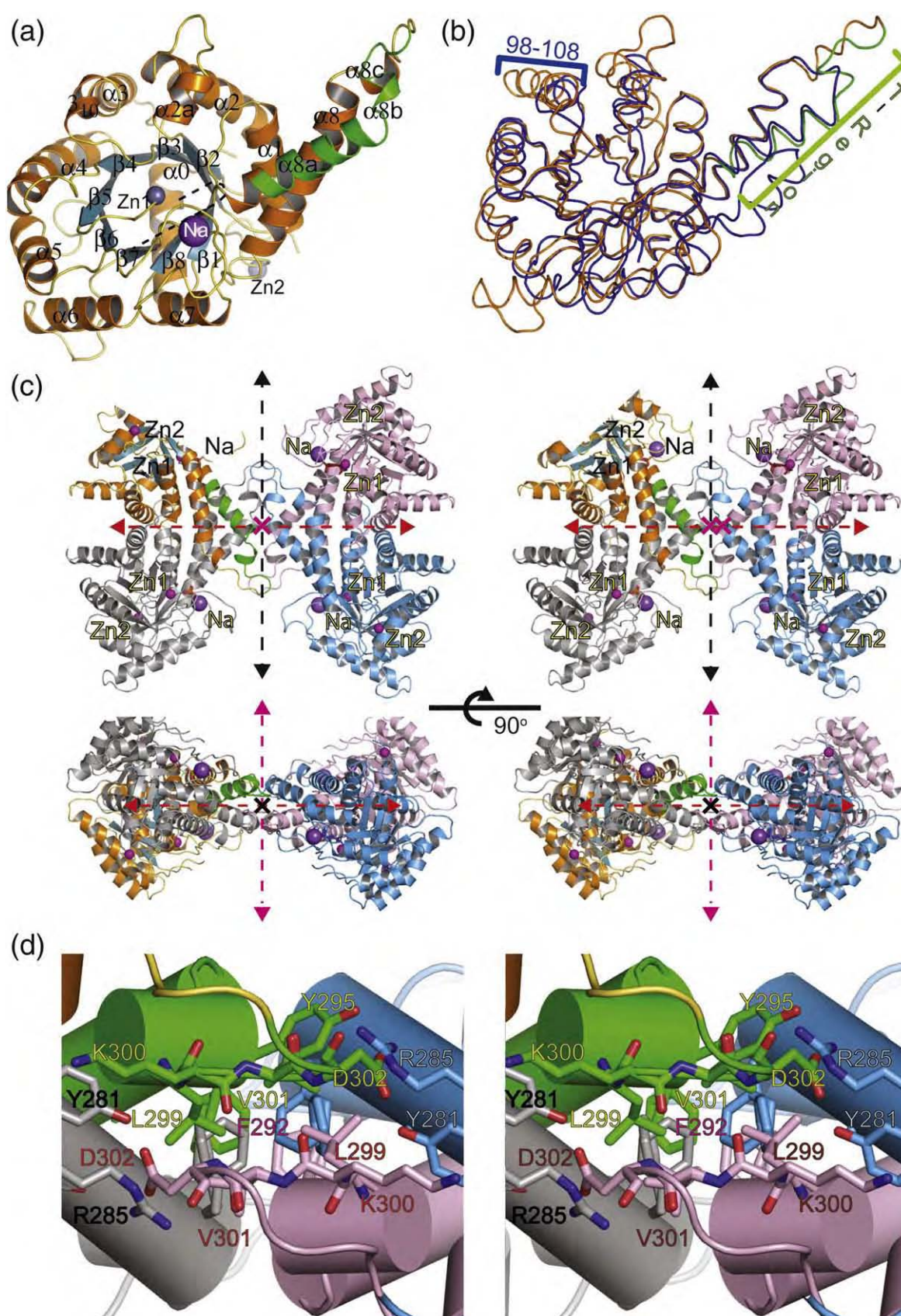


Fig. 2 (legend on previous page)

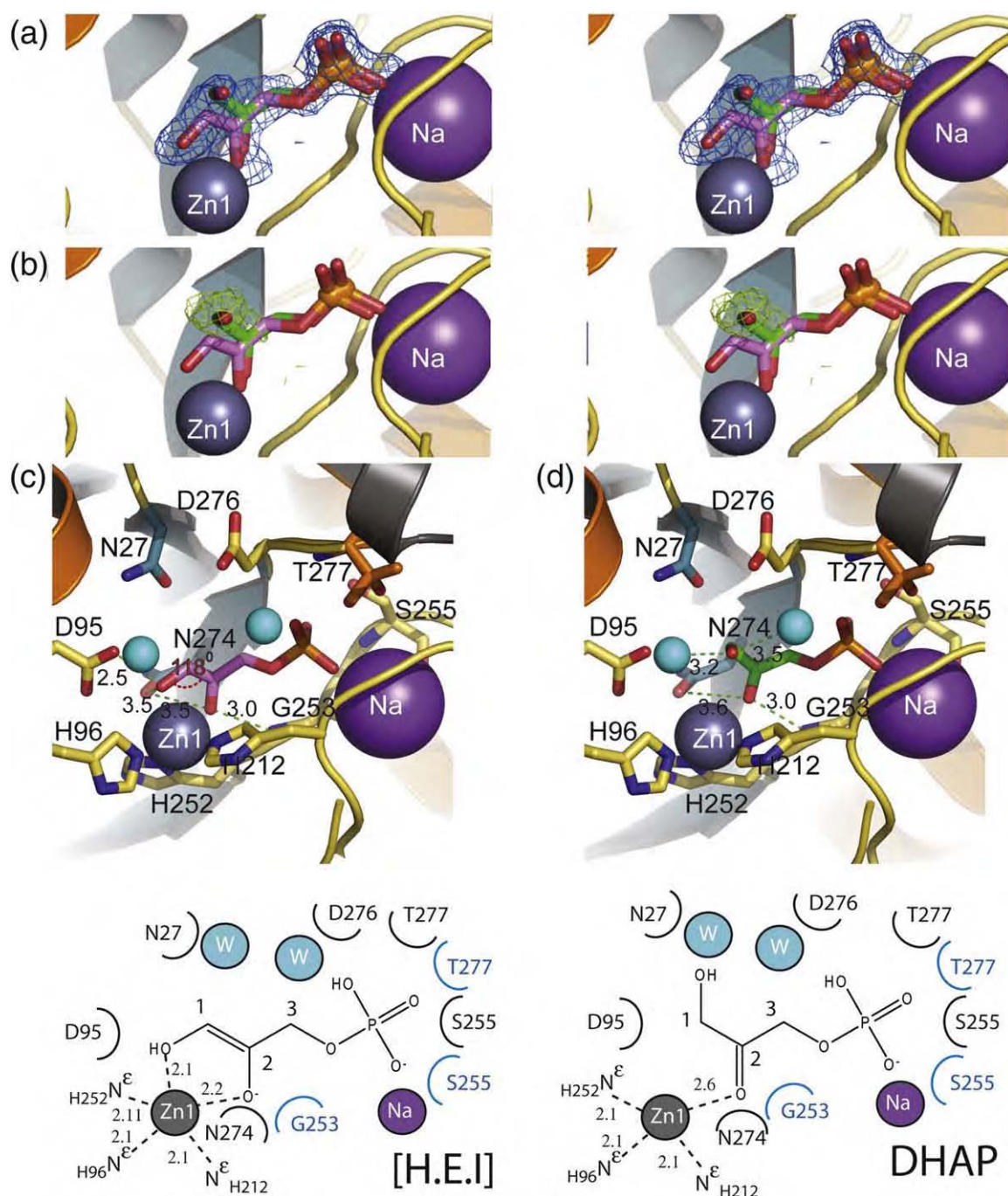


Fig. 3. Active-site structure of the MtFBA–DHAP complex. (a) Divergent-eyed stereo view of MtFBA active site with DHAP (green) and reaction intermediate HEI (violet). Asymmetric protomer carbon atoms are colored according to secondary structure: orange for helix, yellow-orange for loop, and dark cyan for β -strand. Heteroatoms are colored according to their element. Zinc (gray) and sodium (purple) ions are rendered as spheres according to atomic size. The $2F_o - F_c$ density maps calculated with DHAP and HEI present are contoured (blue) at 1σ . (b) $F_o - F_c$ electron density maps, calculated without DHAP present, are contoured (green) at 3σ . Colors for residues, ions, DHAP, and HEI are the same as in (a). (c) The active site of the MtFBA–DHAP complex, with DHAP removed for clarity, is shown at the top panel. Symmetry-related monomer cartoon is depicted in gray. Angles and associated labels are shown in red, with distances and associated labels shown in green. Water molecules (cyan) are depicted as spheres and are scaled to 50% for clarity. All other colors are as in (a). A two-dimensional representation of HEI bound to MtFBA is shown at the bottom panel. Residue labels and crescents are shown in black and illustrate the interaction of residues with HEI mediated through their side chains. Residue labels and crescents shown in cyan represent residues interacting with HEI through backbone heteroatoms. (d) The active site of the MtFBA–DHAP complex, with HEI removed for clarity, is shown at the top panel. Lines and associated labels for distance are shown in green. Water molecules (cyan) are depicted as spheres and are scaled to 50% for clarity. All other colors are as in (a). A two-dimensional representation of DHAP bound to MtFBA is shown at the bottom panel. Residue labels and crescents in black illustrate interaction of residues with HEI mediated through their side chains. All colors are as in (c).

the monomer observed in the asymmetric unit is likely only the protomer of a larger symmetrical tetramer. Analysis of the symmetry-related monomers within the unit cell of the *I*222 space group suggests that MtFBA exists as a dimer of dimers, with D2 quaternary symmetry consistent with the tetrameric species observed from size-exclusion chromatography. The monomer-monomer interface of the dimer has a total contact surface area of 2617 Å². This value compares well with the expected ranges of subunit interfacial surface areas for proteins with similar subunit molecular weights.²³ The monomer-monomer interactions within the dimer are facilitated by a mix of H bonds, salt bridges, and hydrophobic packing, which are also observed at the interface of the dimeric *E. coli* FBA.²² In summary, the monomer-monomer interface of the dimer is facilitated by the packing of α2a against its symmetry-related self and α8, α8a, and α8b on the arm of the monomer crossing over its symmetry-related counterpart (Fig. 2c).

The dimer-of-dimers interface of the tetramer involves a total contact surface area of 1220 Å², which is somewhat less than any value between ~2500 and 3600 Å², which is a general range for tetramers with similar molecular weights.²³ There are, however, a number of major interactions between the two dimers formed from a series of residues spanning from Y281 on the α8a helix to D302 just slightly beyond helix α8b. This region is designated the tetramerization region or "T region" (Figs. 1 and 2b–d).²⁴ The T region mediates tetramer formation by its interactions with other symmetry-related T regions (Fig. 2c). At the core of this interaction are residues F292 and Y295, which form interdimer hydrophobic interactions. Another set of hydrophobic interactions located at the T-region interface is observed between L299 and V301. In addition to hydrophobic interactions, the side-chain hydroxyl group of Y295 also forms an H bond with the side chain of R285. The side chain of R285 also participates in an H-bond network with the side chains of Y281 and D302. There is also an interdimer main-chain interaction formed by the amide of K300 and carbonyl of D302 from different dimers (Fig. 2d).

MtFBA–DHAP-bound active site

Examination of $F_o - F_c$ electron density difference maps within the active site of the MtFBA–DHAP complex revealed strong residual density not only for the substrate, DHAP, but, remarkably, also for its HEI. Under normal solvent conditions in the absence of enzyme, the C1 atom of DHAP is in an sp³ hybridized orbital with tetrahedral geometry. However, when bound to the active site, the bulk of the electron density associated with DHAP in the active site surrounding the C1–C2 bond of DHAP is planar, suggesting that the C1 atom is mainly in an sp² hybridized orbital consistent with a double bond between C1 and C2. This observation lends support for an HEI-like intermediate being bound within the active site. The geometry at the C1 position is similar to that of the FBA inhibitor PGH. Modeling and

refinement of an HEI molecule within the electron density accounted for the bulk of the electron density within the difference maps (Fig. 3a). However, a significant peak ($>3\sigma$) in the $F_o - F_c$ difference maps still remained and was only fully accounted for when the substrate DHAP was modeled into the density and refined at an occupancy DHAP/HEI ratio of 30:70 (Fig. 3a and b). Finally, the average B -factor of 20.6 Å² for the ligands is near the average value of 19.8 Å² for the protein (Table 1).

The active site of the HEI/DHAP-bound form of MtFBA closely resembles the active sites of other bacterial class II aldolase structures bound with the inhibitor PGH.^{6,25} For HEI, both the C1 hydroxyl and C2 enolate oxygen coordinate directly to the catalytic zinc, Zn1, which is coordinated directly to the enzyme by three histidines, H96, H212, and H256. As a result, the coordination number of Zn1 is 5 (T₅), and its geometry is that of a nonideal trigonal bipyramid.²⁶ The C1 hydroxyl of HEI also forms an H bond with D95 (2.5 Å), while the C2 enolate oxygen forms an H-bond interaction with the backbone amide group of G253 (3.0 Å) (Fig. 3c). Similar to HEI, the C2 ketone oxygen of DHAP forms an H bond with the backbone amide of G253 and coordinates to Zn1 with a bond distance of 2.6 Å, which is a bit longer than the bond distance between the enolate oxygen of HEI and Zn1, which is 2.2 Å. The C1 hydroxyl group of DHAP forms H-bond interactions with the side chain of D295 (3.0 Å) and with nearby active-site water molecules (Fig. 3d). The remaining MtFBA–HEI/DHAP interactions are indistinguishable between one another. The phosphate groups of the HEI and DHAP form H bonds with the side-chain hydroxyl and backbone amide groups of S255 and T277, as well as an ionic interaction with Na⁺ (Fig. 3d).

MtFBA–G3P–DHAP precatalysis structure

MtFBA is observed to have a sharp pH optimum of 7.8.⁴ Above or below this pH level, MtFBA quickly loses its ability to mediate the enol condensation of DHAP and G3P or its reversible reaction.^{4,7} The crystallization conditions of MtFBA–DHAP involved preincubation of the enzyme with the substrate DHAP with buffering at approximately pH 8.0 and then setting up crystallization trials with buffering at pH 4.8. The drop in pH upon crystallization suggests that we have trapped MtFBA with DHAP and an HEI-like intermediate bound in a catalytically unreactive form. In the case of HEI, this may actually result in the formation of an enediol intermediate (see Discussion).

We took advantage of this low pH trapping approach and soaked MtFBA–DHAP/HEI crystals for 24 h in mother liquor containing 2 mM concentration of the substrate G3P prior to X-ray data collection. A complete X-ray data set of 2.1 Å was obtained and refined against the MtFBA–DHAP/HEI structure (Table 1). Overall, the tertiary structure of MtFBA remained unchanged. However, additional and strong ($>3\sigma$) electron density in $F_o - F_c$ difference maps was observed within the active site

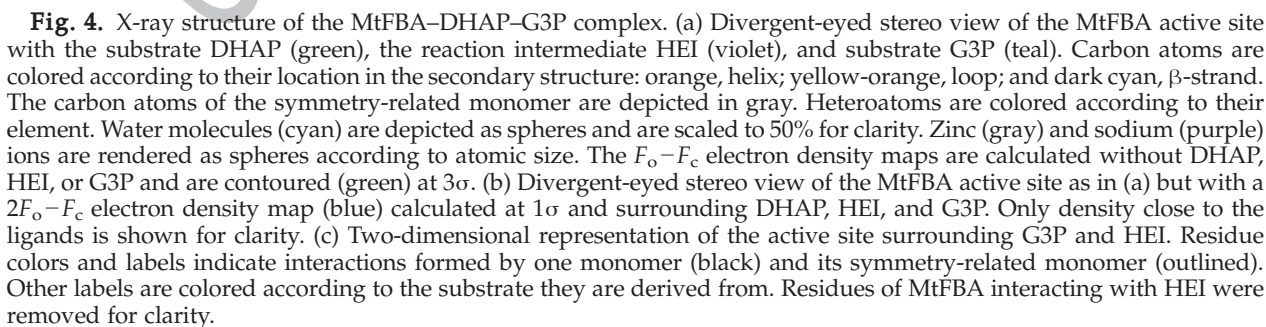


(Fig. 4a). Examination of both $F_o - F_c$ and $2F_o - F_c$ weighted maps proved the density to be that for G3P and DHAP/HEI and not for fructose 1,6-biphosphate (Fig. 4a and b). Thus, we effectively trapped the Michaelis complex for the MtFBA-catalyzed reaction. Final refinement of the structure with HEI/DHAP and G3P resulted in R_{work} and R_{free} values of 15.8% and 18.1%, respectively.

Within the active site of the MtFBA-G3P-DHAP/HEI structure, the position of the HEI molecule remained unchanged, compared with the DHAP/HEI complex, but the DHAP molecule was pushed slightly deeper into the active-site pocket, with the C1 hydroxyl group rotating away from the water molecule it had previously formed an H bond with (Fig. 4). In the end, this placed the C1 of DHAP about 4.4 Å from the C1 of G3P in comparison with the distance of 3.3 Å between the C1 of HEI and C1 of G3P (Fig. 4c). In comparison with the DHAP/HEI binding site that used cations and backbone amide groups, G3P binding is facilitated mostly through interactions with side chains and water molecules (Fig. 4c). Specifically, the C2 hydroxyl of G3P forms H bonds with active-site water molecules that are also shared with the DHAP binding site. This hydroxyl also forms a direct H bond (3.0 Å) with the side chain of D276, which also forms a weak H bond (3.4 Å) with the phosphoester oxygen as well as H bonds with water molecules directly hydrogen bonded to the phosphate moiety.

The C6-phosphate moiety is G3P's main source of interaction with MtFBA. The phosphate oxygen atoms form H bonds with the side chain of S53 and with the side-chain guanidinium group of R314 from a symmetry-related monomer at the dimer interface. The remaining H bonds are formed with water molecules and the side chains of K308 and R314, which are contributed by symmetry-related monomers. The importance of the interaction between R314 and the C6 phosphate of FBP and G3P has been shown through mutagenesis and modeling experiments with *E. coli* FBA.^{27,28} When the equivalent residue (R331) in *E. coli* is mutated to an alanine residue, a 26-fold increase in the K_M value for FBP and a 29-fold decrease in k_{cat} are observed.²⁷

MtFBA-FBP structure

Since the interaction of FBA with the substrate FBP has not been reported for any class II or bacterial aldolase, it was therefore of great interest to determine. We first attempted to co-crystallize FBP with MtFBA, which produced crystals suitable for X-ray diffraction. We collected a 1.7-Å data set and refined the model against the MtFBA-DHAP structure with DHAP removed. Unfortunately, only density supporting the presence of DHAP/HEI was observed, indicating that FBP had undergone complete cleavage. Evidently, the resulting steady-state concentration of G3P was insufficient to adequately occupy the G3P site (Fig. 1S). Cleavage of the FBP in these drops was not a complete surprise since FBP was added directly to the protein

solution buffered at pH 8.0 prior to conducting crystallization trials.

To overcome this issue, we took advantage of the low pH conditions of the preformed MtFBA-HEI/DHAP crystals and attempted to trap FBP in the active site by soaking the crystals overnight in mother liquor containing 10 mM FBP. A 1.3-Å X-ray data set was collected, and the data were refined against the MtFBA-DHAP structure with ligands removed. Under these conditions, strong ($>3\sigma$) and continuous electron density was apparent in $F_o - F_c$ and $2F_o - F_c$ difference maps, which was consistent with a fully occupied FBP molecule (Fig. 5a). The average B -factor value of 17.2 Å² for the ligands was also found to be slightly lower than the average value of 18.4 Å² for the protein (Table 1). Thus, under the experimental conditions employed, the bound DHAP and HEI molecules were able to exchange with free FBP from solvent.

The active-site structure of the MtFBA-FBP structure was remarkably similar to the other two complexes in that the residues, ions, and water molecules forming interactions between the enzyme and FBP are similar to those involved in binding DHAP/HEI and G3P (Fig. 5). The C1-phosphate moiety of FBP is bound by the same residues and sodium ion as observed for DHAP/HEI and DHAP/G3P (Fig. 5a and b). The C3 hydroxyl oxygen coordinates with the catalytic zinc with a short bond distance of 2.2 Å, whereas the C2 ketone and C4 hydroxyl groups coordinate with the zinc with slightly longer bonds of 2.6 and 2.4 Å, respectively. In addition to coordinating to Zn1, the C4 hydroxyl group, which would be deprotonated during the cleavage of FBP in the glycolytic direction, forms an H-bond interaction with an active-site water molecule (2.7 Å), and it comes in close proximity to D276 (3.7 Å), which is proposed to accept the proton from the C4 hydroxyl.

Discussion

Modes of tetramerization among class II FBAs

The structure of MtFBA highlights the structural divergence of tetramer formation between class IIa and class IIb FBAs. Similar to class IIa MtFBA, *Thermus aquaticus* FBA forms a tetramer through a dimer-dimer interaction. However, the dimer-dimer interaction is formed along helices $\alpha 3$ and $\alpha 4$ in *T. aquaticus* FBA, whereas the tetramer interface lies on the other side of the dimer along $\alpha 8a$ and the previously unobserved single helical turn $\alpha 8c$ in MtFBA. The preference for one form of tetramerization over the other can be deciphered from the sequences and structural comparison of MtFBA and *T. aquaticus* FBA. MtFBA, as with other class II FBAs, possesses a conserved insert of 10 residues (98–108) comprising a 3_{10} -helix and a four-residue insertion (121–124) that accommodates the 3_{10} -helix (Figs. 1 and 2b). These additional residues of MtFBA and

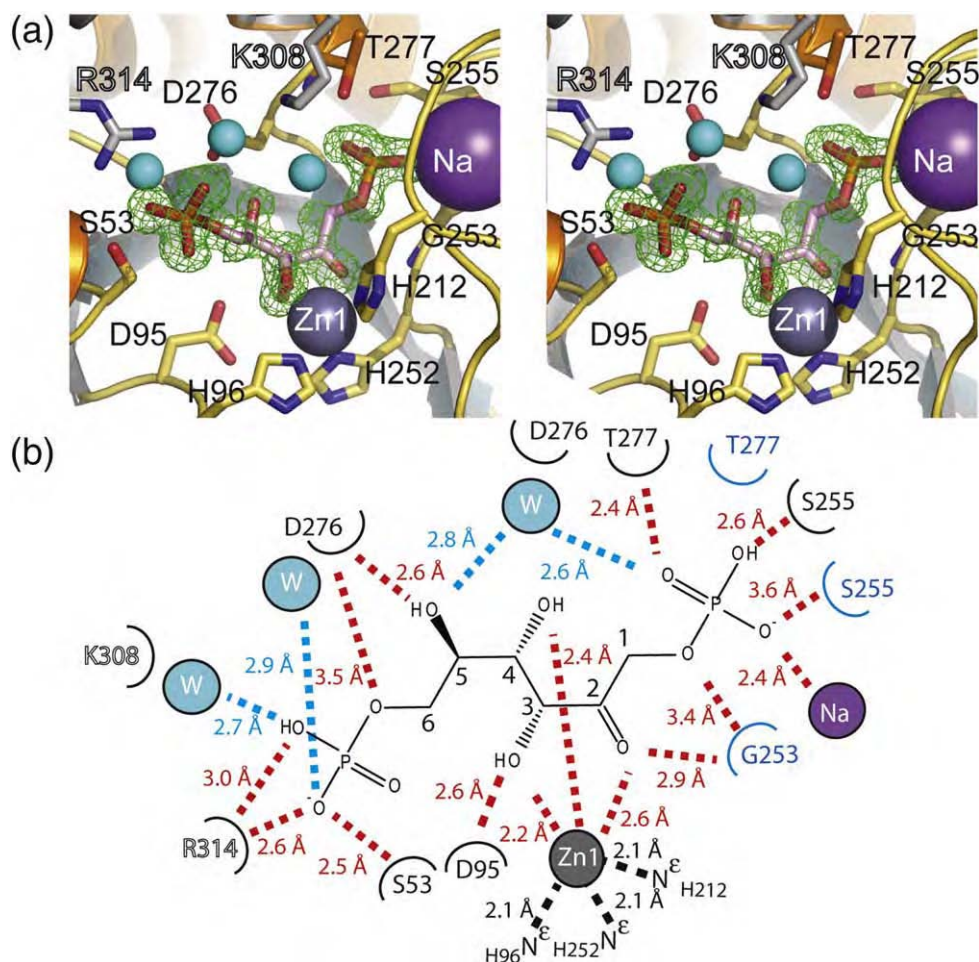


Fig. 5. X-ray structure of the MtFBA active site with FBP bound. (a) Divergent-eyed stereo view of the MtFBA-FBP active site. Residues are colored according to the secondary structure: orange, helix; dark cyan, β -strand; and yellow-orange, loop. Symmetrically related monomers are depicted in gray. All heteroatoms are colored according to their respective elemental colors. Water molecules (cyan), zinc (gray), and sodium (purple) are rendered as spheres. Zinc and sodium are scaled to their atomic radii, with water molecules at 50% scaling for clarity. The $F_o - F_c$ electron density map (green) was calculated in the absence of FBP and is contoured at 3σ . (b) Two-dimensional illustration of the active site surrounding FBP. Monomer residues are in continuous black labels, and symmetry-related monomer residues have outlined black labels.

other class IIa FBAs create a steric clash if packed in the same manner of the *T. aquaticus* tetramer. Thus, the *T. aquaticus*-like tetramer cannot form.

Just as structural features of MtFBA inhibit tetramer formation in the manner of *T. aquaticus*, the lack of structural features in *T. aquaticus* in the tetramerization domain of MtFBA inhibits *T. aquaticus* FBA from forming such tetramers as MtFBA. *T. aquaticus* FBA does not possess an insertion of 13–18 residues in length (MtFBA 294–306) that is present in the majority of class IIa FBAs, MtFBA (*E. coli* FBA and *S. galbus* FBA; Fig. 1). These 13 residues in MtFBA form a significant part of the T region and form five hydrophobic and two ionic interactions essential to tetramer formation (Fig. 2b and d). Interestingly, the presence of an insert at the T-region location does not automatically infer tetrameric assembly among class IIa FBAs. *E. coli* FBA contains an insert at this location but is a dimer, leading to the conclusion that certain key sequence positions must contain specific amino acids in order

to produce a tetrameric species. With the nature of MtFBA and *T. aquaticus* FBA's tetrameric assembly now known, the potential of predicting other class IIa and class IIb FBA tetramers can be realized.

Divergent methods of oligomerization among isoenzymes have been reported for other enzymes. Glutamate racemases 1 and 2 have been observed to adopt different dimer-dimer interactions despite high sequence similarity.²⁹ Both class I and class II FBAs have been observed to form multiple oligomeric states. Class I FBAs have primarily been characterized as tetrameric species in eukaryotes, with a few bacterial class I FBAs forming monomeric-to-decameric oligomeric states.⁴ Previously, only class IIb FBAs were determined to have the same oligomeric range as class I FBAs.^{4,21,22} The evolutionary pressure for FBAs forming oligomeric structures is currently unknown. However, the prevalence of FBAs forming higher-order oligomeric states, primarily tetramers, coupled with the appearance that these enzymes have independently

evolved to form these higher oligomers suggests an evolutionary advantage for organisms carrying higher oligomeric FBAs.

Reaction mechanism for MtFBA

In contrast to previously determined X-ray structures of class II FBAs in complex with the inhibitor PGH, which only represents an intermediate/analog state of the substrate DHAP, the X-ray structures of MtFBA reported here represent bona fide substrate-, product-, and intermediate-bound states along the entire reaction pathway. A superposition of the X-ray structures for these complexes is shown in Fig. 6. Analysis of these structures, in conjunction with the available literature on site-directed mutagenesis, kinetic, and solution biochemical studies for the class II FBAs, has led us to add important structural details to the mechanistic scheme presented in Fig. 7 for the reaction catalyzed by these enzymes.

The structure of the MtFBA–DHAP complex helps provide an understanding of how MtFBA can bind DHAP and carry out its conversion to HEI. Within the MtFBA–DHAP structure, we observed both DHAP and a molecule with geometry analogous to HEI. The molecules are found bound in a 30:70 ratio of DHAP to HEI. The predominance of an HEI-like intermediate suggests that deprotonation of DHAP occurred prior to or during crystallization. Since MtFBA was first incubated with DHAP at pH 8.0 before crystallization, deprotonation of DHAP could have occurred during the preincubation period, thereby forming HEI (steps 1 and 2 in Fig. 7). Since the enzyme was added to an acidic crystallization solution, solvent-derived protons could help stabilize the MtFBA–HEI complex by

protonating the enolate oxygen, essentially trapping an enediol intermediate (steps 2 and 3). Unfortunately, it is impossible to distinguish between the two possible intermediates (HEI or an enediol) by X-ray crystallography since they have the same geometry, a problem that neutron diffraction studies could more directly address.

Deprotonation of DHAP during steps 1 and 2 is likely catalyzed by a glutamate residue (E169 in MtFBA). Studies have suggested that a highly conserved glutamate residue located between $\beta 5$ and $\alpha 5$ (residues 168–180 in MtFBA) is involved in the extraction of the C1 proton from DHAP for class II FBAs (Fig. 1).³⁰ This loop region is analogous to the well-characterized E165 of loop 7 in chicken triose-phosphate isomerase (TIM) responsible for deprotonation of DHAP in TIM. Multiple studies have directly linked increased and decreased flexibility of loop 7 in TIM to a proportional response in k_{cat} .³¹

Unfortunately, in all structures of MtFBA, amino acid E169 and the other residues (168–180) within the loop are structurally unresolved. This observation is similar for all other class II FBA structures that have been elucidated. Electron density for the putative catalytic glutamate can only be visualized in the structure of the *E. coli* class IIa FBA in complex with the inhibitor PGH, which was formed under a high (2–5 mM) concentration of zinc.²⁵ In this structure [Protein Data Bank (PDB) code 1B57], the glutamate points toward PGH but is too far away to abstract a proton. However, the position of glutamate may be contorted by the presence of a spurious zinc atom bound near the active site, a zinc not observed in any of the MtFBA structures crystallized in the presence of 0.1 M zinc. Additionally, the position of the loop could be pH dependent as the *E. coli* homolog was crystallized at pH 7.5, instead of

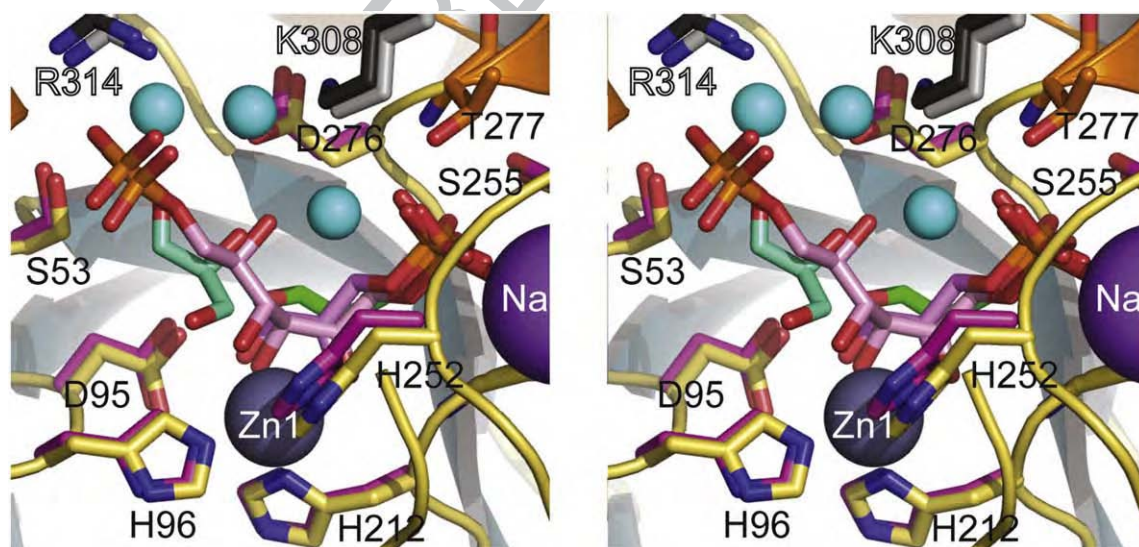


Fig. 6. Divergent-eyed stereo view of a superposition of the MtFBA–FBP and MtFBA–DHAP–G3P complexes. Residues of MtFBA–FBP are colored according to their secondary structure location: orange, helix; dark cyan, β -strand; and yellow-orange, loop. Symmetrically related monomers are depicted in gray. All heteroatoms are colored according to their respective elemental colors: (cyan), zinc (gray), and sodium (purple) are rendered as spheres. Zinc and sodium are scaled to their atomic radii, with water molecules at 50% scaling for clarity. The MtFBA–DHAP–G3P structure is represented in magenta, with symmetry-related monomers in dark gray.

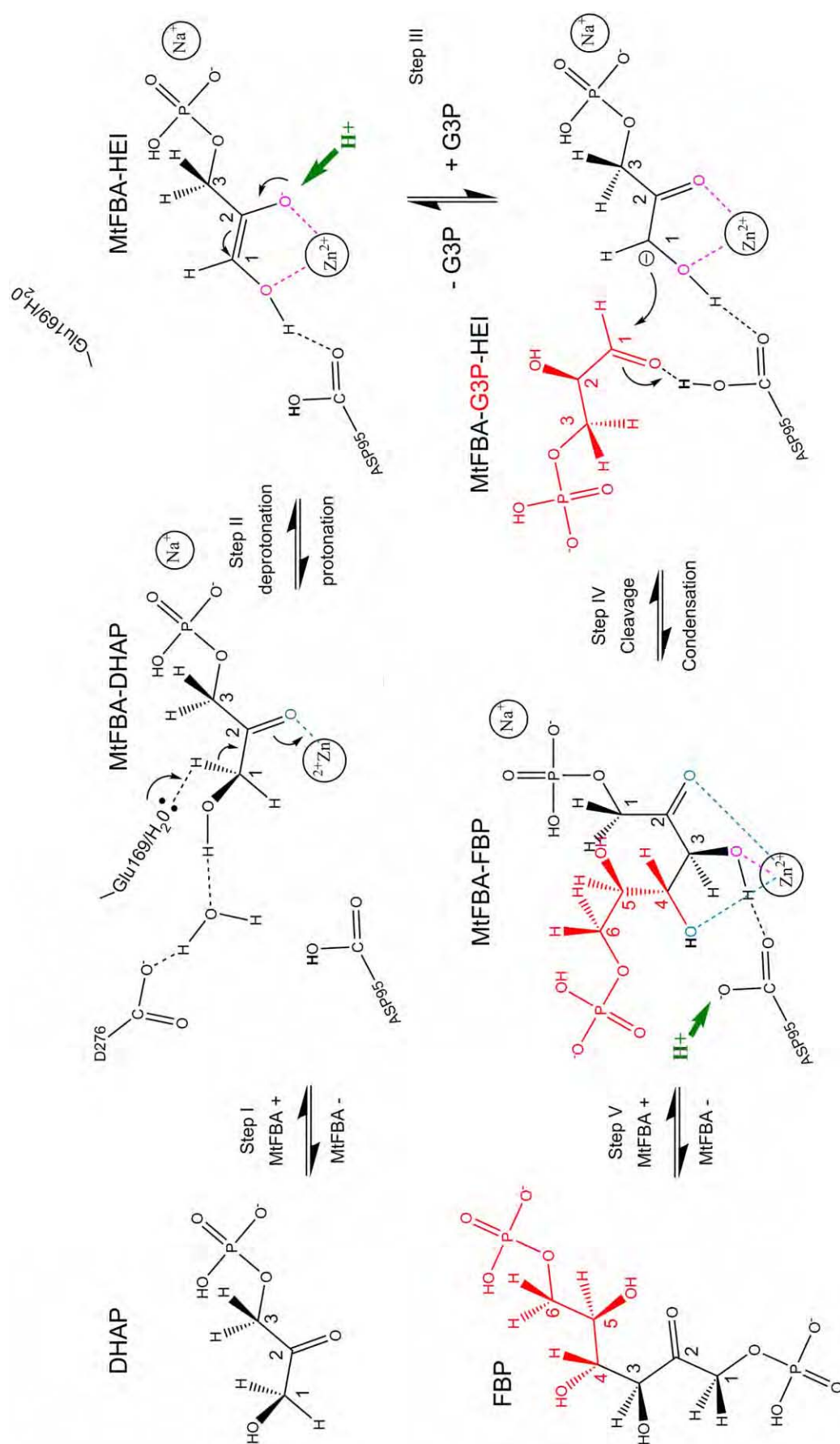


Fig. 7. Proposed reaction mechanism for MtFBA, with elements sourced from G3P in red. Blue and magenta denote coordination and H bonds formed with the Zn1, respectively. Green highlights places in the mechanism where proton trapping could occur.

MtFBA's pH 4.8. To date, this residue has not been observed in any class II FBA structure to be positioned in a manner that would allow deprotonation of DHAP. However, the presumed proximity of this loop and the associated glutamate to several water molecules suggests that it may alternatively activate water molecules via a proton shuttle in the solvent-rich MtFBA active site. At a minimum, the MtFBA-DHAP-G3P and MtFBA-FBP structures assert that the glutamate side chain must be allowed to leave the active site to expose it to solvent and thereby allow G3P or FBP to bind (Fig. 6). The inherent flexibility of this loop is critical for proper deprotonation/protonation and substrate-product binding events, which have been demonstrated for class II FBA from *E.coli*³⁰ (Fig. 7).

The presence of both DHAP and HEI within the active site allows for independent elucidation of their respective interactions with MtFBA. The C1 hydroxyl group of DHAP undergoes H bonding with active-site water molecules anchored by side chains of D276 and symmetry-related K308 instead of the side chain of D95 (Fig. 3d). Moreover, neither of the oxygen atoms in DHAP is located close enough to the Zn1 to form what would be considered a strong first-coordination sphere bond. At 2.6 Å, the ketone of DHAP is the closest, but at this distance, it is more suitably classified as a second-sphere H-bond interaction (Fig. 3d).²⁶ Only upon extraction of the proton from C1 and its conversion to HEI are full coordination bonds observed between the intermediate and MtFBA, placing the catalytic zinc in nonideal trigonal bipyramidal geometry (Fig. 3c and d).

In addition to the required movement of the glutamate out of the active site so that G3P can bind, the coordination state of the catalytic zinc changes upon G3P binding. The active-site structure of the MtFBA-DHAP-G3P complex shows that only the

C1 hydroxyl oxygen maintains a short bond distance of ~2.2 Å with the Zn1 cation. The C2 oxygen bond distance of HEI to Zn1 increases to 2.6 Å (Fig. 4c). This suggests that the electronic nature surrounding the C2 ketone or hydroxyl (enediol) may change after proton extraction from C1 and subsequent binding of G3P.

The MtFBA-G3P-DHAP/HEI structure also adds clarity to step 4 of the reaction mechanism (Figs. 6 and 7). Previous studies have proposed an interaction between the aldehyde on G3P with D95 (MtFBA residue number) in the DHAP-G3P complex prior to catalysis.^{25,30,32} The X-ray structures of the MtFBA-DHAP-G3P and MtFBA-HEI-G3P complexes add important new details to this part of the catalytic reaction. The structure of the MtFBA-DHAP-G3P complex shows that prior to catalysis, this bond has not yet formed since the G3P ketone is incorrectly oriented to create this interaction (Fig. 4). Analysis of the MtFBA-HEI-G3P structure suggests that during the formation of this complex, a significant movement of the ketone oxygen occurs during the condensation reaction such that D95 can interact with the oxygen and thereby protonate the developing negative charge (Fig. 7). In addition, the MtFBA-FBP structure illustrates that the resulting hydroxyl (C4 on FBP or C1 from G3P) forms a coordination bond with Zn1, suggesting that the zinc atom serves to activate G3P in addition to D95 (Figs. 5 and 6).

Finally, by comparing the MtFBA-G3P-DHAP and MtFBA-FBP active sites, the formation of the C3 and C4 bond of FBP during the condensation step of the reaction can be envisioned. The C1 of G3P moves within 3.3 Å of the C1 of HEI before catalysis while simultaneously rotating the oxygen of the aldehyde of G3P toward the zinc atom (Fig. 5c). Upon formation of FBP, the C2, C3, and C4 oxygen atoms all coordinate to the zinc atom, albeit

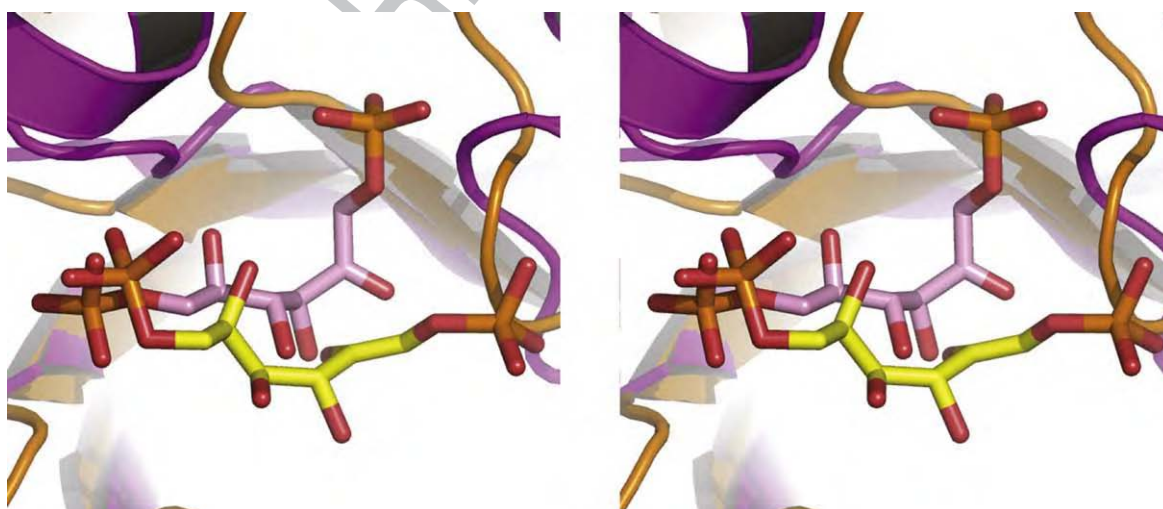


Fig. 8. Different binding orientations for FBP to class I and class II FBAs. A stereo view of the MtFBA-FBP active site is shown superposed with human muscle aldolase bound with FBP (4ALD). The MtFBA-FBP structure is shown in orange, with FBP shown in pink. Human aldolase is shown in purple with the bound FBP molecule shown in yellow. The Zn1 and Na molecules have been removed from the MtFBA active site for clarity.

to varying extents (Fig. 7), and the C4 hydroxyl oxygen comes within hydrogen-bonding distance of D95. This latter residue has been shown via site-directed mutagenesis studies to be critical for deprotonation of FBP in the forward/glycolytic reaction direction.^{30,32}

Specificity of class I and class II FBAs for FBP

In addition to clarifying the final steps of the FBA mechanism, the MtFBA-FBP structure also provides information for future structure-based design endeavors aimed at inhibiting class II FBAs. The conformation that FBP adopts when bound to MtFBA is divergent to conformations observed in class I FBA structures. When MtFBA-FBP is aligned via secondary structure matching with human aldolase complexed with FBP, the conformational differences become clear (Fig. 8).³³ When bound to MtFBA, FBP adopts a more constrained orientation where the hydroxyls of C3, C4, and the ketone of C2 point toward the zinc ion, forming coordination bonds. In the human class I FBA structure, only two hydroxyls on C3 and C4 face themselves in the same direction with the C2 ketone, which is oriented in the opposite direction (Fig. 8). Small molecules designed to exploit the conformational differences of FBP between classes I and II FBAs could enhance selectivity.

In conclusion, the structures of MtFBA bound to DHAP/HEL, DHAP-G3P, and FBP provide new and valuable information toward our understanding of the class II FBA reaction mechanism and subunit association of class IIa FBAs, thereby providing greater predictability of FBA oligomeric states across species in general. The structures of MtFBA and the structures of the human class I FBAs should now provide a basis for structure-based inhibitor design studies aimed at selectively targeting MtFBA.

Materials and Methods

Construction of MtFBA expression vectors

The *M. tuberculosis fba* gene (Rv0363c) was PCR amplified from *M. tuberculosis* H₃₇RV genomic DNA using the oligonucleotides 5'-GGTGGT**CATATG**CC-TATCGCAACGCC-3' and 5'-GAAGATCTAATGGT-GATGGT**GATG** GTGGGTTAGGGACTTTC-3' as the forward primer and the reverse primer, respectively. NdeI and BglII restriction sites (in bold) were incorporated into the two primers. Five histidine codons were also added into the reverse primer. The PCR product was cleaned by a QIAquick PCR purification kit (Qiagen) and digested with NdeI and BglII enzymes. The digested fragment was purified and cloned into the expression vector pET17b using NdeI and BamHI ends to form the pET-fbaH construct, which produces a C-terminal His-tagged fusion protein referred to as MtFBA. The construct was introduced into *E. coli* BL21(DE3) cells by heat-shock transformation. The resulting pET-fbaH plasmid was then purified, restriction analyzed, and sequenced to verify the construct.

Production and purification of MtFBA

E. coli harboring pET-fbaH was grown at 37 °C in 8 L of 825 LB broth containing 100 µg/mL of ampicillin until the 829 OD₆₀₀ was about 0.6 and then induced by 0.4 mM IPTG. 830 The culture was further grown for 4–6 h at 25 °C and then 831 centrifuged at 3000g for 15 min. Cells were washed with 832 phosphate-buffered saline and stored at –20 °C until use. 833 The cell pellets collected from the 8-L culture were lysed 834 by the addition of BugBuster Master Mix (Novagen) 835 following the manufacturer's instructions. Insoluble cell 836 debris was removed by centrifugation at 16,000g for 837 20 min at room temperature. The clarified extract was 838 loaded directly onto Ni-NTA Bind Resin (Novagen) 839 preequilibrated in buffer A (50 mM sodium phosphate 840 buffer, pH 8.0, and 300 mM NaCl) with 10 mM imidazole. 841 MtFBA bound to the Ni-NTA column, which was then 842 washed with 32 column volumes of buffer A plus 20 mM 843 imidazole followed by 40 column volumes of buffer A 844 plus 50 mM imidazole. MtFBA was eluted from the 845 column with 6 column volumes of buffer A plus 250 mM 846 imidazole. The eluate was subsequently concentrated in 847 an Amicon-15 Ultracel 100K (Millipore) centrifuge con- 848 centrator and dialyzed against an exchange buffer [20 mM 849 Tricine (N-[2-hydroxy-1,1-bis(hydroxymethyl)ethyl]gly- 850 cine) buffer, pH 8.0, 100 mM NaCl, 0.1 mM ZnCl₂, and 851 2 mM DTT] prior to application to gel filtration. 852

MtFBA was applied to a Superdex-200 Hiload 26/60 853 FPLC column preequilibrated with the exchange buffer 854 and eluted at a flow rate of 4 mL/min. Fractions were 855 pooled according to the chromatogram, concentrated to 856 12 mg/mL in an Amicon-15 Ultracel 100K (Millipore) 857 centrifuge concentrator, and filtered through a 0.65-µm 858 membrane filter. Approximately, 80 mg of protein was 859 obtained from 8 L of culture medium. 860

MtFBA crystallization

Initial crystal conditions for MtFBA were determined 862 from high-throughput screening of Qiagen Nextel Screens, 863 Classics, Classics II, PEGs (polyethylene glycols), PEGs II, 864 Anion, Cation, PhClear I, and PhClear II suites in a 96-well 865 sitting-drop format using a Tecan Freedom Evo 200 liquid 866 handling robot. Drops were 1 µL of protein solution to 867 1 µL of precipitate with a 100-µL reservoir volume. 868 Samples of 12-mg/mL protein solutions in 20 mM Tricine 869 buffer, pH 8.0, 100 mM NaCl, 0.1 mM ZnCl₂, and 2 mM 870 DTT were used for the screening. Initial screening resulted 871 in several hits, all in conditions containing high PEGs with 872 weights greater than 3350 and pH above 7.5. Crystals 873 resulting from these conditions appeared to be bipyrami- 874 dal in morphology and proved to provide poor diffraction 875 (data not shown). 876

Subsequently, a second screen using the same 768 877 conditions and protein concentration was conducted with 878 MtFBA in the presence of 270 µM DHAP (Sigma D7137) or 879 FBP (Sigma F0752) added to the protein solution prior to 880 crystallization. Results of this screen largely mirrored 881 those of the apo screen but had a few additional hits. 882 Analysis of these additional hits revealed one condition 883 that formed MtFBA crystals that were cubic in morphol- 884 ogy and formed in a relatively divergent condition, 30% 885 PEG 300, and 0.1 M Na-acetate, pH 4.8. Final crystals for 886 all structures were obtained by vapor diffusion with 887 500 µL of reservoir and 4 µL of hanging drops mixed 1:1 888 with protein solution and precipitant, 26% PEG 300, and 889 0.1 M Na-acetate, pH 4.8. Co-crystals for the MtFBA– 890 DHAP complex were sourced from drops in which the 891

MtFBA protein solution containing 270 μ M DHAP was used. MtFBA-FBP complex crystals were sourced from crystals co-crystallized in the presence of protein solution containing 270 μ M FBP and then soaked in mother liquor containing 2 mM FBP for 24 h. MtFBA-DHAP-G3P complex crystals were derived from crystals generated by co-crystallization of MtFBA-DHAP and soaked with 2 mM G3P (Sigma G5251) for 24 h.

X-ray structural determination of MtFBA-DHAP, DHAP-G3P, and FBP complexes

The X-ray data set for MtFBA-DHAP-G3P was collected on our in-house HR200 Rigaku rotating copper anode source using a 1.54-Å wavelength X-ray beam. X-ray data sets for MtFBA-DHAP and MtFBA-FBP were collected at SER-CAT beamline 22-BM and 22-ID, respectively. All crystals were mounted on nylon loops and submerged in a 5- μ L cryo-solution of 30% PEG 300 and 0.1 M Na-acetate, pH 4.8. Crystals were subsequently flash frozen in liquid nitrogen. Frozen crystals were mounted under stream of dry N₂ at 100 K. All data sets were collected using 0.5-deg oscillations using either an area RAXIS IV⁺⁺ detector (MtFBA-DHAP-G3P) or CCD detectors MAR 225 (MtFBA-DHAP) and MAR 300 (MtFBA-FBP). X-ray images were indexed, processed, integrated, and scaled together using the program HKL2000.³⁴

A molecular replacement solution for MtFBA-DHAP was obtained using the CCP4 suite and the molecular replacement tool Phaser with a 3D-JIGSAW homology protomer model of MtFBA based on *E. coli* FBA (1B57).^{35,36} WinCoot was used for model building, and Refmac5.2 from the CCP4 suite was used for refinement.³⁶ Coordinates and molecular library files for the ligands DHAP, G3P, HEI, and FBP were built using the program CCP4 suite program Sketcher. Final refinement was conducted using TLS (translation-libration-screw) restraints from TLS motion determination.³⁷ Isotropic temperature factors were refined for the MtFBA-DHAP and MtFBA-DHAP-G3P structures, whereas anisotropic temperature factors were used for the MtFBA-FBP structure. Water molecules were added to $F_o - F_c$ density peaks that were greater than 3 σ using the "Find Water" WinCoot program function. The final models were checked for structural quality using the CCP4 suite programs Procheck and Sfccheck.

Accession codes

Structure factors and coordinates have been deposited with the PDB and assigned with codes 3EKL, 3EKZ, and 3ELF.

Acknowledgements

This research was supported in part by the National Institutes of Health (grant P01AI060915; S.D.P. and A.D.M.), Department of Defense (grant W81XWH0710445 USAMRAA; A.D.M.), and National Center for Genetic Engineering and Biotechnology (Thailand; K.R.). Data were collected at the Southeast Regional Collaborative Access Team (SER-CAT) 22-ID and 22-BM beamlines at

the Argonne National Laboratory Advanced Photon Source. Supporting institutions may be found at www.ser-cat.org/members.html. Use of the Advanced Photon Source was supported by the U.S. Department of Energy, Office of Science, Office of Basic Energy Sciences, under contract no. W-31-109-Eng-38.

References

- World Health Organization. (2008). Global tuberculosis control—surveillance, planning, financing. 957
- World Health Organization. (2008). Tuberculosis MDR-TB & XDR-TB. February. 958
- Rutter, W. J. (1964). Evolution of aldolase. *Fed. Proc.* **23**, 1248–1257. 959
- Ramsaywak, P. C., Labbe, G., Siemann, S., Dmitrienko, G. I. & Guillemette, J. G. (2004). Molecular cloning, expression, purification, and characterization of fructose 1,6-bisphosphate aldolase from *Mycobacterium tuberculosis*—a novel class II A tetramer. *Protein Expression Purif.* **37**, 220–228. 960
- Izard, T. & Sygusch, J. (2004). Induced fit movements and metal cofactor selectivity of class II aldolases: structure of *Thermus aquaticus* fructose-1,6-bisphosphate aldolase. *J. Biol. Chem.* **279**, 11825–11833. 961
- Galkin, A., Kulakova, L., Melamud, E., Li, L., Wu, C., Mariano, P. *et al.* (2007). Characterization, kinetics, and crystal structures of fructose-1,6-bisphosphate aldolase from the human parasite, *Giardia lamblia*. *J. Biol. Chem.* **282**, 4859–4867. 962
- Marsh, J. J. & Lebherz, H. G. (1992). Fructose-bisphosphate aldolases: an evolutionary history. *Trends Biochem. Sci.* **17**, 110–113. 963
- Gerdes, S. Y., Scholle, M. D., Campbell, J. W., Balazsi, G., Ravasz, E., Daugherty, M. D. *et al.* (2003). Experimental determination and system level analysis of essential genes in *Escherichia coli* MG1655. *J. Bacteriol.* **185**, 5673–5684. 964
- Stribling, D. & Perham, R. N. (1973). Purification and characterization of two fructose diphosphate aldolases from *Escherichia coli* (Crookes' strain). *Biochem. J.* **131**, 833–841. 965
- Baba, T., Ara, T., Hasegawa, M., Takai, Y., Okumura, Y., Baba, M. *et al.* (2006). Construction of *Escherichia coli* K-12 in-frame, single-gene knockout mutants: the Keio collection. *Mol. Syst. Biol.* **2**, 2006.0008. 966
- Scamuffa, M. D. & Caprioli, R. M. (1980). Comparison of the mechanisms of two distinct aldolases from *Escherichia coli* grown on gluconeogenic substrates. *Biochim. Biophys. Acta*, **614**, 583–590. 967
- Davis, E. O., Jones-Mortimer, M. C. & Henderson, P. J. (1984). Location of a structural gene for xylose-H⁺ symport at 91 min on the linkage map of *Escherichia coli* K12. *J. Biol. Chem.* **259**, 1520–1525. 968
- Rosenkrands, I., Slayden, R. A., Crawford, J., Aagaard, C., Barry, C. E., 3rd & Andersen, P. (2002). Hypoxic response of *Mycobacterium tuberculosis* studied by metabolic labeling and proteome analysis of cellular and extracellular proteins. *J. Bacteriol.* **184**, 3485–3491. 969
- Bai, N. J., Pai, M. R., Murthy, P. S. & Venkitesubramanian, T. A. (1974). Effect of oxygen tension on the aldolases of *Mycobacterium tuberculosis* H37Rv. *FEBS Lett.* **45**, 68–70. 970
- Rukseree, K. (2007). Fructose-1,6-bisphosphate aldolase as a potential drug target for tuberculosis. Ph.D. dissertation, Mahidol University. 971

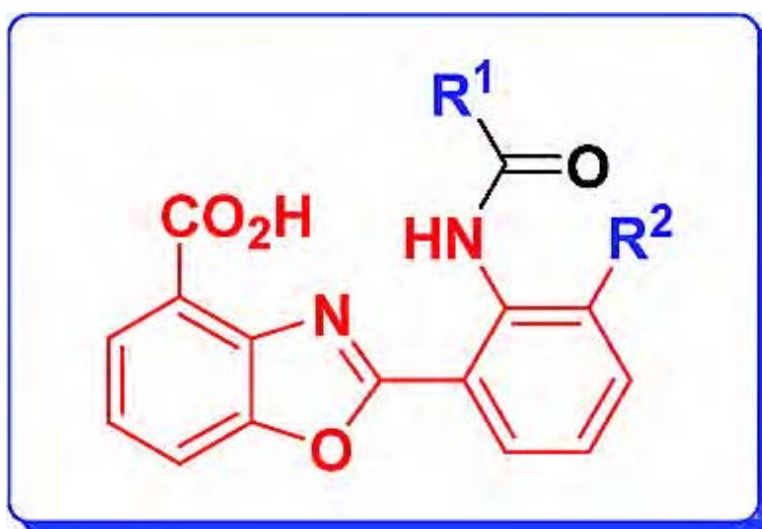
- 1015 16. Zhang, Y. (2005). The magic bullets and tubercu- 1063
1016 losis drug targets. *Annu. Rev. Pharmacol. Toxicol.* **45**, 1064
1017 529–564.
- 1018 17. Fonvielle, M., Weber, P., Dabkowska, K. & Therisod, 1066
1019 M. (2004). New highly selective inhibitors of class II 1067
1020 fructose-1,6-bisphosphate aldolases. *Bioorg. Med.* 1068
1021 *Chem. Lett.* **14**, 2923–2926.
- 1022 18. Gavalda, S., Braga, R., Dax, C., Vigroux, A. & 1070
1023 Blonski, C. (2005). *N*-Sulfonyl hydroxamate deriva- 1071
1024 tives as inhibitors of class II fructose-1,6-diphosphate 1072
1025 aldolase. *Bioorg. Med. Chem. Lett.* **15**, 5375–5377.
- 1026 19. Nakahara, K., Yamamoto, H., Miyake, C. & Yokota, A. 1074
1027 (2003). Purification and characterization of class-I and 1075
1028 class-II fructose-1,6-bisphosphate aldolases from the 1076
1029 cyanobacterium *Synechocystis* sp. PCC 6803. *Plant Cell* 1077
1030 *Physiol.* **44**, 326–333.
- 1031 20. Plaumann, M., Pelzer-Reith, B., Martin, W. F. & 1080
1032 Schnarrenberger, C. (1997). Multiple recruitment of 1081
1033 class-I aldolase to chloroplasts and eubacterial origin 1082
1034 of eukaryotic class-II aldolases revealed by cDNAs 1083
1035 from *Euglena gracilis*. *Curr. Genet.* **31**, 430–438.
- 1036 21. Sauve, V. & Sygusch, J. (2001). Molecular cloning, 1084
1037 expression, purification, and characterization of fruc- 1085
1038 tose-1,6-bisphosphate aldolase from *Thermus aquati-* 1086
1039 *cus*. *Protein Expression Purif.* **21**, 293–302.
- 1040 22. Cooper, S. J., Leonard, G. A., McSweeney, S. M., 1088
1041 Thompson, A. W., Naismith, J. H., Qamar, S. *et al.* 1089
1042 (1996). The crystal structure of a class II fructose-1,6- 1090
1043 bisphosphate aldolase shows a novel binuclear metal- 1091
1044 binding active site embedded in a familiar fold. 1092
1045 *Structure*, **4**, 1303–1315.
- 1046 23. Janin, J., Miller, S. & Chothia, C. (1988). Surface, 1094
1047 subunit interfaces and interior of oligomeric proteins. 1095
1048 *J. Mol. Biol.* **204**, 155–164.
- 1049 24. Krissinel, E. & Henrick, K. (2007). Inference of 1096
1050 macromolecular assemblies from crystalline state. *J.* 1097
1051 *Mol. Biol.* **372**, 774–797.
- 1052 25. Hall, D. R., Leonard, G. A., Reed, C. D., Watt, C. I., 1100
1053 Berry, A. & Hunter, W. N. (1999). The crystal structure 1101
1054 of *Escherichia coli* class II fructose-1, 6-bisphosphate 1102
1055 aldolase in complex with phosphoglycolohydroxa- 1103
1056 mate reveals details of mechanism and specificity. *J.* 1104
1057 *Mol. Biol.* **287**, 383–394.
- 1058 26. Alberts, I. L., Nadassy, K. & Wodak, S. J. (1998). 1105
1059 Analysis of zinc binding sites in protein crystal 1106
1060 structures. *Protein Sci.* **7**, 1700–1716.
- 1061 27. Qamar, S., Marsh, K. & Berry, A. (1996). Identification 1107
1062 of arginine 331 as an important active site residue in 1108
1111 the class II fructose-1,6-bisphosphate aldolase of 1109
1112 *Escherichia coli*. *Protein Sci.* **5**, 154–161.
28. Zgiby, S. M., Thomson, G. J., Qamar, S. & Berry, A. 1065
(2000). Exploring substrate binding and discrimina- 1066
tion in fructose 1,6-bisphosphate and tagatose 1,6- 1067
bisphosphate aldolases. *Eur. J. Biochem.* **267**, 1068
1858–1868.
29. May, M., Mehboob, S., Mulhearn, D. C., Wang, Z., Yu, 1070
H., Thatcher, G. R. *et al.* (2007). Structural and 1071
functional analysis of two glutamate racemase iso- 1072
zymes from *Bacillus anthracis* and implications for 1073
inhibitor design. *J. Mol. Biol.* **371**, 1219–1237.
30. Zgiby, S., Plater, A. R., Bates, M. A., Thomson, G. J. & 1075
Berry, A. (2002). A functional role for a flexible loop 1076
containing Glu182 in the class II fructose-1,6-bispho- 1077
sphate aldolase from *Escherichia coli*. *J. Mol. Biol.* **315**, 1078
131–140.
31. Thanki, N., Zeelen, J. P., Mathieu, M., Jaenicke, R., 1080
Abagyan, R. A., Wierenga, R. K. & Schliebs, W. (1997). 1081
Protein engineering with monomeric triosephosphate 1082
isomerase (monoTIM): the modelling and structure 1083
verification of a seven-residue loop. *Protein Eng.* **10**, 1084
159–167.
32. Plater, A. R., Zgiby, S. M., Thomson, G. J., Qamar, S., 1086
Wharton, C. W. & Berry, A. (1999). Conserved 1087
residues in the mechanism of the *E. coli* class II FBP- 1088
aldolase. *J. Mol. Biol.* **285**, 843–855.
33. Dalby, A., Dauter, Z. & Littlechild, J. A. (1999). Crystal 1090
structure of human muscle aldolase complexed with 1091
fructose 1,6-bisphosphate: mechanistic implications. 1092
Protein Sci. **8**, 291–297.
34. Otwinowski, Z. & Minor, W. (1997). Processing of X- 1094
ray diffraction data collected in oscillation mode. In 1095
Macromolecular Crystallography, Part A (Carter Jr, C. W. 1096
& Sweet, R. M., eds), *Macromolecular Crystallography*, 1097
Part A, 276, pp. Academic Press, New York, NY.
35. Bates, P. A., Kelley, L. A., MacCallum, R. M. & 1099
Sternberg, M. J. (2001). Enhancement of protein 1100
modeling by human intervention in applying the 1101
automatic programs 3D-JIGSAW and 3D-PSSM. 1102
Proteins, 39–46.
36. Collaborative Computational Project No. 4. (1994). 1104
The CCP4 suite: programs for protein crystallography. 1105
Acta Crystallogr., Sect. D: Biol. Crystallogr. **50**, 760–763.
37. Painter, J. & Merritt, E. A. (2006). Optimal description 1107
of a protein structure in terms of multiple groups 1108
undergoing TLS motion. *Acta Crystallogr., Sect. D: Biol.* 1109
Crystallogr. **62**, 439–450.

In Pursuit of Natural Product Leads: Synthesis and Biological Evaluation of 2-[3-hydroxy-2-[(3-hydroxypyridine-2-carbonyl)amino]phenyl]benzoxazole-4-carboxylic acid (A-33853) and Its Analogues: Discovery of *N*-(2-Benzoxazol-2-ylphenyl)benzamides as Novel Antileishmanial Chemotypes

Suresh K. Tipparaju, Sipak Joyasawal, Marco Pieroni, Marcel Kaiser, Reto Brun, and Alan P. Kozikowski

J. Med. Chem., **2008**, 51 (23), 7344-7347 • DOI: 10.1021/jm801241n • Publication Date (Web): 07 November 2008

Downloaded from <http://pubs.acs.org> on January 27, 2009



More About This Article

Additional resources and features associated with this article are available within the HTML version:

- Supporting Information
- Access to high resolution figures
- Links to articles and content related to this article
- Copyright permission to reproduce figures and/or text from this article

[View the Full Text HTML](#)

Letters

**In Pursuit of Natural Product Leads:
Synthesis and Biological Evaluation of
2-[3-hydroxy-2-[(3-hydroxypyridine-2-
carbonyl)amino]phenyl]benzoxazole-
4-carboxylic acid (A-33853) and Its
Analogues: Discovery of
N-(2-Benzoxazol-2-ylphenyl)benzamides as
Novel Antileishmanial Chemotypes**

Suresh K. Tipparaju,^{†,§} Sipak Joyasawal,^{†,§} Marco Pieroni,[†]
Marcel Kaiser,[‡] Reto Brun,[‡] and Alan P. Kozikowski^{*,†}

*Drug Discovery Program, Department of Medicinal Chemistry and
Pharmacognosy, University of Illinois at Chicago, 833 S. Wood Street,
Chicago, Illinois 60612, and Parasite Chemotherapy, Swiss Tropical
Institute, Socinstrasse, 57, P.O. Box CH-4002, Basel, Switzerland*

Received September 30, 2008

Abstract: The first synthesis and biological evaluation of antibiotic **31** (A-33853) and its analogues are reported. Initial screening for inhibition of *L. donovani*, *T. b. rhodesiense*, *T. cruzi*, and *P. falciparum* cultures followed by determination of IC₅₀ in *L. donovani* and cytotoxicity on L6 cells revealed **31** to be 3-fold more active than miltefosine, a known antileishmanial drug. Compounds **14**, **15**, and **25** selectively inhibited *L. donovani* at nanomolar concentrations and showed much lower cytotoxicity.

Leishmaniasis are parasitic diseases caused by several protozoan parasites of the genus *Leishmania*. These parasitic agents are transmitted to humans by the bite of an insect vector, namely, the phlebotomine sand fly. Visceral leishmaniasis or Kala-azar is one of the most common pathological forms in which the disease occurs. It is mainly transmitted by *L. donovani* and is lethal in 100% of the cases when left untreated.¹ Among all parasitic infections, leishmaniasis are the second most important from a socioeconomic point of view.² They affect 12 million people in 88 countries,³ there are 1.5–2 million new cases and 70 000 deaths each year, and 350 million more are at risk of infection.^{4a}

Despite the increasing concerns about this disease, little effort has been made toward the development of new antileishmanial chemotherapeutics. In fact, antimonial derivatives were the first-line therapeutic option for more than 50 years.^{4b,c} Only recently have novel antileishmanial agents such as amphotericin B, pentamidine, and the new oral drug miltefosine been added to the current therapeutic arsenal.^{5a} However, all of these drugs suffer from several moderate to severe drawbacks. Antimonials may cause acute pancreatitis and cardiac arrhythmia and can even lead to death in extreme cases.^{5b} Hypokalemia and nephrotoxicity are the most common side effects triggered by

amphotericin B, not to mention life-threatening first-dose anaphylaxis. Pentamidine, an aromatic diamidine, is not active orally and can lead to renal, pancreatic, and hepatic toxicity along with hypotension and dysglycemia.⁶ Miltefosine, a phosphocholine analogue, is the first oral antileishmanial agent used to cure both visceral and cutaneous leishmaniasis. Despite its great efficacy, miltefosine is limited by its extremely long half-life (6–8 days), low therapeutic index, and teratogenicity in animals.^{7a} Moreover, given the unsatisfactory results of miltefosine when administered to HIV co-infected patients,^{7b} the role of this drug for treatment of leishmaniasis needs to be reconsidered.

In view of the foregoing facts, there is an urgent need for the development of antileishmanial agents based on new molecular scaffolds endowed with improved efficacy and lacking toxicity. Unfortunately, our limited understanding of leishmanial biology complicates the rational design of antileishmanial agents. Thereby new drugs are often discovered serendipitously by testing large chemical libraries or by modifying structures already known to possess anti-infective activity. The latter is the case, for example, of the newly developed antileishmanial agents paromomycin⁸ and sitamaquine.⁹

Compound **31**¹⁰ (Chart 1) is an antibiotic isolated a couple of decades ago from a culture broth of *Streptomyces* sp. NRRL 12068. The biological data revealed a high antibacterial activity for this natural product, leading to some speculation that this new benzoxazole based scaffold could be an attractive lead for the development of novel anti-infective agents. In spite of its interesting antibacterial profile, there are no reported efforts to chemically synthesize the parent natural product or to systematically explore the SAR of its analogues against various pathogens. Thus, as part of our continuing efforts toward the design and synthesis of novel anti-infective agents,¹¹ we synthesized the parent natural product **31** and a number of its derivatives and evaluated them for their antiparasitic activity.

The new structures were initially screened for their ability to inhibit the growth of *L. donovani* and three other parasites, namely, *T. b. rhodesiense*, *T. cruzi*, and *P. falciparum*, at two different concentrations, i.e., 4.8 and 0.8 $\mu\text{g mL}^{-1}$. Most of the synthesized derivatives showed selective inhibition against the amastigote forms of *L. donovani*, and we thus ruled out the possibility of general cytotoxicity. Further determination of IC₅₀ in amastigotes of *L. donovani* and L6 cells furnished derivatives with activity comparable to that of miltefosine and a significantly improved toxicity profile.

We envisaged that the antibiotic **31** and its analogues described in this paper could be synthesized from a common aminophenol intermediate **6**. The synthesis of **6** is outlined in Scheme 1. Esterification of 2-nitro-3-hydroxybenzoic acid followed by protection of the phenolic hydroxyl group as a benzyl ether resulted in the intermediate **1**. Saponification of the ester gave the benzoic acid derivative **2**. Methyl benzoate intermediate **3** was obtained from readily available 3-hydroxy-anthranilic acid. Intermediates **2** and **3** were coupled using carbonyldiimidazole to give the amide **4**. Benzoxazole intermediate **5** was obtained by heating intermediate **4** to high temperatures. Hydrogenation of intermediate **5** in the presence of Pd/C resulted in the aminophenol intermediate **6** in good

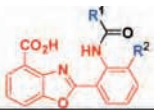
* To whom correspondence should be addressed. Phone: 312-996-7577. Fax: 312-413-0577. E-mail: kozikowa@uic.edu.

[†] University of Illinois at Chicago.

[§] These authors contributed equally to this work.

[‡] Swiss Tropical Institute.

Chart 1. Structure of inhibitors 14–31



| Compd. | R ¹ | R ² |
|--------|----------------|----------------|
| 31 | | OH |
| 14 | | OH |
| 15 | | OH |
| 16 | | OH |
| 17 | | OH |
| 18 | | OH |
| 19 | | OH |
| 20 | | OMe |
| 21 | | OH |
| 22 | | OH |
| 23 | Ph | OH |
| 24 | Ph | H |
| 25 | | OH |
| 26 | | OH |
| 27 | | OMe |
| 28 | | OH |
| 29 | | OH |
| 30 | | OH |

yield. However, subsequent coupling of intermediate **6** with 3-hydroxypyridine-2-carbonyl chloride to give intermediate **7** proceeded in poor yield. The harsh reaction conditions required for the cyclization of intermediate **4** and the poor yields in the subsequent coupling reaction have prompted us to explore an alternative synthetic strategy for the synthesis of **31** and its analogues.

An alternative synthetic route for the synthesis of **31** is shown in Scheme 2. The benzoxazole intermediate **9b** was prepared by oxidative cyclization of the Schiff base obtained from commercially available 3-methoxy-2-nitrobenzaldehyde and aminophenol **3**¹² or via cyclization–dehydration reaction of amide **8** using POCl₃ in refluxing xylene. Reduction of the nitro functionality of intermediate **9b** resulted in amine **10b**. Selective O-benzoylation of 3-hydroxypicolinic acid followed by hydrolysis of the benzyl ester led to the formation of the intermediate **11**

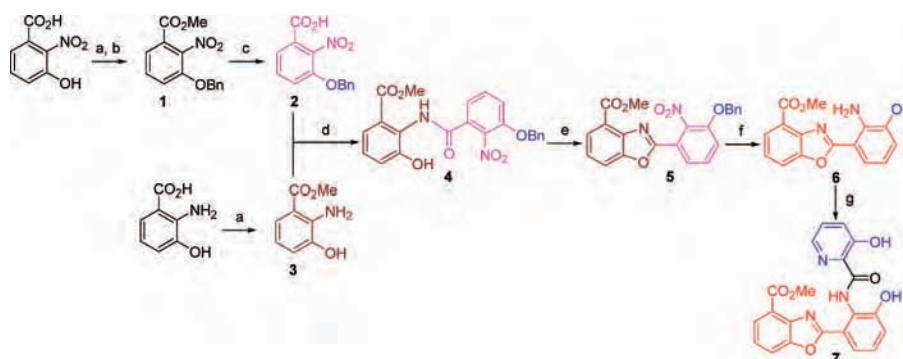
in very good yield. Coupling of 3-benzoyloxypicolinic acid prepared from **11** with the amine **10b** resulted in intermediate **13**. Treatment of **13** with excess BBr₃ gave antibiotic **31** in good overall yield. We found this synthetic strategy to be amenable for the ready scale-up of intermediates **10** and for the quick and easy synthesis of a small library of analogues of **31**. Analogues **14**–**30** (Chart 1) of **31** were synthesized starting from the common intermediates **10a** and **10b** (Scheme 3). Intermediates **14a**–**30a** were obtained by coupling intermediate **10a** or **10b** with an appropriate acid chloride. The acid chlorides were commercially available or were prepared from the readily available carboxylic acids by treating them with oxalyl chloride in the presence of catalytic DMF. Phenolic compounds **14**–**19**, **21**–**23**, **25**, **26**, and **28**–**30** were obtained upon prolonged reaction of the corresponding methoxy intermediates with excess BBr₃. Compounds **20**, **24**, and **27** were obtained by hydrolysis of the corresponding intermediates **19a**, **24a**, and **26a** with LiOH, respectively.

Antibiotic **31** was initially tested for its ability to inhibit the growth of four protozoans, namely, *T. b. rhodesiense*, *T. cruzi*, *P. falciparum*, and *L. donovani*, at two different concentrations (4.8 and 0.8 μg mL^{−1}). It showed 100% inhibition of *L. donovani* at both concentrations. However, **31** also showed notable activity against *T. cruzi* (96% inhibition) and *P. falciparum* (97% inhibition) at 4.8 μg mL^{−1}. Thus, to rule out the possibility that this activity was due to general cytotoxicity, we determined its IC₅₀ against axenic amastigote forms of *L. donovani* MHOM/ET/67/L82,¹³ as well as toxicity to L6 cells.¹³ Miltefosine, a known antileishmanial agent, was included in the study as a control drug (Table 1). Compound **31** was found to be 3-fold more active (IC₅₀ = 80 nM) than miltefosine, but it also showed modest toxicity toward the L6 cells (IC₅₀ = 14 μM).

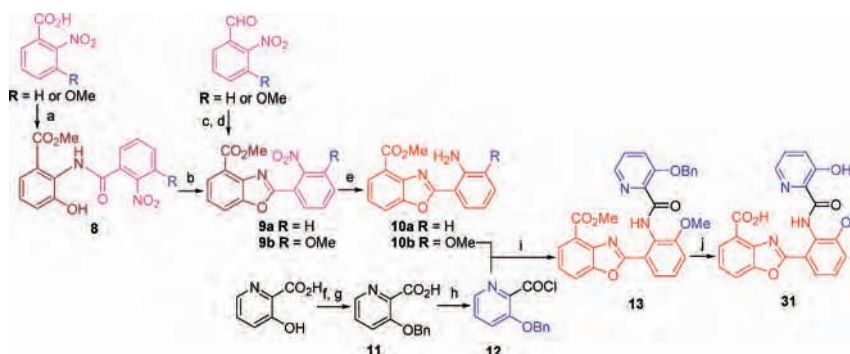
Thus, to circumvent the cytotoxicity of **31**, we undertook the synthesis of a variety of structural analogues in the hope of improving the activity against *L. donovani* while reducing the cytotoxicity. The first set of structural changes were made by modifying the picolinic acid group (R¹ group) while retaining the benzoxazole moiety. For all the analogues of **31** that showed reasonable activity against *L. donovani* (>60% inhibition at 0.8 μg mL^{−1}), along with good selectivity (absence of growth inhibition against the other parasites), IC₅₀ values in the axenic amastigote form of *L. donovani* and in L6 cells were determined. The results are shown in Table 1. Among the analogues made, **14**, **15**, and **25** displayed the most noticeable activity, with IC₅₀ in the nanomolar range and comparable to that of miltefosine.

We were pleased to note that **15**, a 3-fluoropyridine analogue of **31**, maintained good parasitic activity while showing lower toxicity toward the L6 cells than miltefosine itself. For **14**, in which the hydroxyl group of the 3-hydroxypyridine moiety has been deleted, a drop in activities against the parasite and the L6 cells was observed.

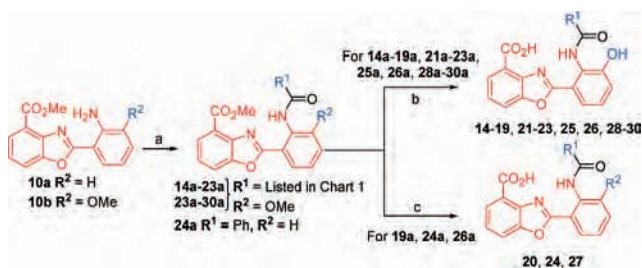
In contrast, replacement of the hydroxyl group with a fluorine atom led to a considerable reduction in cytotoxicity while maintaining good antiparasitic activity. A 10-fold reduction in antileishmanial activity was observed when the 3-hydroxypyridine group of the parent natural product was replaced by a 2-hydroxyphenyl group (**16**). A similar trend was also found upon comparing the activity of the pyridyl derivative **14** and the phenyl derivative **23**, leading to the suggestion that a nitrogen containing ring imbues better activity than the phenyl ring as the R¹. Further, it is interesting to note a considerable shift in the activity profile when the R¹ group is changed from a 2-pyridyl unit (**14**) to a 3-pyridyl unit (**18**), indicating that the

Scheme 1. Synthesis of Common Intermediate 6^a

^a Reagents and conditions: (a) $(\text{CH}_3)_3\text{SiCHN}_2$, $\text{Et}_2\text{O}/\text{MeOH}$ (1:1), 0 °C, 2 h (96%); (b) BnBr , K_2CO_3 , $\text{CH}_2\text{Cl}_2/\text{MeOH}$, reflux, 8 h (95%); (c) 1.4 N NaOH , dioxane, reflux, 3 h (94%); (d) CDI , THF , reflux, 18 h (94%); (e) 230 °C, 3 h (33%); (f) Pd/C , H_2 , MeOH , room temp, 12 h (76%); (g) 3-hydroxypyridine-2-carbonyl chloride, pyridine, DMAP (cat.), CH_2Cl_2 , room temp, 16 h (5%).

Scheme 2. Synthesis of Antibiotic 31^a

^a Reagents and conditions: (a) **3**, CDI , THF , reflux, 18 h (60%); (b) POCl_3 , xylene, 140 °C, 3 h (58%); (c) **3**, MeOH , 40 °C, 12 h; (d) DDQ , CH_2Cl_2 , room temp, 12 h (37%); (e) Pd/C , H_2 , MeOH , room temp, 12 h (80%); (f) BnBr , Ag_2O , $\text{CH}_2\text{Cl}_2/\text{DMSO}$ (1:1), 4 Å, room temp, 12 h (70%); (g) LiOH , $\text{THF}/\text{H}_2\text{O}/\text{MeOH}$ (3:1:1), room temp, 12 h (94%); (h) $(\text{COCl})_2$, room temp, 3 h; (i) pyridine, DMAP (cat.), CH_2Cl_2 , room temp, 12 h (34%); (j) excess BBr_3 , CH_2Cl_2 , -78 °C to room temp, 16 h (81%).

Scheme 3. Synthesis of Inhibitors 14–30^a

^a Reagents and conditions: (a) R^1COCl , pyridine, DMAP (cat.), CH_2Cl_2 , room temp, 12 h; (b) excess BBr_3 , CH_2Cl_2 , -78 °C to room temp, 16 h; (c) LiOH , $\text{THF}/\text{H}_2\text{O}/\text{MeOH}$ (3:1:1), room temp, 12 h.

presence of a nitrogen atom ortho to the amide linkage is important for activity and for reducing the cytotoxicity of this series of compounds.

If hydroxylation of the aromatic ring is considered to be an advantageous substitution based upon the activities of derivative **16** vs **23** as well as **31** vs **14**, the lack of activity of **22** may be attributed to poor penetration through the protozoan membrane due to its greater hydrophilic character. Seemingly the presence of a fluorinated aromatic ring as the R^1 group has a favorable effect on the cytotoxicity of these compounds. For example, **15** is 7-fold less toxic to L6 cells when compared to the unfluorinated **14**. Although polyfluorinated derivative **21** is moderately active, it is considerably less toxic to L6 cells than miltefosine and **31**. The presence of a chlorine substituent on

Table 1. Activity of **31** and Its Analogues in Axenic Amastigote Cultures of *L. donovani*

| compd | IC_{50} (μM) | L6 cells, IC_{50} (μM) | SI^c |
|------------------------|------------------------------------|--|-----------------|
| miltefosine | 0.26 | 147.0 | 565 |
| 31 | 0.08 | 14.2 | 185 |
| 14 | 0.31 | 30.6 | 99 |
| 15 | 0.52 | 203.7 | 392 |
| 16 | 0.85 | 85.1 | 100 |
| 17 | 1.93 | 143.0 | 74 |
| 18 | 4.36 | 240.0 | 55 |
| 19 ^b | NA ^a | NA ^a | NA ^a |
| 20 ^b | NA ^a | NA ^a | NA ^a |
| 21 | 1.90 | 210.0 | 111 |
| 22 ^b | NA ^a | NA ^a | NA ^a |
| 23 | 1.73 | > 240.0 | > 138 |
| 24 | 0.96 | 114.4 | 118 |
| 25 | 0.51 | 94.4 | 185 |
| 26 | 0.68 | 212.3 | 312 |
| 27 | 3.07 | 211.0 | 69 |
| 28 | 1.17 | 108.0 | 92 |
| 29 | 0.93 | 141.0 | 152 |
| 30 ^b | NA ^a | NA ^a | NA ^a |

^a NA: not attainable. ^b Only <30% inhibition of *L. donovani* was observed at 0.8 $\mu\text{g mL}^{-1}$ concentration of the inhibitor. Cytotoxicity assay for these compounds was not performed. ^c SI: selectivity index is the ratio of IC_{50} values of inhibitors against L6 cells to those against *L. donovani* amastigotes.

the aryl ring of the R^1 group seemingly has a detrimental effect on antileishmanial activity (compare **16** vs **17**, **18** vs **19**).

Since a clear improvement in the activity was observed when R^1 is a pyridine ring, we designed inhibitors with the R^1 group comprising other nitrogen containing heterocyclics. Compound

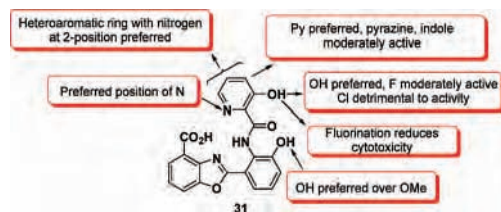


Figure 1. Preliminary SAR of the compounds synthesized.

25 with a pyrazine ring as R^1 showed moderate activity and modest cytotoxicity. Although the activity against *L. donovani* remained the same upon replacing the pyrazine moiety in **25** with an indole ring (compound **26**), significant reduction in the cytotoxicity was observed. Surprisingly, the bulkier 2-phenylquinolin-4-yl derivative **28** showed appreciable activity and low cytotoxicity. The fact that **29**, bearing a 5-phenylisoxazole group linked to the amide linker, showed good antiparasitic activity and low toxicity while the 5-methylisoxazole derivative **30** was inactive suggests a possible existence of an extended hydrophobic pocket in the target binding site.

An unsubstituted phenyl ring as R^2 group appears to be more active than a hydroxyl derivative (**23** vs **24**), while an OH substituent seems to be a more favorable substitution than OMe (**26** vs **27**). Figure 1 summarizes our preliminary SAR for this series of compounds. Encouraged by these results in amastigote cultures of *L. donovani*, we tested derivatives **14–16**, **24–26**, and **29** for their antiparasitic activity on infected mouse peritoneal macrophages. Surprisingly, none of these compounds displayed activity at $10 \mu\text{g mL}^{-1}$. The sharp difference in efficacy against the axenic amastigotes and their corresponding intracellular form raises questions about the penetration of these derivatives through the cell membrane.

In summary, we report the first synthesis of the natural product **31** and a number of its analogues. Biological evaluation of these new chemical entities revealed that they are able to block the growth of the protozoan parasite *L. donovani*, with several of them being active in the submicromolar range and with activities comparable to that of miltefosine. The lead compound **31** is 3-fold more active than miltefosine. While all of the analogues of **31** studied to date are less active than the lead structure, many of them do show an improved selectivity index. Our findings underscore the importance of the *N*-(2-benzoxazole-2-ylphenyl)benzamides as an important lead scaffold in the design and synthesis of antileishmanial agents. While results obtained in mouse peritoneal macrophages were not satisfactory, further work is being directed toward addressing the apparent cellular penetration issues.

Acknowledgment. We thank Drs. Andrew Mesecar and Jimmy Orjala for providing us with information on **31**. We acknowledge support from DOD (W81XWH-07-1-0445).

Supporting Information Available: Biological methods, synthetic experimental details, and analytical data of compounds. This material is available free of charge via the Internet at <http://pubs.acs.org>.

References

- (1) <http://www.who.int/tdr/diseases/leish/diseaseinfo.htm>.
- (2) Chung, M. C.; Ferreira, E. I.; Santos, J. L.; Giarolla, J.; Rando, D. G.; Almeida, A. E.; Bosquesi, P. L.; Menegon, R. F.; Balu, L. Prodrugs for the treatment of neglected diseases. *Molecules* **2008**, *13*, 616–677.
- (3) http://www.dndi.org/cms/public_html/insidcategoryListing.asp?CategoryId=89.
- (4) (a) Desjeux, P. Leishmaniasis: current situation and new perspectives. *Comp. Immunol. Microb.* **2004**, *27*, 305–318. (b) Croft, S. L.; Yardley, V. Chemotherapy of leishmaniasis. *Curr. Pharm. Des.* **2002**, *8*, 319–342. (c) Berman, J. D. Human leishmaniasis: clinical, diagnostic, and chemotherapeutic developments in the last 10 years. *Clin. Infect. Dis.* **1997**, *24*, 684–703.
- (5) (a) Croft, S. L.; Seifert, K.; Yardley, V. Current scenario of drug development for leishmaniasis. *Indian J. Med. Res.* **2006**, *123*, 399–410. (b) Murray, H. W.; Berman, J. D.; Davies, C. R.; Saravia, N. G. Advances in leishmaniasis. *Lancet* **2005**, *366*, 1561–1577.
- (6) Poola, N. R.; Kalis, M.; Plakogiannis, F. M.; Taft, D. R. Characterization of pentamidine excretion in the isolated perfused rat kidney. *J. Antimicrob. Chemother.* **2003**, *52*, 397–404.
- (7) (a) Herwaldt, B. L. Miltefosine—the long-awaited therapy for visceral leishmaniasis. *N. Engl. J. Med.* **1999**, *341*, 1840–1842. (b) Sindermann, H.; Engel, K. R.; Fischer, C.; Bommer, W. Oral miltefosine for leishmaniasis in immunocompromised patients: compassionate use in 39 patients with HIV infection. *Clin. Infect. Dis.* **2004**, *39*, 1520–1523.
- (8) (a) den Boer, M.; Davidson, R. N. Treatment options for visceral leishmaniasis. *Expert Rev. Anti-Infect. Ther.* **2006**, *4*, 187–197. (b) Chappuis, F.; Sundar, S.; Hailu, A.; Ghalib, H.; Rijal, S.; Peeling, R. W.; Alvar, J.; Boelaert, M. Visceral leishmaniasis: what are the needs for diagnosis, treatment and control? *Nat. Rev. Microbiol.* **2007**, *5*, 873–882.
- (9) Jha, T. K.; Sundar, S.; Thakur, C. P.; Felton, J. M.; Sabin, A. J.; Horton, J. A phase II dose-ranging study of sitamaquine for the treatment of visceral leishmaniasis in India. *Am. J. Trop. Med. Hyg.* **2005**, *73*, 1005–1011.
- (10) Michel, K. H.; Boeck, L. D.; Hoehn, M. M.; Jones, N. D.; Chaney, M. O. The discovery, fermentation, isolation, and structure of antibiotic A-33853 and its tetraacetyl derivative. *J. Antibiot.* **1984**, *37*, 441–445.
- (11) (a) Tipparaju, S. K.; Mulhearn, D. C.; Klein, G. M.; Chen, Y.; Tapadar, S.; Bishop, M. H.; Yang, S.; Chen, J.; Ghassemi, M.; Santarsiero, B. D.; Cook, J. L.; Johlfs, M.; Mesecar, A. D.; Johnson, M. E.; Kozikowski, A. P. Design and synthesis of aryl ether inhibitors of the *Bacillus anthracis* enoyl-ACP reductase. *ChemMedChem* **2008**, *3*, 1250–1268. (b) Tipparaju, S. K.; Joyasawal, S.; Forrester, S.; Mulhearn, D. C.; Pegan, S.; Johnson, M. E.; Mesecar, A. D.; Kozikowski, A. P. Design and synthesis of 2-pyridones as novel inhibitors of the *Bacillus anthracis* enoyl-ACP reductase. *Bioorg. Med. Chem. Lett.* **2008**, *18*, 3565–3569.
- (12) Chang, J. Z. K.; Pan, S. Synthesis of 2-arylbenzoxazoles via DDQ promoted oxidative cyclization of phenolic Schiff bases—a solution-phase strategy for library synthesis. *Tetrahedron Lett.* **2002**, *43*, 951–954.
- (13) Nguyen, C.; Kasinathan, G.; Leal-Cortijo, I.; Musso-Buendia, A.; Kaiser, M.; Brun, R.; Ruiz-Páez, L. M.; Johansson, N. G.; González-Pacanoska, D.; Gilbert, I. H. Deoxyuridine triphosphate nucleotidohydrolase as a potential antiparasitic drug target. *J. Med. Chem.* **2005**, *48*, 5942–5954.

JM801241N



Pharmaceutical Nanotechnology

VIP-grafted sterically stabilized phospholipid nanomicellar 17-allylamino-17-demethoxy geldanamycin: A novel targeted nanomedicine for breast cancer

Hayat Önyüksel^{a,b}, Prem S. Mohanty^a, Israel Rubinstein^{a,c,d,*}^a Department of Biopharmaceutical Sciences, University of Illinois at Chicago, Chicago, IL 60612, USA^b Department of Bioengineering, University of Illinois at Chicago, Chicago, IL 60612, USA^c Department of Medicine, University of Illinois at Chicago, Chicago, IL 60612, USA^d Jesse Brown VA Medical Center, Chicago, IL 60612, USA

ARTICLE INFO

Article history:

Received 19 May 2008

Received in revised form 29 July 2008

Accepted 13 August 2008

Available online 27 August 2008

Keywords:

Nanomedicine

Cancer

MCF-7 cells

Chemotherapy

Water-insoluble drugs

17-AAG

Hsp90

Targeting

DSPE-PEG₂₀₀₀

ABSTRACT

17-Allylamino-17-demethoxy geldanamycin (17-AAG), an inhibitor of heat shock protein 90 (Hsp90) function, is being developed as antitumor drug in patients with breast cancer. However, water-insolubility and hepatotoxicity limit its use. The purpose of this study was to begin to address these issues by determining whether 17-AAG can be formulated in long-circulating (PEGylated), biocompatible and biodegradable sterically stabilized phospholipid nanomicelles (SSM) to which vasoactive intestinal peptide (VIP) was grafted as an active targeting moiety and, if so, whether these nanomicelles are cytotoxic to MCF-7 human breast cancer cells. We found that particle size of 17-AAG loaded in VIP surface-grafted SSM was 16 ± 1 nm and drug content was $97 \pm 2\%$ (300 $\mu\text{g}/\text{ml}$). Cytotoxicity of 17-AAG loaded in VIP surface-grafted SSM to MCF-7 cells was significantly higher than that of 17-AAG loaded in non-targeted SSM ($p < 0.05$) and similar to that of 17-AAG dissolved in dimethylsulfoxide. Collectively, these data demonstrate that 17-AAG is solubilized at therapeutically relevant concentrations in actively targeted VIP surface-grafted SSM. Cytotoxicity of these nanomicelles to MCF-7 cells is retained implying high affinity VIP receptors overexpressed on these cells mediate, in part, their intracellular uptake thereby amplifying drug potency. We propose that 17-AAG loaded in VIP surface-grafted SSM should be further developed as actively targeted nanomedicine for breast cancer.

Published by Elsevier B.V.

1. Introduction

It is well established that heat shock protein 90 (Hsp90), a ubiquitous intracellular molecular chaperone involved in folding and activation of several signaling proteins, is overexpressed in various cancers, most notably breast cancer (Ferrarini et al., 1992; Workman, 2004). This, in turn, promotes growth and survival of tumor cells (Whitesell et al., 1994; Hanahan and Weinberg, 2000). Accordingly, inhibition of the biologic function of Hsp90 represents

an important target for cancer therapeutics, including breast cancer (Workman, 2004; Maloney and Workman, 2002; Neckers, 2002; Belikoff and Whitesell, 2004; Modi et al., 2007).

To this end, 17-allylamino-17-demethoxy geldanamycin (17-AAG), a semi-synthetic derivative of ansamycin antibiotic geldanamycin, binds to ATP binding site in N-terminal domain of Hsp90 thereby mitigating its chaperone activity (Workman, 2004; Whitesell et al., 1994; DeBoer et al., 1970). This, in turn, promotes proteasomal-mediated degradation of its client proteins and inhibits cancer cell proliferation (Workman, 2004; Whitesell et al., 1994; Hanahan and Weinberg, 2000; DeBoer et al., 1970). However, clinical use of 17-AAG is hampered by its water-insolubility and hepatotoxicity (Modi et al., 2007; Solit et al., 2007; Weigel et al., 2007). Attempts to overcome these problems by formulating 17-AAG in solvents, such as dimethylsulfoxide (DMSO) and cremophor are fraught with potentially serious adverse events (Modi et al., 2007; Solit et al., 2007; Weigel et al., 2007; Rowinsky et al., 1993). Given Hsp90 are also expressed in normal cells (Ferrarini et al., 1992; Workman, 2004), administration of these and other non-actively targeted formulations of 17-AAG could also be associ-

Abbreviations: 17-AAG, 17-allylamino-17-demethoxy geldanamycin; SSM, sterically stabilized nanomicelles; SSP, sterically stabilized drug particles; VIP, vasoactive intestinal peptide; DMSO, dimethylsulfoxide; DSPE-PEG₂₀₀₀, poly(ethylene glycol)-2000-grafted distearoylphosphatidylethanolamine; DSPE-PEG₃₄₀₀-SPA, 1,2-distearoyl-*sn*-glycero-3-phosphoethanolamine-*N*-[methoxy(polyethylene glycol)-3400]-succinimidyl propionate; Hsp90, heat shock protein 90.

* Corresponding author at: Department of Medicine (M/C 719), University of Illinois at Chicago, 840 South Wood Street, Chicago, IL 60612-4325, USA. Tel.: +1 312 996 8039; fax: +1 312 996 4665.

E-mail address: irubinst@uic.edu (I. Rubinstein).

ated with collateral damage to healthy tissues (Modi et al., 2007; Solit et al., 2007; Weigel et al., 2007). Hence, there is an ongoing need to develop new formulations of 17-AAG with improved water-solubility and therapeutic index.

To address both water-insolubility and toxicity of potent anti-cancer drugs, we developed long-circulating, actively targeted, sterically stabilized phospholipid nanomicelles (~16 nm) using U.S. FDA generally regarded as safe (GRAS) compounds, 1,2-distearoyl-*sn*-glycero-3-phosphoethanolamine-*N*-[methoxy(polyethylene glycol)-2000] (DSPE-PEG₂₀₀₀) to which vasoactive intestinal peptide (VIP), a ubiquitous 28-amino acid pleiotropic mammalian peptide (Gomariz et al., 2001), was grafted to the tip of PEG molecule as an active targeting moiety (Krishnadas et al., 2003; Koo et al., 2005; Working and Dayan, 1996).

These phospholipid nanomicelles are simple to prepare, form spontaneously above their critical micellar concentration (micromolar range), stable upon dilution in aqueous environment with reproducible size distribution and are lyophilized without cryo- and lyoprotectants for long-term storage (Krishnadas et al., 2003; Koo et al., 2005; Ashok et al., 2004; Arleth et al., 2005). Given numerous cancers, most notably breast cancer, overexpress high affinity VIP (VPAC₁) receptors on plasma membrane of tumor cells, surface grafting of SSM with VIP could promote active targeting of these drug-loaded nanocarriers selectively to cancer through local microvascular enhanced permeability and retention (EPR) effect and subsequent binding of VIP to its cognate receptors on cancer cells (Dagar et al., 2001; Dagar et al., 2003; Gespach et al., 1988; Reubi, 1996; Rubinstein et al., 2008). This, in turn, will improve the therapeutic index of the anti-cancer drug (Krishnadas et al., 2003; Koo et al., 2005). Accordingly, we found that VIP surface-grafted SSM solubilize high concentrations of paclitaxel and camptothecin, two potent, albeit water-insoluble, anti-cancer drugs, within their hydrophobic core and amplified the anti-cancer effects of both drugs (Krishnadas et al., 2003; Koo et al., 2005). Taken together, these data suggest that VIP surface-grafted SSM could also be used to solubilize and actively target 17-AAG to breast cancer.

Thus, the purpose of this study was to begin to address this issue by determining whether 17-AAG can be formulated in VIP surface-grafted SSM and, if so, whether these nanomicelles are cytotoxic to MCF-7 human breast cancer cells which are known to over express VIP receptors (Gespach et al., 1988).

2. Materials and methods

2.1. Chemicals

N-[Methoxy (polyethylene glycol-2000)] carbonyl-1,2-distearoyl-*sn*-glycero-3-phosphoethanolamine (DSPE-PEG₂₀₀₀) was obtained from Lipoid GmbH (Ludwigshafen, Germany). *N*-[Methoxy (polyethylene glycol-3400)] carbonyl-1,2-distearoyl-*sn*-glycero-3-phosphoethanolamine-succinimidylpropionate (DSPE-PEG₃₄₀₀-SPA) was purchased from Nektar Therapeutics (Huntsville, AL). 17-AAG was procured from A.G. Scientific (San Diego, CA). Vasoactive intestinal peptide was synthesized by Protein Research Laboratory, Research Resources Center, University of Illinois at Chicago. MCF-7 cells (#HTB-22), fetal bovine serum, trypsin-EDTA and Eagle's Minimum Essential Medium (EMEM) with Earle's Balanced Salt System (BSS) were obtained from American Type Culture Collection (Manassas, VA). Bovine insulin, DMSO, HEPES buffer, glycine, Tris-HCl, sulforhodamine B, trichloroacetic acid were purchased from Sigma-Aldrich Chemical Co. (St. Louis, MO). Phosphate buffered saline (PBS) was obtained from Mediatech Cellgro (Herndon, VA). HPLC-grade methanol and acetonitrile were procured from Fisher Scientific (Itasca, IL). All chemicals were of analytical grade and used as received.

2.2. Preparation and characterization of 17-AAG in phospholipid nanomicelles

Dispersions of 17-AAG solubilized in SSM were prepared by the co-precipitation/reconstitution method as previously described in our laboratory (Krishnadas et al., 2003; Ashok et al., 2004; Koo et al., 2005). Briefly, varying concentrations of 17-AAG and 5 mM DSPE-PEG₂₀₀₀ were dissolved in methanol. Solvent was then removed using vacuum rotary evaporator to form a dry film. Complete dryness was accomplished by desiccation under vacuum overnight. Thereafter, the film was rehydrated with HEPES buffer (10 mM; pH 7.4) and resulting dispersion vortexed followed by bath sonication. The dispersion was flushed with argon, sealed and equilibrated for 3 h at room temperature in complete darkness. Excess unsolubilized 17-AAG was removed by centrifugation at 13,000 × *g* for 5 min to obtain a clear dispersion. Optimal SSM formulations were chosen for further studies based on formation of a homogenous system with maximum solubilization of 17-AAG (see below).

Particle size of aqueous dispersions of 17-AAG in different formulations of SSM were determined by quasi-elastic light scattering using a NICOMP 380 Submicron Particle Sizer (Particle Sizing Systems Inc., Menlo Park, CA) equipped with a temperature controlled cell holder, a 5-mW helium-neon laser (excitation at 632.8 nm) with detection at a fixed scattering angle of 90°. Data were analyzed by volume and intensity-weighted distributions (Krishnadas et al., 2003; Ashok et al., 2004; Koo et al., 2005).

Content of 17-AAG in SSM was determined by RP-HPLC as previously described in our laboratory (Krishnadas et al., 2003; Ashok et al., 2004; Koo et al., 2005). Clear aqueous drug containing micellar dispersions were dissolved in methanol. Each sample preparation was injected (20 µl injection volume) in triplicate through a Spectra System AS3500 autosampler (Thermo Separation Products, Waltham, MA) into a Zorbax SB-C18 column (5 µm pore size, 4.6 mm ID, 25 cm length; Agilent Technologies, Santa Clara, CA) equipped with a C18 column guard. The column was eluted with mobile phase composed of acetonitrile and water (70:30, v/v) at 1.0 ml/min flow rate (Spectra System P2000). Detection was by UV absorption measurement at 330 nm (Spectra Focus). Chromatographic peak areas were integrated by using Chromquest™ 4.0 software, (Thermo Separation Products). A standard curve was generated using 17-AAG dissolved in methanol and sample concentrations were determined by regression analysis of standard curve. The assay was linear over tested concentration range, and there was no interference of phospholipids with the assay (Krishnadas et al., 2003; Ashok et al., 2004; Koo et al., 2005).

VIP was conjugated to distal end of PEG moiety of DSPE as previously described in our laboratory (Krishnadas et al., 2003; Dagar et al., 2003). Briefly, activated 1,2-distearoyl-*sn*-glycero-3-phosphoethanolamine-*N*-[methoxy(polyethylene glycol)-3400]-succinimidyl propionate (DSPE-PEG₃₄₀₀-SPA) was used to conjugate VIP to DSPE-PEG₃₄₀₀. For conjugation reaction, VIP and DSPE-PEG₃₄₀₀-SPA in molar ratio of 1:5 (VIP:DSPE-PEG₃₄₀₀-SPA) were dissolved separately in cold HEPES buffer (10 mM, pH 6.6). DSPE-PEG₃₄₀₀-SPA solution was added in small increments to VIP solution at 4 °C with gentle stirring. The reaction was allowed to proceed for 2 h at 4 °C and then stopped by adding 1 M glycine solution to reaction mixture to consume remaining NHS moieties. Conjugation was ascertained by SDS-PAGE electrophoresis. Thereafter, DSPE-PEG₃₄₀₀ reaction mixture was added to 17-AAG loaded in SSM to obtain final concentration of 5 mM phospholipid and 0.3 mM VIP conjugate. The mixture was equilibrated in darkness at 25 °C for 30 min to yield VIP surface-grafted SSM loaded with 17-AAG. Particle size and drug content of this formulation was determined as outlined above.

2.3. Cytotoxicity of 17-AAG loaded SSM to MCF-7 cells

Cytotoxicity of 17-AAG loaded in SSM with and without surface-grafted VIP to MCF-7 cells was determined as previously described in our laboratory (Krishnadas et al., 2003; Koo et al., 2005; Rubinstein et al., 2008). Cells were maintained in humidified atmosphere with 5% CO₂ at 37 °C in EMEM with 2 mM L-glutamine and Earle's BSS adjusted to contain 1.5 g/l sodium bicarbonate, 0.1 mM non-essential amino acids, 1 mM sodium pyruvate and supplemented with 0.01 mg/ml bovine insulin and 10% fetal bovine serum. Cells (6 × 10⁴ cells/ml) were plated in 96-well plate in triplicate. Drugs and controls were serially diluted and added to each well. The concentration of 17-AAG was 0.0025–1.0 µg/ml. Empty SSM and empty VIP surface-grafted SSM at lipid concentration similar to that of highest concentration of micellar 17-AAG (1 µg/ml), DMSO (10%) and HEPES buffer were used as vehicle controls. In addition, 17-AAG (1.0 µg/ml) dissolved in DMSO (10%) was used as positive control. Final concentration of DMSO in each well was 0.5%. Plates were incubated for 72 h in 5% CO₂ humidified atmosphere at 37 °C. Thereafter, sulforhodamine B cytotoxicity assay was used to determine cell viability spectrophotometrically as previously described (Vichai and Kirtikara, 2006) by measuring optical density (O.D.) of acetic acid fixed, sulforhodamine B-treated cells at 515 nm (Spectra-Max Plus³⁸⁴, Molecular Devices, Sunnyvale, CA). Readings obtained for buffer controls were used to define 100% growth. Percent cell survival was calculated as:

$$\% \text{ Survival} = \frac{\text{O.D. Sample well} - \text{O.D. zero day}}{\text{O.D. Solvent well} - \text{O.D. zero day}} \times 100$$

Growth curves of percent survival versus 17-AAG concentration were plotted and GI₅₀ values calculated using nonlinear regression analysis.

2.4. Data and statistical analyses

Data are expressed as means ± S.D. Analysis of variance followed by Tukey's post hoc test were used for statistical analysis. *p* < 0.05 was considered statistically significant.

Table 1

Formulation characteristics of 17-allylamino-17-demethoxy geldanamycin self-associated with sterically stabilized phospholipid nanomicelles^a

| Lipid:17-AAG ratio | 17-AAG concentration (µg/ml) in 5 mM SSM | Particle size (nm) (n = 3) | SSP |
|--------------------|--|----------------------------|-----|
| Blank SSM | 0 | 15 ± 1 | No |
| 1:0.035 | 100 | 15 ± 1 | No |
| 1:0.05 | 150 | 15 ± 1 | No |
| 1:0.07 | 200 | 15 ± 1 | No |
| 1:0.085 | 250 | 15 ± 1 | No |
| 1:0.1 | 300 | 14 ± 1 | No |
| 1:0.12 | 350 | 16 ± 1 | Yes |
| 1:0.13 | 375 | 15 ± 1 | Yes |
| 1:0.14 | 400 | 13 ± 2 | Yes |

17-AAG, 17-allylamino-17-demethoxy geldanamycin; SSM, sterically stabilized nanomicelles; SSP, sterically stabilized drug particles.

^a Data are means ± S.D.

3. Results

Table 1 depicts formulation characteristics of 17-AAG self-associated with SSM. At 17-AAG concentrations up to 300 µg/ml, only single homogenous particle species was detected by quasi-elastic light scattering while above it sterically stabilized drug particles (SSP) ranging from 100 to 400 nm in size were observed as well (Fig. 1A) (Krishnadas et al., 2003). At 17-AAG concentration of 400 µg/ml, clear precipitation was seen after centrifugation. Thus, lipid:17-AAG molar ratio of 1:0.1 corresponding to 300 µg/ml drug in 5 mM was determined as optimal solubilization ratio for 17-AAG in SSM with drug content of 93 ± 3% by RP-HPLC analysis (*n* = 3). Particle size (16 ± 1 nm) and drug content (97 ± 2%) of VIP surface-grafted SSM (5 mM) loaded with 17-AAG (300 µg/ml) were similar to those of non-targeted SSM loaded with 17-AAG (Fig. 1B and C).

Cytotoxicity and GI₅₀ of various 17-AAG formulations to MCF-7 human breast cancer cells are shown in Figs. 2 and 3. Cytotoxicity of VIP surface-grafted SSM loaded with 17-AAG was significantly higher than that of non-targeted SSM loaded with 17-AAG (Figs. 2 and 3; each, *n* = 3; *p* < 0.05). The cytotoxic effects of VIP

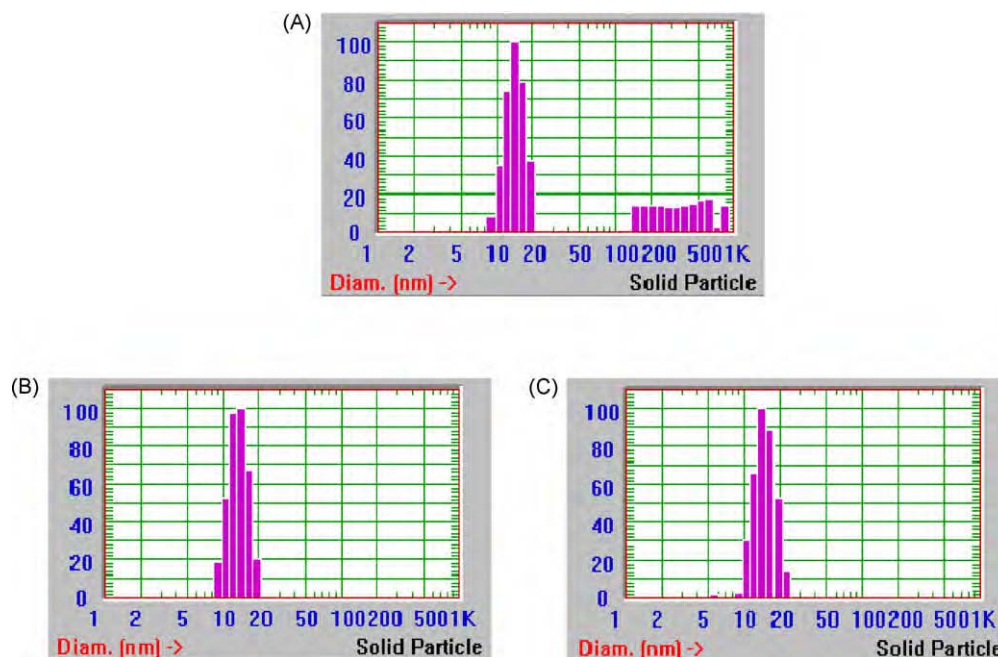


Fig. 1. Representative particle size distribution of 17-allylamino-17-demethoxy geldanamycin nanoformulations. (A) 17-AAG loaded in SSM with SSP; (B) 17-AAG loaded in SSM; (C) 17-AAG loaded in VIP surface grafted SSM. 17-AAG, 17-allylamino-17-demethoxy geldanamycin; SSM, sterically stabilized nanomicelles; SSP, sterically stabilized drug particles; VIP, vasoactive intestinal peptide.

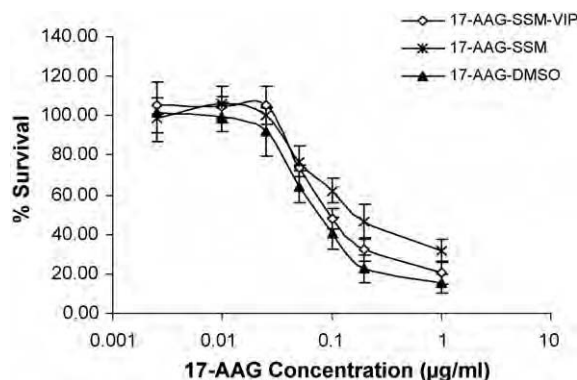


Fig. 2. Cytotoxicity of various 17-allylamino-17-demethoxy geldanamycin formulations to MCF-7 human breast cancer cells. Data are means \pm S.D. after 72-h incubation (each data point, $n = 3$ experiments). Significance markers were omitted for clarity (see Results and Fig. 3 for explanation). 17-AAG, 17-allylamino-17-demethoxy geldanamycin; SSM; sterically stabilized nanomicelles; VIP, vasoactive intestinal peptide; DMSO, dimethylsulfoxide.

surface-grafted SSM loaded with 17-AAG was similar to that of 17-AAG dissolved in DMSO (Figs. 2 and 3; each, $n = 3$; $p > 0.5$). Empty SSM, VIP surface-grafted empty SSM, DMSO and HEPES buffer had no significant effects in MCF-7 cells ($n = 3$; $p > 0.5$; data not shown).

4. Discussion

The new findings of this study are that 17-AAG was successfully solubilized and monodispersed at therapeutically relevant concentrations (300 µg/ml) in long-acting (PEGylated), biocompatible and biodegradable sterically stabilized phospholipid nanomicelles in absence and presence of surface-grafted VIP as an active targeting moiety. In addition, cytotoxicity of VIP surface-grafted SSM loaded with 17-AAG to MCF-7 human breast cancer cells was similar to that of the drug dissolved in DMSO and superior to that of non-targeted drug-loaded phospholipid nanomicelles. Taken together, these data indicate that 17-AAG formulated in SSM retains its cytotoxicity to MCF-7 human breast cancer cells and that high affinity overexpressed VIP (VPAC₁) receptors on these cells mediate, in part, intracellular uptake of 17-AAG-loaded phospholipid nanomicelles thereby amplifying drug potency.

The results of this study extend previous reports from our laboratory where both water-insoluble paclitaxel and camptothecin,

two potent anti-cancer drugs, were successfully formulated in VIP surface-grafted SSM at therapeutically relevant concentrations in the absence of secondary species, i.e. sterically stabilized drug particles (Krishnadas et al., 2003; Koo et al., 2005). Accordingly, we propose that VIP surface-grafted SSM loaded with 17-AAG should be further developed as actively targeted nanomedicine for breast cancer.

We found that unlike VIP surface-grafted SSM loaded with 17-AAG, cytotoxic effects of non-targeted 17-AAG-loaded SSM were smaller than that of 17-AAG dissolved in DMSO. This phenomenon may be related, in part, to greater ability of free 17-AAG molecules to interact with and penetrate plasma membrane of MCF-7 cells and accumulate intracellularly (Workman, 2004; Whitesell et al., 1994; Neckers, 2002; Belikoff and Whitesell, 2004; DeBoer et al., 1970). By contrast, self-association of 17-AAG with nanomicelles may impede its interactions with plasma membrane over the observation period (72 h) because drug molecules must be first released from the nanocarrier, a time-dependent phenomenon, before interaction with plasma membrane ensues. This, in turn, may attenuate cytotoxic effects of nanomicellar 17-AAG.

Alternatively, non-targeted 17-AAG-loaded SSM may be internalized into MCF-7 cells as nanoparticles through various pathways, such as phagocytosis, macropinocytosis, clathrin-mediated endocytosis and caveolae-mediated endocytosis, that express slower kinetics relative to that of free 17-AAG molecules (Working and Dayan, 1996). This hypothesis is supported, in part, by recent study from our laboratory showing slower intracellular accumulation of non-targeted hydrophobic quantum dots-loaded sterically stabilized nanomicelles in MCF-7 cells relative to that of nanomicelles decorated with VIP (Rubinstein et al., 2008). The results of this study extend these observations by demonstrating that cytotoxicity of VIP surface-grafted SSM loaded with 17-AAG is significantly higher in comparison to non-targeted 17-AAG-loaded nanomicelles in these cells.

Conceivably, the nanosize of VIP surface-grafted SSM loaded with 17-AAG (~16 nm) coupled with their steric stabilization conferred by PEG₂₀₀₀ moiety and absence of VIP receptors on plasma membrane of endothelial cells could prolong their circulation time because these nanoparticles will not extravasate from intact microvascular beds nor removed by the reticuloendothelial system (Reubi, 1996; Working and Dayan, 1996; Dagar et al., 2001, 2003; Krishnadas et al., 2003). This, in turn, would enable active targeting of VIP surface-grafted SSM loaded with 17-AAG to breast cancer through local enhanced permeability and retention (EPR) effect and VIP binding to its high affinity overexpressed cognate receptors on cancer cells thereby improving therapeutic index of the drug (Gespach et al., 1988; Reubi, 1996; Gomariz et al., 2001; Krishnadas et al., 2003; Dagar et al., 2001, 2003; Rubinstein et al., 2008). Clearly, additional in vivo studies are warranted to support or refute this hypothesis.

In summary, we found that 17-AAG is solubilized at therapeutically relevant concentrations in actively targeted VIP surface-grafted SSM. Cytotoxicity of these nanomicelles to MCF-7 human breast cancer cells is retained implying high affinity VIP (VPAC₁) receptors overexpressed on these cells mediate, in part, their intracellular uptake thereby amplifying drug potency. We propose that 17-AAG loaded in VIP surface-grafted SSM should be further developed as actively targeted nanomedicine for breast cancer.

Acknowledgments

We thank Ernest Gemeinhart for assistance with cell culture experiments. This study was supported, in part, by NIH grants RO1

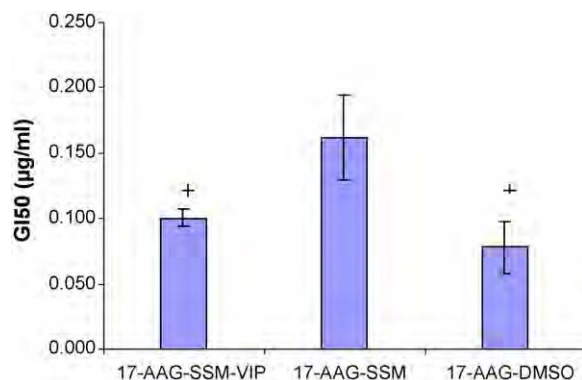


Fig. 3. GI₅₀ (concentration of drug at which 50% growth inhibition is seen) of various 17-allylamino-17-demethoxy geldanamycin formulations to MCF-7 human breast cancer cells. Data are means \pm S.D. after 72-h incubation (each data point, $n = 3$ experiments). * $p < 0.05$ in comparison to 17-AAG-SSM. 17-AAG, 17-allylamino-17-demethoxy geldanamycin; SSM; sterically stabilized nanomicelles; VIP, vasoactive intestinal peptide; DMSO, dimethylsulfoxide.

AG024026 and R01 CA121797, VA Merit Review and Department of Defense (DOD) grant BCRP DAMD 17-02-1-0415 and DOD contract W81XWH-07-1-0445. Research was conducted in a facility constructed with support from Research Facilities Improvement Program Grant Number C06 RR15482 from the National Center for Research Resources.

References

- Arleth, L., Ashok, B., Önyüksel, H., Thiagarajan, P., Jacob, J., Hjelm, R.P., 2005. Detailed structure of hairy mixed micelles formed by phosphatidylcholine and PEGylated phospholipids in aqueous media. *Langmuir* 21, 3279–3290.
- Ashok, B., Arleth, L., Hjelm, R.P., Rubinstein, I., Önyüksel, H., 2004. In vitro characterization of PEGylated phospholipid micelles for improved drug solubilization: effects of PEG chain length and PC incorporation. *J. Pharm. Sci.* 93, 2476–2487.
- Belikoff, J., Whitesell, L., 2004. Hsp 90: an emerging target for breast cancer therapy. *Anticancer Drugs* 15, 651–662.
- Dagar, S., Sekosan, M., Lee, B.S., Rubinstein, I., Önyüksel, H., 2001. VIP receptors as molecular targets of breast cancer: implications for targeted imaging and drug delivery. *J. Control Release* 74, 129–134.
- Dagar, S., Krishnadas, A., Rubinstein, I., Blend, M.J., Önyüksel, H., 2003. VIP grafted sterically stabilized liposomes for targeted imaging of breast cancer: in vivo studies. *J. Control Release* 91, 123–133.
- DeBoer, C., Meulman, P.A., Wnuk, R.J., Peterson, D.H., 1970. Geldanamycin, a new antibiotic. *J. Antibiot. (Tokyo)* 23, 442–447.
- Ferrarini, M., Heltai, S., Zocchi, M.R., Rugarli, C., 1992. Unusual expression and localization of heat-shock proteins in human tumor cells. *Int. J. Cancer* 51, 613–619.
- Gespach, C., Bawab, W., de Cremoux, P., Calvo, F., 1988. Pharmacology, molecular identification and functional characteristics of vasoactive intestinal peptide receptors in human breast cancer cells. *Cancer Res.* 48, 5079–5083.
- Gomariz, R.P., Martinez, C., Abad, C., Leceta, J., Delgado, M., 2001. Immunology of VIP: a review and therapeutic perspectives. *Curr. Pharm. Des.* 7, 89–111.
- Hanahan, D., Weinberg, R.A., 2000. The hallmarks of cancer. *Cell* 100, 57–70.
- Koo, O.M., Rubinstein, I., Önyüksel, H., 2005. Camptothecin in sterically stabilized phospholipid micelles: a novel nanomedicine. *Nanomedicine* 1, 77–84.
- Krishnadas, A., Rubinstein, I., Önyüksel, H., 2003. Sterically stabilized phospholipid mixed micelles: in vitro evaluation as a novel carrier for water-insoluble drugs. *Pharm. Res.* 20, 297–302.
- Maloney, A., Workman, P., 2002. HSP90 as a new therapeutic target for cancer therapy: the story unfolds. *Expert Opin. Biol. Ther.* 2, 3–24.
- Modi, S., Stopeck, A.T., Gordon, M.S., et al., 2007. Combination of trastuzumab and tanespimycin (17-AAG, KOS-953) is safe and active in trastuzumab-refractory HER-2 overexpressing breast cancer: a phase I dose-escalation study. *J. Clin. Oncol.* 25, 5410–5417.
- Neckers, L., 2002. Heat shock protein 90 is a rational molecular target in breast cancer. *Breast Dis.* 15, 53–60.
- Reubi, J.C., 1996. In vitro identification of VIP receptors in human tumors: potential clinical implications. *Ann. N.Y. Acad. Sci.* 805, 753–759.
- Rowinsky, E.K., Eisenhauer, E.A., Chaudhry, V., Arbuck, S.G., Donehower, R.C., 1993. Clinical toxicities encountered with paclitaxel (Taxol). *Semin. Oncol.* 20, 1–15.
- Rubinstein, I., Soos, I., Önyüksel, H., 2008. Intracellular delivery of VIP-grafted sterically stabilized phospholipid mixed nanomicelles in human breast cancer cells. *Chem. Biol. Interact.* 171, 190–194.
- Solit, D.B., Ivy, S.P., Kopil, C., et al., 2007. Phase I trial of 17-allylamino-17-demethoxy geldanamycin in patients with advanced cancer. *Clin. Cancer Res.* 13, 1775–1782.
- Vichai, V., Kirtikara, K., 2006. Sulforhodamine B colorimetric assay for cytotoxicity screening. *Nat. Protoc.* 1, 1112–1116.
- Weigel, B.J., Blaney, S.M., Reid, J.M., et al., 2007. A phase I study of 17-allylamino-17-demethoxy geldanamycin in relapsed/refractory pediatric patients with solid tumors: a Children's Oncology Group study. *Clin. Cancer Res.* 13, 1789–1793.
- Whitesell, L., Mimnaugh, E., Costa, B., Myers, C., Neckers, L., 1994. Inhibition of heat shock protein HSP90-pp60v-src heteroprotein complex formation by benzoquinone anamycins: essential role for stress proteins in oncogenic transformation. *Proc. Natl. Acad. Sci. U.S.A.* 91, 8324–8328.
- Working, P.K., Dayan, A.D., 1996. Pharmacological-toxicological expert report. CAE-LYX. (Stealth liposomal doxorubicin HCl). *Hum. Exp. Toxicol.* 15, 751–785.
- Workman, P., 2004. Combinatorial attack on multistep oncogenesis by inhibiting the Hsp90 molecular chaperone. *Cancer Lett.* 206, 149–157.



ELSEVIER

Available online at www.sciencedirect.com

ScienceDirect

Nanomedicine: Nanotechnology, Biology, and Medicine xx (2009) xxx–xxx

nanomedicine

www.nanomedjournal.com

Self-associated indisulam in phospholipid-based nanomicelles: a potential nanomedicine for cancer

Hacer Cesur, MS,^a Israel Rubinstein, MD,^{b,c,d} Ashwini Pai, PhD,^b Hayat Önyüksel, PhD^{a,b,*}

^aDepartment of Bioengineering, University of Illinois at Chicago, Chicago, Illinois, USA

^bDepartment of Biopharmaceutical Sciences, University of Illinois at Chicago, Chicago, Illinois, USA

^cDepartment of Medicine, University of Illinois at Chicago, Chicago, Illinois, USA

^dJesse Brown VA Medical Center, Chicago, Illinois, USA

Abstract

This study aimed to begin development of a nanomedicine containing indisulam solubilized in sterically stabilized micelles (SSMs) composed of DSPE-PEG₂₀₀₀ or sterically stabilized mixed micelles (SSMMs) composed of DSPE-PEG₂₀₀₀ plus egg phosphatidylcholine. Micelles were prepared by co-precipitation and reconstitution of drug and lipids. Particle size distributions of micellar formulations were determined by quasi-elastic light scattering. Amounts of solubilized drug were determined by reverse-phase high-performance liquid chromatography (RP-HPLC). In vitro cytotoxicity of indisulam in nanocarrier was determined on the MCF-7 cell line by the National Cancer Institute–developed sulforhodamine B assay. Optimal solubilized indisulam concentrations in 5 mM total lipid were 10 µg/mL for SSMMs and 400 µg/mL for SSMs. HPLC results demonstrated that the encapsulation capacity of both micelles was over 95%. In vitro studies showed that indisulam in micellar system was more effective than free indisulam. The optimized formulation was successfully freeze-dried without any addition of lyoprotectants or cryoprotectants. We conclude that SSMs are a promising nanocarrier for indisulam, and indisulam-SSMs should be developed further as a novel targeted nanomedicine.

© 2009 Elsevier Inc. All rights reserved.

Key words:

DSPE-PEG₂₀₀₀ and EPC; PEGylated phospholipids; Water-insoluble anticancer drug; Indisulam; Sterically stabilized simple micelles; Sterically stabilized mixed micelles

Recently our laboratory has reported on the use of PEGylated phospholipids such as 1,2-distearoyl-*sn*-glycero-3-phosphoethanolamine-*N*-methoxy-poly(ethylene glycol 2000)(DSPE-PEG₂₀₀₀), to form sterically stabilized micelles (SSMs) or DSPE-PEG₂₀₀₀ plus egg phosphatidylcholine

(EPC) to form sterically stabilized mixed micelles (SSMMs) as targeted nanocarriers for the delivery of poorly water-soluble drugs.^{1,2} Components of these micelles are approved by the U.S. Food and Drug Administration, safe, biocompatible, and relatively nontoxic.^{2,3} The PEG on the surface of the micelles sterically stabilizes them, preventing opsonization and reticuloendothelial system uptake.⁴

These sterically stabilized micelles, because of their low critical micellar concentration values and most likely because of strong interactions between the acyl chains in the core region, are also relatively stable on dilution.^{1,5} In addition, the small size (~15 nm) of these carrier systems can provide targeted delivery to cancer tissue or other injured tissues by selective extravasation through leaky

Received 31 December 2007; accepted 1 September 2008.

This work was supported, in part, by Eisai Inc., National Institutes of Health grants RO1 CA121797, AGC24026-01 and C06RR15482, VA Merit Review, and Department of Defense contract W81XWH-07-1-0445.

*Corresponding author. Department of Biopharmaceutical Sciences (M/C 865), College of Pharmacy, University of Illinois at Chicago, Chicago, Illinois 60612-7231, USA.

E-mail address: hayat@uic.edu (H. Önyüksel).

1549-9634/\$ - see front matter © 2009 Elsevier Inc. All rights reserved.

doi:[10.1016/j.nano.2008.09.001](https://doi.org/10.1016/j.nano.2008.09.001)

vasculature.⁶ Furthermore, preparation of SSMs is simple and efficient compared with bile salt/phospholipid mixed micelles or liposomes.^{7–9}

Indisulam—also called E7070, *N*-(3-chloro-7-indolyl)-1,4-benzenedisulfonamide—is a sulfonamide anticancer agent that disrupts the cell cycle progression at the G1/S phase.^{10–12} Although the exact mechanism of action remains uncertain, some identified effects include induced expression of p53 and p21, inhibition of phosphorylation of the tumor suppressor retinoblastoma (RB) protein, reduced expression of cyclins and cyclin-dependent kinases,^{13,14} and inhibition of carbonic anhydrase IX.¹⁵ Currently, indisulam is being tested in combination with capecitabine and carboplatin for clinical trials.^{16,17} Indisulam alone has been shown to be effective on human breast cancer by *in vitro* and *in vivo* studies.^{12,18,19} It was found to be considerably different from conventional anticancer drugs in clinical use with respect to its cell cycle effect and its tumor type selectivity.^{14,20} However, its efficacy in clinical trials for breast cancer did not meet expectations as a result of dose-limiting toxicities.^{19,21} Aqueous indisulam formulations tested in clinical trials are not made of nanoparticles, and drug molecules can extravasate in any vasculature in the body, resulting in high toxicity to healthy tissues. One of the reasons for the hematological toxicity in these formulations tested in clinical trials is that indisulam binds to plasma proteins (albumin) and to erythrocytes (carbonic anhydrase) in a saturable manner.²² However, if indisulam is solubilized in micelles, then the drug will not be free to interact with blood components and the nanosize of micelles will significantly reduce drug distribution and toxicity to normal tissues. In addition, the drug will be accumulated by passive targeting at the tumor sites by extravasations due to leaky vasculature.⁴ Furthermore, nanomicelles can improve the solubility of hydrophobic compounds (aqueous solubility of indisulam is less than 5 µg/mL at 37°C, provided by Eisai, Inc., Tokyo, Japan) in the aqueous medium to render them suitable for parenteral administration. We have shown elsewhere the improved solubility of other anticancer drugs such as camptothecin and paclitaxel using simple and mixed micelles.^{2,7} The purpose of this study was to investigate the solubility potential of SSMs and SSMMs for indisulam, and to determine an optimized formulation to initiate the development of a novel nanomedicine for targeted treatment of breast cancer.

Methods

Chemicals

1,2-Distearoyl-*sn*-glycero-3-phosphoethanolamine-*N*-methoxy-poly(ethylene glycol 2000) (DSPE-PEG₂₀₀₀) and EPC were obtained from LIPOID GmbH (Ludwigshafen, Germany). Indisulam was a gift from Eisai Inc. All lipid samples were purified by high-performance liquid chromatography (HPLC). HPLC-grade methanol, acetonitrile, and phosphoric acid were purchased from Fisher Scientific

(Itasca, Illinois). Eagle's minimal essential medium (EMEM) was purchased from American Type Culture Collection (ATCC; Manassas, Virginia). All other reagents were of analytical grade.

Preparation of aqueous dispersions of indisulam

Simple and mixed micelles containing indisulam were prepared by co-precipitation method.^{1,2} Briefly, for simple micelles, indisulam and DSPE-PEG₂₀₀₀ were dissolved in methanol. For mixed micelles, DSPE-PEG₂₀₀₀ and EPC at optimal molar ratio (90:10) were co-precipitated along with indisulam.¹ The solvent was then removed by vacuum rotary evaporation under a stream of argon. Obtained dry film was further dried under vacuum overnight to remove any traces of remaining solvent. The dried film was rehydrated with isotonic 0.01 M phosphate buffer pH 6.0, at which indisulam is in the most stable form. The solution was then flushed with argon, sealed, and equilibrated for 2 hours for simple micelles and 12 hours for mixed micelles at room temperature which was approximately 25°C. The excess of unsolubilized indisulam was removed by centrifugation at 13,000 g for 5 minutes to obtain a clear dispersion. The maximum solubility of indisulam was determined in simple micelles of DSPE-PEG₂₀₀₀ by keeping the phospholipid concentration fixed and changing the drug concentration (drug-to-phospholipid molar ratios ranged from 0.005 to 1.04 for simple micelles, and 0.001 to 0.52 for mixed micelles) until a homogeneous system was determined by a quasi-elastic light scattering (QELS) as a single-size peak population. Each formulation was prepared in triplicate. The prepared dispersions were then characterized for their particle size and assayed for the drug content. The optimal formulations of SSMs or SSMMs were chosen according to their formation of a homogeneous system with maximum solubilization potential for indisulam.

Particle size determination

Particle size distribution and mean diameter of the prepared aqueous dispersions of indisulam were determined by QELS using a NICOMP 380 submicron Particle Sizer (Particle Sizing Systems, Santa Barbara, California) equipped with a 35-mW helium-neon laser at 632.8 nm. Mean hydrodynamic particle diameters (\bar{d}_h) in the aqueous dispersions were obtained from the Stokes-Einstein relation using the measured diffusion of particles in solution ($\eta = 0.933$, $T = 23^\circ\text{C}$, $n = 1.33$). Data were analyzed in terms of volume- and intensity-weighted distributions. Each reported experimental result is the average of at least three \bar{d}_h values obtained from analysis of the autocorrelation function accumulated for at least 20 minutes.

Assay of solubilized indisulam

The amounts of indisulam solubilized in both the SSMs and the SSMMs were determined by reverse-phase HPLC (RP-HPLC). The clear aqueous dispersion was diluted with

methanol, and 20 μL of each sample were injected into YMC-Pack-Pro- C_{18} column (5 μm , 250 mm \times 4.6 mm, 120 Å pore size (YMC, Tokyo, Japan)). The column was eluted with acetonitrile–water–phosphoric acid (430:570:1, v/v/v) at a flow rate of 1.2 mL/min. Ultraviolet absorbance was measured at 223 nm. The drug concentration was calculated from standard curves. Each solution was analyzed in triplicate.

In vitro cytotoxicity

The MCF-7 breast cancer cell line was used to evaluate the *in vitro* activity of the formulations. The cell line was maintained in EMEM containing 2 mM L-glutamine and Earle's balanced salt solution adjusted to contain 1.5 g/L sodium bicarbonate, 0.1 mM nonessential amino acids, 1 mM sodium pyruvate, and supplemented with 0.01 mg/mL fetal bovine insulin at 37°C in a humidified, 5% CO_2 atmosphere.

Optimum solutions of indisulam-SSMs (composed of 5 mM DSPE-PEG₂₀₀₀, 400 $\mu\text{g/mL}$ indisulam) chosen from the solubilization studies were used as the test solutions. Drug-free SSMs in 0.01 M phosphate buffer (pH 6.0) were prepared at the same concentrations as the test solution and used as a negative control. Indisulam in 4% dimethyl sulfoxide (DMSO) was used as a positive control. *In vitro* indisulam cytotoxicity was assessed using the sulforhodamine B assay adopted for a routine antitumor screening test at the National Cancer Institute (NCI).^{23,24} Briefly, serial dilutions with either phosphate buffer containing lipid or 4% DMSO were made to obtain indisulam concentrations from 0.1 to 50 mg/mL. MCF-7 cells (190 μL) were trypsinized and plated at a density of 1000 cells per well in a 96-well plate (final DMSO concentration was <0.5%). A total of 27 μL per well of the test solutions and control groups of solvents were added to the microtiter plates. Each sample was evaluated in triplicate. The plates were then incubated for 72 hours in a humidified, 5% CO_2 atmosphere.

After the incubation period, the cells were fixed to the plates by adding 100 μL per well of cold 20% trichloroacetic acid and incubated for 1 hour at 4°C. The plates were then washed, air-dried, and stained with 100 μL /well of 0.4% sulforhodamine B in 1% acetic acid for 30 minutes. Then the plates were washed with 1% acetic acid, and 200 μL /well of 10 mM Tris ([tris-hydroxymethyl]-aminomethane) buffer were added. The optical density was then read at 515 nm, and the readings obtained for the solvent controls were used to define 100% growth after normalizing for the value obtained for the zero-day control. These data were then expressed as survival percentage versus drug concentration, and ED_{50} values were calculated using nonlinear regression analysis.

Freeze-drying of indisulam-SSMs

The optimal solubilization ratio of indisulam in DSPE-PEG₂₀₀₀ micelles was determined as drug-to-lipid molar ratio 0.2:1. In our lyophilization studies, final lipid concentration of indisulam-SSMs was 10 mM so as to

Table 1

Solubility of indisulam in 5 mM SSMs and SSMMs, and particle sizes of SSMs and indisulam-SSMs before and after lyophilization

| Formulation | Mean particle diameter | | Optimum drug concentration |
|-------------------------------|--------------------------------|-------------------------------|----------------------------|
| Indisulam-SSMMs (5 mM lipids) | 12.6 ± 2.9 nm (<i>n</i> = 20) | | 10 µg/mL |
| Indisulam-SSMs (5 mM lipids) | 13.0 ± 2.5 nm (<i>n</i> = 20) | | 400 µg/mL |
| | | | |
| | Before lyophilization | After lyophilization | |
| SSMs (10 mM lipids) | 10.4 ± 1.8 nm (<i>n</i> = 3) | 10.7 ± 2.2 nm (<i>n</i> = 3) | 0 |
| Indisulam-SSMs (10 mM lipids) | 10.8 ± 3.1 nm (<i>n</i> = 3) | 10.3 ± 2.2 nm (<i>n</i> = 3) | 800 µg/mL |

More (40-fold) drug solubilization was achieved in SSMs than in SSMMs (n = 20, mean \pm SD, P > .05, SSMs mean particle diameter compared with SSMMs). Particle sizes of SSMs and indisulam-SSMs before and after lyophilization did not significantly change (P > .05).

form a good visually appealing “cake”.²⁵ The optimal indisulam-SSM formulation (composed of 10 mM DSPE-PEG₂₀₀₀, 800 $\mu\text{g/mL}$ indisulam) based on indisulam solubilization experiments, without any modification or any addition of a cryoprotectant or lyoprotectant, was placed into 1.5-mL glass vials at fill volumes of 1 mL and subjected to a lyophilization cycle by FreeZone 6 (Labconco, Kansas City, Missouri).²⁶ Briefly, prepared samples were stored at –20°C overnight, followed by freezing in liquid nitrogen for 3 minutes. Then frozen samples and controls were lyophilized. Micellar size and indisulam concentration were compared for stability before and after lyophilization.

Data and statistical analysis

All the data are expressed as means \pm SD. Formulations and characterization data are averages of at least triplicate. *In vitro* cytotoxicity data are average of triplicates. ED_{50} values were calculated for each formulation and compared statistically using one-way analysis of variance. A P value less than 0.05 was considered statistically significant.

Results

Particle size

A given phospholipid concentration can solubilize poorly water-soluble drug only up to a certain concentration of the drug.²⁶ Once this maximal threshold is attained, populations of other species are observed by QELS. Those particles that do not settle after centrifugation are named as sterically stabilized particles (SSPs), because most likely they are stabilized by DSPE-PEG₂₀₀₀ on their surfaces. Mean hydrodynamic diameters of SSMs and SSMMs without any presence of SSPs were 12.6 \pm 2.9 nm (n = 20) and 13.0 \pm 2.5 nm (n = 20), respectively (Table 1).

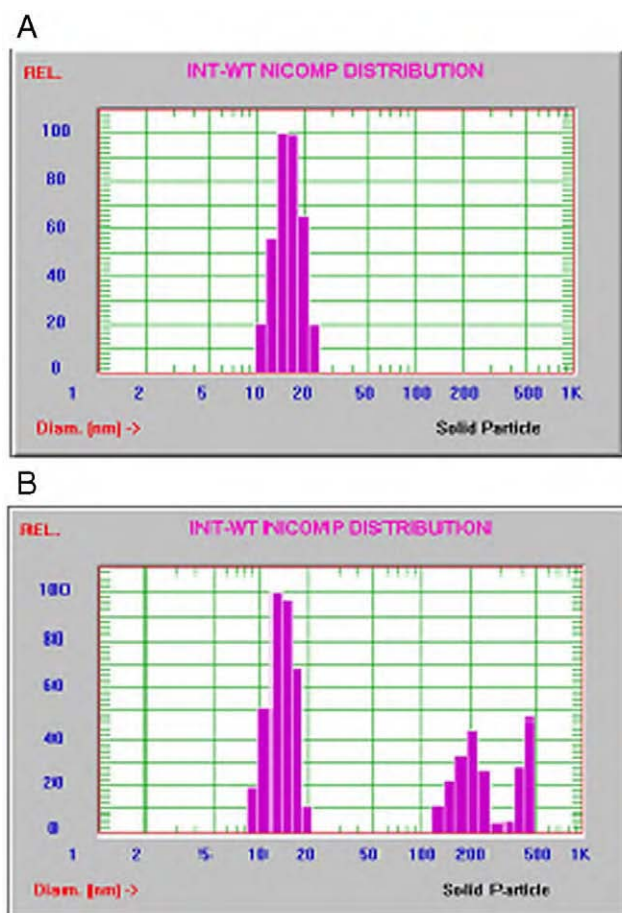


Figure 1. Representative NICOMP size distribution of indisolam with SSMMs. (A) Indisolam-SSMMs at optimum drug concentration of 10 µg/mL; (B) indisolam-SSMMs at excessive drug concentration of 25 µg/mL.

Solubilization of indisolam

With 5 mM fixed total phospholipid concentration of SSMMs, we performed experiments at different indisolam concentrations ranging from 2 µg/mL to 1000 µg/mL. For concentrations at and below 10 µg/mL, one uniform size distribution was observed by NICOMP analysis (Figure 1, A). Above this concentration there were other populations of lipid-coated particles coexisting with indisolam-SSMMs as indicated by size distribution (Figure 1, B). Therefore, solubilization potential of 5 mM SSMMs for indisolam was low, and only 10 µg/mL (drug-to-lipid molar ratio 0.005:1).

Next we tested SSMMs for their potential to solubilize indisolam. Sixteen different indisolam concentrations ranging from 2 to 2000 µg/mL were tested with 5 mM SSMMs composed of DSPE-PEG₂₀₀₀ alone. Surprisingly, all samples at and below 400 µg/mL of indisolam had a single uniform size distribution, and above this concentration SSPs were observed (Figure 2, A and B).

The amount of solubilized drug in the system was calculated by standard curves of RP-HPLC. All standard curves were linear over the tested indisolam concentration

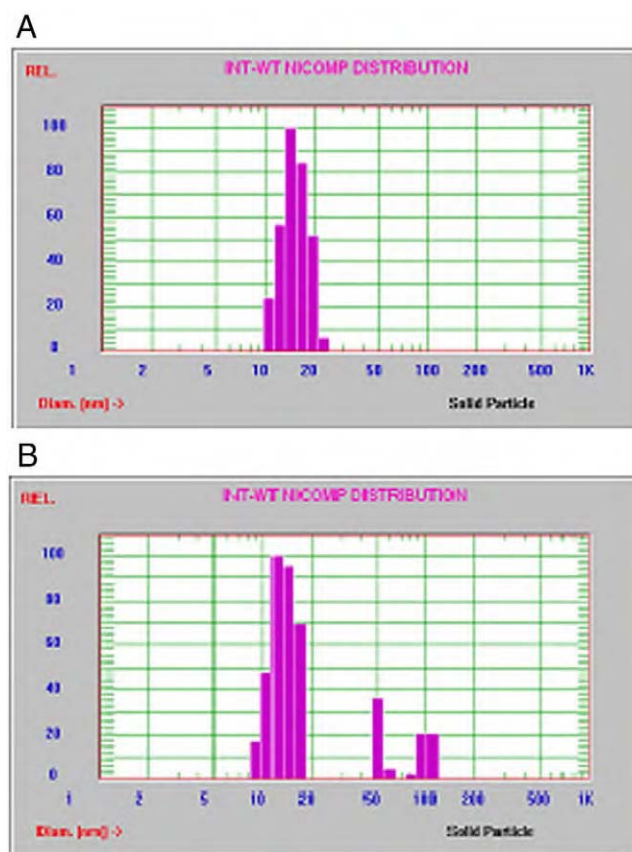


Figure 2. Representative NICOMP size distribution of indisolam with SSMMs. (A) Indisolam-SSMMs at optimum drug concentration of 400 µg/mL; (B) indisolam-SSMMs at excessive drug concentration of 500 µg/mL.

range of 20 to 100 µg/mL. RP-HPLC results showed that at least 95% of the drug was incorporated in the system for all optimum drug concentrations.

In vitro cytotoxicity

We investigated whether the interaction between indisolam and the lipids in the formulation affected the anticancer activity of the drug. Because the solubility of indisolam in SSMMs was 40-fold higher than its solubility in SSMMs, we performed in vitro cytotoxicity studies only with indisolam-SSMMs. The formulations of free indisolam in DMSO and indisolam-SSMMs were tested against MCF-7, a human breast cancer cell line.

As shown in Figure 3, indisolam in simple micelles was readily available to interact with cancer cells and retained its anticancer activity. As shown in Figure 4, ED₅₀ of indisolam in DMSO was 36.3 ± 3.6 µM, which is similar to the value reported by Nakatsu et al.¹⁸ Indisolam in SSMMs proved to be more effective with an ED₅₀ value of 16.2 ± 2.7 µM.

Freeze-drying

PEGylated lipids are unstable in aqueous media and are subject to degradation by hydrolysis and oxidation.²⁷ Therefore, we tested the option of keeping the optimal

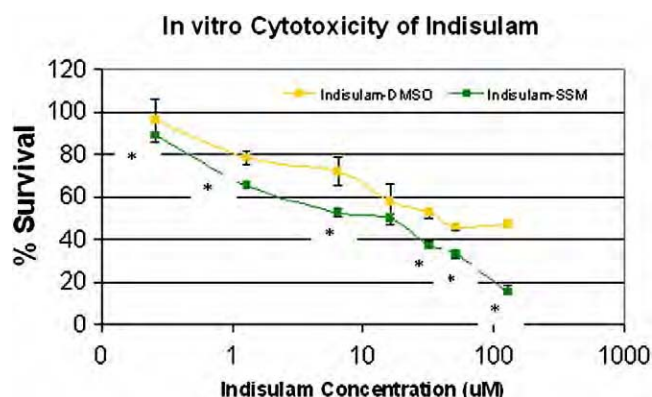


Figure 3. In vitro cytotoxicity of indisulam-SSMs after 72 hours by sulforhodamine B assay ($n = 3$, mean + SD, $*P < .05$ compared to respective samples of indisulam in DMSO).

indisulam-SSM formulation in dry form after lyophilization. The visual appearance of lyophilized cakes of indisulam-SSMs was similar to SSM controls: white, cotton-like cakes pleasing in appearance. Particle sizes of both SSM alone and indisulam-SSMs were not significantly different before and after lyophilization (Table 1). According to the HPLC results, all the drug molecules were incorporated into the micelles after lyophilization.

Discussion

Drug incorporation did not change the particle size of simple and mixed micelles (Table 1), most probably because of the dominating effect of the PEG molecules in the overall size of micelles. Similarly, addition of small-sized drug molecules into the core did not bring about a significant change in size of either SSMs or SSMMs.

Indisulam was 40-fold more soluble in SSMs than in SSMMs. The big difference in the solubilization potential between SSMs and sSSMM can be explained by the observation that indisulam is located at the interface between the hydrophobic core and relatively hydrophilic palisade region. For SSMMs, most of this area may be occupied by EPC molecules, allowing only very few molecules of indisulam to reside, causing lower drug solubilization in SSMMs.

According to in vitro cytotoxicity experiments on the MCF-7 cell line, indisulam in SSMs proved to be more effective than in DMSO (Figure 4). The reason for the increased activity is yet to be investigated. However, it was not due to the additive effect of PEGylated lipids, because PEGylated lipids alone did not show any significant toxicity up to 150 µM.

Micellar formulations were successfully lyophilized. We believe that the slightly smaller size for indisulam-SSMs prepared for freeze-drying (Table 1) is due to the higher concentration of lipids (5 mM vs. 10 mM), which may affect the extension of flexible PEG chains. However,

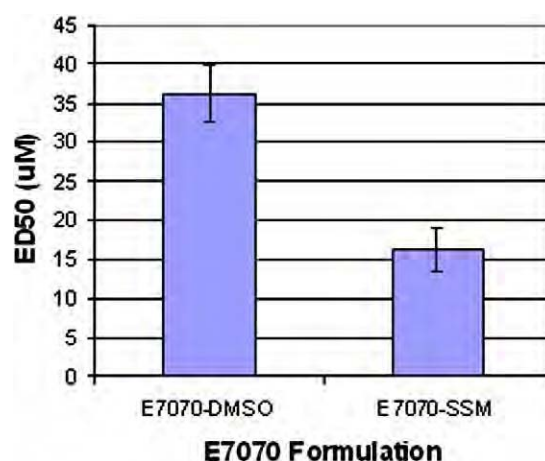


Figure 4. ED₅₀ values of indisulam in DMSO and indisulam-SSMs (3.6.3 + 3.6 µM and 16.2 + 2.7 µM, respectively).

particle size of samples in each case was not significantly different ($P > .05$ for 5 mM micellar samples as compared with 10 mM micellar samples).

In conclusion, molecular dispersion of indisulam in aqueous media was increased at least 80-fold when solubilized in SSMs (drug concentration in aqueous media ≤ 5 µg/mL vs. in SSMs 400 µg/mL). SSMMs were not as efficient as solubilizers as were SSMs, and SSMMs only improved aqueous solubility by two fold. This was probably due to competition of indisulam molecules with EPC for the same location in SSMMs. Drug incorporation did not change the mean size of the micelles. According to the HPLC results, more than 95% of the drug was incorporated in the optimized micellar system with no precipitation or SSP formation. In vitro studies using the MCF-7 breast cancer cell line showed that indisulam-SSMs are more effective than indisulam in DMSO. The optimized indisulam-SSM formulation was successfully lyophilized without any addition of lyoprotectants or cryoprotectants, indicating that acceptable shelf life can be achieved for this optimized indisulam formulation. We propose that indisulam-SSMs should be further developed as a novel nanomedicine for targeted treatment of breast cancer.

References

- Ashok B, Arleth L, Hjelm RP, Rubinstein I, Önyüksel H. In vitro characterization of PEGylated phospholipid micelles for improved drug solubilization: effects of PEG chain length and PC incorporation. *J Pharm Sci* 2004;93:2476–87.
- Krishnadas A, Rubinstein I, Önyüksel H. Sterically stabilized phospholipid mixed micelles: in vitro evaluation as a novel carrier for water-insoluble drugs. *Pharm Res* 2003;20:297–302.
- Önyüksel H, Ikezaki H, Patel M, Gao XP, Rubinstein I. A novel formulation of VIP in sterically stabilized micelles amplifies vasodilation in vivo. *Pharm Res* 1999;16:155–60.
- Koo OM, Rubinstein I, Önyüksel H. Role of nanotechnology in targeted drug delivery and imaging: a concise review. *Nanomedicine* 2005;1: 193–212.

5. Lukyanov AN, Torchilin VP. Micelles from lipid derivatives of water-soluble polymers as delivery systems for poorly soluble drugs. *Adv Drug Deliv Rev* 2004;56:1273-89.
6. Lukyanov AN, Gao Z, Mazzola L, Torchilin VP. Polyethylene glycol-diacyllipid micelles demonstrate increased accumulation in subcutaneous tumors in mice. *Pharm Res* 2002;19:1424-9.
7. Koo OM, Rubinstein I, Önyüksel H. Camptothecin in sterically stabilized phospholipid micelles: a novel nanomedicine. *Nanomedicine* 2005;1:77-84.
8. Hammad MA, Muller BW. Solubility and stability of lorazepam in bile salt/soya phosphatidylcholine-mixed micelles. *Drug Dev Ind Pharm* 1999;25:409-17.
9. Gabizon A, Shmeeda H, Horowitz AT, Zalipsky S. Tumor cell targeting of liposome-entrapped drugs with phospholipid-anchored folic acid-PEG conjugates. *Adv Drug Deliv Rev* 2004;56:1177-92.
10. Owa T, Yoshino H, Okauchi T, Yoshimatsu K, Ozawa Y, Sugi NH, et al. Discovery of novel antitumor sulfonamides targeting G1 phase of the cell cycle. *J Med Chem* 1999;42:3789-99.
11. Yamada Y, Yamamoto N, Shimoyama T, Horiiike A, Fujisaka Y, Takayama K, et al. Phase I pharmacokinetic and pharmacogenomic study of E7070 administered once every 21 days. *Cancer Sci* 2005;96:721-8.
12. Ozawa Y, Sugi NH, Nagasu T, Owa T, Watanabe T, Koyanagi N, et al. E7070, a novel sulphonamide agent with potent antitumour activity in vitro and in vivo. *Eur J Cancer* 2001;37:2275-82.
13. Smyth J, Aamdal S, Awada A, Ditttrich C, Caponigro F, Schoffski P, et al. Phase II study of E7070 in patients with metastatic melanoma. *Ann Oncol* 2005;16:158-61.
14. Fukuoka K, Usuda J, Iwamoto Y, Fukumoto H, Nakamura T, Yoneda T, et al. Mechanisms of action of the novel sulfonamide anticancer agent E7070 on cell cycle progression in human non-small cell lung cancer cells. *Invest New Drugs* 2001;19:219-27.
15. Abbate F, Casini A, Owa T, Scozzafava A, Supuran CT. Carbonic anhydrase inhibitors: E7070, a sulfonamide anticancer agent, potently inhibits cytosolic isozymes I and II, and transmembrane, tumor-associated isozyme IX. *Bioorg Med Chem Lett* 2004;14:217-23.
16. Tripathy D. Capecitabine in combination with novel targeted agents in the management of metastatic breast cancer: underlying rationale and results of clinical trials. *Oncologist* 2007;12:375.
17. Ditttrich C, Zandvliet AS, Gneist M, Huitema AD, King AA, Wanders J. A phase I and pharmacokinetic study of indisulam in combination with carboplatin. *Br J Cancer* 2007;96:559-66.
18. Nakatsu N, Yoshida Y, Yamazaki K, Nakamura T, Dan S, Fukui Y, et al. Chemosensitivity profile of cancer cell lines and identification of genes determining chemosensitivity by an integrated bioinformatical approach using cDNA arrays. *Mol Cancer Ther* 2005;4:399-412.
19. Raymond E, ten Bokkel Huinink WW, Taieb J, Beijnen J, Faivre S, Wanders J, et al. Phase I and pharmacokinetic study of E7070, a novel chloroindolyl sulfonamide cell-cycle inhibitor, administered as a one-hour infusion every three weeks in patients with advanced cancer. *J Clin Oncol* 2002;20:3508.
20. Yokoi A, Kuromitsu J, Kawai T, Nagasu T, Sugi NH, Yoshimatsu K, et al. Profiling novel sulfonamide antitumor agents with cell-based phenotypic screens and array-based gene expression analysis. *Mol Cancer Ther* 2002;1:275-86.
21. Punt C, Fumoleau P, van de Walle B, Faber M, Ravic M, Campone M. Phase I and pharmacokinetic study of E7070, a novel sulfonamide, given at a daily times five schedule in patients with solid tumors. A study by the EORTC–Early Clinical Studies Group (ECSG). *Ann Oncol* 2001;12:1289-93.
22. Zandvliet AS, Copalu W, Schellens JH, Beijnen JH, Huitema AD. Saturable binding of indisulam to plasma proteins and distribution to human erythrocytes. *Drug Metab Dispos* 2006;34:1041-6.
23. Papazisis KT, Geromichalos GD, Dimitriadis KA, Kortsaris AH. Optimization of the sulforhodamine B colorimetric assay. *J Immunol Methods* 1997;208:151-8.
24. Vichai V, Kirtikara K. Sulforhodamine B colorimetric assay for cytotoxicity screening. *Nat Protoc* 2006;1:1112-6.
25. Lim SB, Rubinstein I, Önyüksel H. Freeze drying of peptide drugs self-associated with long-circulating, biocompatible and biodegradable sterically stabilized phospholipid nanomicelles. *Int J Pharm* 2008;356:345-50.
26. Zhang JX, Hansen CB, Allen TM, Boey A, Boch R. Lipid-derivatized poly (ethylene glycol) micellar formulations of benzoporphyrin derivatives. *J Control Release* 2003;86:323-38.
27. Hauss JD. Oral lipid-based formulations: enhancing the bioavailability of poorly water-soluble drugs (drugs and the pharmaceutical sciences), 170. New York: Informa Healthcare; 2007. p. 158-68.

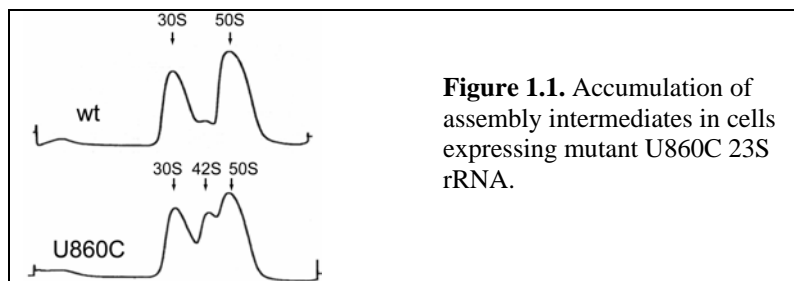
Hye-Yeong Kim, Gregory R. J. Thatcher, et al. Poster: Synthesis of Estradiol-Cyclodextrin Conjugates toward Studying Extranuclear Estrogen Signaling Pathway. Division of Medicinal Chemistry. The American Chemical Society 235th National Meeting & Exposition, New Orleans, LA, April 2008.

Cyclodextrin (CD) is a well known drug carrier and has been used as an excipient for low solubility and labile drug molecules, however, limited examples have been reported of the potential therapeutic use of derivatized CDs. The bioavailability and membrane permeability of CDs is problematic because of hydrophilicity and molecular weight. CDs were modified with 17-beta estradiol (E_2) using a number of different methodologies, leading to derivatives including aminocyclodextrins (ACDs) in which the primary face amino groups blunt the inclusion capability of the CD cavity. The estrogen receptor is a high affinity cytosolic sensor for E_2 allowing the sensitive assay of membrane permeability. Two different synthetic approaches resulted in E_2 -modified ACDs from an ethynyl- E_2 -aldehyde (nEACD) and E_2 -modified CD (nEqCD) resulting from 'click chemistry' of azido-CD and 17-beta ethynylestradiol (EE). Mono-substituted and per-substituted ECDs from both reactions were obtained in good yields under mild reaction conditions, and structures characterized by MALDI-TOF, HPLC, and 1H and ^{13}C NMR; showing no inclusion of free EE. The biological properties of these compounds were tested in ER α -positive MCF-7 breast cancer and Ishikawa endometrial cell lines. ERE-luciferase, alkaline phosphatase, and ER binding assays were performed to measure ER signaling. In cell culture, both EACD and EqCD derivatives were estrogenic at submicromolar concentrations showing cell membrane penetration. The facile qCD synthetic methodology and the observation of cell permeability suggest that the qCD scaffold is of use in exploring polyvalent molecular recognition.

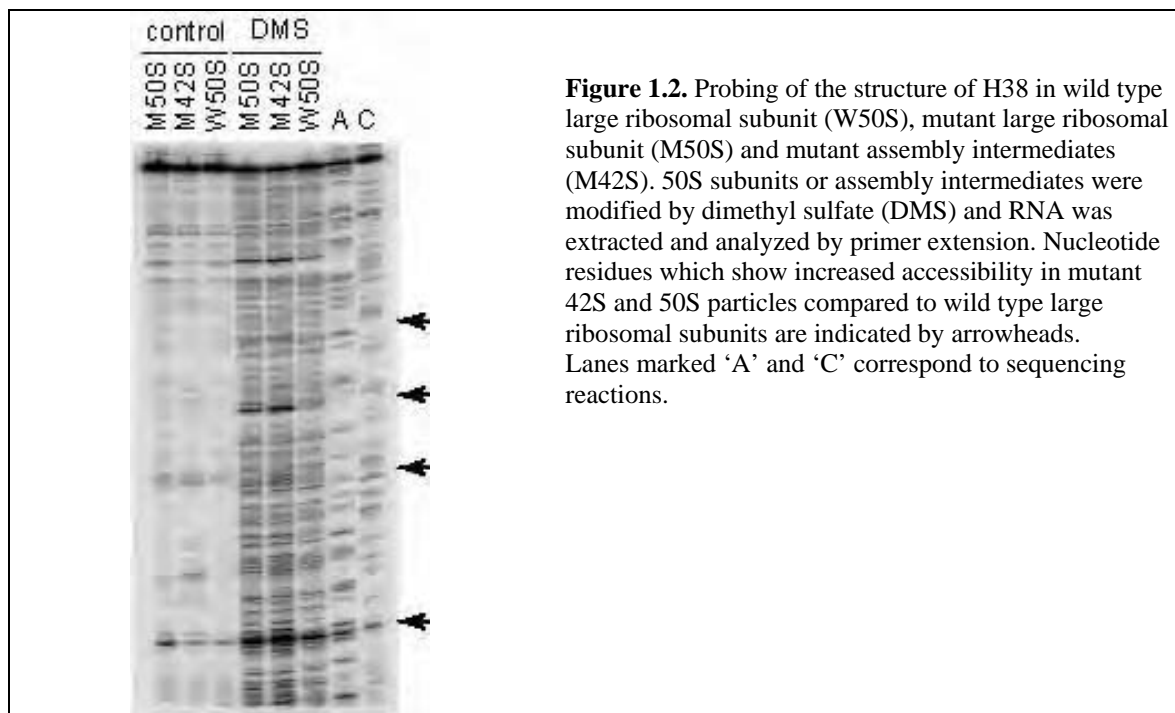
Quarterly Report 1: Project 1. Protein synthesis inhibitors acting upon new sites in bacterial ribosomes.

The aim of the project is to understand the functional significance of helix 38 (H38) in 23S rRNA and develop approaches for identifying protein synthesis inhibitors that act upon this rRNA element.

In the run-up period we found that two of the mutations in H38, U860C and A864G, are strongly deleterious and interfere with either the assembly or function of the large ribosomal subunit. Sucrose gradient analyses (Figure 1.1) show that the mutations dramatically change the gradient profile of the ribosomal subunits and reveal accumulation of a 42S assembly intermediate peak (Figure 1.1).



We analyzed the structure of H38 both in the assembly intermediates and mature 50S subunits by RNA chemical probing (Figure 1.2). Several positions in H38 in both 42S and 50S peaks showed increased accessibility to DMS modification, indicating a less tight or misassembled structure of H38 in the mutant ribosomes and precursors. This result is compatible with the idea that mutations in H38 distort its structure and prevent correct ribosomal assembly.

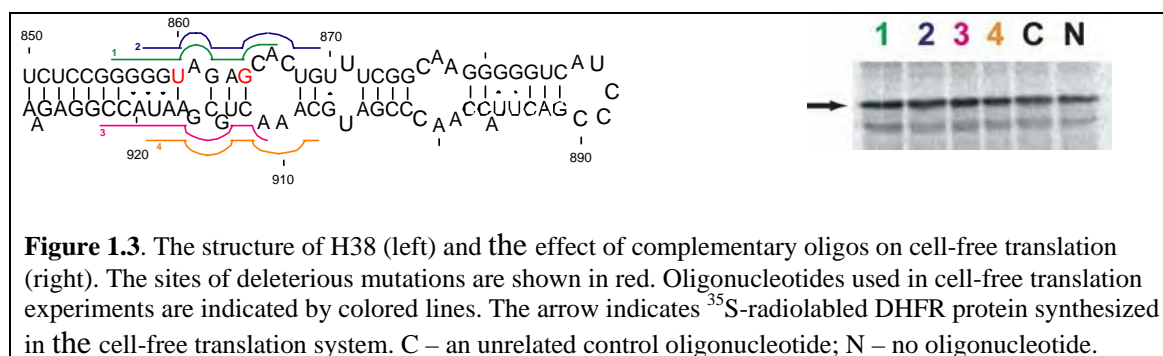


Analysis of the protein composition of the assembly intermediates turned out to be too cumbersome because of contamination of the 42S fraction with mature 50S subunits. Though decreased amounts of some proteins

were noticed, we decided to abandon more detailed characterization of the structure of the assembly intermediates in favor of more promising experiments.

On the basis of the results of sucrose gradient centrifugation and RNA probing, we hypothesized that the deleterious effect of these mutations is primarily due to the inability of the cell to assemble ribosomes. Inhibition of ribosomal assembly is attributed to some of the known protein synthesis inhibitors, however no drugs that inhibit cell proliferation specifically due to interference with ribosome assembly are known. This raises interest in H38 as a potential target for antibiotics with a new mode of action.

If our model is correct and H38 mutations affect primarily the assembly of the ribosome, then oligonucleotides targeting H38 should not inhibit protein synthesis in the cell-free system. However, they would be expected to inhibit translation in the living cell. To verify this assumption, we then carried out experiments that are formally part of Milestone 2 and tested the effects of several oligonucleotides complementary to H38 in the PURE cell-free translation system (Figure 1.3).



As anticipated, addition of up to 1 mM of synthetic oligonucleotides complementary to either of the strands of H38 did not inhibit cell-free translation of the DHFR polypeptide.

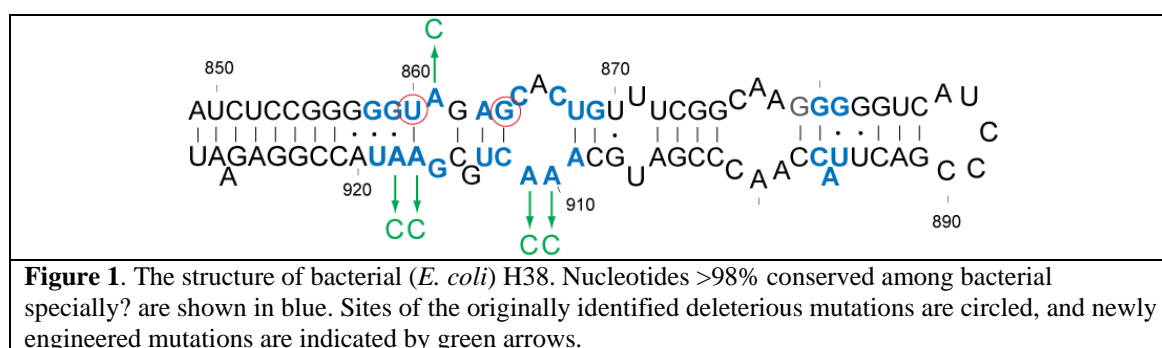
In conclusion, we achieved some of the stated goals of Aim 1 and 2: we characterized the structure of RNA in the assembly intermediates and mature mutant 50S subunits and tested the effect of synthetic oligonucleotides complementary to H38 in cell-free translation system.

In the second quarter we plan to proceed with experiments of Aims 1 and 2. Specifically, we will engineer several new mutations in H38 and will test the effect of synthetic peptide-conjugated oligonucleotides on cell proliferation and protein synthesis in the living cell.

Quarterly Report 2: Project 1. Protein synthesis inhibitors acting upon new sites in bacterial ribosomes. A. Mankin

The aim of the project is to understand the functional significance of helix 38 (H38) in 23S rRNA and develop approaches for identifying protein synthesis inhibitors that act upon this rRNA element.

On the basis of our previous results we hypothesized that the structure of this rRNA segment might be important for the ribosome assembly. Analysis of H38 structure within the context of the ribosome, in conjunction with the nucleotide conservation data, showed that several conserved adenines are involved in interactions with the other functionally-critical elements of the ribosome, including 5S rRNA. These observations prompted us to better define the boundaries of the functionally-critical region in H38. In the second quarter of our work on the project, in accordance with the original plan, we have initiated mutagenesis studies of H38.



Five positions in H38 were chosen for mutagenesis (Figure 1): A861, A910, A911, A917, and A918. In addition, we decided to mutagenize two nucleotides (A78 and 99) in 5S rRNA which directly participate in interactions with H38. 35 nt-long oligonucleotides encompassing the sites of mutations were synthesized and used for mutagenesis of pLK35 plasmid containing the complete *rrnB* operon of *E. coli*. With the use of a Multi site-directed mutagenesis kit offered by Stratagene we obtained several transformants but none of the sequenced clones carried the desired mutations. It is possible that multi-site kit is poorly applicable to such a large plasmid as pLK35 (ca. 10 kb). We are currently repeating the mutagenesis using a different kit, QuickChange II XL, specifically designed for introducing mutations in the large plasmids.

In our original proposal, in order to validate H38 as an antibiotic target we planned to synthesize peptide-conjugated peptide nucleic acid (PNA) oligos and test their inhibitory action *in vivo*. Unfortunately, our planned collaboration with Dr. Bruce Geller of the Oregon State University and his company AVI BioPharma did not go through because of the new focus of the company's effort. Our inquiries with the other commercial suppliers of peptide-conjugated PNA oligos showed that the cost of even limited number of oligos (4-6) would be prohibitively expensive (\$25,000 - \$40,000). Therefore, we decided to modify the research strategy. Our original plan was to validate the new site of antibiotic action and then develop a fluorescence-based binding assay to identify compounds that bind to bacterial H38. However, we were aware of three potential problems with this approach: 1) Designing of a "good" fluorescence-based assay for monitoring binding of small molecules to RNA is not straightforward; 2) Compounds that 'simply' bind to H38 will not necessarily inhibit protein synthesis; 3) Compounds that bind to the target *in vitro* might not be able to get into the living cell. To overcome these problems, we designed an alternative strategy that will

combine two goals in one experimental design: validation of the drug-target site and identification of selective compounds that can reach the target in the living cell.

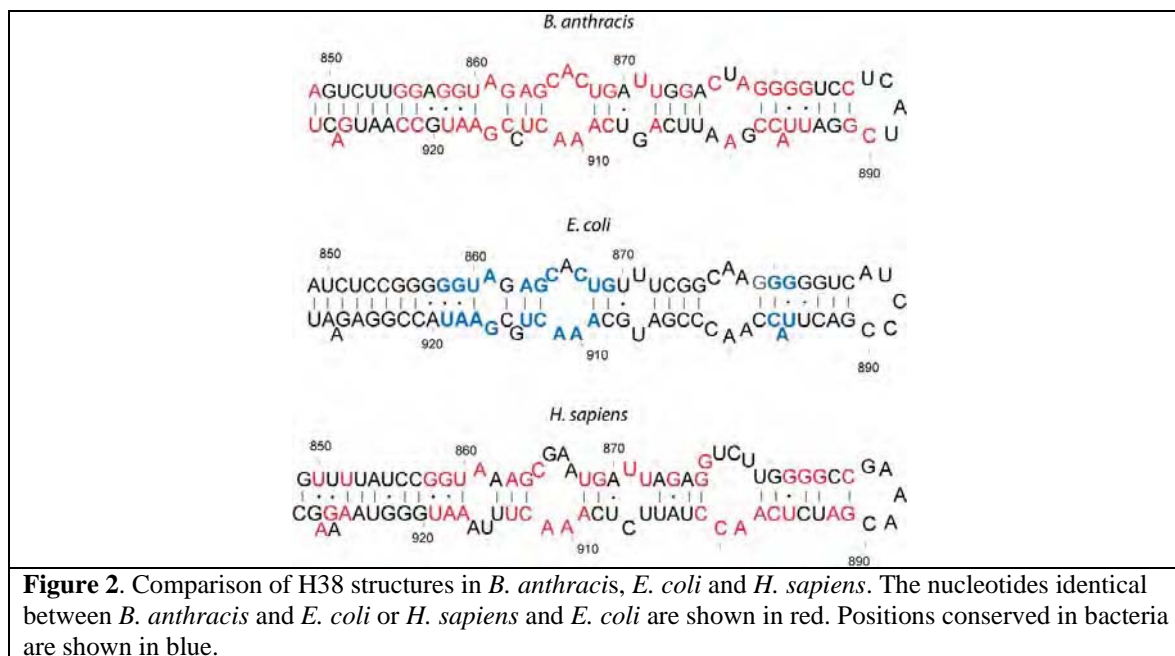


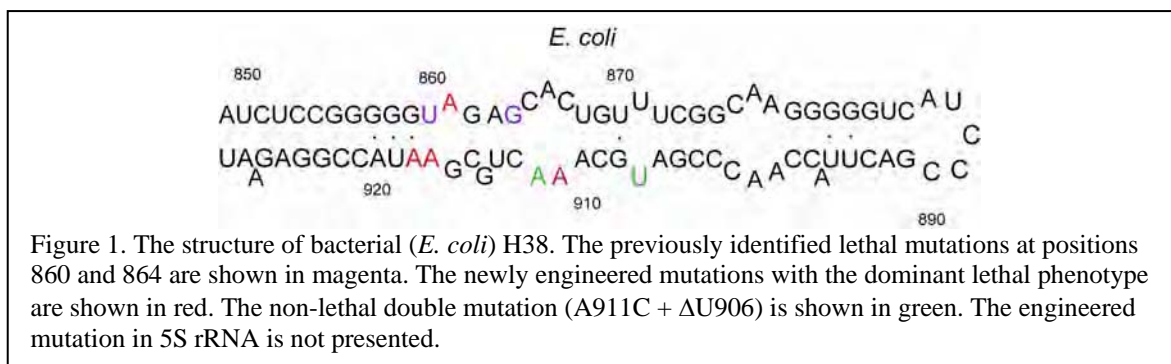
Figure 2 shows H38 sequences of *E. coli*, *B. anthracis* and human cytoplasmic ribosomes. There are significant variations between bacterial and human sequence (potentially allowing for selectivity of an inhibitor). However, most of nucleotides conserved in bacteria are also conserved in the human ribosome. Therefore, we believe that exchanging the sequence of bacterial H38 for the human H38 will preserve the ribosome function. In the third quarter of our work on the project, we will replace H38 in *E. coli* ribosome with H38 of *B. anthracis* or H38 of the human ribosome. The mutated rRNA genes will be introduced into the *E. coli* strain that lacks chromosomal wild type rRNA operons so that all the ribosomes in the cell will carry the mutant H38. We will then use high-throughput screening (in collaboration with Dr. Mesecar) to identify compounds that inhibit growth of cells expressing ‘anthracized’ ribosomes, but not cells with the ‘humanized’ ribosome. The only difference between the tester cells will be the structure of H38. Therefore, if selectively-inhibitory compounds are found, we can be sure that they target H38. Furthermore, since screening will be done using a whole-cell assay, we will be sure that the identified compounds can reach their target in the living bacterial cell. In order to construct the ‘anthracized’ and ‘humanized’ ribosome, a 709 bp-long segment of 23S rRNA gene enclosed between unique restriction sites *Sna*B1 and *Sph*1 will be synthesized by Bio Basic, Inc. so to include the *B. anthracis* or *H. sapiens* sequence of H38 (at a cost of \$ 460 each). The synthetic DNA fragment will be used to replace the corresponding region in pLK35 plasmid. Functionality of the mutant ribosomes will be tested and the whole cell HTS assay will be carried out.

Quarterly Report 3: Project 1. Protein synthesis inhibitors acting upon new sites in bacterial ribosomes.

A. Mankin

The overall aim of the project is to understand the functional significance of helix 38 (H38) in bacterial 23S rRNA and identify protein synthesis inhibitors that act upon this rRNA element.

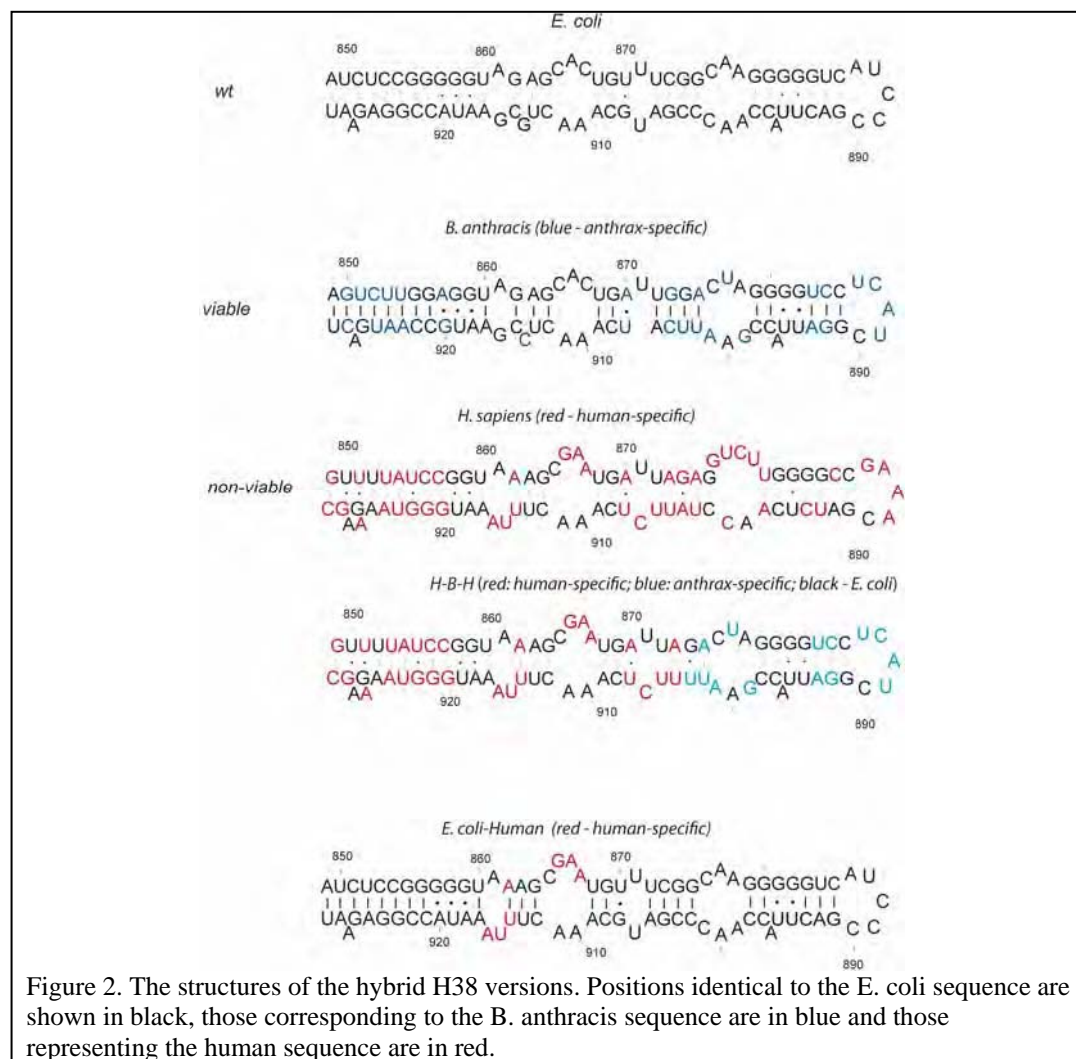
In the third quarter, the work focused on two main areas: delineating the critically-important region of H38, and generating the ‘humanized’ and ‘anthracized’ versions of H38 in the context of the *E. coli* ribosome.



Several positions in H38 in the vicinity of the originally identified lethal mutations (shown in magenta in Figure 1) were chosen for mutagenesis. A to C transversions were introduced at the conserved positions 861, 910, 911, 917, and 918. Four of the engineered H38 point mutations showed dominant lethal phenotypes: plasmids expressing mutant 23S rRNA with the mutations A861C, A910C, A917C and A918C failed to transform JM109 cells in which the P_L promoter controlling rRNA operon expression is constitutively active. This result demonstrates that the structure of the central region of H38 is critical for ribosome function or assembly and thus, justifies the attempts to identify inhibitors acting upon this site in rRNA. Neither the A911C mutation, nor a spontaneous deletion of U906 in conjunction with this mutation were notably deleterious. Therefore, the most critical part of H38 appears to be confined to its relative short segment. Lethal mutations in this rRNA segment (and therefore, small organic molecules binding to the hairpin core) are likely to disrupt ribosome function by forcing H38 into an inactive conformation resulting in inhibition of protein synthesis.

As a new way to identify selective compounds that inhibit cell growth due to their binding to the selected rRNA structure in the ribosome, we proposed a new approach – to engineer the anthrax and human sequences of H38 in the context of the *E. coli* ribosome and to screen a library of chemical compounds for selective inhibitors of the function of the ‘anthracized’, but not ‘humanized’ ribosome. The sequence of the *B. anthracis* and *H. sapiens* versions of H38 are significantly different from that of *E. coli* (Figure 2) and could be engineered by site-directed mutagenesis. Therefore, we have ordered the designed 716-nt and 713-nt sequences of a segment of 23S rRNA gene that contained the human or *B. anthracis* versions of H38, respectively, from a commercial source (Bio Basic Inc.). After the sequences of the synthetic fragment were verified, they were used to replace the corresponding segment in the plasmid-encoded 23S rRNA gene and then expressed in *E. coli*.

Both engineered plasmids were able to transform POP2136 cells in which the mutant rRNA operon is inducibly expressed at 42°C. Furthermore, transformed cells were able to grow at 42°C suggesting the lack of the dominant lethal phenotype. We then introduced the mutant plasmids into the *E. coli* SQ171 strain in which all chromosomal *rrn* alleles are deleted and rRNA is expressed from a Kan^r plasmid pCSacB. We were able to select cells that exclusively express ribosomes with the *B. anthracis* version of H38. These cells form normal size colonies and their growth rate in the liquid culture did not differ significantly from that of wild type control. This strain can be used in the screening protocol.



Unfortunately, the ribosomes with the ‘humanized’ version of H38 did not support cell growth in the absence of wild type ribosomes. Most likely the structure of the entirely-humanized H38 differed too much from the bacterial sequence. In an attempt to confine the ‘humanized’ sequence to a shorter segment of H38, we mutated the apex segment of the ‘H38 human’ sequence to the bacterial one. Since our ultimate goal is to find compounds that distinguish between *B. anthracis* and human ribosomes, the tip of the human version of H38 was mutated towards the anthrax sequence (Figure 2, H-B-H H38 construct). We are currently in the process of screening the clones for the presence of the mutation. Once mutant plasmids are identified, the phenotypes will be tested. In case the new construct is still lethal, we will further decrease the number of ‘humanizing’ mutations. Since our engineered point mutations indicate that the functionally-important part of H38 is confined to the segment 855-868/909-922, we are currently in the process of generating a construct where only 7 mutations will be introduced in the *E. coli* sequence (Figure 2, *E. coli*-Human H38 construct). These mutations will convert the central segment of H38 into the human H38 structure. We hope that this version, which carries much fewer mutations than the original ‘humanized’ construct, but still provides the structure of the human ribosome within the region that we want to target by antibiotics, will be viable and adequate for the subsequent screening library screening.

If our expectations turn out to be correct, we will have constructed a pair of clones that would be amenable for use in a HTS protocol in search for the selective compounds that inhibit protein synthesis in *B. anthracis* by interacting with H38 in the large ribosomal subunit.

Quarterly Report 4: Project 1. Protein synthesis inhibitors acting upon new sites in bacterial ribosomes.

A. Mankin

The overall aim of the project is to understand the functional significance of helix 38 (H38) in bacterial 23S rRNA and identify protein synthesis inhibitors that act upon this rRNA element.

In this report period, the work was focused on identifying ‘humanizing’ mutations in helix 38 of 23S rRNA that would be tolerated by *E. coli* cells. After having tried several mutant variants of H38 representing hybrid sequences of bacterial and human ribosome, we have identified the version that contains ‘humanizing’ mutations in one of the critical segments of H38 and yet is tolerated by the bacterial cell (Figure 1)

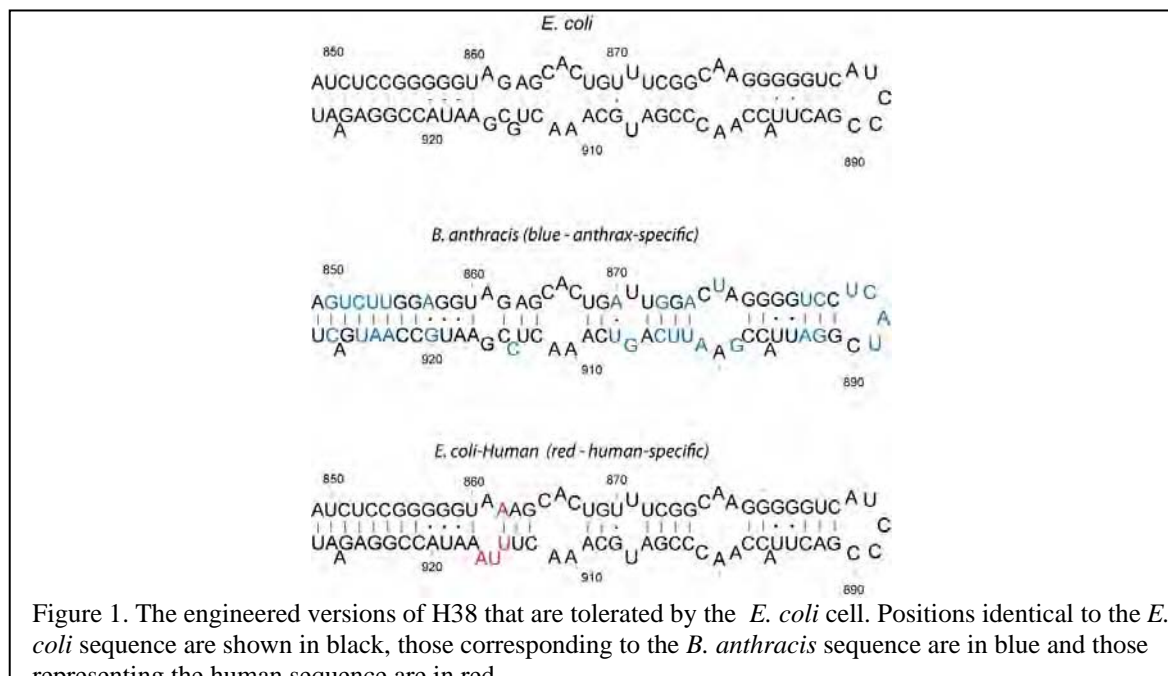


Figure 1. The engineered versions of H38 that are tolerated by the *E. coli* cell. Positions identical to the *E. coli* sequence are shown in black, those corresponding to the *B. anthracis* sequence are in blue and those representing the human sequence are in red.

In the final humanized version (“*E. coli*-Human” in Figure 1), positions 862, 914, 915 and 916 of the *E. coli* 23S rRNA are mutated to their human counterparts. The pLK35 plasmid carrying the resulting mutant rRNA operon has been introduced (along side with the pLK35 plasmid carrying *B. anthracis* version of H38 and the wild type pLK35) into *E. coli* cells SQ171. This strain lacks chromosomal rRNA operons and rRNA genes are transcribed exclusively from the plasmid-borne rRNA operons. After curing the cells of the plasmid carrying wild type rRNA operon, the resulting clones expressed exclusively mutant 23S rRNA.

In spite of the presence of mutations in the functionally-critical region of H38, *E. coli* cells expressing mutant 23S rRNA carrying the *B. anthracis* and an *E. coli*-human hybrid versions of H38 were found to be viable. Furthermore, testing growth of the resulting clones in the liquid culture did not reveal significant difference in the growth rates of the mutants compared to cells expressing wild type 23S rRNA. The resulting strains are ready for high throughput screening of the chemical library for the selective inhibitory compounds.

As the first step towards this goal, we collaborated with Dr. Mesecar’s laboratory to optimize the whole cell assay that will be used in the HTS protocol. Cells were grown in liquid culture in the wells of a 384-well microtiter plate in the presence of the increasing concentration of several known protein synthesis inhibitors. Our initial plan was to use cell density measurements as a direct readout for cell growth. This approach, however, turned out to be less than optimal and did not provide for a sufficient Z-factor. Therefore, we used the approach which is based on the use of the Alamar blue dye which is metabolized by the living cells; the use of this dye allows for amplification of the cell density signal. Previously, the dye was

used exclusively with Gram-positive bacteria and we needed to optimize the assay for Gram-negative *E. coli*. We found that prolonged (90 min) incubation with the dye at 37° compensates for the low permeability of Gram-negative membrane and provides sufficiently strong signal to be used in the high throughput assay. We are now ready to start the high-throughput screening.

Quarterly Report 5:Project 1. Protein synthesis inhibitors acting upon new sites in bacterial ribosomes.

A. Mankin

In the previous report period we have generated three bacterial strains which carry ribosomes with the E. coli, B. anthracis and the human versions of the helix 38 in 23S rRNA of the large ribosomal subunit.

We have now verified that the three strains exhibit comparable growth characteristics when grown in the wells of 384-well microtiter plate. We have additionally optimized the detection protocol for cell growth suitable for analysis in a high throughput format. However, subsequent progress was delayed because of the access to the library.

Currently, together with Dr. Mesecar, we are waiting for the 60,000 chemical compound ASINEX library. When the library is available (in the next one or two weeks), in collaboration with Dr. Mesecar (HTS Core), we will screen 20,000 compounds for their selective inhibitory action on the growth of the engineered strains.

Quarterly Report 6: Project 1. Protein synthesis inhibitors acting upon new sites in bacterial ribosomes.

A. Mankin

In the previous period, we have engineered three *E. coli* strains which express ribosomes carrying engineered *B. anthracis* and human versions of helix 38 in the large subunit rRNA. We planned to use these strains in a high-throughput screening testing. However, because the library has not been received during the anticipated time, we focus our experimental effort on verifying that the engineered strains have comparable growth characteristics and that they express exclusively mutant ribosomes.

Growth rate of the three strains was tested in a liquid culture in LB media supplemented with 50 ug/ml ampicillin. As the curves in Figure 1 show, all the three strains grew with very similar growth rates. This is an important result because a significant difference in growth rate would dramatically complicate subsequent screening effort.

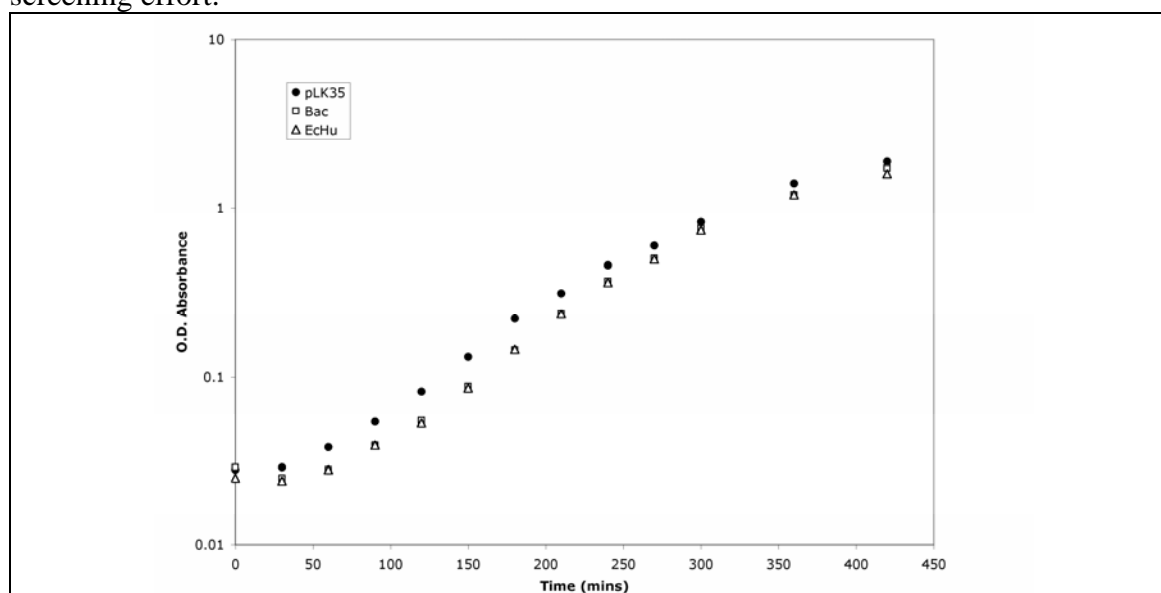


Figure 1. Growth rate of cells expressing plasmid-encoded wild type rRNA (“pLK35”), rRNA with the *B. anthracis* version of helix 38 (“Bac”) and cells with the ‘humanized’ version of helix 38 (“EcHu”).

We additionally verified that cells with the mutated helix 38 express exclusively mutant rRNA. For that, total RNA was prepared from the cells, a specific oligonucleotide primer was annealed to 23S rRNA upstream from the site of the engineered mutation and extended in the presence of three dNTPs and a terminator (ddG). The representative gel, shown in Figure 2 shows that EcHu cells expressed exclusively 23S rRNA with the mutated helix 38. A similar result was obtained for the cells expressing rRNA with the *B. anthracis* version of helix 38.

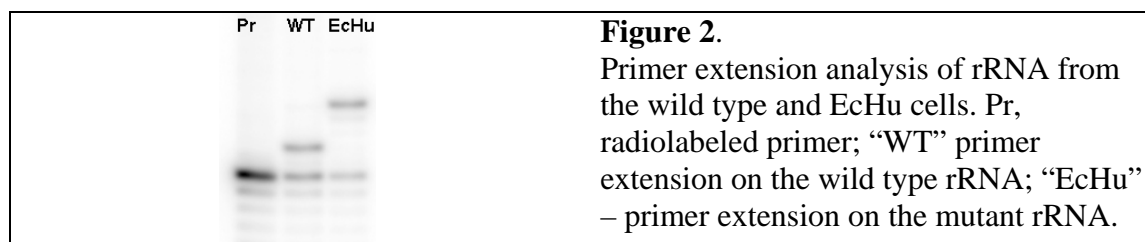


Figure 2. Primer extension analysis of rRNA from the wild type and EcHu cells. Pr, radiolabeled primer; “WT” primer extension on the wild type rRNA; “EcHu” – primer extension on the mutant rRNA.

Quarterly Report 1: Project 2. Multiple target molecular counter-measures to biowarfare pathogens; blockade of infiltration and boosting of host defenses.

The hypothesis of this project is that aminocyclodextrins (ACDs) represent polyvalent ligands that can be synthesized to selectively inhibit the assembly of protective antigen (PA), blocking intracellular delivery of lethal factor (LF) and edema factor (EF); and furthermore, that ACDs can be used to deliver NO to macrophages to supplement pathogen destruction.

Preliminary data on ACDs A number of laboratories including our own, have demonstrated that substituted CDs can show specific recognition of substrates.¹⁻⁹ In order to pursue these studies, we developed, published, and patented novel and highly efficient synthetic techniques.¹⁰⁻¹² Based upon the hypothesis that proteoglycans have neurite growth promoting and inhibitory activity associated with the anionic glycosaminoglycan sulfate (GAGS) side chains,¹³ we synthesized amino-cyclodextrins (ACDs) in which the primary face was persubstituted with an amine and the secondary face was unmodified, methylated or acylated. ACDs were shown to selectively recognize different GAGs and in primary cell culture to inhibit and/or provide a substrate for neurite growth,⁷ showing a surprising degree of selectivity, explored further in studies using small anionic guest molecules, such as nucleotides and aryl phosphates.^{14,15} These studies demonstrated that ACDs differ significantly from other CD derivatives. We observed that ACDs inhibited self-assembly of a potentially neurotoxic form of β -amyloid protein ($A\beta$) implicated in Alzheimer's disease using an $A\beta$ specific immunoassay.¹⁶⁻¹⁹ ACDs inhibit self-assembly of $A\beta$ into neurotoxic soluble oligomers termed ADDLs with nanomolar potency through a combination of electrostatic and hydrophobic recognition.¹⁸ ACDs can be viewed to present a topology of binding sites akin to an antibody-like binding pocket but without the inherent problems in antibody therapeutics.^{20,21} The Specific Aims and the above paraphrased text from the proposal are provided for reference.

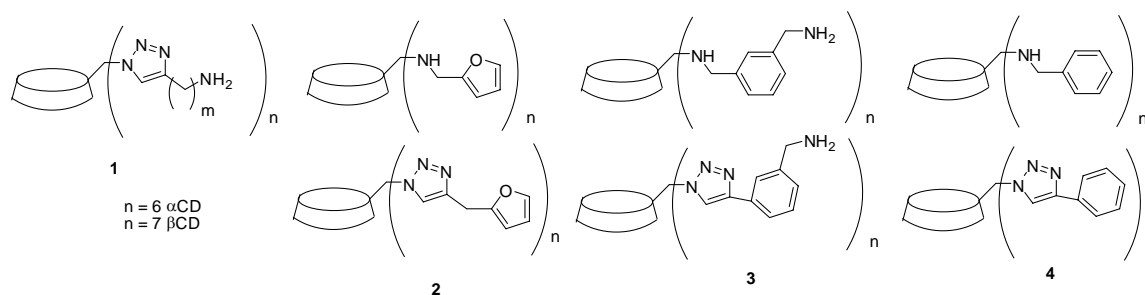
Specific Aims and Progress *Italicized aims have not been a target of this funding period.*

Aim 1. Synthesis of a small library of 18 ACDs derived from α , β , and γ CD that contain pendant groups at the primary face to provide electrostatic or hydrophobic recognition or a combination of both. *Synthesis of a second library of 6 ACDs to extrapolate or optimize interactions with PA and to amplify cytoprotection against LT.* Synthesis of a combinatorial library of >2000 ACDs based upon either an α , β , or γ CD scaffold that utilizes different amine pendant groups in various combinations.

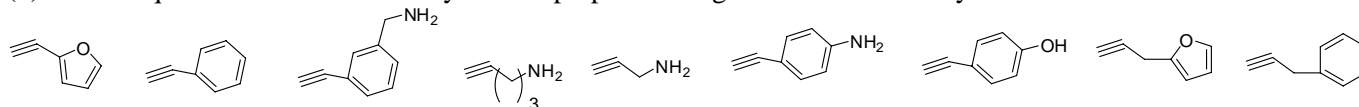
Progress. Three synthetic routes were studied for preparation of CD derivatives: (1) condensation of per-NH₂-ACD with the appropriate aldehydes followed by reduction to the desired ACD; (2) the standard route to derivatized CDs employing reaction of a thiol with per-Br-CD and subsequent functionalization, leading eventually to derivatives which contain amine pendant groups, but which are derivatized CDs, rather than ACD derivatives; (3) a new application of the Cu-catalyzed coupling of azides to alkynes (coined "click chemistry") whereby per-N₃-CD is reacted with the appropriate alkyne to yield a CD with a corona of amine pendant groups and an annulus of triazole groups. Since these may have different properties from CDs, we term these qCD derivatives.

We have further explored routes (1) and (2) in this funding period and confirmed that only in very few cases do reactions go to completion. We have initiated exploration of the qCD derivatives in this funding period and find that in general the reaction is quantitative, although purification using various extraction techniques requires careful optimization. The importance of a quantitative synthetic methodology is (1) that chromatography on multiply substituted CD derivatives is complex, sometimes intractable and unsuitable for scale-up and (2) that preparation of combinatorial libraries requires a clean synthetic procedure that should not be biased towards subsets of synthons. The synthesis leading to qCD derivatives appears to fill these criteria and several examples have been prepared.

Goals for next funding period: (1) Determine the differences in molecular recognition caused by the triazole annulus of qCDs versus ACDs. Accordingly, the following compounds will be prepared:



(2) A small qCD combinatorial library will be prepared using a selection of 9 alkynes:



Aim 2. Assay of binding of ACDs to recombinant PA using pulsed ultrafiltration electrospray mass spectrometry (PUF-LC-MS) to indicate the most potent ACD capable of inhibition of PA self-assembly and to derive a structure-activity relationship for ACDs.

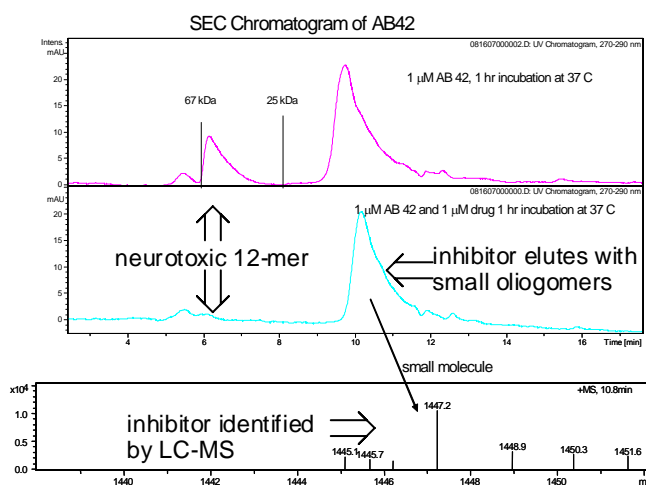
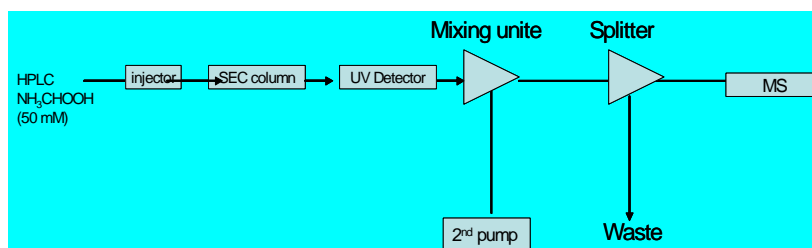
Progress. At present, we do not have immediate access to recombinant PA, so we have adjusted our approach to optimize methods before use of PA itself. In part, the original rationale for use of ACDs in Anthrax treatment was based upon both the simile between PA and other peptides that self-assemble into cytotoxic oligomeric structures as well as the ability of ACDs to inhibit such self-assembly. We have developed an LC-MS method that is improved upon the PUF-LC-MS methodology and for the first time applied it to the inhibition of self-assembly of β -amyloid peptide ($A\beta_{1-42}$) by ACD. This is a significant breakthrough for two reasons: First, it demonstrates that the ACD under testing completely inhibits $A\beta_{1-42}$ self-assembly to the neurotoxic 12-mer form, but does not inhibit assembly of other oligomers. Second, the methodology is not specific to $A\beta$, but is general for screening of inhibitors of peptide self-assembly.

The details of the methodology are as follows: (1) inhibitor and peptide are incubated with stirring allowing assembly; (2) cut-off filters are used to remove uncomplexed inhibitor; prior to (3) elution through size exclusion chromatography (SEC) column separating and detecting oligomeric forms by UV-detection; (4) post-column disaggregation of oligomers; (5) electrospray injection into mass spec and detection of small molecule inhibitors as a function of time. This SEC-LS-MS methodology is shown for the ACD inhibitor (MW = 14472); the neurotoxic 12-mer has MW 56kDa and is not observed in the presence of ACD.

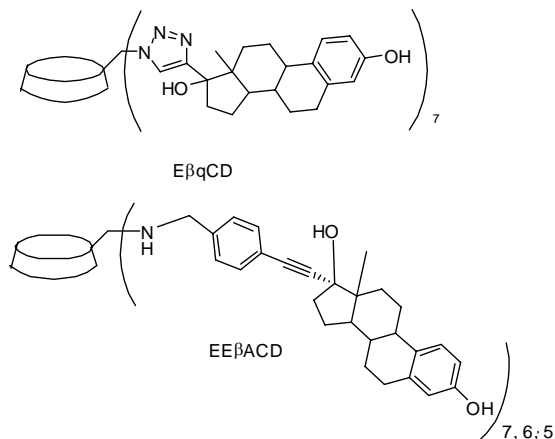
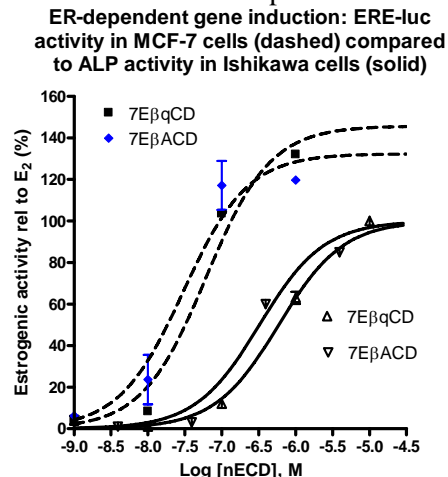
Goals for next funding period: (1) extrapolation of assay to screening libraries of qCD or ACD inhibitors; (2) assay of compounds **1-6** for inhibitor potency towards oligomerization.

Aim 3. Assay of ACD inhibition of LT-induced cytotoxicity in RAW cells. Study of NO donor influence on LT-induced cytotoxicity and any synergism with ACD inhibition.

Progress. We have proposed that CD derivatives inhibit the actions of Anthrax lethal factor by blocking self-assembly of PA in the host cell membrane. The major clinical use of simple CDs has been as drug carriers solubilizing and increasing membrane permeability of these drugs. The question of membrane permeability of derivatized CDs of MW>1500 has not been determined unambiguously. Therefore, in the absence of LT to pursue aim 3, we conducted experiments with a pair of qCD and ACD derivatives to answer the question



of membrane permeability. Experimental hypothesis: the intracellular estrogen receptor (ER) is a high sensitivity reporter with nanomolar affinity for estrogens; estrogen derivatized qCD and ACD will induce estrogen-dependent gene transcription (ERE-luciferase or Alkaline phosphatase expression) if they permeate the cell into the cytosol. We synthesized ethynylestradiol derivative of ACD (EE β qCD) and an estradiol derivative of qCD (E β qCD). ER ligand binding for both compounds compared to estrogenic activity in ER positive endometrial and breast cancer cell confirmed that even these large polyvalent molecules are capable of crossing cell membranes. This is important information for the experiments to be carried out in cells using PA and LT in the next funding period.



Literature Cited

- (1) Palmer, D. R. J.; Buncel, E.; Thatcher, G. R. J. Re-evaluation of cyclodextrin as a model of chymotrypsin: acceleration and inhibition of tertiary anilide hydrolysis. *J. Org. Chem.* **1994**, *59*, 5286-5291.
- (2) Tabushi, I. Cyclodextrin catalysis as a model for enzyme action. *Acc. Chem. Res.* **1982**, *15*, 66-72.
- (3) Breslow, R. Biomimetic chemistry and artificial enzymes: catalysis by design. *Acc. Chem. Res.* **1995**, *28*, 146-153.
- (4) Murakami, Y.; Kikuchi, J.-i.; Hisaeda, Y.; Hayashida, O. Artificial Enzymes. *Chemical Reviews (Washington, D. C.)* **1996**, *96*, 721-758.
- (5) Thatcher, G. R. J. PI-specific phospholipase C: inhibition and enzyme model studies. *Book of Abstracts, 214th ACS National Meeting, Las Vegas, NV, September 7-11 1997*, CARB-058.
- (6) Breslow, R.; Dong, S. D. Biomimetic Reactions Catalyzed by Cyclodextrins and Their Derivatives. *Chem Rev* **1998**, *98*, 1997-2012.
- (7) Borrajo, A. M. P.; Gorin, B. I.; Dostaler, S. M.; Riopelle, R. J.; Thatcher, G. R. J. Derivatized cyclodextrins as peptidomimetics: influence on neurite growth. *Bioorg Med Chem Lett* **1997**, *7*, 1185-1190.
- (8) Karginov, V. A.; Nestorovich, E. M.; Schmidtman, F.; Robinson, T. M.; Yohannes, A. et al. Inhibition of *S. aureus* alpha-hemolysin and *B. anthracis* lethal toxin by beta-cyclodextrin derivatives. *Bioorg Med Chem* **2007**, *15*, 5424-5431.
- (9) Karginov, V. A.; Nestorovich, E. M.; Yohannes, A.; Robinson, T. M.; Fahmi, N. E. et al. Search for cyclodextrin-based inhibitors of anthrax toxins: synthesis, structural features, and relative activities. *Antimicrob Agents Chemother* **2006**, *50*, 3740-3753.
- (10) Gorin, B. D.; Riopelle, R. J.; Thatcher, G. R. J. Efficient perfacial derivatization of cyclodextrins at the primary face. *Tetrahedron Lett* **1996**, 4647-4650.
- (11) Dow, K. E.; Gorine, B. I.; Riopelle, R. J.; Thatcher, G. Cyclodextrin derivatives, preparation thereof, and use as nerve process growth modulators; (Queen's University at Kingston, Can.). Application: WO, 1997; pp 36 pp.

- (12) Vizitiu, D.; Walkinshaw, C. S.; Thatcher, G. R. J. Synthesis of mono-facially functionalized cyclodextrins bearing amino pendent groups. *J. Org. Chem.* **1997**, *62*, 8760-8766.
- (13) Palmer, D. R. J.; Buncel, E.; Thatcher, G. R. J. Re-Evaluation of Cyclodextrin as a Model of Chymotrypsin: Acceleration and Inhibition of Tertiary Anilide Hydrolysis. *Journal of Organic Chemistry* **1994**, *59*, 5286-5291.
- (14) Vizitiu, D.; Thatcher, G. R. J. Binding of phosphates to aminocyclodextrin biomimetics. *Journal of Organic Chemistry* **1999**, *64*, 6235-6238.
- (15) Thatcher, G. R. J.; Borrajo, A. M. P. Molecular recognition of nucleotides and other biologically relevant anions by amino-cyclodextrins. *Abstracts of Papers, 222nd ACS National Meeting, Chicago, IL, United States, August 26-30, 2001* **2001**, ORGN-631.
- (16) Wang, Z.; Fernandez, P. A.; Chang, L.; Klein, W. L.; Venton, D. L. et al. Design and synthesis of functionalized cyclodextrins as inhibitors of amyloid-b-peptide derived toxins. *Abstracts of Papers, 229th ACS National Meeting, San Diego, CA, United States, March 13-17, 2005* **2005**, MEDI-195.
- (17) Venton, D. L.; Klein, W. L.; Thatcher, G. R. J.; Chang, L.; Liu, R. et al. Preparation of per-6-amino-substituted-deoxy-cyclodextrins to treat Alzheimer's diseases; (The Board of Trustees of the University of Illinois, USA; Northwestern University). Application: WO, 2005; pp 54 pp.
- (18) Wang, Z.; Chang, L.; Klein, W. L.; Thatcher, G. R. J.; Venton, D. L. Per-6-substituted-per-6-deoxy beta-cyclodextrins inhibit the formation of beta-amyloid peptide derived soluble oligomers. *J Med Chem* **2004**, *47*, 3329-3333.
- (19) Chang, L.; Bakhos, L.; Wang, Z.; Venton, D. L.; Klein, W. L. Femtomole immunodetection of synthetic and endogenous amyloid-beta oligomers and its application to Alzheimer's disease drug candidate screening. *J Mol Neurosci* **2003**, *20*, 305-313.
- (20) Park, H. S.; Lin, Q.; Hamilton, A. D. Modulation of protein-protein interactions by synthetic receptors: design of molecules that disrupt serine protease-proteinaceous inhibitor interaction. *Proc Natl Acad Sci U S A* **2002**, *99*, 5105-5109.
- (21) Mourez, M.; Kane, R. S.; Mogridge, J.; Metallo, S.; Deschatelets, P. et al. Designing a polyvalent inhibitor of anthrax toxin. *Nat Biotechnol* **2001**, *19*, 958-961.

Quarterly Report 2:

Project 2. Multiple target molecular counter-measures to biowarfare pathogens; blockade of infiltration and boosting of host defenses.

G. Thatcher

The hypothesis of this research is that ACDs represent polyvalent ligands that can be synthesized to selectively inhibit the assembly of PA, blocking intracellular delivery of LF and EF; and furthermore, that ACDs can be used to deliver NO to macrophages to supplement pathogen destruction.

Preliminary data on ACDs. A number of laboratories including our own, have demonstrated that substituted CDs can show specific recognition of substrates.¹⁻¹¹ The hypothesis that proteoglycans have neurite growth promoting and inhibitory activity associated with the anionic glycosaminoglycan sulfate (GAGS) side chains,¹² stimulated the synthesis of amino-cyclodextrins (ACDs) in which the primary face was persubstituted with an amine and the secondary face was unmodified, methylated or acylated. ACDs were shown to selectively recognize different GAGs and in primary cell culture to inhibit and/or provide a substrate for neurite growth,⁶ showing a surprising degree of selectivity, explored further in studies using small anionic guest molecules, such as nucleotides and aryl phosphates.^{13, 14} These studies demonstrated that ACDs differ significantly from other CD derivatives. We observed that ACDs inhibited self-assembly of a potentially neurotoxic form of β -amyloid protein (A β) implicated in Alzheimer's disease using an A β specific immunoassay.¹⁵⁻¹⁸ ACDs can be viewed to present a topology of binding sites akin to an antibody-like binding pocket but without the inherent problems in antibody therapeutics.^{19, 20} The Specific Aims and the above paraphrased text from the proposal are provided for reference.

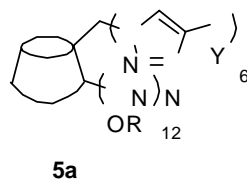
Specific Aims and Progress *Italicized aims have not been a target of this funding period.*

Aim 1. Synthesis of a small library of 18 ACDs derived from α , β , and γ CD that contain pendant groups at the primary face to provide electrostatic or hydrophobic recognition or a combination of both. *Synthesis of a second library of 6 ACDs to extrapolate or optimize interactions with PA and to amplify cytoprotection against LT.* Synthesis of a combinatorial library of >2000 ACDs based upon either an α , β , or γ CD scaffold that utilizes different amine pendant groups in various combinations.

Progress. Previously, 3 synthetic routes were studied for preparation of CD derivatives, including Cu-catalyzed coupling of azides to alkynes (coined "click chemistry") whereby per-N₃-CD is reacted with the appropriate alkyne to yield a CD with a corona of amine pendant groups and an annulus of triazole groups (we term these qCD derivatives). Although the click chemistry proved more general than the first two synthetic methods attempted, drawbacks to this method were seen; in particular, long reaction times and very different rates of reaction with different alkynes. The importance of a quantitative synthetic methodology is that chromatography on derivatized CDs is complex and unsuitable for scale-up. The drawback with varied alkyne reactivity is the problem in preparing combinatorial libraries using different alkynes that react at very different rates.

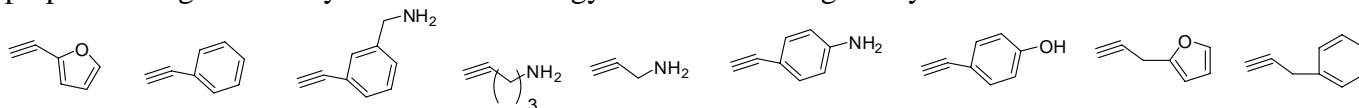
In the present funding period, great progress was made in optimizing the click chemistry for reliable library synthesis. The new method enjoys great advantage: (1) shortened reaction time (2 min in microwave oven versus 2 to 10 days previously); (2) the reaction can be easily monitored by TLC to ensure complete conversion; (3) removal of the new catalyst system CuI-P(OEt)₃ is more convenient than CuI alone, therefore improving the isolated yield.

A small qCD library of 14 compounds was prepared:



5 R = OAc; **6** R = H
a Y = Ph **b** Y = p-BrPh
c Y = p-NH₂Ph **d** Y = pMeOPh
e Y = H **f** Y = HOCH₂
g 2-furfuryl

In the next funding period, homogeneous β qCD derivatives, and a combinatorial library, will be prepared using the new synthetic methodology and the following 9 alkynes:



Aim 2. Assay of binding of ACDs to recombinant PA using pulsed ultrafiltration electrospray mass spectrometry (PUF-LC-MS) to indicate the most potent ACD capable of inhibition of PA self-assembly and to derive a structure-activity relationship for ACDs.

Progress. In our original proposal, recombinant PA was to be provided from Dr. Andy Mesecar's lab, however, Dr Mesecar's lab has ceased to express and purify this protein. We have located BEResources as an alternative source of both Anthrax lethal factor components, PA and LT. The contract and MTA agreement has been completed by UIC and we hope to receive these peptides in the next funding period. We will extend to the Anthrax proteins the LC-MS methodology developed in the previous and current funding periods, which examined the inhibition of self-assembly of β -amyloid peptide ($A\beta_{1-42}$) by ACDs. Goals for next funding period: assay of combinatorial qCD libraries and homogeneous qCD and ACD derivatives.

Aim 3. Assay of ACD inhibition of LT-induced cytotoxicity in RAW cells. Study of NO donor influence on LT-induced cytotoxicity and any synergism with ACD inhibition.

Progress. It has been proposed that CD derivatives inhibit the actions of Anthrax lethal factor by blocking self-assembly of PA in the host cell membrane. The major clinical use of simple CDs has been as drug carriers solubilizing and increasing membrane permeability of these drugs. The question of membrane permeability of derivatized CDs of MW>1500 has not been unambiguously determined. Experiments were conducted with a pair of qCD and ACD derivatives to answer the question of membrane permeability based upon the experimental hypothesis that the intracellular estrogen receptor (ER) is a high sensitivity reporter with nanomolar affinity for estrogens, and therefore estrogen derivatized qCD and ACD derivatives will induce estrogen-dependent gene transcription if they permeate the cell into the cytosol and further penetrate the nuclear membrane. An ethynylestradiol derivative of ACD and an estradiol derivative of qCD were synthesized. In endometrial and breast cancer cell lines both compounds were observed to be estrogenic, confirming that even these large polyvalent molecules are capable of crossing cell membranes. In the current funding period, a new set of compounds were synthesized incorporating a fluorescent pendant group in the qCD structure, in order to use confocal microscopy to localize and quantify cell permeability. This will be explored in the next funding period.

A major goal of the next funding period is to screen all qCD and ACD libraries for effects on RAW cell cultures. Cell viability and markers of inflammatory response (iNOS and PGs) will be measured. These experiments serve as essential controls for the future study of Anthrax proteins in the RAW macrophage like cell line. Compounds that inhibit the induction of inflammatory response by lipopolysaccharide (LPS) may be poorly selective for Anthrax toxins; compounds that are cytotoxic in the absence of LPS may be too broadly cytotoxic for use.

Literature Cited

1. Palmer, D. R. J.; Buncel, E.; Thatcher, G. R. J. Re-evaluation of cyclodextrin as a model of chymotrypsin: acceleration and inhibition of tertiary anilide hydrolysis. *J. Org. Chem.* **1994**, 59, 5286-91.
2. Tabushi, I. Cyclodextrin catalysis as a model for enzyme action. *Acc. Chem. Res.* **1982**, 15, 66-72.
3. Breslow, R. Biomimetic chemistry and artificial enzymes: catalysis by design. *Acc. Chem. Res.* **1995**, 28, 146-153.
4. Murakami, Y.; Kikuchi, J.-i.; Hisaeda, Y.; Hayashida, O. Artificial Enzymes. *Chemical Reviews*

- (Washington, D. C.) **1996**, 96, 721-58.
5. Breslow, R.; Dong, S. D. Biomimetic Reactions Catalyzed by Cyclodextrins and Their Derivatives. *Chem Rev* **1998**, 98, 1997-2012.
 6. Borrajo, A. M. P.; Gorin, B. I.; Dostaler, S. M.; Riopelle, R. J.; Thatcher, G. R. J. Derivatized cyclodextrins as peptidomimetics: influence on neurite growth. *Bioorg Med Chem Lett* **1997**, 7, 1185-1190.
 7. Karginov, V. A.; Nestorovich, E. M.; Schmidtman, F.; Robinson, T. M.; Yohannes, A.; Fahmi, N. E.; Bezrukov, S. M.; Hecht, S. M. Inhibition of *S. aureus* alpha-hemolysin and *B. anthracis* lethal toxin by beta-cyclodextrin derivatives. *Bioorg Med Chem* **2007**, 15, 5424-31.
 8. Karginov, V. A.; Nestorovich, E. M.; Yohannes, A.; Robinson, T. M.; Fahmi, N. E.; Schmidtman, F.; Hecht, S. M.; Bezrukov, S. M. Search for cyclodextrin-based inhibitors of anthrax toxins: synthesis, structural features, and relative activities. *Antimicrob Agents Chemother* **2006**, 50, 3740-53.
 9. Gorin, B. D.; Riopelle, R. J.; Thatcher, G. R. J. Efficient perfacial derivatization of cyclodextrins at the primary face. *Tetrahedron Lett* **1996**, 4647-4650.
 10. Dow, K. E.; Gorine, B. I.; Riopelle, R. J.; Thatcher, G. Cyclodextrin derivatives, preparation thereof, and use as nerve process growth modulators. 97-CA437 9749735, 19970620., 1997.
 11. Vizitiu, D.; Walkinshaw, C. S.; Thatcher, G. R. J. Synthesis of mono-facially functionalized cyclodextrins bearing amino pendent groups. *J. Org. Chem.* **1997**, 62, 8760-8766.
 12. Palmer, D. R. J.; Buncel, E.; Thatcher, G. R. J. Re-Evaluation of Cyclodextrin as a Model of Chymotrypsin: Acceleration and Inhibition of Tertiary Anilide Hydrolysis. *Journal of Organic Chemistry* **1994**, 59, 5286-91.
 13. Vizitiu, D.; Thatcher, G. R. J. Binding of phosphates to aminocyclodextrin biomimetics. *Journal of Organic Chemistry* **1999**, 64, 6235-6238.
 14. Thatcher, G. R. J.; Borrajo, A. M. P. Molecular recognition of nucleotides and other biologically relevant anions by amino-cyclodextrins. *Abstracts of Papers, 222nd ACS National Meeting, Chicago, IL, United States, August 26-30, 2001* **2001**, ORGN-631.
 15. Wang, Z.; Fernandez, P. A.; Chang, L.; Klein, W. L.; Venton, D. L.; Thatcher, G. R. J. Design and synthesis of functionalized cyclodextrins as inhibitors of amyloid-b-peptide derived toxins. *Abstracts of Papers, 229th ACS National Meeting, San Diego, CA, United States, March 13-17, 2005* **2005**, MEDI-195.
 16. Venton, D. L.; Klein, W. L.; Thatcher, G. R. J.; Chang, L.; Liu, R.; Wang, Z.; Holterman, M. Preparation of per-6-amino-substituted-deoxy-cyclodextrins to treat Alzheimer's diseases. 2004-US23854 2005011710, 20040726., 2005.
 17. Wang, Z.; Chang, L.; Klein, W. L.; Thatcher, G. R. J.; Venton, D. L. Per-6-substituted-per-6-deoxy beta-cyclodextrins inhibit the formation of beta-amyloid peptide derived soluble oligomers. *J Med Chem* **2004**, 47, 3329-33.
 18. Chang, L.; Bakhos, L.; Wang, Z.; Venton, D. L.; Klein, W. L. Femtomole immunodetection of synthetic and endogenous amyloid-beta oligomers and its application to Alzheimer's disease drug candidate screening. *J Mol Neurosci* **2003**, 20, 305-13.
 19. Park, H. S.; Lin, Q.; Hamilton, A. D. Modulation of protein-protein interactions by synthetic receptors: design of molecules that disrupt serine protease-proteinaceous inhibitor interaction. *Proc Natl Acad Sci U S A* **2002**, 99, 5105-9.
 20. Mourez, M.; Kane, R. S.; Mogridge, J.; Metallo, S.; Deschatelets, P.; Sellman, B. R.; Whitesides, G. M.; Collier, R. J. Designing a polyvalent inhibitor of anthrax toxin. *Nat Biotechnol* **2001**, 19, 958-61.

Quarterly Report 3: Project 2. Multiple target molecular counter-measures to biowarfare pathogens; blockade of infiltration and boosting of host defenses.

G. Thatcher

My labs in the College of Pharmacy, housing all analytical instrumentation, including HPLC, UV-Vis and fluorescence spectrometers, and mass spectrometers, are 20 yds from the center of the fire. Consequently, our operations have been severely affected from Jan 19th until the present. As of May 5th, one HPLC was restored to service from the total instrumentation affected. Aims 2 and 3 are instrument intensive and no meaningful progress has been possible. Our synthetic operations were partly restored in April, allowing some progress on Aim 1. The graduate student on this project has been writing her PhD thesis since January because of the obstacles to pursuing research.

The hypothesis of this research is that ACDs represent polyvalent ligands that can be synthesized to selectively inhibit the assembly of PA, blocking intracellular delivery of LF and EF; and furthermore, that ACDs can be used to deliver NO to macrophages to supplement pathogen destruction.

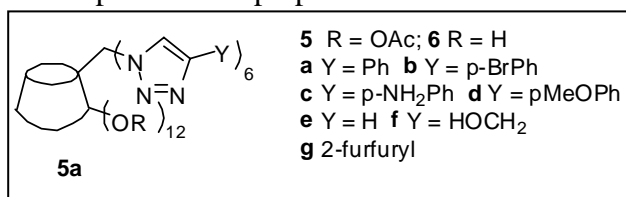
Specific Aims and Progress

Aim 1. Synthesis of a small library of 18 ACDs derived from α , β , and γ CD that contain pendant groups at the primary face to provide electrostatic or hydrophobic recognition or a combination of both. Synthesis of a second library of 6 ACDs to extrapolate or optimize interactions with PA and to amplify cytoprotection against LT. Synthesis of a combinatorial library of >2000 ACDs based upon either an α , β , or γ CD scaffold that utilizes different amine pendant groups in various combinations.

Progress. Three synthetic routes were studied for preparation of CD derivatives, including Cu-catalyzed coupling of azides to alkynes (coined “click chemistry”) whereby per-N₃-CD is reacted with the appropriate alkyne to yield a CD with a corona of amine pendant groups and an annulus of triazole groups (we term these qCD derivatives). Although the click chemistry proved more general than the first two synthetic methods attempted, drawbacks to this method were seen, in particular, long reaction times and very different rates of reaction with different alkynes. The importance of a quantitative synthetic methodology is that chromatography on derivatized CDs is complex and unsuitable for scale-up. The drawback with varied alkyne reactivity is the problem in preparing combinatorial libraries using different alkynes that react at very different rates.

Click chemistry was optimized for reliable library synthesis. The new method enjoys great advantage: (1) shortened reaction time (2 min in microwave oven versus 2 to 10 days previously); (2) the reaction can be easily monitored by TLC to ensure complete conversion; (3) removal of the new catalyst system CuI-P(OEt)₃ is more convenient than CuI alone, therefore improving the isolated yield.

A small qCD library of 14 compounds was prepared:



Progress has been made towards preparation of β qCD derivatives containing combinations of pendant groups, towards synthesis of a combinatorial library, using the new synthetic methodology in combination with alkyne synthons.

Synthesis of NO donor molecules has also been initiated in this funding period, using glucose and deoxyglucose derivatives in which the NO functionality is incorporated in a nitrosothiol group.

Aim 2. Assay of binding of ACDs to recombinant PA using pulsed ultrafiltration electrospray mass spectrometry (PUF-LC-MS) to indicate the most potent ACD capable of inhibition of PA self-assembly and to derive a structure-activity relationship for ACDs.

Progress. In our original proposal, recombinant PA was to be provided from Dr Andy Mesecar's lab, however, Dr Mesecar's lab has ceased to express and purify this protein. We have located BEResources as an alternative source of both Anthrax lethal factor components, PA and LT. The contract and MTA agreement has been completed by UIC and we hope to receive these peptides in the next funding period. We will extend to the Anthrax proteins the LC-MS methodology developed in the previous and current funding periods, which examined the inhibition of self-assembly of β -amyloid peptide ($A\beta_{1-42}$) by ACDs. Goals for next funding period: assay of combinatorial qCD libraries and homogeneous qCD and ACD derivatives.

No progress due to fire in COP and lack of instrumentation.

Aim 3. *Assay of ACD inhibition of LT-induced cytotoxicity in RAW cells. Study of NO donor influence on LT-induced cytotoxicity and any synergism with ACD inhibition.*

A major goal of the next funding period is to screen all qCD and ACD libraries for effects on RAW cell cultures. Cell viability and markers of inflammatory response (iNOS and PGs) will be measured. These experiments serve as essential controls for the future study of Anthrax proteins in the RAW macrophage like cell line. Compounds that inhibit the induction of inflammatory response by lipopolysaccharide (LPS) may be poorly selective for Anthrax toxins; compounds that are cytotoxic in the absence of LPS may be too broadly cytotoxic for use.

No progress due to fire in COP and lack of instrumentation.

Quarterly Report 4: Project 2. Multiple target molecular counter-measures to biowarfare pathogens; blockaed of infiltration and boosting of host defenses.

G. Thatcher

Because of the devastating fire in the College of Pharmacy on January 19, 2008, there is no progress to be reported for this project since the last quarterly update. This project is dependent upon mass spectroscopy, specifically the Agilent ion-trap. This instrument remains in pieces in the College having been disassembled and cleaned post-fire. Last week, the insurance company finally approved replacement of this instrument, so we should be able to report progress in the next quarter.

The synthetic component of the project is complete, therefore, there is little research progress that can be made until the new mass spec is in place and operational.

Quarterly Report 5: Project 2. Multiple target molecular counter-measures to biowarfare pathogens; blockade of infiltration and boosting of host defenses.

G. Thatcher

Lab status after Jan 2008 fire in College of Pharmacy: ion trap mass spec was replaced and installed to working condition in Sept '08; the mass spec was the key instrument for proposed analytical work on this project.

The hypothesis of this research is that ACDs represent polyvalent ligands that can be synthesized to selectively inhibit the assembly of PA, blocking intracellular delivery of LF and EF; and furthermore, that ACDs can be used to deliver NO to macrophages to supplement pathogen destruction.

Specific Aims and Progress

Aim 1. Synthesis The first objective was to study the membrane permeability of CD derivatives because all approaches are intrinsically linked to the ability of these derivatives to incorporate in cell membrane, cytoplasm, or cell nucleus. Ethynyl estradiol was chosen to be conjugated with CD derivatives to provide a highly sensitive reporter of nuclear receptor activity. The following derivatives were synthesized (Tables 1-3):

Table I. Per-6-amino- β -CD derivatives and aldehydes condensation reactions.

| entry | CD | ligand | reaction condition | product |
|----------------|----|-----------|--------------------|------------------|
| 1 ^a | | 8 eq. | r.t, 5 h | |
| 2 ^b | | 8 eq. | r.t, 7 d | |
| 3 ^c | | 8 eq. | 60-70 °C, 18 h | + Other mixtures |
| 4 ^c | | 8 eq. | 60-70 °C, 18 h | S.M recovered |
| 5 ^d | | 10-70 eq. | 60-70 °C, 10 d. | |
| 6 ^d | | 10 eq. | 60-70 °C, 10 d. | S.M recovered |
| 7 ^d | | 21 eq. | 60-70 °C, 10 d. | + Other mixtures |

a. 1. r.t, 5 h, 2.

NaBH₄, MeOH, 2 h; **b.** 1. DMF, r.t, 7 d, 2. NaBH₄, MeOH, 2 h; **c.** 1. DMF, 60-70 °C, 18 h, 2. NaBH₄, MeOH, 2 h; **d.** 1. DMF, 60-70 °C, 10 d, 2. NaBH₄, MeOH, 2 h.

Synthesis of triazole-modified control compound, qE₂ **25**.

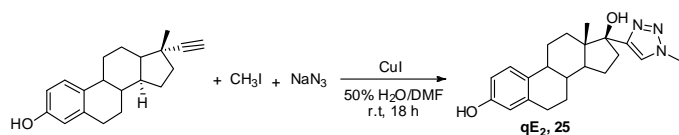


Table II. 'Click chemistry' with hepta- and mono-azido- β -CD **2** and **18** with EE₂.

| entry | CD | ligand | reaction condition | product |
|-----------------|-----------|--------|--------------------|------------------|
| 14 ⁱ | 2 | 7 eq. | r.t, 1 d | 7EqCD, 23 |
| 15 ⁱ | 18 | 1 eq. | r.t, 1 d | 1EqCD, 24 |

i. CuI, DIEA, DMF/MeOH, r.t, 1 d.

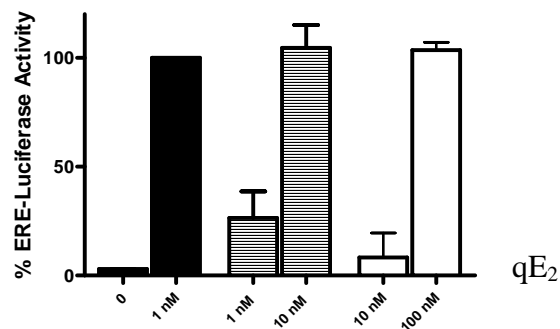
Table III. Substitution reactions and mono-modifications.

| entry | CD | ligand | reaction condition | product |
|-----------------|-----------|-----------|--------------------|------------------|
| 8 ^e | 1 | 15 eq. | r.t, 2 d | 14 |
| 9 ^f | | 10-70 eq. | 60-70 °C, 10 d | S.M recovered |
| 10 ^f | 17 | 21 eq. | 60-70 °C, 7 d | 21 |
| 11 ^g | 19 | 1-3 eq. | 60-70 °C, 3 d. | 1EqCD, 20 |

e. DMF, Cs₂CO₃, r. t, 2 d; f. DMF, 60-70 °C, 10 d.; g. 1. DMF, 60-70 °C, 3 d, 2. NaBH₄, MeOH, 2 h.

Aim 2. Assay of ACD and qCD derivatives used MCF-7 human breast cancer cells grown in estrogen-stripped serum and transiently transfected with a luciferase reporter for activation of the nuclear estrogen receptor element (ERE-luciferase). Induction of luciferase in this assay requires liganded ER binding to the ERE of DNA in the cell nucleus. The CD derivative appears capable of accessing the cell nucleus based upon the submicromolar potency for ERE activation (Fig. 1).

Figure 1. Activation of ERE and induction of luciferase activity in ER(+) MCF-7 cells relative to estradiol. Cells were treated with E₂ (solid bars), or 7EqCD (open bars), or (crossed bars) for 24h.

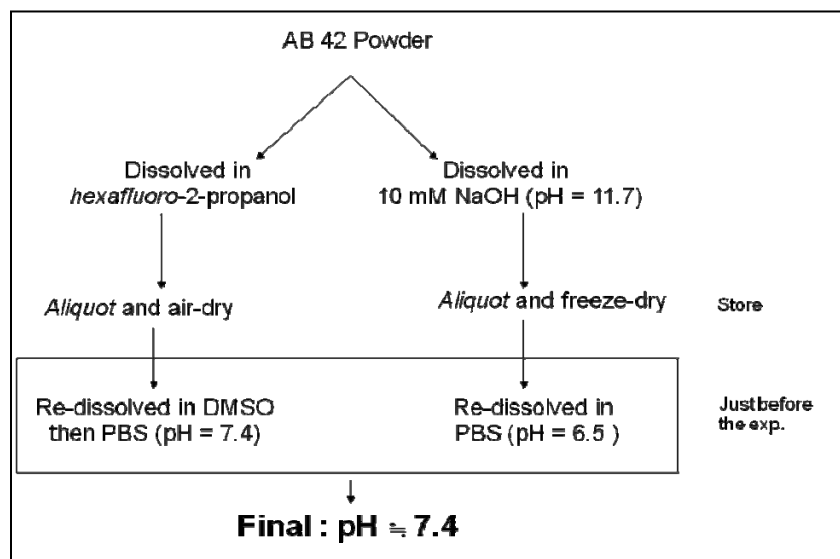


Quarterly Report 6: Project 2. Multiple target molecular counter-measures to biowarfare pathogens; blockade of infiltration and boosting of host defenses.
G. Thatcher

The hypothesis of this research is that aminocyclodextrins (ACDs) represent polyvalent ligands that can be synthesized to selectively inhibit the assembly of polypeptides that are cytotoxic and cause death to humans. The anthrax associated polypeptide protective antigen (PA) forms an organized aggregate that permits access of lethal factor (LF) and edema factor (EF) into the host human cell leading to cell death. It is argued that assembly of multiple PA polypeptides and insertion into the cell membrane results in formation of an ion channel. We have previously demonstrated that ACDs are able to inhibit assembly of β -amyloid peptide into aggregates. These aggregates are soluble oligomers, sometimes coined amyloid derived diffusible ligands (ADDLs). It is currently agreed that these soluble oligomers are the neurotoxic form of amyloid that is causal in Alzheimer's disease, which is a human disease of the brain leading to death. The detailed mechanism of neurotoxicity of these oligomers is not fully elucidated, several proposals involve interaction with a membrane receptor, and one posits formation of an ion channel in the neuronal cell membrane leading to influx of calcium and cell death. Regardless, it has been clearly demonstrated that $A\beta_{1-42}$ forms cyclic oligomers. It should be noted that many researchers study β -amyloid peptides that have little relevance to human disease such as $A\beta_{1-40}$ and $A\beta_{25-35}$, because these peptides do not aggregate and are thus much easier to handle – they are consequently of very little relevance. Therefore, we use only $A\beta_{1-42}$, which requires substantial effort in new method development.

Progress

1. Preparation of $A\beta$ oligomers



2. Trapping of $A\beta$ oligomers by rapid photo-cross-linking using a ruthenium photocatalyst.

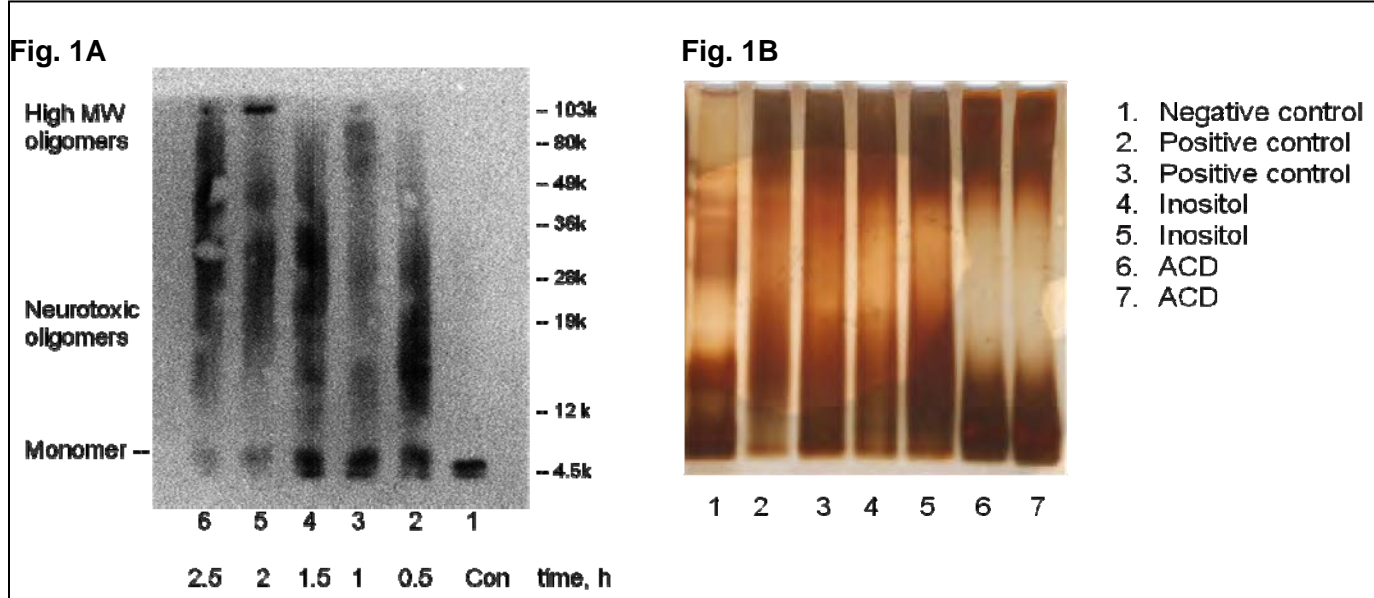
Free radical peptide cross-linking was achieved by photoactivation of ammonium persulfate (10 mM) in the presence of a Ru(II) salt (1 mM) generating oxygen radicals. An apparatus was constructed to focus the light source on the $A\beta$ sample, optimizing: focal length; exposure time (10 s); and sample path length. Sample preparation following cross-linking required considerable optimization to remove ruthenium from the peptide sample.

3. Analysis of cross-linked $A\beta$ oligomers using 1D electrophoresis.

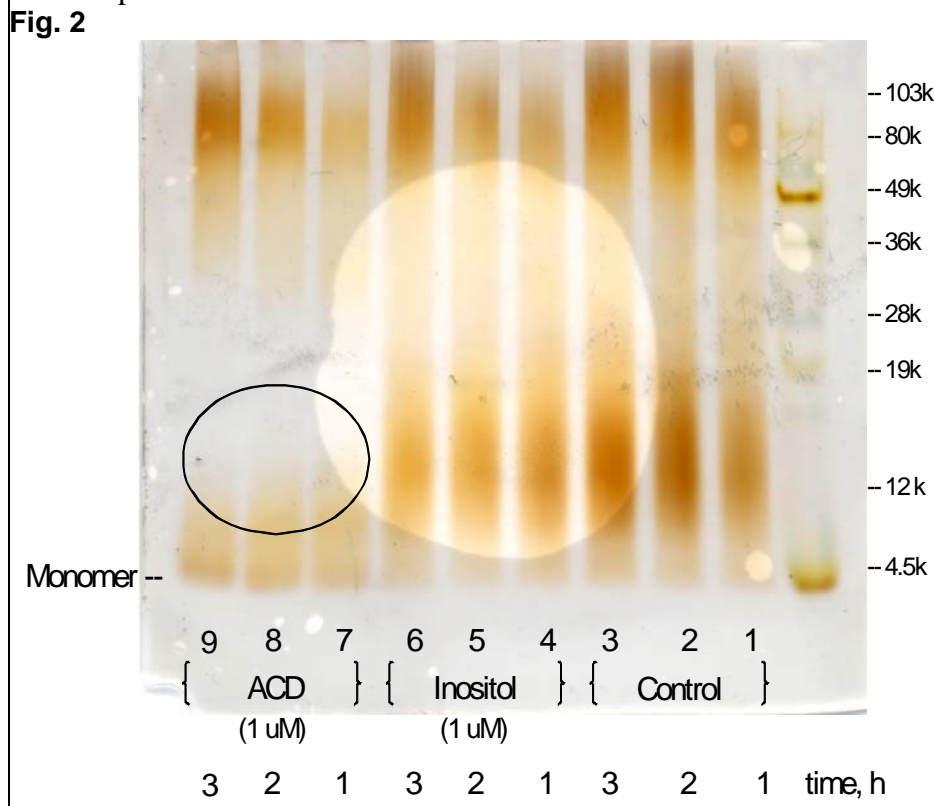
The photo-cross-linked peptide mixtures were run on a 10% NuPAGE gel with MES as the running buffer. The gel was visualized by silver staining. Control experiments were run as a function of $A\beta$ incubation time, showing a time-dependent loss of monomer and formation of oligomers. Notable was the very rapid formation of oligomers with $9,000 < MW < 30,000$, followed by formation of higher molecular weight oligomers at later time points (Fig. 1A).

4. Assay of inhibition of $A\beta$ oligomerization by ACD using gel electrophoresis.

A simple ACD, modified with aminomethylfuran, previously demonstrated to inhibit ADDL formation was tested by co-incubating with A β for 48 h. A second agent was tested in parallel, *scyllo*-inositol, a natural product in Phase 2 clinical trials for Alzheimer's that reportedly inhibits A β aggregation and inhibits formation of A β fibrils and plaques in amyloid transgenic mice. The results were remarkable, in that ACD treatment inhibited formation of the smaller soluble oligomers that are thought to be the amyloid neurotoxic agents in humans (Fig. 1B).



Further examination of the time course of oligomerization confirmed the results observed with ACD (Fig. 2). The sample treated ACD was observed to remain in the monomeric form even after 3 hours of incubation.

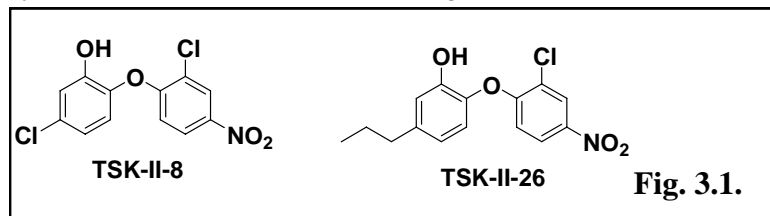


5. Analysis of A β soluble oligomers by MALDI-TOF mass spectroscopy
 Data will be presented in the final report.

Quarterly Report 1: Project 3. Rational Discovery of new FabI inhibitors as biodefense antibacterial therapeutics.

A. Activity analysis of Biphenyl Triclosan Analogs

As planned in the original proposal, we have developed an extended analysis of our two most active analogs synthesized to date, shown below (Fig. 3.1)



To evaluate their spectrum of activity within readily accessible pathogens, we have tested them against a number of clinical isolates. The results are shown in Table 1.

Table 1. MICs and MBCs of FabI inhibitors against *B. anthracis* and other bacterial pathogens.

| Bacteria | Ciprofloxacin ¹ | TSK-II-8 | | | TSK-II-26 | | |
|-------------------------------------|----------------------------|-------------|---------------|---------|-------------|--------------|---------|
| | MIC ² | MIC | MBC | MBC/MIC | MIC | MBC | MBC/MIC |
| ΔΔANR ³ | 0.098 ± 0.01 | 2.19 ± 0.38 | 3.12 ± 1.11 | 1.4 | 2.19 ± 0.01 | 3.91 ± 0.78 | 1.8 |
| Sterne ⁴ | 0.082 ± 0.02 | 1.87 ± 0.31 | 3.91 ± 0.78 | 2.1 | 1.87 ± 0.01 | 3.91 ± 0.78 | 2.1 |
| Staph. aureus | 0.39 ± 0.01 | 0.14 ± 0.06 | 2.93 ± 1.21 | 20.9 | 0.14 ± 0.06 | 2.93 ± 1.21 | 20.9 |
| Methacillin-resistant Staph. Aureus | 0.47 ± 0.17 | 0.28 ± 0.25 | 0.44 ± 0.12 | 1.6 | 0.28 ± 0.25 | 0.54 ± 0.15 | 1.9 |
| E. fecalis | 0.68 ± 0.11 | 4.38 ± 0.77 | 31.25 ± 6.25 | 7.1 | 4.38 ± 0.47 | 12.5 ± 0.01 | 2.9 |
| Vancomycin Resistant E. fecalis | 0.55 ± 0.15 | 5.73 ± 0.57 | 37.50 ± 12.50 | 6.6 | 5.73 ± 0.29 | 15.63 ± 3.13 | 2.7 |
| Listeria mono. | 0.94 ± 0.34 | 2.81 ± 0.31 | 14.06 ± 3.93 | 5.0 | 2.8 ± 0.86 | 14.06 ± 3.93 | 5.0 |
| Pseud. aerug. | 0.26 ± 0.07 | >25 | NT | | >25 | NT | |
| Klebs. pneum. | 0.51 ± 0.11 | 1.76 ± 0.44 | 12.50 | 7.1 | 1.76 ± 0.88 | 8.33 ± 2.08 | 4.7 |
| E. coli | 0.057 ± 0.02 | 0.26 ± 0.07 | 12.50 | 48.0 | 0.26 ± 0.17 | 1.17 ± 0.39 | 4.5 |

¹Drug concentrations = g/ml. Results = mean ± SEM, n = 3.

²MIC = minimum inhibitory concentration; MBC = minimum bactericidal concentration; MBC/MIC: bactericidal drug ≤ 4

³Plasmid-negative strain of anthrax, lacking both pXO1 and pXO2 plasmids

⁴Sterne strain of anthrax that contains pXO1 (toxin production) but lacks pXO2 (capsule)

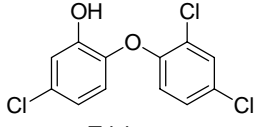
From the data in this table, it is clear that these two analogs exhibit very good activity against a wide spectrum of organisms. We have also tested in the presence of serum, and find that 96-99% of the compounds are bound to protein, requiring higher concentrations in the presence of serum. This high serum binding may be a problem should we test these agents in vivo.

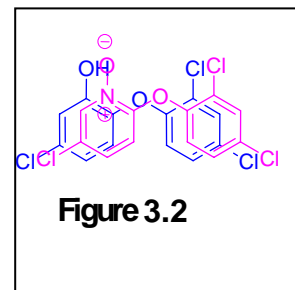
We have also completed formal contractual arrangements with the NIH to permit testing of compounds against fully virulent strains, but have not yet had any of the compounds accepted for testing, which we obviously cannot control.

B. Synthesis of Alternate Scaffold Triclosan Analogues

Triclosan is a well known broad spectrum antibacterial used in a number of consumer products. It has been shown to inhibit the enzyme in a number of microorganisms like *Escherichia coli*, *Pseudomonas aeruginosa* and *Staphylococcus aureus*. Originally, it was believed that triclosan was a nonspecific antibacterial that attacks bacterial cell membranes. Later it was shown to have a specific mode of action and inhibits bacterial fatty acid synthesis at the enoyl-acyl carrier protein reductase (ENR or FabI) step. Triclosan has since been shown to inhibit ENR in a number of microorganisms,

which has led to intense activity in search of new triclosan derived antibacterials. Improvements in the broad spectrum activity of triclosan-like compounds have been deterred by the variability in the effectiveness of triclosan against different species. Table 2 shows the antibacterial activity and FabI inhibition of triclosan in different species. The IC₅₀ values range from 73 nM in malaria to 7.25 μ M for *E. coli*. Due to this large range in activity, it is important that we examine the inhibitory action of more triclosan-type compounds for individual organisms, so as to maximize the specificity.

|  Triclosan | Table 2. FabI Inhibition of triclosan and antibacterial activity. | |
|--|---|--|
| | Species | IC ₅₀ (μ M) MIC (μ g/mL) |
| | <i>E. coli</i> ^{a,g} | 2.07-7.25 0.3-0.5 |
| | <i>S. pneum.</i> ^g | >30 (FabK) 16 |
| | <i>S. aureus</i> ^{c,g} | 0.54 0.03 |
| | <i>H. influenzae</i> ^{d,g} | 0.1- 2.4 0.5 |
| | <i>P.f. ENR</i> ^b | 0.073 |
| | <i>M. tuberculosis</i> ^e | 345.4 |
| | <i>B. anthracis</i> ^f | 0.5 3.12 |



^a Biol. Chem. 1998, 273, 30316 and J. Med. Chem. 2004, 47, 509. ^b Bioorg. Med. Chem. Lett. 2006, 16, 2163. ^{c-e} BRENDA ^f Our assay testing. ^g J. Med. Chem. 2003, 46(9), 1627-1635. ^h Heath, R.J.; Li, J.; Roland, G.E.; Rock, C.O.; J. Biol. Chem. 2000, 275(7) 4654-4659. ⁱ Bhargava, H.N. Leonard, P.A. Am. J. Infect. Control 1996, 24,209-218.

We have examined the activity of pyridone-based analogs, which can mimic triclosan (Figure 3.2.). We had synthesized a series of 2-pyridone-based inhibitors by following the strategy as shown in Scheme 2. Some of our best compounds are shown in the following table (Table 3):

Scheme 2

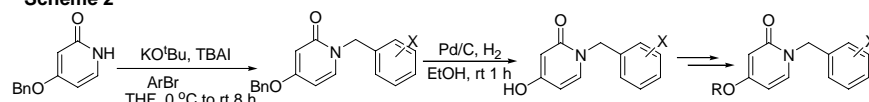
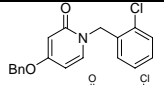
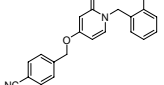
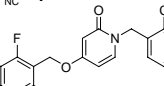
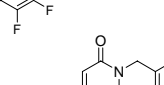
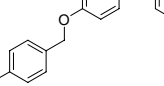
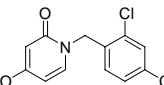
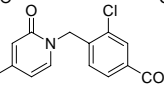
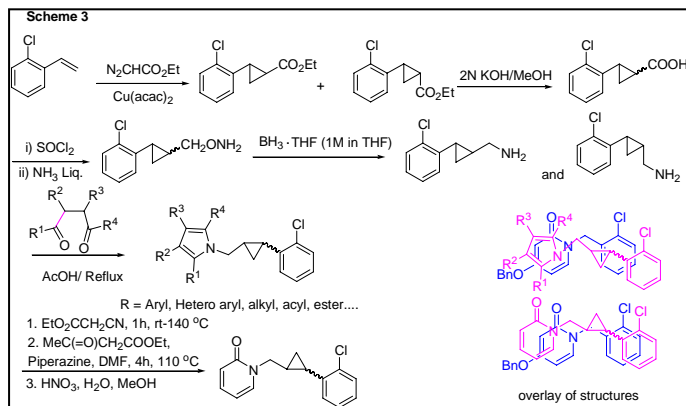


Table 3

| ID# | Structure | MW | % Inhibition | FabI IC50 (μ M) | MIC (μ g/mL)) | MIC(μ M) |
|-------------|---|--------|-----------------------|----------------------|--------------------|---------------|
| TSK-III-34 |  | 325.39 | 83.1(@ 12.5 μ M) | 1.43 \pm 0.08 | 16.3 | 50 |
| SIP-1-42 |  | 350.80 | 61.5 (@ 12.5 μ M) | 2.69 \pm 0.42 | 140.3 | >400 |
| TSK-III-67A |  | 415.74 | 12 | 0.12 \pm 0.08 | | >400 |
| TSK-III-37A |  | 370.79 | 24.2(@ 6.25 μ M) | 0.69 \pm 0.18 | >148.3 | >400 |
| TSK-III-43 |  | 350.80 | 55.6 (@ 12.5 μ M) | 7.02 \pm 1.09 | >140.3 | >400 |
| TSK-III-45 |  | 368.81 | 79.7(@ 25 μ M) | 3.61 \pm 0.29 | >147.5 | >400 |
| TSK-III-46 |  | 369.80 | 75.5(@ 50 μ M) | 23.76 \pm 2.54 | 74 | 200 |



Recently, Professor Kozikowski's group has synthesized a library of 2-aryl-1-aminomethylcyclopropane derivatives. It will be of interest, for example to use the same strategy in preparing cyclopropane derivatives bearing a pyrrole ring (4) or pyridone ring (5). As is apparent from the accompanying overlay, these compounds are related structures and it is worth checking the antibiotic ability of this type of new compounds.

Summary

During this quarter, we have made significant progress in evaluating current compounds, and in preparing for further testing. Our *in vitro* activities are excellent, and demonstrate that the basic approach of FabI inhibition should yield potent antimicrobials that can exhibit wide spectrum activity. We are now preparing to explore alternate scaffolds that should maintain FabI inhibitory activity, while focusing on achieving good bacterial penetration and improved serum characteristics.

Reference:

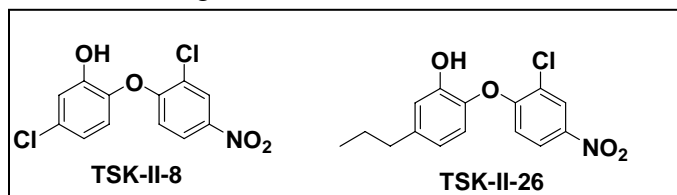
- (1) Huang, S. T., Hsei, I. J., Chen, C. Synthesis and anticancer evaluation of bis(benzimidazoles), bis(benzoxazoles), and benzothiazoles. *Bioorg. Med. Chem.*, **14**, 6106-6119, (2006).
- (2) Chang, J., Zhao, K., Pan, S. Synthesis of 2-arylbenzoxazoles via DDQ promoted oxidative cyclization of phenolic Schiff bases-a solution-phase strategy for library synthesis. *Tetrahedron Lett.* , **43**, 951-954, (2002).
- (3) Adediran, S. A., Cabaret, D., Drouillat, B., Pratt, R. F., Wakselman, M. The synthesis and evaluation of benzofuranones and β -lactamase substrates. *Bioorg. Med. Chem.* , 1175-1183, (2001).
- (4) Paal, C. A density functional theory study of the mechanism of the Paal–Knorr pyrrole synthesis. *Chem. Ber.*, **17**, 2756, (1884).
- (5) U.S. Pat. Appl. Publ. 2004006234.

Report 2: Project 3. Rational discovery of new FabI inhibitors as biodefense antibacterial therapeutics

M. Johnson, A. Kozikowski, A. Mesecar

A. Serum MIC testing of Biphenyl Triclosan Analogs

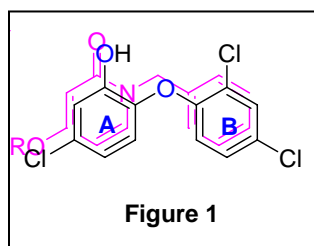
As discussed in the last report's plans for this quarter, we have measured serum MIC values for the two best triclosan analog leads, shown below.



Although both compounds show excellent antibiotic activity against a variety of pathogens in laboratory media, as noted in the last report, serum reduces activity by about two orders of magnitude, limiting their potential application. Consequently, we have developed an alternative pyridone scaffold, described below.

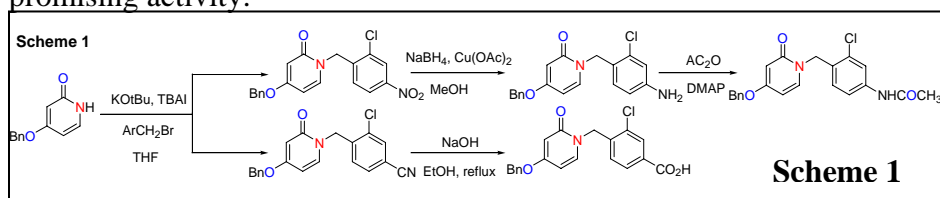
B. Synthesis of 2-pyridones as a novel class of antibacterials:

We have recently reported a number of triclosan-based inhibitors of FabI, the enoyl-ACP reductase from *Bacillus anthracis*.¹ Although very potent inhibitory activity was observed, the metabolic liability of the



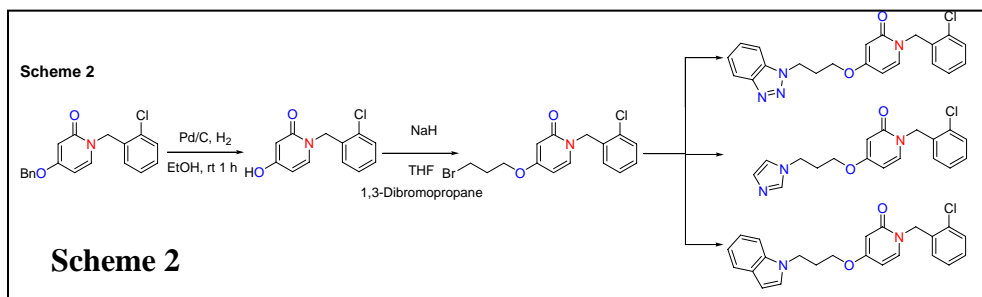
phenolic hydroxyl group would be a major caveat in developing triclosan and its derivatives as drugs.² This bottleneck has prompted us to develop novel scaffolds that replace the phenolic ring of triclosan with other heterocyclic rings that retain the essential binding interactions of triclosan.

The essential interactions of triclosan with the FabI active site include the phenolic 'ring A' binding face-to-face with the nicotinamide ring of NAD⁺ involving a π - π stacking interaction. The hydroxyl group on ring A makes two hydrogen bond contacts, one with Tyr 157 (OH) and the other with the 2'-hydroxyl group of nicotinamide ribose. Based on these findings, we speculated that 2-pyridones would be ideal candidates to mimic all the essential binding features of triclosan, while perhaps minimizing some of the metabolism and solubility problems. Figure 1 illustrates the structural similarity of the triclosan and 2-pyridone scaffolds using a ChemDraw overlay of structures. To this end, we have synthesized a number of 2-pyridone based inhibitors and tested them for their activity against *B. anthracis* (Table). Of these, **TSK-III-56B** and **TSK-III-64** and **TSK-III-92** showed promising activity.



Scheme 1 shows the synthesis of inhibitors **TSK-III-46**, **56R**, **56B** and **64** starting from commercially available 4-benzyloxy-pyridone.

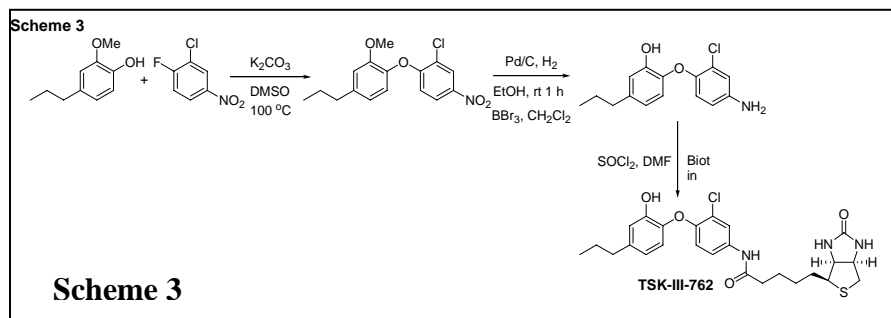
Selective *N*-alkylation of 4-benzyloxy-pyridone using KOtBu in the presence of catalytic tetrabutylammonium bromide resulted in the nitro and cyano substituted pyridone inhibitors. Selective reduction of the nitro-pyridone gave the amine inhibitor **TSK-III-56B**, which was subsequently acetylated using acetic anhydride to obtain **TSK-III-64**. Scheme 2 displays the synthesis of the heteroaromatic tethered pyridone inhibitors. 4-hydroxy-pyridone was prepared by the catalytic hydrogenation of the benzyloxy-pyridone which was



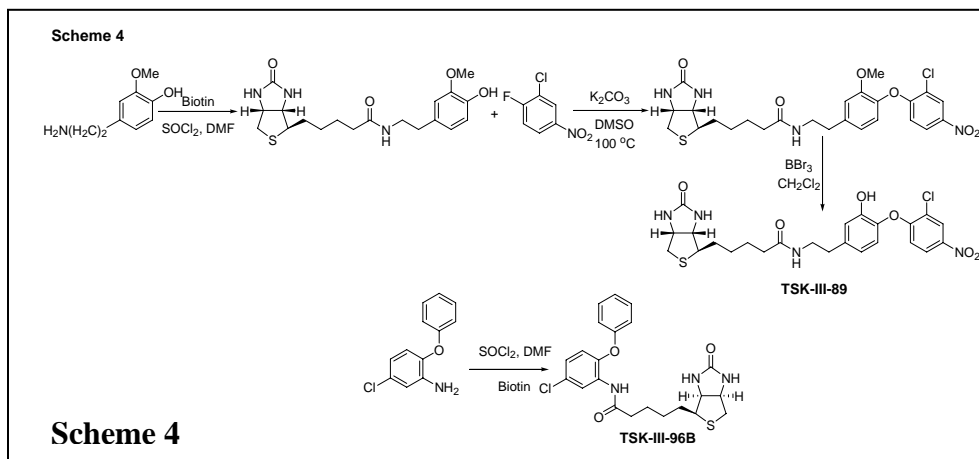
prepared by the procedure shown in Scheme 1. The hydroxy pyridine was alkylated using 1,3-dibromopropane resulting in the bromopropane tethered, common synthetic intermediate. Compounds **TSK-III-92**, **93** and **98B** were prepared from this common intermediate *via* simple alkylation reactions.

C. Synthesis of Triclosan-Based Biotinylated Analogs

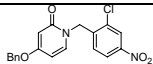
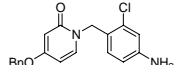
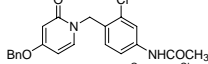
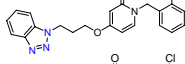
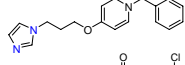
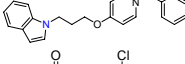
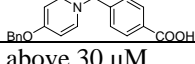
Triclosan is a well known broad spectrum antibacterial used in a number of consumer products. It has been shown to inhibit the enzyme in a number of microorganisms like *Escherichia coli*, *Pseudomonas aeruginosa*, *Staphylococcus aureus*. Originally, it was believed that triclosan was a nonspecific antibacterial that attacks bacterial cell membranes. Later it was shown to have a specific mode of action and to inhibit bacterial fatty acid synthesis at the enoyl-acyl carrier protein reductase (FabI) step. Triclosan has since been shown to inhibit



endogenous nitrate respiration (ENR) in a number of microorganisms, which has lead to intense activity in search of new triclosan derived antibacterials. We have recently reported the design, synthesis and activity of a number of triclosan-based inhibitors.¹ We have now synthesized a number of biotinylated triclosan analogs to study their inhibitory activities against FabI from *Bacillus anthracis* and to investigate the possibility to use such analogs in the design of an improved bioassay to determine inhibitory activity. *Scheme 3* shows the synthesis of the diphenyl ether *via* coupling of the corresponding phenol with the requisite fluoroaromatic compound. Catalytic hydrogenation followed by demethylation using boron tribromide afforded the amino diphenylether which was biotinylated using SOCl₂ and biotin.



Scheme 4 shows synthesis of two additional triclosan-based biotinylated analogs. **TSK-III-89** was prepared from commercially available amino-phenol. Biotinylation of the amino-phenol followed by nucleophilic aromatic substitution with the requisite fluoroaromatic resulted in the diaryl ether which was subsequently demethylated using excess boron tribromide. **TSK-III-96B** was prepared by direct biotinylation of the commercially available amino diphenyl ether. This compound shows an IC₅₀ of 9.6 μM against FabI. The inhibitory activities of some of our best 2-pyridone compounds are shown in the following Table.

| ID# | Structure | MW | FabI IC ₅₀ (μM) | MIC(μM) |
|-------------|---|--------|-------------------------------|---------|
| TSK-III-56R |  | 370.79 | 3.73 ± 1.08 | 50 |
| TSK-III-56B |  | 340.80 | 0.785 ± 0.081 | >400 |
| TSK-III-64 |  | 382.8 | 1.78 ± 0.54 | >400 |
| TSK-III-92 |  | 394.9 | 1.60 ± 0.18 | >200 |
| TSK-III-93 |  | 343.8 | 28.00 ± 1.09 | >200 |
| TSK-III-98B |  | 392.9 | 0.75 ± 0.29* | >200 |
| TSK-III-46 |  | 369.80 | 23.76 ± 2.54 | 200 |

*Precipitation Observed above 30 μM

This design has shown significant success in obtaining enzymatic inhibitory activity against FabI, as shown in the table above, with TSK-III-56B and TSK-III-98B both exhibiting slightly submicromolar activities, and with TSK-III-56R, -64, and -92 also exhibiting low micromolar FabI inhibitory activities. However, only TSK-III-56R exhibits measurable MIC activity, indicating that further chemical modification will be required to obtain good MIC activity. We plan to pursue approaches to improve biological activity during the coming quarter.

Summary

During this quarter, we have made significant progress in the biological evaluation of our current compounds, and have substantially extended the development of a new scaffold that should have better *in vivo* biological properties than the triclosan-based scaffold. During the coming quarter, we will focus on increasing bacterial penetration as a strategy for improving biological activity. More extensive testing of current compounds is also planned.

Literature cited

1. Tipparaju, S. K. M.; Debbie C.; Klien, Gary M.; Chen, Y.; Tapadar, S.; Bishop, Molly H.; Yang, S.; Chen, J.; Ghassemi, M.; Santarsiero, Bernard D.; Cook, James L.; Johlfs, Mary.; Mesecar, Andrew D.; Johnson, Michael E.; Kozikowski, Alan P., Design and synthesis of novel triclosan based inhibitors of the Bacillus anthracis Enoyl-ACP Reductase. *J. Med. Chem.* Submitted-December, 2007.
2. Wang, L. Q.; Falany, C. N.; James, M. O., Triclosan as a substrate and inhibitor of 3'-phosphoadenosine 5'-phosphosulfate-sulfotransferase and UDP-glucuronosyl transferase in human liver fractions. *Drug Metab.Dispos.* **2004**, 32, 1162-9.

Report 3: Project 3. Rational discovery of new FabI inhibitors as biodefense antibacterial therapeutics

M. Johnson, A. Kozikowski, A. Mesecar

A. Work activities during this reporting period.

As detailed in Dr. Beck's summary report, two events on January 19 severely restricted work during this quarter. The fire in the College of Pharmacy building effectively stopped all synthetic work through March 31. The frozen heating coils in the Molecular Biology Building and resulting water damage also stopped most experimental testing and computational design work for a period of approximately one month.

Accordingly, after remediation of water damage in MBRB, we have concentrated on (1) further testing and design analysis of compounds based on the pyridone scaffold that was introduced in the last report; and (2) preparation of manuscripts describing our work to date on both the biphenyl ether and pyridone scaffolds. Two manuscripts have now been accepted for publication, pending minor revision, and are listed at the end of this report.

B. Preparation and testing of 2-pyridone based inhibitors.

As noted in the last report, we have initiated development of inhibitors based on a substitution of 2-pyridone for the phenolic "ring A" that exhibits metabolic lability in triclosan analogs. Our structure optimization studies were based on predicted binding interactions of 2-pyridones with the enzyme active site. Triclosan and synthesized pyridones were docked into the *Ba*ENR (*Ba*FabI) crystal structure using the GOLD docking program. We observed that the 2-pyridones dock to *Ba*ENR in the same binding pocket as that of triclosan, and maintain similar H-bonding interactions with the residues in the active site. Figure 1 shows the similarities in the binding geometry of triclosan and a representative 2-pyridone, **2**.

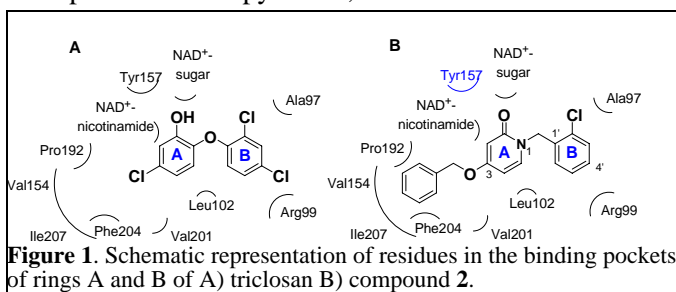


Figure 1. Schematic representation of residues in the binding pockets of rings A and B of A) triclosan B) compound **2**.

In Q2, we reported results for seven initial pyridone structures. We now report more extensive results in Table 1, with results for compounds **3**, **4**, **6**, **8**, **21**, **22** and **23**, reported last time, included for completeness. We explored the SAR by functionalizing ring B. From the docking conformations of the lead compound into the *Ba*ENR X-ray crystal structure, we anticipated that hydrogen bond donors/acceptors at the 4'-position would be positioned to interact with either Ala 97 or Arg 99. We thus synthesized compounds **3–8** with various functional groups at the 4'-position of the ring B. **4**, bearing an amino group at the 4'-position is the best compound with an IC_{50} of 0.8 μ M. Conversion of the amino functionality into an acetamide (**8**) reduced the *Ba*ENR inhibitory activity by half. Thus, it appears that the presence of an electron-donating group at the 4'-position enhances the interaction of the ligand with the enzyme active site. Replacing ring B with an acetylene (**9**) or an isoxazole (**10**) were not successful in improving the activity (Table 2).

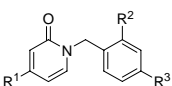
|  | | | | |
|---|--------------------------|----------------|-------------------|-----------------------|
| Compd. | R ¹ | R ² | R ³ | IC ₅₀ (μM) |
| 1 | OH | H | H | > 100 ^a |
| 12 | OH | H | OMe | > 100 ^a |
| 13 | OH | H | OH | > 100 ^a |
| 1 | BnO | H | H | 6.8 ± 0.8 |
| 2^b | BnO | Cl | H | 1.5 ± 0.1 |
| 14 | 4-CN-PhCH ₂ O | Cl | H | 2.7 ± 0.4 |
| 15 | | Cl | H | 1.5 ± 0.8 |
| 16 | | Cl | H | 1.1 ± 0.1 |
| 18 | | Cl | H | > 6 ^c |
| 19 | | H | OMe | > 3 ^d |
| 20 | | H | H | > 100 ^a |
| 21 | | Cl | H | 0.8 ± 0.2 |
| 22 | | Cl | H | 1.6 ± 0.3 |
| 23 | | Cl | H | 28.0 ± 6.2 |
| 5 | BnO | Cl | CN | 7.0 ± 1.1 |
| 7 | BnO | Cl | CONH ₂ | 3.6 ± 0.3 |
| 6^b | BnO | Cl | COOH | 23.8 ± 2.5 |
| 3 | BnO | Cl | NO ₂ | 3.7 ± 1.1 |
| 4 | BnO | Cl | NH ₂ | 0.8 ± 0.1 |
| 8 | BnO | Cl | NHAc | 1.8 ± 0.5 |

Table 1. *Ba*ENR inhibitory activities of compounds

^a *Ba*ENR inhibition was less than 30% at 100 μM.

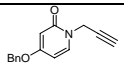
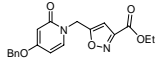
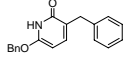
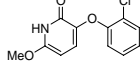
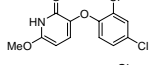
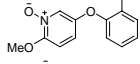
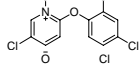
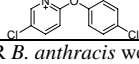
^b MIC values against ΔANR *B. anthracis*¹⁴ for compound **2**: 16 μg/mL, for compound **6**: 74 μg/mL. MICs for all other compounds in the table are > 80 μg/mL.

^c The inhibitor precipitated at concentrations > 6 μM.

^d The inhibitor precipitated at concentrations > 3 μM.

We briefly explored the activities of *C*-substituted 2-pyridones that are structurally similar to the *N*-substituted 2-pyridones discussed above (compounds **33–35**). These *C*-substituted pyridones are capable of existing in their enol form as hydroxypyridines, and thus closely mimic triclosan in structure. The activities of these compounds are shown in Table 2. It is gratifying to note that the novel *C*-substituted 2-pyridone, **35** showed a 10-fold improvement in ENR inhibitory activity over its *N*-substituted analog **1**. The GOLD docking conformation of **35** in Figure 2C suggests a nearly identical orientation of the *C*-substituted 2-pyridones compared to the *N*-substituted pyridones. Although the origin of improved activity of compound **35** is not completely clear at this stage, the pyridone NH and the nicotinamide ring are about 3.6 Å apart and thus ligand binding stabilization from an N–H... π interaction cannot be ruled out.¹⁶ Moderate ENR inhibition was observed by the 3-phenoxy-2-pyridones **33** and **34**. Among the pyridine *N*-oxides, compound **37** exhibited modest ENR inhibition, while compound **30** was inactive.

Table 2. *Ba*ENR inhibitory activities of compounds.

| Compd. ^a | Structure | IC ₅₀ (μM) |
|---------------------|---|-----------------------|
| 9 |  | > 100 ^b |
| 10 |  | > 100 ^b |
| 35 |  | 0.7 ± 0.4 |
| 33 |  | 18.8 ± 4.2 |
| 34 |  | 23.7 ± 11.7 |
| 30 |  | > 100 ^b |
| 37 |  | 21.4 ± 7.7 |
| 37 |  | 21.4 ± 7.7 |

^a MIC values against ANR *B. anthracis* were >100 μg/mL.

^b *Ba*ENR inhibition was less than 30% at 100 μM.

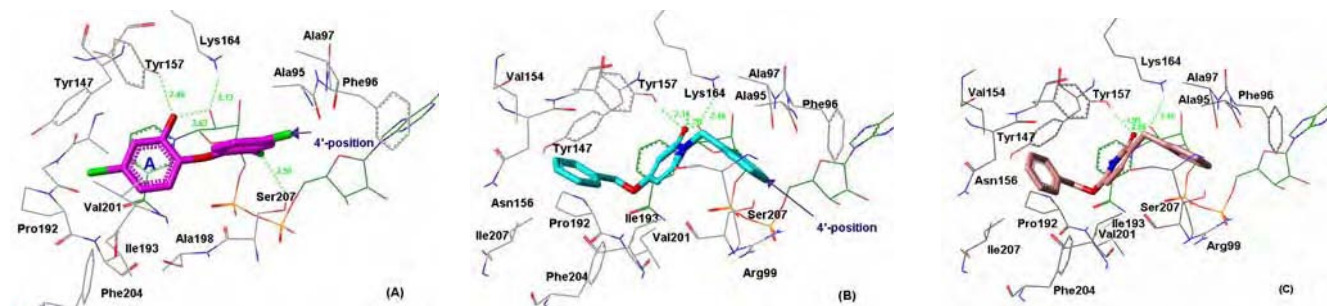


Figure 2. (A) Crystal structure of triclosan bound to *Ba*ENR. ENR atoms are colored by atom type, NAD⁺ is green, and triclosan is pink. (B) GOLD docking conformation of **2** against the crystal structure of *Ba*ENR. ENR atoms are colored by atom type, NAD⁺ is green, and **2** is cyan. Distances between atoms that are close enough to be within hydrogen bonding range are shown in green. (C) GOLD docking conformation of **35** against the crystal structure of *Ba*ENR. ENR atoms are colored by atom type, NAD⁺ is green, and **35** is light pink.

C. Summary

Despite the extensive setbacks to our work due to the two building failures on January 19, we have been able to extensively explore and evaluate the use of the 2-pyridone replacement of the phenolic group of triclosan as an alternate scaffold for ENR inhibition, and have found that this scaffold exhibits good ENR inhibition. MIC values against *B. anthracis*, however, are marginal, even for **2**, the most active compound. We speculate that this is most probably due to limited bacterial membrane permeability. Thus, future work will focus on structural alterations to improve permeability and exploration of alternate scaffolds that may exhibit higher permeability.

D. Publications

- S.K. Tipparaju, D.C. Mulhearn, G.M. Klein, Y. Chen, S. Tapadar, M.H. Bishop, S. Yang, J. Chen, M. Ghassemi, B.D. Santarsiero, J.L. Cook, M. Johlfs, A.D. Mesecar, M.E. Johnson, and A.P. Kozikowski (2008) “Design and synthesis of novel aryl ether inhibitors of the *Bacillus anthracis* enoyl–ACP reductase,” *Current Medicinal Chemistry*, accepted pending minor revision.
- S.K. Tipparaju, S. Joyasawal, S. Forrester, D.C. Mulhearn, S. Pegan, M.E. Johnson, A.D. Mesecar, and A.P. Kozikowski (2008) Design and synthesis of 2-pyridones as novel inhibitors of the *Bacillus Anthracis* enoyl–ACP reductase, *Bioorganic & Medicinal Chemistry Letters*, accepted pending minor revision.

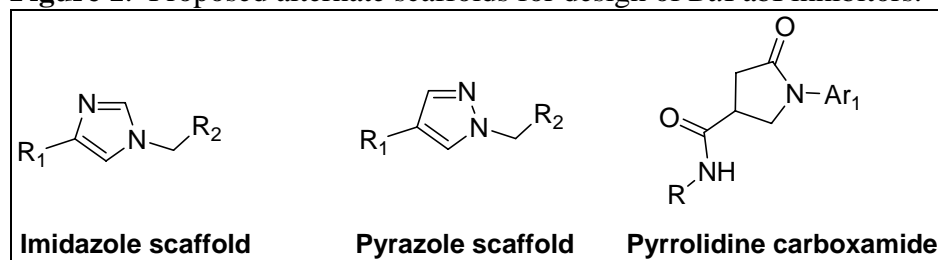
Report 4: Project 3. Rational discovery of new FabI inhibitors as biodefense antibacterial therapeutics

M. Johnson

A. Overview of work activities during this reporting period.

To date, the main focus of our work for discovering inhibitors against FabI, the enzyme that catalyzes the ultimate step in FAS II, has been on triclosan (diaryl ether) based analogs. Unfortunately, due to rapid metabolic processing of the phenolic moiety in triclosan compounds, an alternative scaffold is necessary to discover a more viable antibacterial. Three new base structures, imidazoles, pyrazoles, and pyrrolidine carboxamides, (Figure 1) have been investigated utilizing computational modeling methods, docking the small compounds against *Ba*FabI with GOLD. All three of the new scaffolds have been reported to be good inhibitors against the enoyl acyl carrier protein reductases from other organisms, such as *S. pneumoniae*, *S. aureus*, *E. coli*, *P. falciparum*, or *M. tuberculosis*, organisms for which triclosan has also been effective. (Detailed references below.) In this period, we have pursued initial exploration of these new scaffolds as new inhibitors against *Ba*FabI.

Figure 1. Proposed alternate scaffolds for design of *Ba*FabI inhibitors.

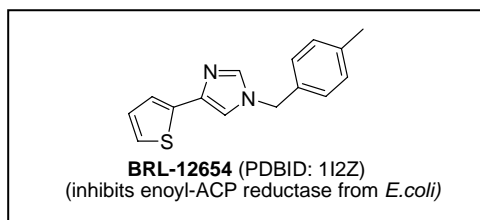


B. Detailed evaluations.

Substituted imidazoles and pyrazoles

Glaxo-Smith Kline reported in 2001 on 1,4-disubstituted imidazoles showing inhibitory activity against FabI from *S. aureus* and *E. coli*, IC₅₀ as low as 250nM (Heerding, et.al. 2001). Crystal structure (PDBID: 1I2Z) of a 1-thiophene-4-benzyl-imidazole derivative, BRL-12654 (Figure 2), indicates that the unsubstituted imidazole nitrogen is involved in a crucial hydrogen bond to the active site Tyr156, as well as showing π -stacking of the thiophene with the nicotinamide ring of NAD⁺. (Heerding, et.al., 2001) This indicates that the substituted imidazole is behaving in a similar fashion to ring A of triclosan, and is a very good replacement for the troubling phenolic group. A more recent report (Kitagawa, et.al., 2007) indicates that phenylimidazoles are also good inhibitors of FabK, the enoyl-ACP reductase from *S. pneumoniae* (IC₅₀ =140nM). The phenylimidazoles also show antibacterial activity against *S. pneumoniae* (MIC = 0.5 μ g/mL).

Figure 2

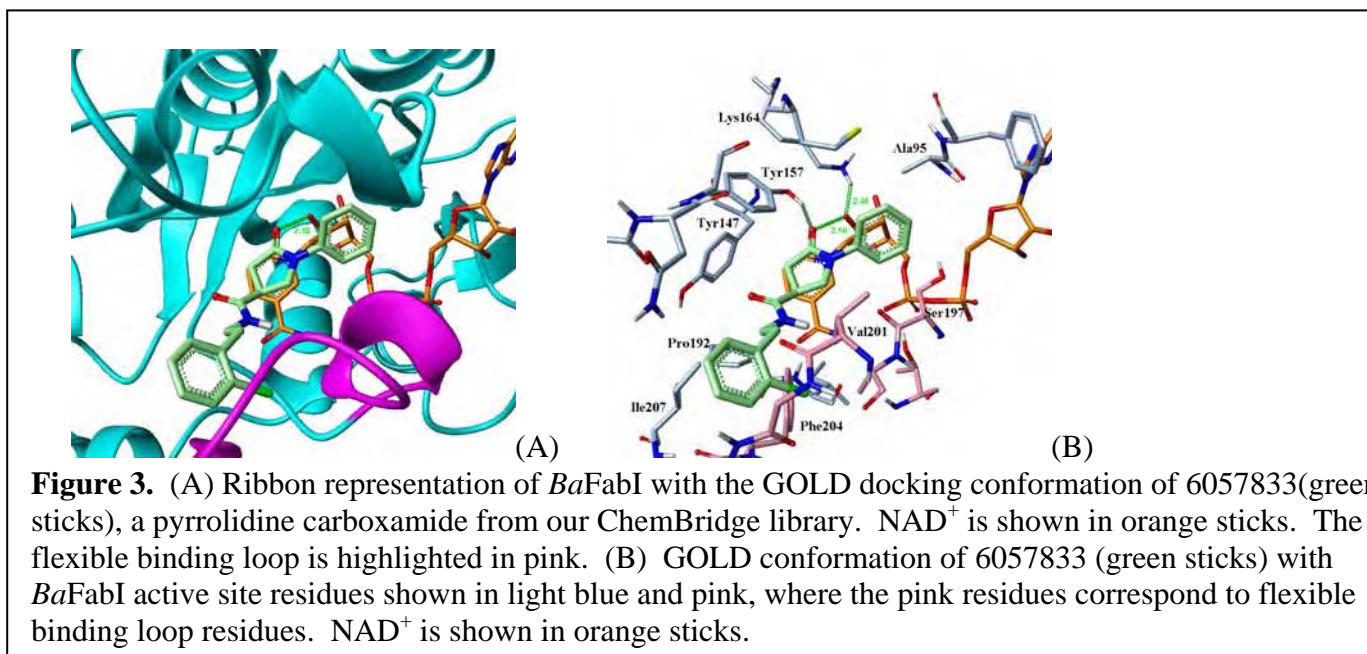


Pyrazoles, structurally very close to imidazoles, have also been shown to be effective inhibitors against enoyl-ACP reductase (FabI) from *P. falciparum*. 1,3- and 1,5-diaryl imidazoles showed inhibitory activity in the 30-50 μ M range for *P. falciparum* FabI (Kumar, et.al., 2006). Unfortunately, no crystal

structures have been reported for these compounds, but due to their similarities to the imidazoles, they are expected to bind in a similar fashion.

Preliminary docking of imidazoles and pyrazoles like those mentioned above, against the *B.anthraxis* FabI suggests that they bind in a fashion similar to the crystal structure of imidazole BRL-12654 from GSK. The R₁ group needs to be a hydrophobic group such as thiophene, phenyl, or benzyl, to reside in the hydrophobic pocket. R₂ is best if it is an aromatic ring with smaller substituents (Cl, Me) in the *ortho* and *meta* position, and larger hydrogen bonding substituents at the *para* position as this is oriented similar to ring B of triclosan, where this position can interact with residues 95-99, and points toward the enzyme surface.

Pyrrolidine carboxamides



Pyrrolidine carboxamides were reported in 2006 to be effective inhibitors against the enoyl-ACP reductase from *M. tuberculosis*, InhA (He, et.al., 2006). Substitution of the two rings attached to the pyrrolidine carboxamide core resulted in an IC₅₀ of 140nM for racemic compound, which when separated found the active enantiomer to be 62nM, against InhA. The crystal structure of one of these compounds, PDBIDs 2H7M and 2H7P, indicate that the pyrrolidine carboxyl group is hydrogen bonding with the active site tyrosine, and the pyrrolidine ring overlaps nicely with the nicotinamide ring from NAD⁺, much in the same way as ring A from triclosan. Substitution of the pyrrolidine carboxamide core is attractive for FabI, as they point in the two directions where the active site can accommodate more atoms. A search of our current 50K DiverSet library from ChemBridge has found over 100 analogs of the pyrrolidine carboxamide. GOLD docking of these compounds against *BaFabI* has found that these fit very comfortably in the active site, and orient as reported in the crystal structure noted above. Figure 3 shows the orientation of one of the pyrrolidines from the database, 6057833, with respect to NAD⁺. In the ribbon representation, it is clear that the group off the carboxamide resides in a hydrophobic pocket pushing up against the flexible binding loop. The aromatic group off of the pyrrolidine nitrogen is positioned toward the entrance of the pocket, toward the Ala95 loop, suggesting that modifications on the phenyl ring might be beneficial to binding. Due to the number of the pyrrolidine carboxamides present in our ChemBridge library, this scaffold will be tested against *BaFabI* first.

C. Publications

- S.K. Tipparaju, D.C. Mulhearn, G.M. Klein, Y. Chen, S. Tapadar, M.H. Bishop, S. Yang, J. Chen, M. Ghassemi, B.D. Santarsiero, J.L. Cook, M. Johlfs, A.D. Mesecar, M.E. Johnson, and A.P. Kozikowski (2008) "Design and synthesis of novel aryl ether inhibitors of the *Bacillus anthracis* enoyl-ACP reductase," *ChemMedChem*, in press.
- S.K. Tipparaju, S. Joyasawal, S. Forrester, D.C. Mulhearn, S. Pegan, M.E. Johnson, A.D. Mesecar, and A.P. Kozikowski (2008) Design and synthesis of 2-pyridones as novel inhibitors of the *Bacillus Anthracis* enoyl-ACP reductase, *Bioorganic & Medicinal Chemistry Letters*, **18**(12), 3565-3569.

D. References

- He, X., Alian, A., Stroud, R., Ortiz de Montellano, P.R. *J. Med. Chem.*, **2006**, *49*, 6308-6323. "Pyrrolidine Carboxamides as a Novel Class of Inhibitors of Enoyl Acyl Carrier Protein Reductase from *Mycobacterium tuberculosis*".
- Heerding, D.A., Chan, G., DeWolf, Jr., W.E., Fosberry, A.P., Janson, C.A., Jaworski, D.D., McManus, E., Miller, W.H., Moore, T.D., Payne, D.J., Qui, X., Rittenhouse, S.F., Slater-Radosti, C., Smith, W., Takata, D.T., Vaidya, K.S., Yuan, C.C.K., Huffman, W.F. *Bioorg. Med. Chem. Lett.* **2001**, *11*, 2061-2065. "1,4-Disubstituted Imidazoles are Potential Antibacterial Agents Functioning as Inhibitors of Enoyl Acyl Carrier Protein Reductase (FabI).
- Kitagawa, H., Ozawa, T., Takahata, S., Iida, M. *Bioorg. Med. Chem. Lett.* **2007**, *17*, 4982-4986. "Phenylimidazole derivatives as new inhibitors of bacterial enoyl-ACP reductase FabK".
- Kumar, S., Kumar, G., Kapoor, M., Surolia, A. *Synthetic Comm.* **2006**, *36*, 215-226. "Synthesis and Evaluation of Substituted Pyrazoles: Potential Antimalarials Targeting the Enoyl-ACP Reductase of *Plasmodium Falciparum*"

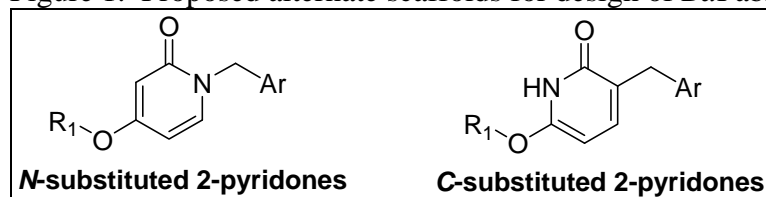
Report 5: Project 3. Rational discovery of new FabI inhibitors as biodefense antibacterial therapeutics

M. Johnson

A. Overview of work activities during this reporting period.

As noted in the last report, the main focus of our work to date for discovering inhibitors against FabI, the enzyme that catalyzes the ultimate step in FAS II, has been on triclosan (diaryl ether) based analogs. Unfortunately, due to rapid metabolic processing of the phenolic moiety in triclosan compounds, an alternative scaffold is necessary to discover a more viable antibacterial. In the prior quarter, we reported on three new base structures, imidazoles, pyrazoles, and pyrrolidine carboxamides, that were investigated utilizing computational modeling methods, docking the small compounds against *Ba*FabI with GOLD. In this period, we have focused on N- and C-substituted pyridones (Figure 1) as additional scaffolds for alternative *Ba*FabI inhibitors.

Figure 1. Proposed alternate scaffolds for design of *Ba*FabI inhibitors.



B. Detailed evaluations.

We have synthesized and tested more than 30 *N*-substituted 2-pyridones to date, with a number of them showing *Ba*ENR inhibitory activities in the micromolar range (Tipparaju et al., 2008). The best inhibitor synthesized of the *N*-substituted group has R₁ = benzyl and Ar = 2-chloro-4-aminobenzene, with an IC₅₀ = 800 nM. Antibacterial activity has been more elusive in this set of compounds, with only 2 compounds having measurable MICs. Turning our synthetic efforts to the *C*-substituted 2-pyridones, we have synthesized and tested about 10 compounds. Preliminary data indicates that a *C*-substituted 2-pyridone with R₁ = benzyl and Ar = phenyl has an IC₅₀ = 700 nM. Considering the simplicity of this compound, numerous substituents can be added onto R₁ and Ar to maximize interactions with other regions in the active site. Utilizing our knowledge from the both the *N*-substituted 2-pyridones as well as the 100+ triclosan analogs synthesized, we are initially focusing on the expansion of the Ar group, as this has the most opportunities for ligand-enzyme interactions. GOLD docking of both classes of 2-pyridones indicates that both show van der Waals interactions, and excellent hydrophobic complementarity. Also seen is retention of the hydrogen bonds between the Tyr157, as well as with the NAD⁺ sugar, with either the carbonyl oxygen (*N*-substituted) or the NH (*C*-substituted) pyridones. The orientations of the amide unit of the *C*-substituted 2-pyridones is flipped from that of the *N*-substituted, so as to maximize hydrogen bonding opportunities with the NAD⁺ sugar and Tyr157. A GOLD conformation of a *C*-substituted 2-pyridone with R₁=benzyl and Ar=phenyl clearly shows there to be ample space to add substituents onto the R₁ benzyl group, and places the Ar phenyl group deep in the hydrophobic region of the active site (Figure 2).

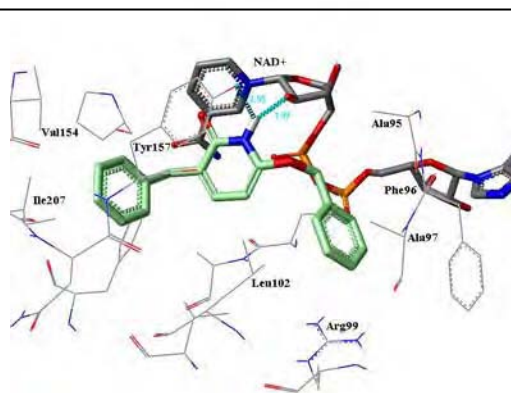


Figure 2. Stick representation of *Ba*FabI with the GOLD docking conformation of a *C*-substituted pyridone (green carbons) shown stacked adjacent to the NAD⁺ (grey carbons), with substantial space near the Ar phenyl group.

With additional future funding, we hope to be able to explore the experimental validation of these computational designs.

C. Publications (previously reported as in press; full citation now provided)

S.K. Tipparaju, D.C. Mulhearn, G.M. Klein, Y. Chen, S. Tapadar, M.H. Bishop, S. Yang, J. Chen, M. Ghassemi, B.D. Santarsiero, J.L. Cook, M. Johlfs, A.D. Mesecar, M.E. Johnson, and A.P. Kozikowski (2008) "Design and synthesis of novel aryl ether inhibitors of the *Bacillus anthracis* enoyl-ACP reductase," *ChemMedChem*, **3**(8), 1250-1268.

D. References

S.K. Tipparaju, S. Joyasawal, S. Forrester, D.C. Mulhearn, S. Pegan, M.E. Johnson, A.D. Mesecar, and A.P. Kozikowski (2008) Design and synthesis of 2-pyridones as novel inhibitors of the *Bacillus Anthracis* enoyl-ACP reductase, *Bioorganic & Medicinal Chemistry Letters*, **18**(12), 3565-3569.

Report 6: Project 3. Rational discovery of new FabI inhibitors as biodefense antibacterial therapeutics

M. Johnson

A. Overview of work activities during this reporting period.

As noted in the last report, the main focus of our work to date has been on discovering inhibitors against FabI, the enzyme that catalyzes the ultimate step in FAS II. In the Q2 and Q3 reports, we have reported on the computational exploration of a few high priority scaffolds derived from literature studies. During this past quarter, we have expanded our studies in two directions: (a) We have used computational (“*in silico*”) screening to dock the ZINC library of approximately 800,000 compounds against the *Ba*FabI enzyme as a further approach for discovering novel scaffolds for developing further inhibitors; and (b) based on recent literature reports that targeting metabolic pathways is more effective than targeting individual enzymes, we have expanded the targets within the fatty acid biosynthetic pathway to include FabD, FabG, FabF and FabH, which are corollary enzymes that are essential for a variety of bacterial pathogens, including some or all of the Category A agents. This work has included cloning and expression of all of these enzymes plus the acyl carrier protein, demonstration of enzymatic assay feasibility for inhibitor discovery, and computational screening of the ZINC database against the enzymes.

B. Detailed evaluations.

Fab I *in silico* computational screening of the ZINC dataset. The full ZINC database contains approximately 5.6 million compounds, many of which are not suitable for therapeutic lead development. Four subsets of this database were selected with reactive and other unsuitable compounds eliminated, including “lead-like” compounds with molecular weights below 350, H-bond donors and acceptors conforming to Lupinski-type rules, and with additional subsets including groups for facile derivatization, following the guidelines of Hubbard and co-workers (2). An example plot, showing the results of this computational screening using the program Surflex-Dock is provided in Figure 1, below. The results demonstrate that only 10-20% of the compounds bind to the enzyme with high affinity. We thus plan to use further computational methods to evaluate the approximately 100,000 compounds showing the highest affinity. This will include doing a consensus docking with other software programs, including Gold, Autodock, Glide and Dock, followed by short molecular dynamics simulations that allow the protein to flex and provide potential for induced fit. Consensus among several scoring and docking methods is known to provide more reliable rankings of compounds than any one method alone. Rescoring the binding following MD simulation will further allow the enzyme to undergo induced fit accommodation of compounds that may simulate the slow, tight binding that is observed with some inhibitors such as triclosan. Subject to funding, we plan to subsequently experimentally evaluate the compounds predicted to be most active, with 1,000 to 10,000 to be chosen for experimental evaluation.

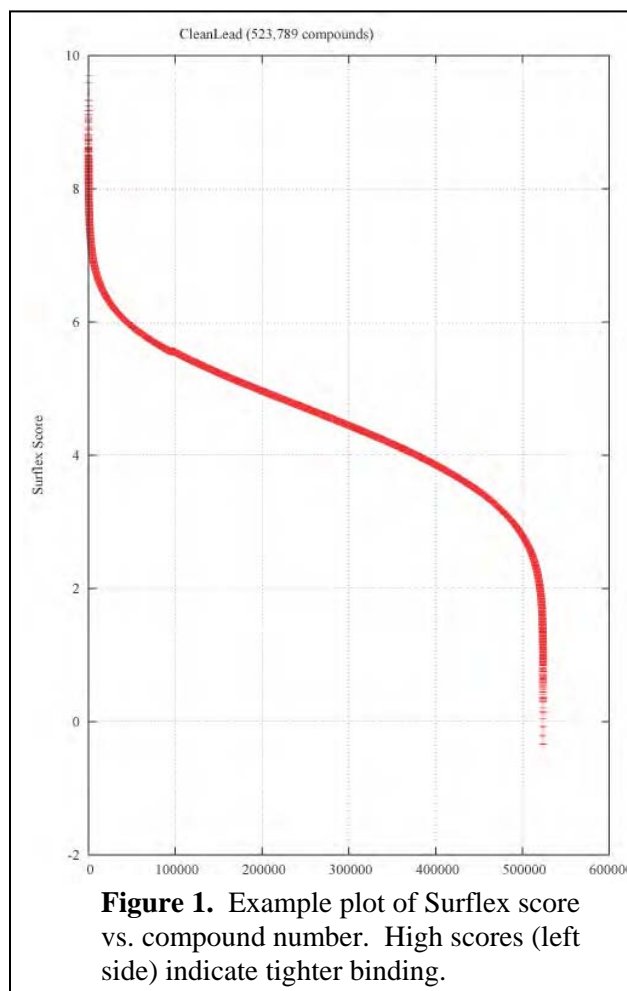
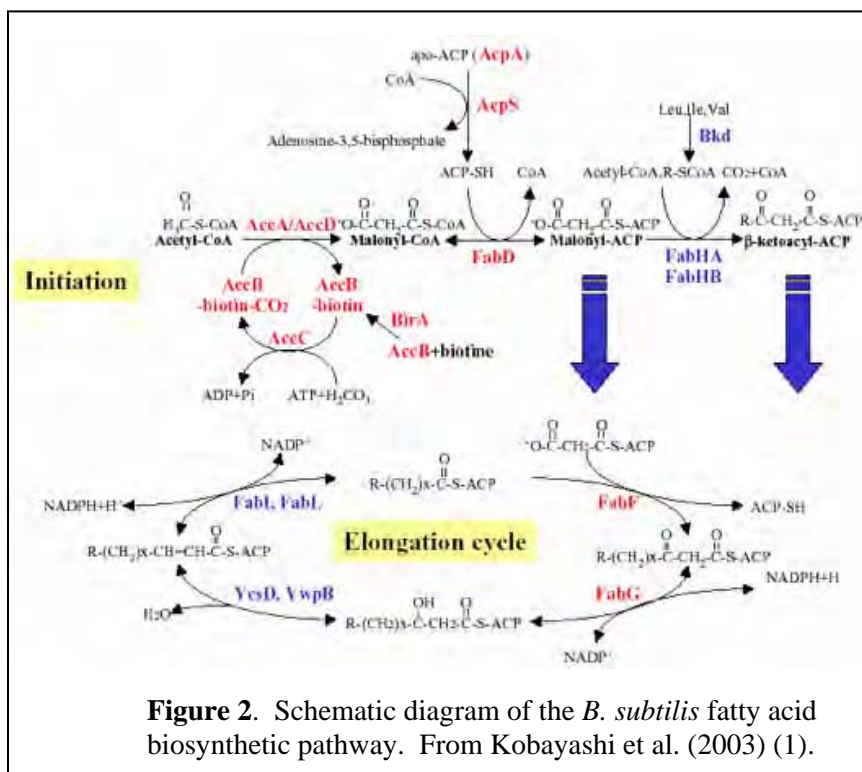


Figure 1. Example plot of Surflex score vs. compound number. High scores (left side) indicate tighter binding.

Development of additional targets in the fatty acid biosynthetic pathway. Antibiotic resistance arises partly since most antibiotics target a single enzyme active site or receptor site where one mutation can compromise antibiotic activity.

Recent studies suggest that polypharmacology, or drugs acting on multiple biological targets within a metabolic pathway, may be therapeutically beneficial (3). A schematic of the fatty acid metabolic pathway for *B. subtilis* is shown below in Figure 2. Enzymes shown in red are essential for that organism.

Additionally, Fab H is essential in other pathogens. We have accordingly cloned and expressed *B. anthracis* FabD, FabF, FabG and FabH from this pathway. We have computationally screened the ZINC library subsets described above against FabF, FabG and FabH, and have also established activity assays for FabD/FabF. We plan to complete computational screening against FabD and to establish assays for FabG and FabH as well.



Recent work has demonstrated that two natural products, platensimycin and platencin, demonstrate antibiotic activity against several gram positive organisms, including *S. aureus*, *S. pneumoniae*, *E. faecalis* and *E. faecium* (4). In collaboration with us, Professor Daesung Lee has synthesized both platencin and platensimycin, as well as related analogs. In collaboration with Professor James Cook, in the Department of Medicine, we have successfully established an antibacterial assay for these compounds that replicates literature values, and we plan to extend testing against *B. anthracis* and other Category A and B agents. Plans for future work include development of this initial foundation to discover lead inhibitors against these various targets that can be pursued for therapeutic development.

With additional future funding, we hope to be able to explore the experimental validation of these computational and experimental approaches.

C. Publications

All publications previously reported.

D. References

1. Kobayashi K, Ehrlich SD, Albertini A, et al: Essential *Bacillus subtilis* genes. *Proc Natl Acad Sci U S A* 2003; 100:4678-4683
2. Baurin N, Baker R, Richardson C, et al: Drug-like annotation and duplicate analysis of a 23-supplier chemical database totalling 2.7 million compounds. *J Chem Inf Comput Sci* 2004; 44:643-651
3. Hopkins AL: Network pharmacology. *Nat Biotechnol* 2007; 25:1110-1111
4. Wang J, Kodali S, Lee SH, et al: Discovery of platencin, a dual FabF and FabH inhibitor with in vivo antibiotic properties. *Proc Natl Acad Sci U S A* 2007; 104:7612-7616

Quarterly Report 1: Project 4. Natural products-based discovery of therapeutics for biodefense

Summary

During this first quarter, we have successfully completed the total synthesis of **Antibiotic A-33853**. In addition, we have synthesized 6 first-generation analogs of A-33853 and have evaluated their antibiotic activities against the *Bacillus anthracis* Δ ANR strain (see Figure 1). Antibiotic A-33853 was the most potent inhibitor against *Bacillus anthracis* in cell culture with a minimum inhibitor concentration (MIC) of approximately 6 μ M. We tested all of the A-33853 compounds for their ability to inhibit the enzyme enoylreductase (ENR) from *B. anthracis*. However, none of the compounds inhibited the enzyme suggesting that this enzyme is not the target for these compounds. We also evaluated a series of natural Ambiquine and Hapalindole compounds isolated from a cyanobacteria strain for inhibitory activity towards *B. anthracis* (see Figure 2). We found that Ambiquine A has an MIC value of 1 to 3 μ M placing it in the potency range of A-33853.

Plans

Antibiotic A-33853 was found to potently inhibit anthrax in cell culture, whereas the 6 first generation analogs were all weaker. Based upon the activity of and the structure of the compounds, we will continue to pursue the synthesis and evaluation of 2nd and 3rd generation A-33853 compounds during this next quarter. We will also initiate scale-up strategies so that we can produce enough of the A-series of compounds for more extensive testing. We will also test the A-series compounds for their ability to inhibit other enzymes in *Bacillus anthracis*.

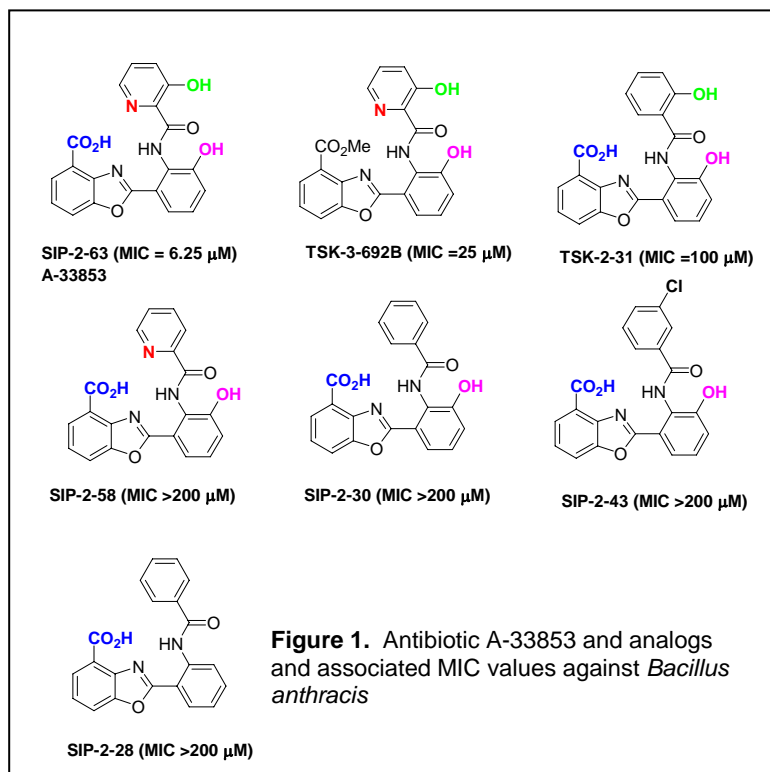


Figure 1. Antibiotic A-33853 and analogs and associated MIC values against *Bacillus anthracis*

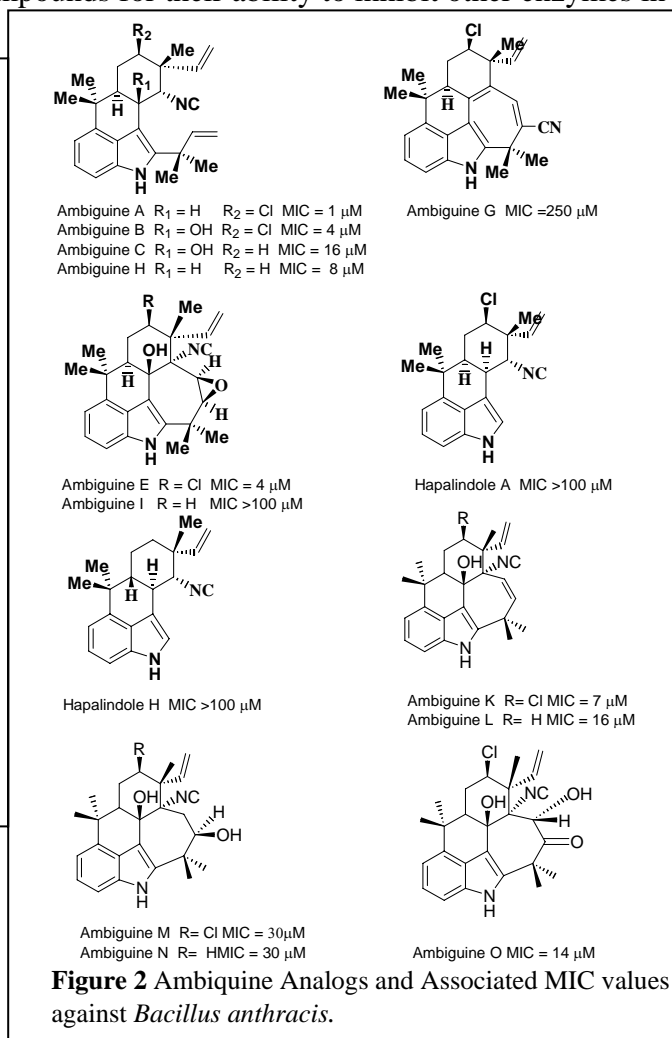
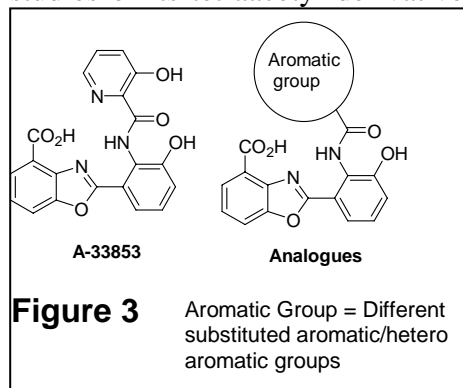


Figure 2 Ambiquine Analogs and Associated MIC values against *Bacillus anthracis*.

Detailed Progress Report

Synthesis of Antibiotic A-33853 and Its Analogues:

Antibiotic A-33853 was produced by aerobic fermentation from a new *Streptomyces* sp. that was isolated from an Illinois soil sample. Antibiotic A-33853 and its diacetyl and triacetyl derivatives have shown antibacterial and antiviral activities. The structure of A-33853 has been elucidated through X-ray diffraction studies of its tetraacetyl derivative (Figure 3). The biological data reveal that **Antibiotic A-33853** is a very

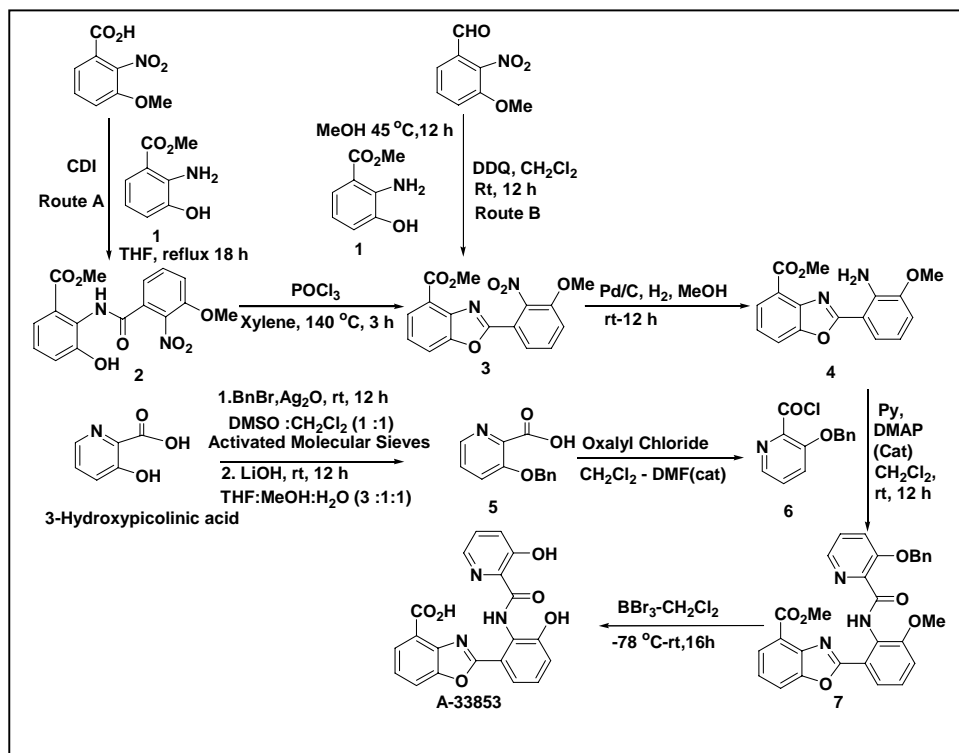


attractive lead compound and worthy of further evaluation and SAR studies. The total synthesis of natural product A-33853 has been carried out in our laboratories with the synthetic strategies shown below. The key intermediate **3** can be obtained via either route A or B. In route A, the amide **2** was prepared from commercially available 3-Methoxy-2-nitrobenzoic acid and amine **1** by CDI mediated amide coupling reaction and was then transformed to benzoxazole **3** via cyclization-dehydration reaction using POCl₃ in refluxing xylene (1). In route B, the Schiff base, prepared from commercially available 3-methoxy-2-nitro-benzaldehyde and amino phenol **1**, was transformed to 2-aryl bezoxazole **3** by oxidative cyclization using DDQ (2). The nitro functionality of compound **3** was reduced to amine **4** by catalytic hydrogenation. The acid chloride **6** was prepared by treating 3-benzoyloxypicolinic acid (**5**) with oxalyl

hydrogenation. The acid chloride **6** was prepared in two steps, by treating 3-hydroxypicolinic acid with benzyl bromide and silver oxide followed by hydrolysis of benzyl ester with LiOH. The natural product **A-33853** was obtained by the coupling reaction of amine **4** and acid chloride **6** followed by removal of the protecting group (3) (Scheme 1).

To date, we have synthesized compounds in Figure 1 for the testing against *Bacillus Anthracis* (Anthrax). Classical medicinal chemistry plays an invaluable role in drug discovery, especially at the stage where a screening program has been initiated and a lead candidate found. As a wide variety of A-33853 analogs can be envisioned, we plan to

synthesize a library of analogues from the intermediate **4** by using the same chemistry (with little modification in case of some analogues) as shown in Figure 4.



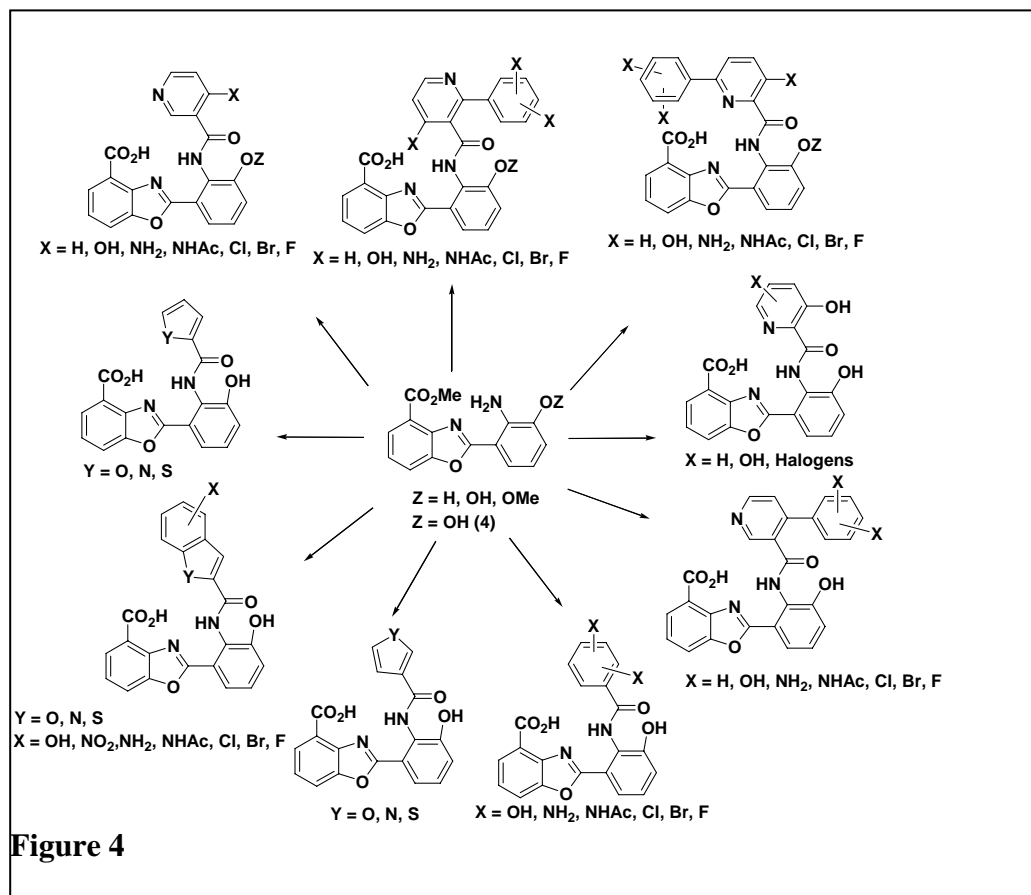


Figure 4

References:

- (1) Huang, S. T., Hsei, I. J., Chen, C. Synthesis and anticancer evaluation of bis(benzimidazoles), bis(benzoxazoles), and benzothiazoles. *Bioorg. Med. Chem.*, **14**, 6106-6119, (2006).
- (2) Chang, J., Zhao, K., Pan, S. Synthesis of 2-arylbenzoxazoles via DDQ promoted oxidative cyclization of phenolic Schiff bases-a solution-phase strategy for library synthesis. *Tetrahedron Lett.*, **43**, 951-954, (2002).
- (3) Adediran, S. A., Cabaret, D., Drouillat, B., Pratt, R. F., Wakselman, M. The synthesis and evaluation of benzofuranones and β -lactamase substrates. *Bioorg. Med. Chem.*, 1175-1183, (2001).
- (4) Paal, C. A density functional theory study of the mechanism of the Paal-Knorr pyrrole synthesis. *Chem. Ber.*, **17**, 2756, (1884).
- (5) U.S. Pat. Appl. Publ. 2004006234.

Quarterly Report 2: Project 4. Natural products-based discovery of therapeutics for biodefense

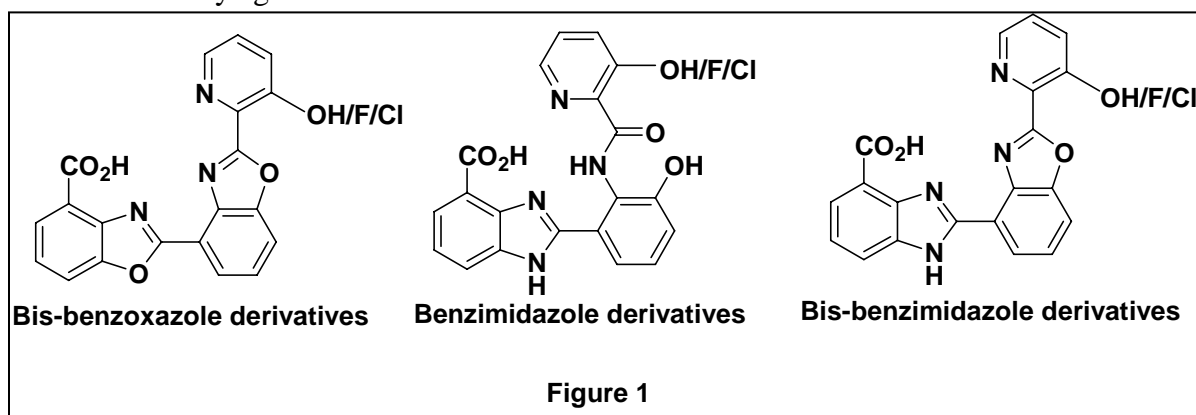
A. Mesecar and A. Kozikowski

Summary

During this second quarter, we have successfully completed the synthesis of a series of 2nd and 3rd generation derivatives of **Antibiotic A-33853** and have tested them against the *Bacillus anthracis* Δ ANR strain. This completes the 2nd quarter milestones. Thus far, Antibiotic A-33853 is still the most potent inhibitor against *Bacillus anthracis* in cell culture tested to date with a minimum inhibitory concentration (MIC) of approximately 6.25 μ M (Table 1). However, we have now achieved the synthesis of one compound (compound **8** in Table 1) that has an MIC value of 12.5 μ M which is near that of A-33853.

Plans

Based upon the activity of and the structure of the compounds presented in Tables 1 and 2, below, we will continue our efforts and generate more potent, A-33853 derivative compounds during this next quarter. We will focus on the synthesis of bis-benzoxazole, benzimidazole and bis-benzimidazole derivatives (Figure 1) and will test their efficacy against the *Bacillus anthracis* Δ ANR strain.



Detailed progress report

Natural product A-33853 was synthesized in a single step by treatment of **7** with excess BBr_3 ⁵ (**Scheme 1**). The resulting product was tested against *Bacillus anthracis* (MIC 6.26 μ M). Classical medicinal chemistry plays an invaluable role in drug discovery, especially at the stage where a screening program has been initiated and a lead candidate found. As planned, we have synthesized a library of analogues from the intermediate **4** and tested against *Bacillus anthracis*. Structure and MIC values of synthesized compounds are given in Table 1 and Table 2. To synthesize A-33853 analogues 3-hydroxyl pyridinyl moiety was replaced with different substituted heterocyclic aromatic ring (**Table 1**) and with substituted benzene ring (**Table 2**). After testing all the synthesized compounds against anthrax, it was found that A-33853 is more active (MIC 6.25 μ M) and some analogues having moderate activities (Table 1, entries 2,3,8, 9, 10 and 12).

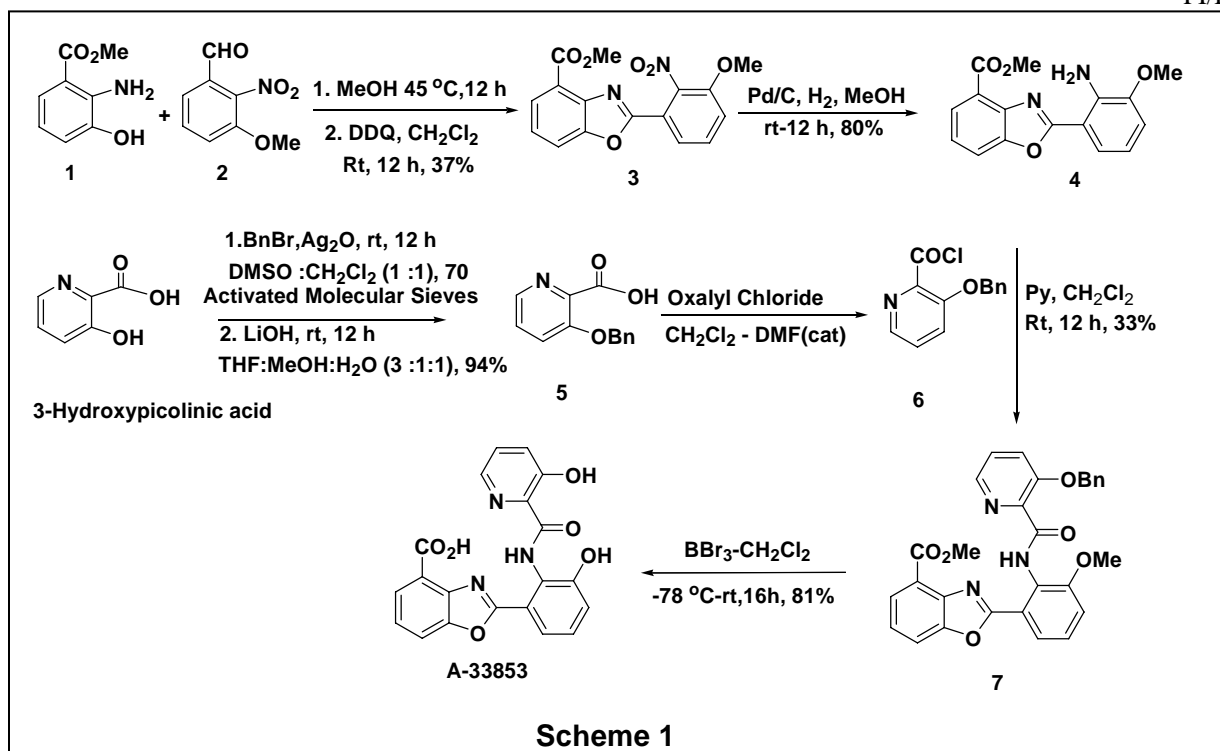
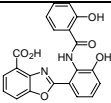
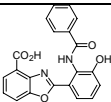
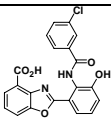
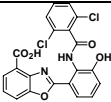
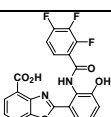
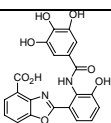
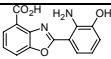


Table 1:

| Compounds | Structure of acids | MIC (μ M) | Compounds | Structure of acids | MIC (μ M) |
|-----------|--------------------|-------------------|-----------|--------------------|-------------------|
| 1 | A-33853 | 6.25 | 7 | | >200 |
| 2 | | 25 | 8 | | 50 |
| 3 | | 25 | 9 | | 12.5 |
| 4 | | 200 | 10 | | 50 |
| 5 | | 200 | 11 | | >200 |
| 6 | | >200 | 12 | | 50 |

Table 2:

| Compounds | Structure of acids | MIC (μ M) |
|-----------|---|----------------|
| 1 |  | 100 |
| 2 |  | >200 |
| 3 |  | 200 |
| 4 |  | 100 |
| 5 |  | 200 |
| 6 |  | >200 |
| 7 |  | >200 |

*Acid chlorides are commercially available or synthesized from corresponding acid by treating with oxalyl chloride.

Quarterly Report 3:Project 4. Natural products-based discovery of therapeutics for biodefense

A. Mesecar and A. Kozikowski

Summary

During this quarter, we have successfully completed the synthesis of additional analogs of Antibiotic A-33853 and have tested them against the *Bacillus anthracis* ΔANR strain. In addition, we have tested A-33853 against a series of other pathogens to test for its spectrum of activity. This completes the 3rd quarter milestones. Significantly, during this quarter we have been able to improve upon the potency of the original lead, A-33853, against *B. anthracis*. Compound SIP-3-4 (MIC 3.125 μM) is 2-fold more potent. In addition, we have found that A-33853 potently inhibits another of other pathogens including various *Staphylococcus*, *Salmonella*, *Pasteurella*, *Mycoplasma* and *Aermonas* strains.

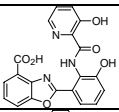
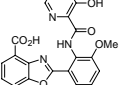
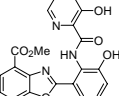
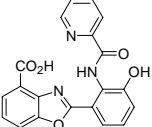
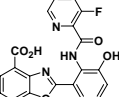
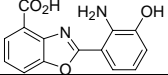
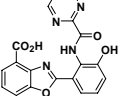
Plans

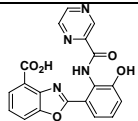
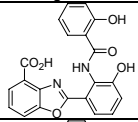
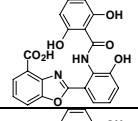
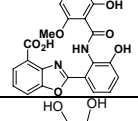
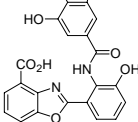
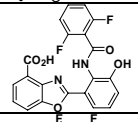
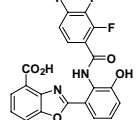
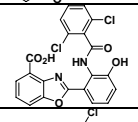
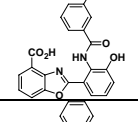
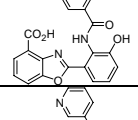
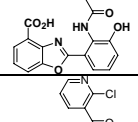
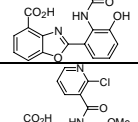
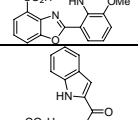
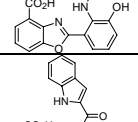
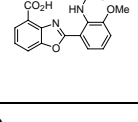
Based upon the activity of and the structured of the compounds tested so far, we will continue our efforts and generate more potent derivatives of A-33853 during this next quarter. We will test the efficacy of all the compounds against the *Bacillus anthracis* ΔANR strain, and we will test our most potent compounds against other bacteria.

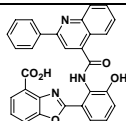
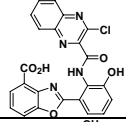
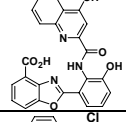
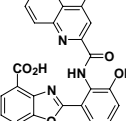
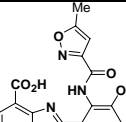
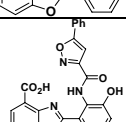
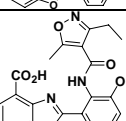
Detailed Progress Report

By following the chemistry we reported in the previous progress report, we have synthesized a library of A-33853 analogs and tested then against *Bacillus anthracis*. The structure and MIC values of synthesized compounds are given in Table 1 below.

Table 1. Activity of Antibiotic A-33853 against *Bacillus anthracis*

| Entry | ID# | Acids | MIC(μM) |
|-------|-------------|---|---------|
| 1 | SIP-2-63 |  | 6.25 |
| 2 | SIP-2-93 |  | 25 |
| 3 | TSK-III-692 |  | 25 |
| 4 | SIP-2-77 |  | 200 |
| 5 | SIP-2-88 |  | 200 |
| 6 | SIP-2-100 |  | >100 |
| 7 | SIP-3-3 |  | >200 |

| | | | |
|----|----------------------|---|------|
| 8 | SIP-2-86 |  | >200 |
| 9 | SIP-2-31 |  | 100 |
| 10 | SIP-3-13(1) |  | >200 |
| 11 | SIP-3-13(2) ***** |  | >200 |
| 12 | SIP-2-72 |  | >200 |
| 13 | SIP-3-14 |  | >200 |
| 14 | SIP-2-87 |  | 200 |
| 15 | SIP-2-98 |  | >100 |
| 16 | SIP-2-43 |  | 200 |
| 17 | SIP-2-30(BB) |  | >200 |
| 18 | SIP-2-58 |  | >200 |
| 19 | SIP-2-68 |  | >200 |
| 20 | SIP-2-67 |  | >200 |
| 21 | SIP-2-71 |  | 50 |
| 22 | SIP-2-74 |  | >200 |

| | | | |
|----|----------|--|-------|
| 23 | SIP-2-85 |  | 12.5 |
| 24 | SIP-2-97 |  | 50 |
| 25 | SIP-3-5 |  | 200 |
| 26 | SIP-3-4 |  | 3.125 |
| 27 | SIP-2-89 |  | 50 |
| 28 | SIP-2-90 |  | >200 |
| 29 | SIP-2-91 |  | >100 |

We also tested for inhibition of other bacteria by A-33853. As shown in Table 2 below, A-33853 effectively inhibits a number of bacteria suggesting that it may have potential to be developed as a broad-spectrum antibiotic.

Table 2. Activity of Antibiotic A-33853 vs Bacteria Pathogenic to animals (in vitro)

| Entry | Test Organism | MIC (µg/ml) |
|-------|-------------------------------------|-------------|
| 1 | <i>Staphylococcus aureus</i> 3055* | 2.0 |
| 2 | <i>Staphylococcus aureus</i> 3074** | 2.0 |
| 3 | <i>Salmonella typhosa</i> SA12*** | 2.0 |
| 4 | <i>Staphylococcus</i> sp. | 3.12 |
| 5 | <i>Streptococcus</i> sp. | 6.25 |
| 6 | <i>Pasteurella multocida</i> | |
| | Bovine | 1.56 |
| | Turkey | 6.25 |
| 7 | <i>Bordetella bronchiseptica</i> | >50.0 |
| 8 | <i>Escherichia coli</i> | >50.0 |

| | | |
|----|---------------------------------|-----------------|
| 9 | <i>Salmonella dublin</i> | >50.0 |
| 10 | <i>Pseudomonas (animal)</i> | >50.0 |
| 11 | <i>Mycoplasma gallisepticum</i> | 1.56 |
| 12 | <i>Mycoplasma synoviae</i> | 1.56 |
| 13 | <i>Mycoplasma hyorhinis</i> | 1.56 |
| 14 | <i>Mycoplasma hyopneumoniae</i> | <0.78 |
| 15 | <i>Pseudomonas (fish)</i> | 50.0 |
| 13 | <i>Aeromonas liquefaciens</i> | 3.12 |
| 16 | <i>Bacillus Anthracis</i> | 6.25 (μ M) |

* Benzylpenicillin-susceptible, clinical isolate

** Benzylpenicillin-resistant, clinical isolate

***Clinical isolate

Together, the biological data presented above reveal that antibiotic A-33853 remains a very attractive lead compound and worthy of further evaluation and SAR studies. Classical medicinal chemistry plays an invaluable role in drug discovery, especially at the stage where a screening program has been initiated and a lead candidate found. Compound SIP-3-4 (MIC 3.125 μ M) is the most active compounds in this series.

Note: This DOD sub-project has been affected by the fire on 01/19/2008 in the College of Pharmacy. No experiment has been carried out from 01/19/2008-03/01/2008. At this moment, the lab is still not fully functional because of the damage to our HPLC instruments.

Quarterly Report 4: Project 4. Natural products-based discovery of therapeutics for biodefense

A. Mesecar and A. Kozikowski

Summary

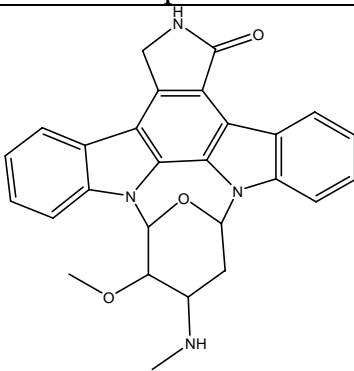
During this second quarter, we have successfully completed the synthesis of a series of additional analogs of Antibiotic A-33853 and the staurosporine-like lead natural product and have tested them against the *Bacillus anthracis* ΔANR strain. This completes the 4th quarter milestones. Significantly, during this quarter we have been able to improve upon the inhibitory potency of the original lead of the GSP series against *B. anthracis*. Compound GSP3-32 has an MIC value of 1.56 μM).

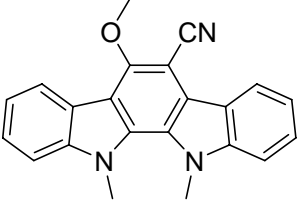
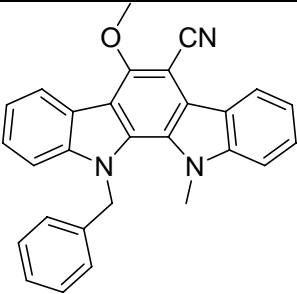
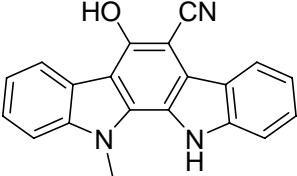
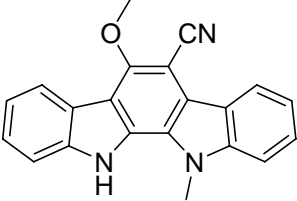
Plans

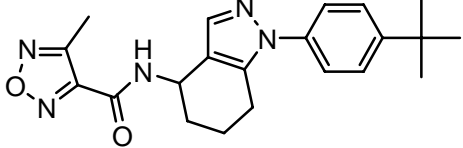
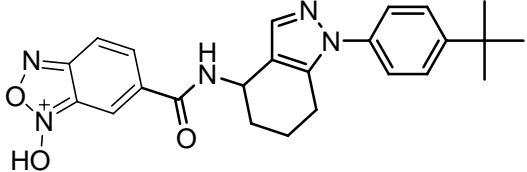
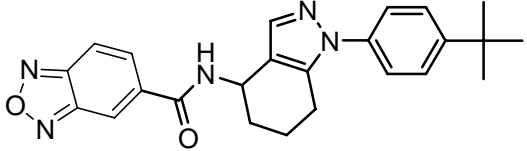
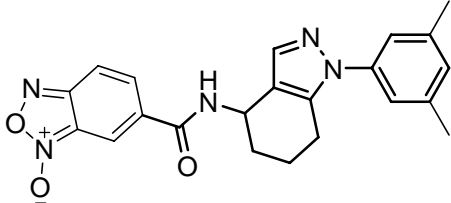
Based upon the activity of and the structured of the compounds tested so far, we will continue our efforts and generate more potent derivatives during this next quarter. We will test the efficacy of all the compounds against the *Bacillus anthracis* ΔANR strain, and we will test our most potent compounds against other bacteria.

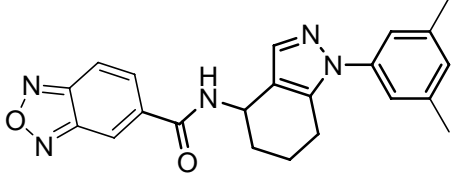
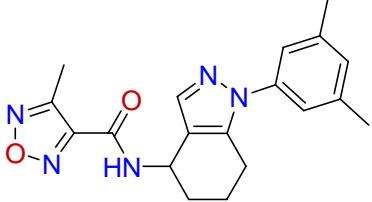
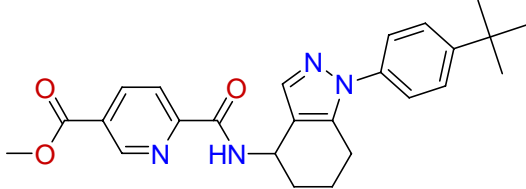
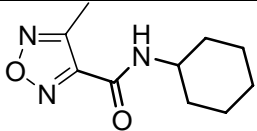
Detailed Progress Report

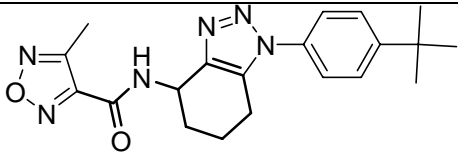
By following the chemistry we reported in the previous progress report, we have synthesized a library of A-33853 analogs and tested then against *Bacillus anthracis*. The structure and MIC values of synthesized compounds are given in Table 1 below.

| Compounds | MIC Values |
|--|------------|
|  <p>Staurosporine C: 12.8 mM in DMSO C₂₇H₂₄N₄O₃ Mol. Wt.: 452.50</p> | 128 μM |

| | |
|--|----------------------------------|
|  <p>GSP3-4 Amount: 1.15 mg $C_{22}H_{17}N_3O$ Mol. Wt.: 339.1372 Soluble in DMSO</p> | <p>>200 μM</p> |
|  <p>GSP3-23 Amount: 1.1 mg $C_{28}H_{21}N_3O$ Mol. Wt.: 415.49 Soluble in DMSO</p> | <p>6.25 μM</p> |
|  <p>GSP3-32 Amount: 1.0 mg $C_{20}H_{13}N_3O$ Mol. Wt.: 311.34 Soluble in DMSO</p> | <p>1.56 μM</p> |
|  <p>GSP3-46 Amount: 1.0 mg $C_{21}H_{15}N_3O$ Mol. Wt.: 325.3633 Soluble in DMSO</p> | <p>>200 μM</p> |

| | |
|--|--------------|
|  <p>GSP3-53 Amount: 2.1 mg $C_{21}H_{25}N_5O_2$ Mol. Wt.: 379.46 Soluble in DMSO</p> | 200 μ M |
|  <p>GSP3-56 Amount: 1.6 mg $C_{24}H_{25}N_5O_3$ Mol. Wt.: 431.49 Soluble in DMSO</p> | >200 μ M |
|  <p>GSP3-58 Amount: 1.0 mg $C_{24}H_{25}N_5O_2$ Mol. Wt.: 415.49 Soluble in DMSO</p> | >200 μ M |
|  <p>GSP3-63 Amount: 2.0 mg $C_{22}H_{21}N_5O_3$ Mol. Wt.: 403.43 Soluble in DMSO</p> | >200 μ M |

| | |
|--|----------------------------------|
|  <p>GSP3-64 Amount: 1.5 mg $C_{22}H_{21}N_5O_2$ Mol. Wt.: 387.43 Soluble in DMSO</p> | <p>>200 μM</p> |
|  <p>GSP3-65 Amount: 2.8 mg $C_{19}H_{21}N_5O_2$ Mol. Wt.: 351.40 Soluble in DMSO</p> | <p>>200 μM</p> |
|  <p>GSP3-66 Amount: 1.5 mg $C_{25}H_{28}N_4O_3$ Mol. Wt.: 432.51 Soluble in DMSO</p> | <p>>200 μM</p> |
|  <p>GSP3-74 Amount: 1.0 mg $C_{10}H_{15}N_3O_2$ Mol. Wt.: 209.24 Soluble in DMSO</p> | <p>>200 μM</p> |

| | |
|--|--------------|
|  <p>GSP3-85 Amount: 1.8 mg $C_{20}H_{24}N_6O_2$ Mol. Wt.: 380.44 Soluble in DMSO</p> | >200 μ M |
|--|--------------|

Quarterly Report 1: High Throughput Screening (HTS) Core

Summary

During this first quarter, the HTS Core has worked to develop a HTS assay capable of detecting natural products that inhibit or eliminate growth of *B. anthracis*. We explored the adaptation of the Alamar Blue dye, a popular colorimetric assay, to our HTS platform. This assay has been shown to be successful for a wide range of mammalian, fungal, and bacteria cell assays¹⁻³. Over the course of this quarter we were able to successfully adapt and miniaturize this assay for use in HTS of *B. anthracis*. Details of these studies are given below.

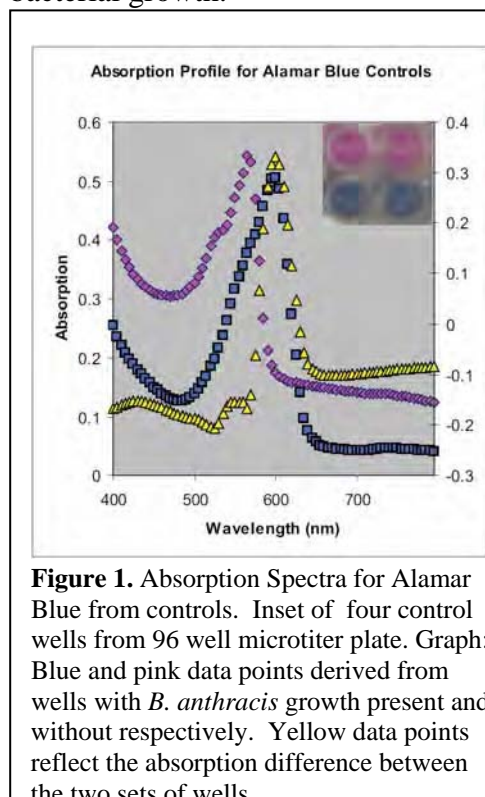
Plans

During the next quarter, we plan to implement the Alamar Blue *Bacillus anthracis* (ABBA) assay and screen over 2,500 natural product extracts and compounds. We anticipate obtaining a number of hits that we will follow-up on over the course of the next few months.

Detailed Progress Report

1) Adaptation of Alamar Blue Assay for *B. anthracis* Stern Δ ANR Strain

To examine the practicality of using the Alamar Blue cell viability assay to screen for inhibitors against the *B. anthracis* Δ ANR strain, we sought first to confirm the wavelength range that we could utilize in detecting bacterial growth.

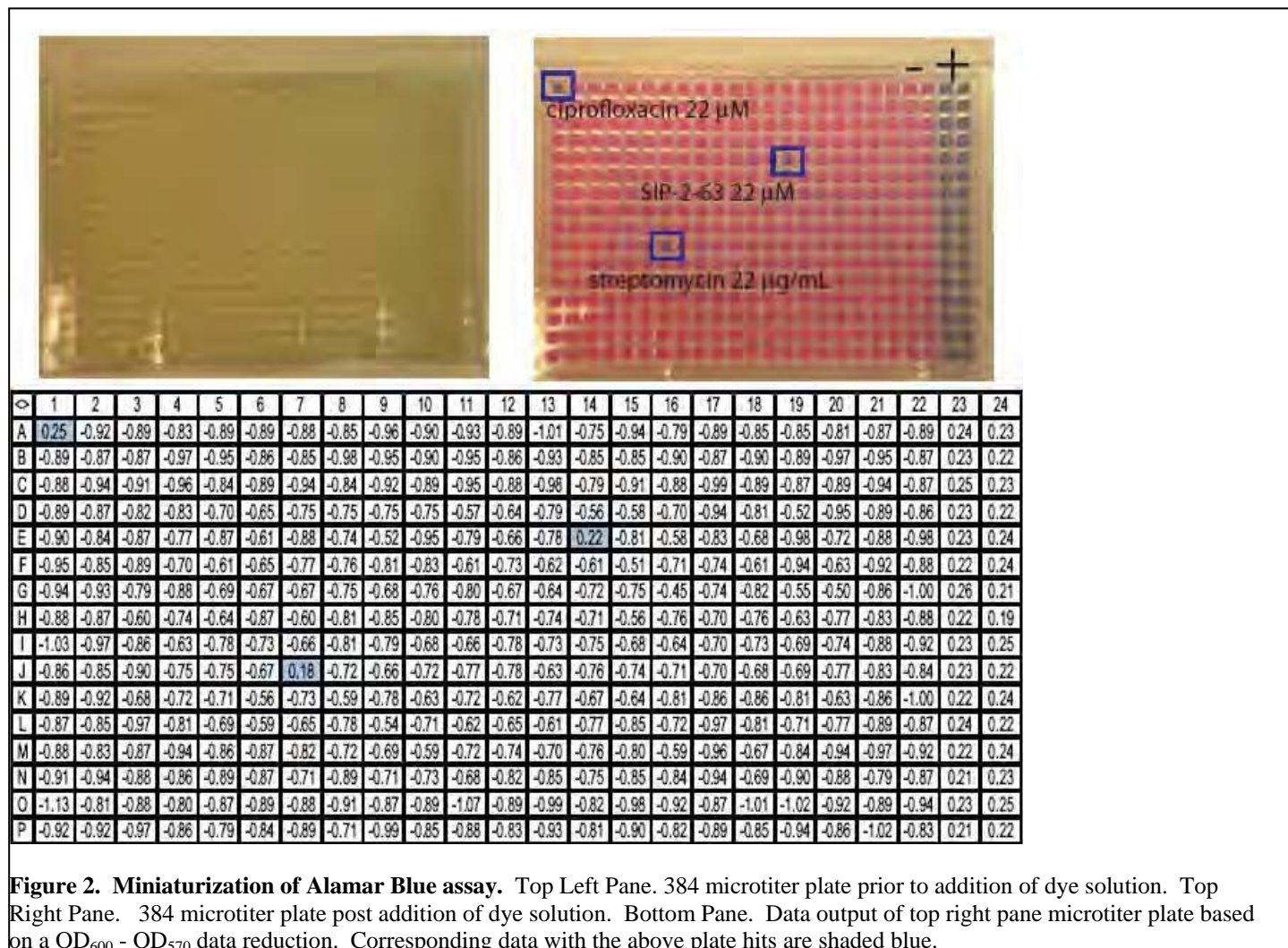


Currently there are two detection methods for determining cell viability of alamar blue, a florescence method and an absorbance based one. The florescence method requires the excitation of the sample at 530 nm and detection of emission at 590 nm. Although valid, we chose to employ the absorbance method of subtracting OD₅₇₀ from the OD₆₀₀. Selection of the absorbance method was rooted in our experience that most natural products and natural product extracts tend to absorb light at lower wavelengths e.g. in the 200 to 400 nm range. By selecting a detection method based on longer wavelengths, we hope to avoid as much inference from overlapping absorbance spectra as possible during HTS screens.

In order to test the use of the visible-absorbance method using our in-house HTS core instrumentation as well as to establish our *B. anthracis* growth protocols, we grew the bacteria overnight in a 96 microtiter plate in Cation Adjusted Muller Hinton media (CAMH). CAMH was selected for use in our studies based on its compliance with the National Committee on Clinical Laboratory Standards (NCCLS). As observed in Figure 1, once the alamar blue dye solution was added to the wells, the wells that contain viable *B. anthracis* cells turn a pinkish color. Wells containing no bacteria remain the blue color of the Almar Blue dye. These results are consistent with those obtained from similar studies with other bacterial systems². To more accurately quantitate the absorbance differences between wells with cells and those without, we utilized our variable wavelength spectrometer to scan for the wavelength signature that results from the differences between the positive and negative control wells (Figure 1). Subtraction of the OD₅₇₀ from the OD₆₀₀ (yellow data points in Figure 1) exemplifies the large signal that results from this assay.

2) Reproducibility and Miniaturization test of the assay in 384 microtiter plate format

Miniaturization of the cell viability assay has many benefits for our planned HTS of natural extracts and products. The two main benefits are savings in reagent costs and increased throughput. However, difficulties can arise by miniaturization of some assays. In the current assay, use of Alamar Blue in cell viability assays had been performed using only 96 well formats¹⁻³. We probed the possibility of reducing the format to a 384 well format.



As observed in Figure 2, there is difficulty in rapidly assessing the growth of *B. anthracis* by eye alone in the 384 microtiter format. However, once the Alamar Blue dye solution is added, the color change and therefore the wells that contain the bacteria, become readily apparent. For validation of our assay, we included 16 positive control wells that were not exposed to the bacteria, and 16 samples that were exposed and will serve as a negative control leaving 320 fir assay sample wells. These data from the control wells provided us with a Z-factor value of .807 consistent with categorization of an excellent assay⁴. To ensure that our assay would be sensitive to detecting lead compounds we also spiked three of the wells with the following, 22 μ M ciprofloxin, 22 μ g/mL streptomycin, and one of our synthetically produced natural product based compounds, SIP-2-63. The concentrations of the test compounds were selected because the were within our proposed screening concentration of 20-30 μ M or μ g/mL depending on whether we were screening pure compounds or biological extracts respectively.

3) Automation of MIC determination with the use of Alamar Blue and automation

To rapidly follow up the lead hits in our 384 microtiter screening, we also developed an automated MIC determination strategy. The automation setup in our facility favored the use of the 96 microtiter plate in creating sequential dilutions while maintaining sterility.

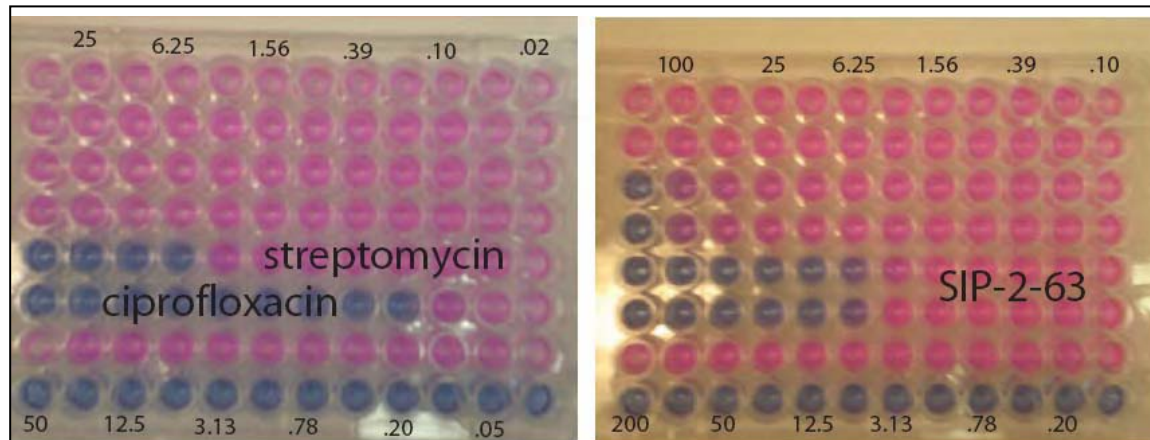
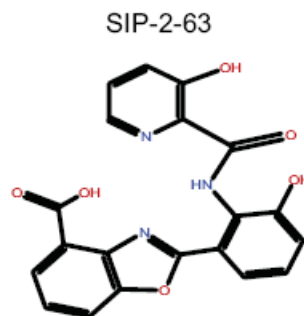


Figure 3 Automated MIC. Left pane. *B. anthracis* MIC determination of Ciprofloxacin and streptomycin via automated MIC strategy. X-axis is in μM for ciprofloxacin and $\mu\text{g/mL}$ for streptomycin. Right pane. *B. anthracis* MIC determination of SIP-2-63 via automated MIC strategy. X-axis is in μM .

MICs determined via the automated MIC strategy for *B. anthracis* of ciprofloxacin and streptomycin was determined to be 0.20 μM and 6.25 $\mu\text{g/mL}$ respectively (Figure 3). These values are consistent with those reported by the CDC.

| Compound | MIC (mM) |
|--------------|----------|
| SIP-2-31 | 100 |
| SIP-2-58 | >200 |
| SIP-2-43 | 200 |
| SIP-2-63 | 6.25 |
| SIP-2-28B | >200 |
| TSK-III-692B | >200 |
| SIP-2-30B | >200 |



The automated MIC strategy was employed for the rapid determination of the MICs of the synthetically produced natural product based SIP-2-63 and its derivatives. As observed in Figure 3 and Table 1, the MIC for SIP-2-63 was determined to be 6.25 μM .

References

- Breinholt, V.; Larsen, J. C., Detection of weak estrogenic flavonoids using a recombinant yeast strain and a modified MCF7 cell proliferation assay. *Chem Res Toxicol* **1998**, 11, (6), 622-9.
- Collins, L.; Franzblau, S. G., Microplate alamar blue assay versus BACTEC 460 system for high-throughput screening of compounds against *Mycobacterium tuberculosis* and *Mycobacterium avium*. *Antimicrob Agents Chemother* **1997**, 41, (5), 1004-9.

3. Repp, K. K.; Menor, S. A.; Pettit, R. K., Microplate Alamar blue assay for susceptibility testing of *Candida albicans* biofilms. *Med Mycol* **2007**, 1-5.
4. Zhang, J. H.; Chung, T. D.; Oldenburg, K. R., A Simple Statistical Parameter for Use in Evaluation and Validation of High Throughput Screening Assays. *J Biomol Screen* **1999**, 4, (2), 67-73.

Quarterly Report 2: High Throughput Screening (HTS) Core

A. Mesecar and S. Pegan

Summary

During this second quarter, the HTS Core was highly successful in implementing the *Bacillus anthracis* (ABBA) assay on our robotics platform. We met our second quarter milestone which was to screen over 2,500 natural product extracts and compounds. In fact, our new assay and robotics protocols were so successful, we were able to screen over 50,080 compounds in addition to over 2,500 extracts.

Plans

During the next or 3rd quarter, we plan to perform follow-up, confirmatory assays on our primary hits. We will then perform a structure-activity analysis on all of the data from the pure compounds to come up with substructures/templates of lead compound classes. We will then use this data to search through the literature and patent database in an attempt to identify the potential protein target(s) for these compounds.

Detailed progress report

After developing an Alamar Blue cell viability assay for *B. anthracis* Δ ANR strain in the first quarter, we designed a high through robotics scheme for the assay whereby a single concentration was used for the screening of a large, chemically diverse library. Our automated HTS method, coupled with a lower throughput minimum inhibition concentration (MIC) version of the screen, allowed us to screen 50,080 pure compounds from our library and 3,997 extracts that were produced from marine microorganism, cyanobacteria, and plant natural sources. Below, the description of designed and optimized HTS method and results are described.

1) Design of robot schemes for single and multiple Concentration assays.

Expanding on our first quarter success in creating a cell viability assay for HTS use with the *B. anthracis* Stern Δ ANR Strain, we sought to develop the a set of robotic schemes that would adapt the HTS screen to our current robotics capability. As shown in Figure 1a, we split the process into three phases. Phase 1 consisted of media and library compound addition to the plates. During the course of the day, 60 assay plates were processed through Phase 1 in the morning. As we preformed our screening in duplicate, this translated into 30 daughter plates being screened for an average output of 9,600 a day. All plates were sealed at the end of Phase 1 to prevent contamination during storage for Phase 2 which involved the inoculation of the wells with *B. anthracis* Δ ANR strain. The bacteria were added via addition of a 45 μ L aliquot at an OD of 0.004 at 600 nm. Following inoculation, the plates were covered with lids and then sealed with parafilm for incubation overnight at 37°C. Development of the plates by addition of Alamar Blue followed the Phase 3 scheme.

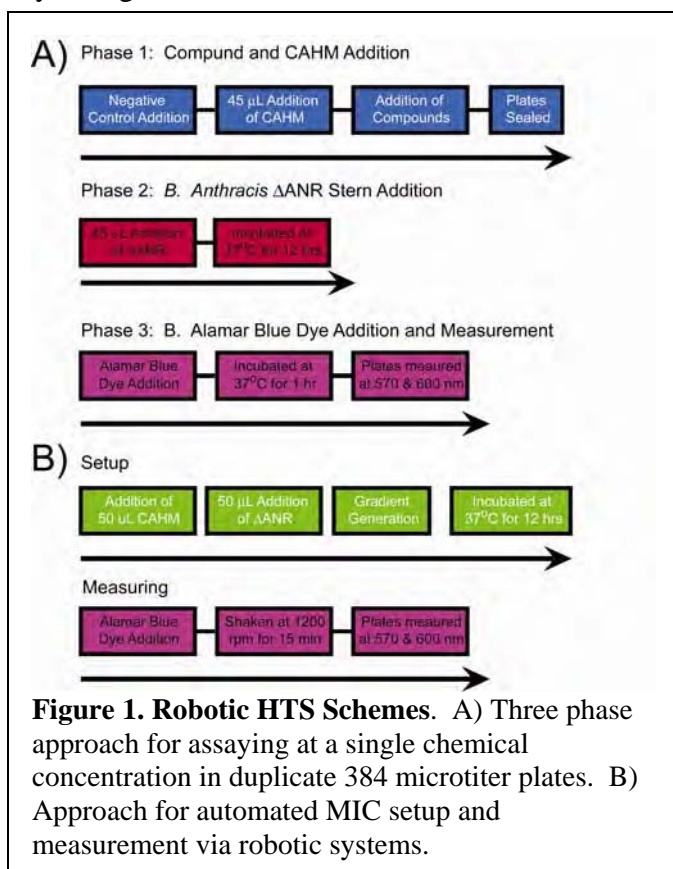


Figure 1. Robotic HTS Schemes. A) Three phase approach for assaying at a single chemical concentration in duplicate 384 microtiter plates. B) Approach for automated MIC setup and measurement via robotic systems.

In addition to the 384 single-concentration schemes developed during the first quarter, a standardized scheme was also finalized for implementation of the gradient concentration screen to measure MIC values (Figure 1b). Due to the low throughput of this version, this scheme only consisted of two steps, Setup and Measurement.

2) 384 High Throughput Screening Results of Deep Ocean Marine Extract Library.

The first library screened consisted of extracts sourced from deep ocean bacterial strains. These extracts were provided by Dr. Bill Fenical's laboratory located at Scripps Institution of Oceanography (SIO). We were provided with 2800 distinct solutions comprised of fractionated extracts from 28 separate growths. Growths contained either one bacterial strain or two grown together. Subsequently after growth, each underwent a rough extraction and was fractionated via a HPLC reverse phase C8 column. Consequently, 9 fractions and a wash fraction were generated for 10 fractions total. All fractions were desiccated and re-suspended to 4 mg/ml in DMSO. Due to the previously observed hit rate with this library against individual enzymatic targets, we opted initially screen *B. anthracis* Δ ANR strain in duplicate at a final concentration of 4.4 μ g/ml.

Overall, the screening can be characterized as excellent according to previously established HTS standards [1]. Of 2800 fractionated extracts, 192 fractionated extracts exhibited a mean inhibition of bacterial growth over 70% (6.8 % hit rate) and had similar inhibition values in both replicate test wells (Figure 2a). Furthermore, positive controls that were not inoculated with bacteria had an average value of 0.25 with a standard deviation of only 0.008. Negative controls containing no fractionated extracts had an average value -0.927 with a standard deviation of 0.04. These values resulted in a per plate set Z-factor value ranging from 0.55-0.79 with an average of 0.70, which is consistent with the excellent assay classification [1].

Comparison of the data with other already tested antibiotic enzyme targets resulted in the identification of at five extracts that also inhibit *B. anthracis* enzymes. In order to follow-up on these and other hits, we are currently in the process of triaging the hits to determine the priority order for follow-up experimentation. Since these hits are extracts that contain 3-5 unique compounds, collaboration with Dr. Bill Fenical's group for de-replication and identification of chemical structures will be required prior to elucidation of their protein targets

3) 384 High Throughput Screening Results of Cyanobacteria.

In addition to the bacterial extracts from the deep ocean, 40 additional extracts from cyanobacteria strains, provided by Dr. Jimmy Orjala's laboratory, were also screened. The cyanobacteria library consisted of 320 distinct solutions generated by only fractionation by a SP-20 column which resulting in 7 fractions and 1 wash fraction for a total of 8 fractions per strain. As with the SIO library screening, we opted initially screen *B. anthracis* Δ ANR strain in duplicate at a final concentration of 4.4 μ g/ml.

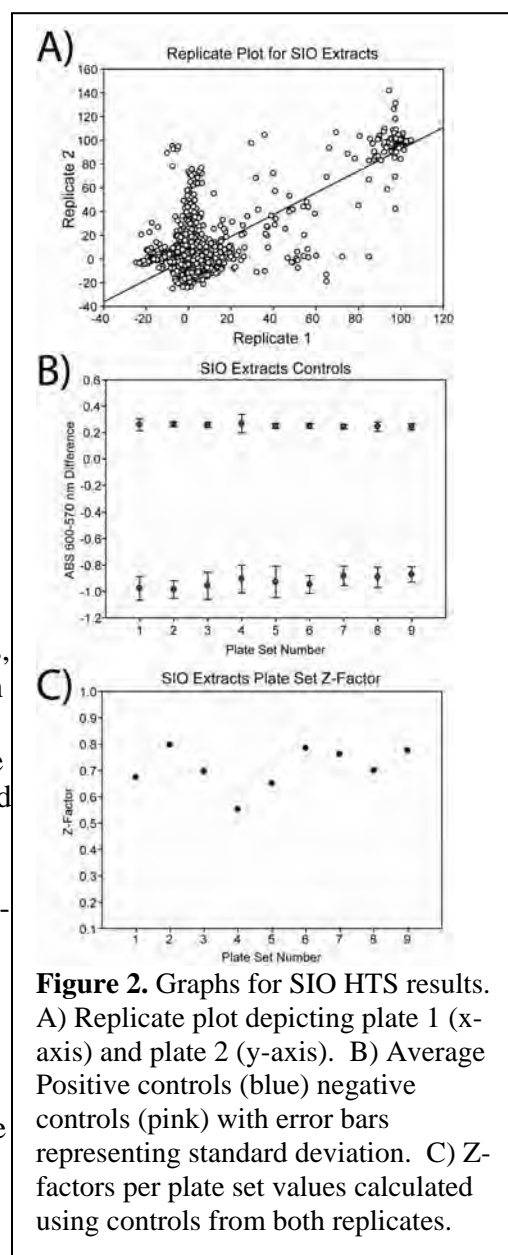


Figure 2. Graphs for SIO HTS results. A) Replicate plot depicting plate 1 (x-axis) and plate 2 (y-axis). B) Average Positive controls (blue) negative controls (pink) with error bars representing standard deviation. C) Z-factors per plate set values calculated using controls from both replicates.

As with the SIO HTS screen, this screening can be characterized as excellent according to previously established HTS standards [1]. Of the 320 fractionated extracts, 9 fractionated extracts exhibited a mean inhibition of bacterial growth over 70% (2.8 % hit rate) and had similar inhibition values in both replicate test wells (Figure 3a). Furthermore, positive controls that were not inoculated with bacteria had an average value of 0.24 with a standard deviation of only 0.018. Negative controls containing no fractionated extracts had an average value -0.91 with a standard deviation of 0.07. These values resulted in a per plate set Z-factor for the one plate of 0.77, which is consistent with the excellent assay classification[1].

Comparison of the data with other already tested antibiotic enzymatic targets resulted in the identification of at two extracts that share inhibition qualities with *B. anthracis* enzymes that have been screened. In contrast to the SIO library fractionation, the cyanobacteria library was less vigorously fractionated. Subsequently, each fraction contains approximately 5-15 unique compounds and will be undergoing further fractionation in collaboration with Dr. Jimmy Orjala's laboratory.

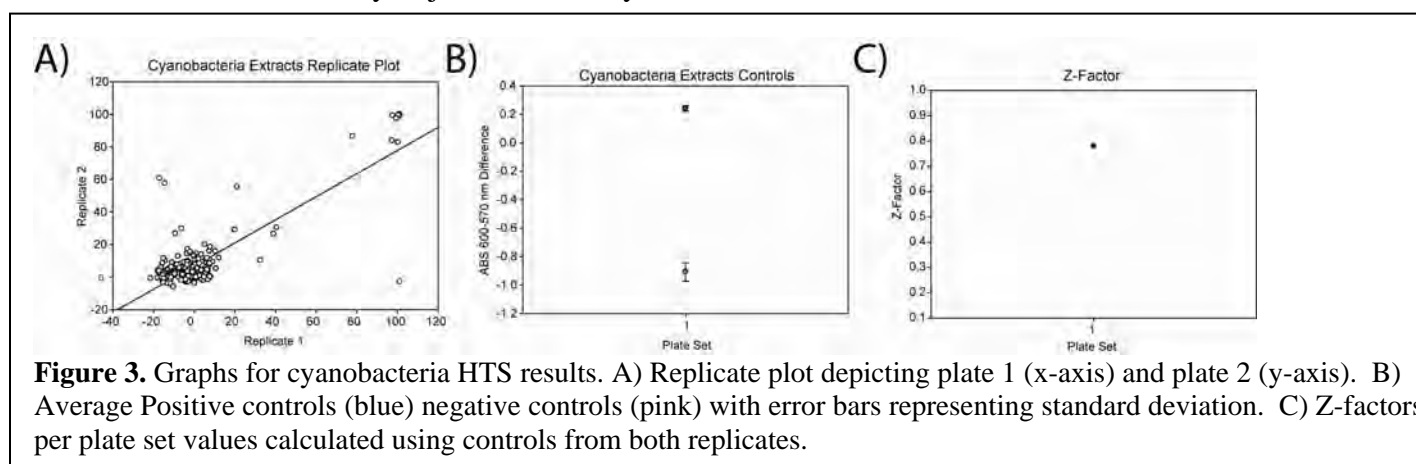


Figure 3. Graphs for cyanobacteria HTS results. A) Replicate plot depicting plate 1 (x-axis) and plate 2 (y-axis). B) Average Positive controls (blue) negative controls (pink) with error bars representing standard deviation. C) Z-factors per plate set values calculated using controls from both replicates.

4) 384 High Throughput Screening Results of Compounds and Extracts from other Sources.

To achieve partial coverage of eukaryotic organisms that may produce metabolites with antibiotic activity, a third library of plant extracts was screened. This library comprised of raw extracts derived from 877 species of plants. Scripps Research Institute in Florida provided 458 of the extracts with various PIs located in the Republic of China providing the remaining 419 species. Screening was performed in duplicate at a final concentration of 10 µg/ml.

As with the other extract HTS screens, this screening can be characterized as excellent according to previously established HTS standards [1]. Of the 878 extracts, 9 fractionated extracts exhibited a mean inhibition of bacterial growth over 70% (1.0 % hit rate) and had similar inhibition values in both replicate test wells (Figure 4a). Furthermore, positive controls that were not inoculated with bacteria had an average value of 0.25 with a standard deviation of only 0.018. Negative controls containing no fractionated extracts had an average value -0.92 with a standard deviation of 0.07 (Figure 4b). These values resulted in a per plate set Z-factor average of 0.77, which is consistent with the excellent assay classification (Figure 4c)[1].

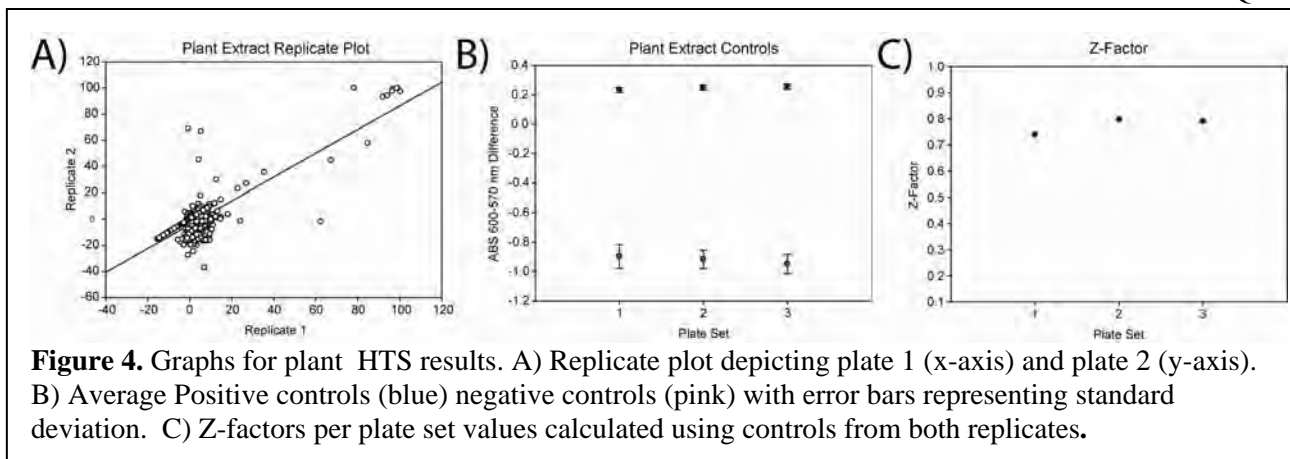


Figure 4. Graphs for plant HTS results. A) Replicate plot depicting plate 1 (x-axis) and plate 2 (y-axis). B) Average Positive controls (blue) negative controls (pink) with error bars representing standard deviation. C) Z-factors per plate set values calculated using controls from both replicates.

Comparison of the data with other already tested antibiotic enzymatic targets resulted in the identification of at three extracts that share inhibition qualities with *B. anthracis* enzymes that have been screened. In contrast to the SIO and UIC sourced libraries, no current collaboration has been established for further fractionation, de-replication, or de-convolution.

5) 384 High Throughput Screening Results of 50,000 Pure Compounds from the TB Global Alliance.

In addition to screening extracts that contain a mixture of compounds, we also screened a library of known pure compounds that have been screened against *Mycobacterium tuberculosis* for antibiotic lead discovery. The library (ChemBridge NovaCore) was generated by using ~47 core chemical templates with different chemical groups added onto the core. This reduced the diversity of the library but increased the likelihood of an SAR analysis being successfully conducted without additional compounds needed. In contrast to the extract libraries, the ChemBridge NovaCore library was screened at a final concentration of 22.2 μ M.

As with the extract HTS screens, this screening can be characterized as excellent according to previously established HTS standards [1]. Of the 50,000 compounds, 44 compounds exhibited a mean inhibition of bacterial growth over 35% (0.08 % hit rate) with each replicate exhibiting at least 30% inhibition (Figure 5a). Furthermore, positive controls that were not inoculated with bacteria had an average value of 0.21 with a standard deviation of only 0.014. Negative controls containing no fractionated extracts had an average value -0.80 with a standard deviation of 0.05 (Figure 5b). These values resulted in a per plate set Z-factor average of 0.82 with a 0.5 standard deviation, which is consistent with the excellent assay classification (Figure 5c) [1].

Literature cited

1. Zhang, J.H., T.D. Chung, and K.R. Oldenburg, A Simple Statistical Parameter for Use in Evaluation and Validation of High Throughput Screening Assays. *J Biomol Screen*, 1999. **4**(2): p. 67-73.

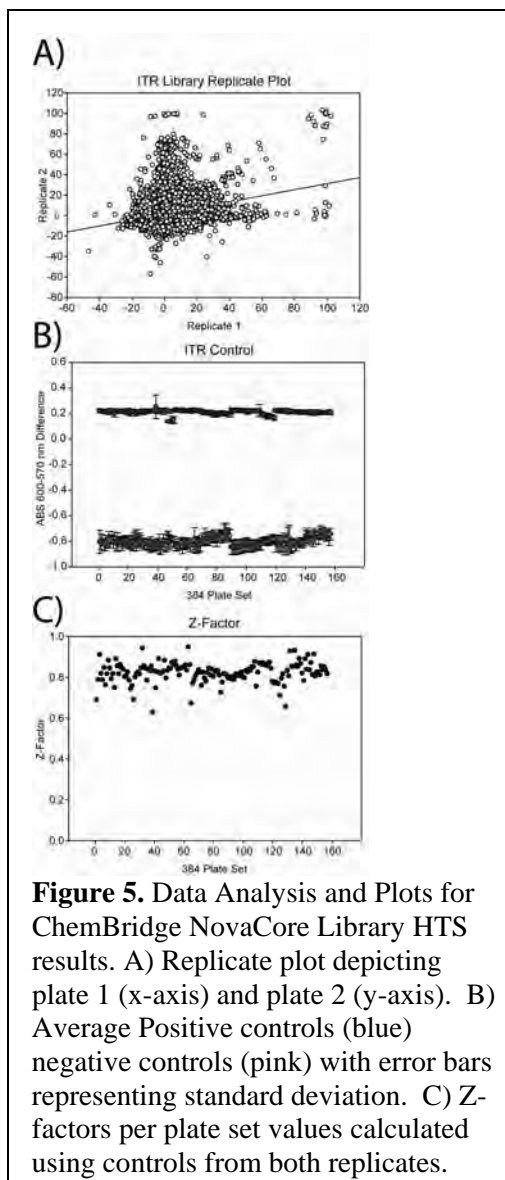


Figure 5. Data Analysis and Plots for ChemBridge NovaCore Library HTS results. A) Replicate plot depicting plate 1 (x-axis) and plate 2 (y-axis). B) Average Positive controls (blue) negative controls (pink) with error bars representing standard deviation. C) Z-factors per plate set values calculated using controls from both replicates.

Quarterly Report 3: High Throughput Screening (HTS) Core

A. Mesecar and S. Pegan

Summary

During the 3rd Quarter, the HTS core was able to meet all of its milestones. We completed an SAR analysis of the HTS data acquired during the second quarter and arrived different structural templates that served as our leads to perform follow-up analysis on. Follow-up included performing MICs on three distinct structural templates which identified one compound with an MIC value of 12.5 μ M. We also performed an extensive literature search and found a patent that states that one of our templates, a β -carboline, is an inhibitor of the enzyme Phosphopantetheine adenylyltransferase (PPAT) from *E.coli*. To follow-up on this possibility, we successfully cloned and expressed PPAT from *Bacillus anthracis*, *Mycobacterium tuberculosis* and *E.coli* so that we can test for inhibition of these enzymes by our identified lead compounds.

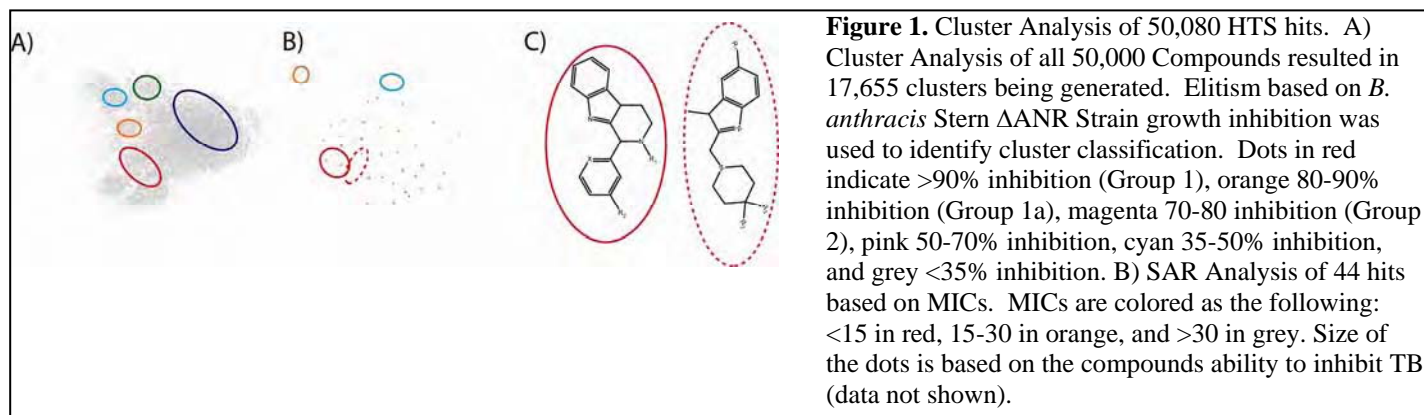
Plans

Our plans for the 4th quarter are to now test the hypothesis that β -carbolines inhibit *B. anthracis*, *M. tuberculosis* and *E.coli* PPAT. We will develop an assay to measure the kinetic activity of enzymes, and we will then measure the kinetic constants, K_m and V_{max} for their substrates. We utilize this information to setup assays so that we may test for inhibition of PPAT by the β -carbolines and the other structural templates that we identified. If the PPAT enzyme is inhibited by these compounds, it will be of significance since it will help to define a new class of antibacterial target and lead compounds for further therapeutic development.

Detailed Progress Report

1. Follow-up SAR Analysis on the ChemBridge NovaCore Library

Cluster analysis using SARnavigator by Tripos was used to identify possible templates for further optimization and validation experiments. Based on similarity of chemical structure, 17,655 cluster for comparing were generated. Each cluster was represented by the compound in the cluster that exhibited the highest inhibition properties. Upon first review, five areas were deemed hotspots (Figure 1a). To narrow the field to those of the highest potency further MIC determination using the 96 well format gradient was used. The highest concentration of inhibitor used for the gradient screen was 30 μ M. Of the 44 original hits, 13 had MICs of 30 μ M or less with three compounds exhibiting MICs of less than 15 μ M. All three of these compounds were found to be in the hotspot indicated by the red ring in Figure 1. Using the MICs as an indicator of potency, an SAR map of the 44 compounds was created (Figure 1b). Examination of this map indicated that the hotspot red contained two distinct chemical templates and could be broken into two groups (Figure 1b). Each subgroups primary scaffold is depicted in Figure 6c. Currently we are performing further SAR analysis and prioritizing these two scaffolds for synthetic chemistry.



2) Confirm MIC's of commercially purchased hit compounds.

Three groups of compounds, 1, 1a, 2, were identified in the 2nd QTR by cluster analysis by the alamar blue based assay to inhibit the growth of Δ ANR strain of *B. anthracis*. Of the twelve compounds selected, seven were of group 1, five of group 1a and one from group 2. These compounds were commercially purchased from Chembridge Corporation the originator of the library. MICs were conducted using the automated MIC version of the alamar blue assay developed in the 2nd QTR. Range of concentrations for the MIC assay was 200 μ M to 97 nM. Group 1 compound MES# 63818 had the lowest MIC of the twelve.

| Table 1: MICs of Groups 1, 1a, and 2 | | | |
|--------------------------------------|------|-------|-----|
| MES # | MIC | MES # | MIC |
| 63818 | 12.5 | 54669 | 50 |
| 64347 | 25 | 61500 | 25 |
| 83483 | 25 | 86143 | 50 |
| 84996 | 50 | 87748 | 50 |
| 85833 | 100 | 99216 | 100 |
| 76062 | 25 | | |
| 51262 | 50 | | |

3) Cloning and Purification of Phosphopantetheine adenylyltransferase (PPAT) from *Bacillus anthracis*, *Mycobacterium tuberculosis*, and *Escherichia coli*.

To test if *B. anthracis*' PPAT was the target of group 1 compounds and other hit compounds in our screen we sought to clone, over-express, and purify PPAT for testing. The nucleotide sequence of *B. anthracis* PPAT was gathered from the NCBI database and was codon optimized. The gene was inserted into a pET28a vector using *NdeI* and *BamHI* sites. The final construct contained a hexa-histidine tag and a thrombin cleavage site. Subsequently, the plasmid was transformed into *E. coli* BL21 (DE3) cells. The cells were then grown at 37 °C to an OD₆₀₀ of 0.6 and induced with 1 mL of 0.5 M IPTG and incubated at 37 °C for 3 hrs. Cells were lysed through sonication and spun at high speed to pellet insoluble proteins and membranes in a pH 8 environment. The supernatant was poured over a Qiagen Ni-NTA affinity column to select for the His-tagged PPAT. PPAT was eluted off with imidazole and under went either; buffer exchange to a pH 5 environment, was incubated with thrombin for tag cleave, or was unadulterated. PPAT was then loaded on to a Superdex 200 sizing column in a minimal salt buffer. PPAT in all condition tested eluted as a hexamer, which is consistent with previous studies performed on other bacterial PPAT enzymes. To determine protein quality a 15% polyacrylamide gel was used (Figure 2). A Band is present at 20 kDa standard band and is consistent with the expected monomeric PPAT weight of 20 kDa. Furthermore, upon thrombin cleave the band drops the approximate 2 kDa expected confirming this to be PPAT. By using our purification strategy we were able to purify 26.5 mgs of 99% pure *B. anthracis* PPAT from a 4 L growth.

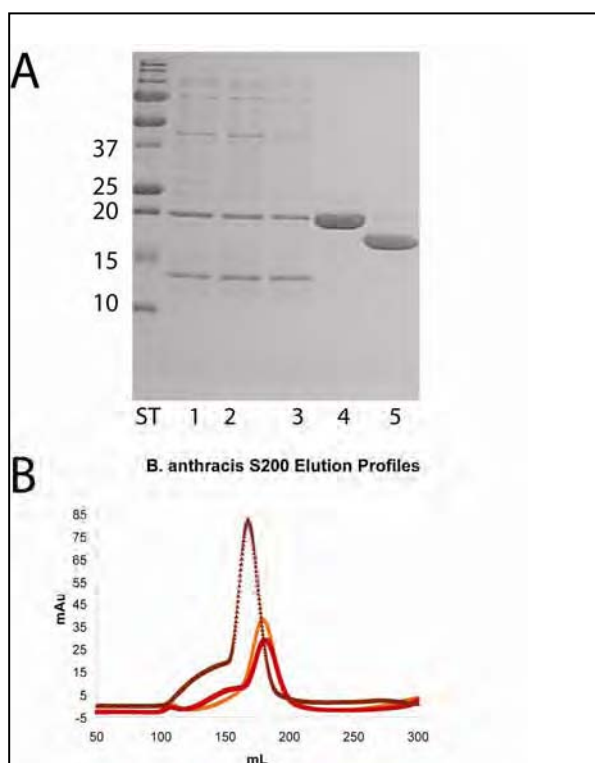
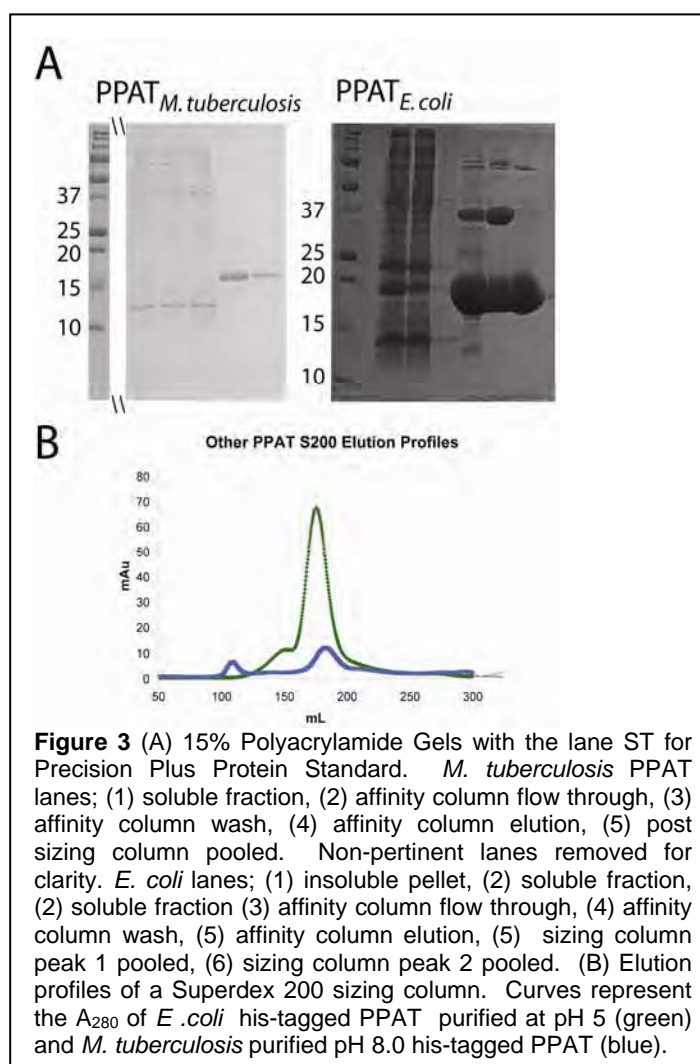


Figure 2 (A) 15% Polyacrylamide Gel with the following lanes: (ST) Precision Plus Protein Standard, (1) soluble fraction, (2) affinity column flow through, (3) affinity column wash, (4) affinity column elution, (5) post-thrombin cleaved *B. anthracis* PPAT. (B) Elution profiles of a superdex 200 sizing column. Curves represent the A₂₈₀ of *B. anthracis* PPAT purified at pH 8.5; his-tagged (orange), his-tagged cleaved (red), as well as his-tagged purified at pH 5 (brown).

In addition to acquiring *B. anthracis* PPAT, we also sought to obtain PPAT from *E. coli* and *M. tuberculosis*. As the original study linking PPAT to compounds similar to group 1 was performed in *E. coli*, we sought to compare directly group 1 compounds with PPAT from the original study. *M. tuberculosis* was added as the library used for HTS screening of Δ ANR strain of *B. anthracis* was also screened locally against *M. tuberculosis*. Similar compounds from group 1, 1a, and 2 were also identified in that screen to inhibit *M. tuberculosis* growth. As with the *B. anthracis* PPAT, *M. tuberculosis* PPAT was obtained through the NCBI database and codon optimized for *E. coli*, inserted using *NdeI* and *BamHI* sites and a pET28a vector. *E. coli* PPAT was sourced from the ASKA library on a pCA24N expression plasmid with a hexa-histadine tag with no thrombin cleavage site (1). Both *E. coli* and *M. tuberculosis* PPATs were grown, expressed and purified using the purification protocol for *B. anthracis* PPAT. Both enzymes eluted from the sizing columns as hexamers. Results of a 15% polyacrylamide gel indicated that both proteins were at least 99% pure and ran consistent with expected molecular weights of *M. tuberculosis* PPAT, 17 kDa, and *E. coli* PPAT 20 kDa (Figure 3). Overall yield for the 4 L preps were 10.0 mgs for *M. tuberculosis* and 17.1 mgs for *E. coli*.



References

1. M. Kitagawa *et al.*, *DNA Res* **12**, 291 (2005).

Quarterly Report 4:High Throughput Screening (HTS) Core

A. Mesecar and S. Pegan

Summary

During this Fourth Quarter, the HTS core was able to meet all of its milestones. We tested the hypothesis that β -carboline inhibit the enzyme PPAT from *B. anthracis*, *M. tuberculosis* and *E.coli*. Most significantly, we found that the β -carboline do not act as inhibitors of PPAT in our current in vitro enzyme assays suggesting that they have a different molecular target in bacteria.

Plans

Since our current PPAT enzyme assay only measures the reverse reaction catalyzed by the enzyme, we will work to develop an activity assay based on measuring the rate of the forward reaction catalyzed by PPAT and retest the ability of the compounds to inhibit PPAT. If we find that these compounds do not inhibit PPAT, it will bring into question the validity of the patent that reported that β -carboline inhibit bacterial PPAT enzymes.

Detailed Progress Report

We developed an assay to measure the kinetic activity of the PPAT enzymes based upon the reverse reaction. This direction was chosen since the reagents for running the reaction in reverse are commercially available. We optimized the assay and then measured the kinetic constants, K_m and V_{max} for the substrates. We used this information to setup assays so that we could test for inhibition of PPAT by the β -carboline and the other structural templates that we identified. We attempted to measure the IC_{50} values for these compounds at substrate concentrations near their K_m values. However, we were unable to detect any inhibition of the *B.anthraxis*, *M. tuberculosis* and *E.coli* PPAT enzymes up to 100 μM .

Project personnel (in alphabetical order)

Salaried:

Name

Beck, William
Forrester, Sara
Gao, Kuanquang
Gemeinhart, Ernest
Guo, Songpo
Joyasawal, Sipak
Kadari, Sudhakar
Kim, Hye Yeong
Klepacki, Dorota
Kuzmis, Antonina
Llano-Sotelo, Beatriz
Mittal, Anuradha
Mulhearn, Debbie
Pegan, Scott
Ramy, Abdelhamid
Suresh, Tipparaju
Thatcher, Gregory
Turski, Sondra
Vaskova, Martina

Non salaried:

Name

Bauman, Jerry
Gemeinhart, Richard
Johnson, Michael
Kozikowski, Alan
Mankin, Alexander
Mesecar, Andrew
Onyuksel, Hayat